The application of PEEK to the packaging of implantable electronic devices

A thesis submitted in partial fulfilment of
the requirements for the degree of
Doctor of Philosophy

Nathaniel Dahan

DEPARTMENT OF MEDICAL PHYSICS AND BIOENGINEERING
UNIVERSITY COLLEGE LONDON

Supervisor: Pr Nick Donaldson
Second Supervisor: Dr Stephen Taylor

2010-2013

Declaration

I, Nathaniel Dahan, confirm that the work presented in this thesis is my own. Where information has been derived from other sources, I confirm that this has been indicated in the thesis

'*Concentration applied to solve a problem does not mean focusing on the solution – you do not have the solution to focus on yet. Concentration simply means clearing the mind of extraneous thoughts and mental 'noise', clearing a space in the mind – and the solution appears. An idea is not created, it happens. In Yiddish an 'idea' is an 'einfal': it* falls in. *There is a humility in that term, a recognition that a new insight comes from outside as a gift, that the word 'idea' can never convey.'*

(Tatz & Gottlieb 2004)

Acknowledgments

I would like to express my greatest thanks to my supervisors, Prof. Nick Donaldson and Dr Stephen Taylor, for providing structure, help, and guidance during my PhD. Their direction, insight and knowledge have been essential to the good conduct of this study and to my development as a PhD student. I would like to thank them especially for getting right that delicate balance between letting me work autonomously, while always being available to answer all my questions whenever I needed help.

I would like to thank my sponsor Invibio Ltd. for enabling this work, and in particular Dr Nuno Sereno for his general help in answering my questions, for always ensuring that I received the parts I needed for my research as promptly as possible, and for keeping an open mind and suggesting potential innovative solutions.

I would also like to thank Dr Anne Vanhoestenberghe for her good company and her availability in providing invaluable help in all aspects of my work on a daily basis. Thanks also to Dr Adam Wojcik (UCL Mechanical engineering) for his help with the lap shear test experiments; to Dominik Cirmirakis for his help with the telemetry system used in this study; to Dr Jane Galbraith for her help with statistics and power calculations; to Sacha Noimark and Andreas Kafizas for their help with TiO_2 coatings; to Dr Antonio Santana (Ionbond), William Easley (SMD), Prof. Ivan Parkin (UCL Chemistry), Xiaoling Zhang (Teer coatings Ltd), Godfried Knut, Lutz Hofmann (Fraunhofer ENAS), Peter Franks (dual Metallising) and Dr Carsten Gollasch (Southampton Nanofabrication Centre) for their help with the metallisation of PEEK.

On a more personal level, I would like to express my greatest thanks to all my family, especially to my parents, and to my beloved Anat, for their unconditional love, support and pride in me, which has enabled me to go through with this work in the best conditions I could have wished for.

I would also like to thank all my friends and fellow PhD students in Medphys: Kylie, Runhan, Nooshin, Bret, Hwan, James, etc. for their good company and sharing their doubts and encouragements on the PhD student life.

Finally, I would also like to express my thanks to my housemates Dave, Jonny and Lauren, for their support and all the fun we have had in the last couple of years, which played a great part in making this an enjoyable journey.

Abstract

PEEK is a polymer that is used in many orthopaedic implants because of its favourable mechanical properties and its biocompatibility. High-reliability electronic implants such as pacemakers have 'hermetic' enclosures with the electronic components in dry gas. This type of package, generally made of metal or ceramic, guarantees a very long lifetime, but is also expensive. PEEK can be easily machined or injection-moulded, it is an attractive material for implant manufacturers and it may be that by novel design based on established material properties, PEEK may be used in some applications.

This thesis examines the case of PEEK as a packaging material for applications which only require a more limited lifetime (less than three years). The process of moisture ingress through polymers is analysed, and a novel calculation method to quantify it is developed, based on an electrical analogy and Tencer's approximation of the full solution to Fick's laws of diffusion. A telemetry system is designed, which allows measuring the relative humidity inside a PEEK capsule. Diagrams, PCB layouts, microcontroller program and component lists are provided, making this design easily reproducible.

The lifetime of PEEK packages is investigated, as well as the contribution of the adhesive seal vs. the package walls. In order to prolong this lifetime, the use of desiccant and thin film coating is suggested. The calculation method we developed is extended to the case of the use of desiccant. This model is found accurate in predicting the time constant when silica gel is used (Type IV isotherm), but not in the case of molecular sieve (Type I isotherm), because of the type of isotherm characterising the desiccant behaviour.

Thin film coating of PEEK is also investigated as a means to reduce permeability. It is found that most PVD techniques do not provide a significant improvement, due to high residual stress and the porous morphology of the films. Nevertheless, applying a coating prior to deposition proves effective in mitigating these, and improves the time constant of the package by a factor of 2.3. Atomic Layer Deposition also shows an improvement in time constant of similar magnitude.

Finally, guideline graphs and tables combining calculations and experimental results are presented, providing a quick way for the implant designer to evaluate which size package is required for their application. It is found that time constants in excess of 2.5 years are achievable, using the right combination of coating and desiccant.

Contents

DECLARATION 2

ACKNOWLEDGMENTS 4

ABSTRACT 5

CONTENTS 6

LIST OF TABLES 11

LIST OF FIGURES 12

NOMENCLATURE 16

CHAPTER 1 INTRODUCTORY SUMMARY 18

CHAPTER 2 PEEK, HERMETICITY, AND MOISTURE INGRESS – AN INTRODUCTION 20

2.1 Introduction 20

2.2 PEEK as a material, properties 20

2.2.1 Chemical structure and properties 20

2.2.2 Barrier properties 20

2.2.3 Joining technology 20

2.2.4 Mechanical properties 21

2.2.5 Surface activation and coating of PEEK 21

2.2.6 Benefits of PEEK 22

2.3 Encapsulation and hermetic packages 22

2.3.1 Encapsulation 22

2.3.2 Hermetic packages 23

2.3.3 The importance of sealing 23

2.4 Joining technologies for thermoplastic polymers and the case of PEEK and implanted electronic devices 24

2.4.1 Fusion bonding 24

2.4.2 Adhesive bonding 29

2.5 Flow of gas in and out of sealed packages 29
2.5.1 Viscous, molecular and diffusive flow 29
2.5.2 Origin 29
2.5.3 Consequences 30
2.5.4 Failure criteria 30
2.5.5 Helium leak tests 31
2.5.6 Formulas for the flow of gases and leak rates 31
2.5.7 The case of permeation through a solid 33

2.6 Expected lifetime of a polymer package 33
2.6.1 Full transient model – Analogy with heat conduction problem 33
2.6.2 Tencer's approximation 34

2.7 Difference between the solubility (S), diffusion (D) and permeation (K) constants 36

2.8 Conclusion 36

CHAPTER 3 MOISTURE INGRESS IN AN ADHESIVELY JOINED POLYMER PACKAGES - THEORETICAL CONSIDERATIONS AND A NOVEL CALCULATION METHOD 37

3.1 Objectives and failure mechanisms 37
3.1.1 Useful lifetime and objectives 37
3.1.2 Failure mechanisms and criterion 38
3.1.3 Description of the package 39

3.2 Is the Tencer approximation a good representation of the full transient model? 39
3.2.1 Transient model 40
3.2.2 Tencer's approximation 40
3.2.3 Comparison of the two models 42

3.3 A new calculation method for polymer packages with walls of varying thickness/properties. 43
3.3.1 Electrical analogy, making sense of the time constant 44
3.3.2 Calculation method for package made with walls of different properties 45
3.3.3 Experimental results 47
3.3.4 Discussion 48

3.4 Interpreting experimental results 49
3.4.1 Normalising the lifetime 49
3.4.2 Determining the experimental time constant 49

3.5 Conclusion 50

CHAPTER 4 MEASURING THE HUMIDITY INSIDE THE CAPSULE: METHOD AND SET UP 51

4.1 Telemetry using electromagnetic inductive coupling 51
4.1.1 How does it work? 51
4.1.2 Description of the receiver side (implant) of the telemetry system 52
4.1.3 Description of the transmitter side of the telemetry system 53
4.1.4 Attenuation issues 54

4.2 Measuring the humidity level inside the PEEK capsule 58
4.2.1 The humidity sensor 58
4.2.2 The PIC Microcontroller and the program 59

4.3 Circuit design 61
4.3.1 The receiver 61
4.3.2 The transmitter 65

4.4 Experimental set up 68

4.5 Sample size 69

4.6 Conclusion 70

CHAPTER 5 MOISTURE INGRESS IN ADHESIVELY JOINED PEEK CAPSULES: EXPERIMENTAL WORK 71

5.1 Adhesive bonding – Literature review 71
5.1.1 Intramolecular forces 71
5.1.2 Intermolecular forces 74
5.1.3 Surface energy 75
5.1.4 Work of cohesion and work of adhesion 76
5.1.5 Theories of adhesion 77
5.1.6 Effect of moisture on an adhesive joint 78
5.1.7 Promoting adhesion 79

5.2 Lifetime of adhesively joined PEEK packages – experimental work 79
5.2.1 Selection of adhesives 79
5.2.2 Preliminary experiment 80
5.2.3 Lifetime of adhesively joined PEEK packages 82

5.3 Influence of the wall thickness on the lifetime 94

5.4 Summary and conclusion 96

CHAPTER 6 PROLONGING THE LIFETIME USING A DESICCANT 98

6.1 Desiccants and adsorption – Literature review 98
6.1.1 Introduction on adsorbents 98
6.1.2 Types of desiccant 98
6.1.3 Adsorption equilibrium 103
6.1.4 Rate of adsorption 106

6.2 Selection of an appropriate desiccant 107

6.3 Influence of the temperature on the adsorption capacity 109

6.4 Lifetime calculations and preliminary experiments 110
6.4.1 Calculation method 110
6.4.2 Preliminary experiment – amount of water adsorbed by silica gel at high humidity levels 112
6.4.3 Calculated lifetime 113

6.5 Experimental results 114
6.5.1 Using molecular sieve desiccant 114
6.5.2 Using silica gel desiccant 115
6.5.3 Comparison and validity of the calculation method 115

6.6 Maximum lifetime achievable using a desiccant 117

6.7 Conclusion 119

CHAPTER 7 PROLONGING THE LIFETIME USING A THIN FILM COATING 120

7.1 Vacuum deposition techniques – Literature review 120
7.1.1 Physical vapour deposition (PVD) 120
7.1.2 Chemical vapour deposition (CVD) 127
7.1.3 Film growth and properties 128
7.1.4 Adhesion and loss of adhesion 129

7.2 PVD coating on PEEK 130
7.2.1 Evaporation coating 130
7.2.2 Reasons for failure 135
7.2.3 Sputtering coating 142

7.3 Plasma enhanced CVD 147

7.4 Other coating techniques 149
7.4.1 Atomic Layer Deposition of alumina 149
7.4.2 Electrodeposition with copper 152
7.4.3 Dip coating with titania 153
7.4.4 Dip coating with ceramic 155

7.5 Summary and conclusion 157

CHAPTER 8 SUMMARY, DISCUSSION, AND FUTURE WORK 159

8.1 Summary, discussion and maximum achievable lifetime 159

8.2 Future work 166

8.3 Conclusion 166

APPENDIX 1. ASSEMBLER CODE FOR THE RECEIVER CIRCUIT 168

APPENDIX 2. LIST OF COMPONENTS FOR THE TELEMETRY SYSTEM 171

APPENDIX 3. SOLID TITANIUM CAPSULE AND FEEDTHROUGH 172

BIBLIOGRAPHY 174

List of tables

TABLE 1-1 ELECTRONIC IMPLANT APPLICATIONS AND THEIR LIFETIMES 18
TABLE 3-1 CALCULATIONS 47
TABLE 4-1 ATTENUATION OF SIGNAL DUE TO METAL COATING 57
TABLE 4-2 DATA FOR POWER CALCULATION 69
TABLE 5-1 TYPES OF INTRAMOLECULAR BONDS 73
TABLE 5-2 TYPES OF VAN DER WAALS BONDS 74
TABLE 5-3 TIME CONSTANTS FOR DIFFERENT TYPES OF SEAL 83
TABLE 5-4 SUMMARY OF RESULTS 97
TABLE 6-1 REPRESENTATIVE COMMERCIAL ADSORPTION SEPARATIONS - FROM (KELLER II 1987) 99
TABLE 6-2 COMMERCIAL MOLECULAR SIEVE ADSORBENTS AND PROPERTIES - FROM (KELLER II 1987) 100
TABLE 6-3 TYPICAL PROPERTIES OF ADSORBENT-GRADE SILICA GEL (FROM (KELLER II 1987)) 101
TABLE 6-4 TYPICAL PROPERTIES OF ADSORBENT-GRADE ACTIVATED ALUMINA - FROM (KELLER II 1987) 102
TABLE 6-5 REGENERATION CONDITIONS FOR DESICCANTS 107
TABLE 6-6 VALUES USED FOR CALCULATION OF MOISTURE INGRESS 113
TABLE 6-7 TIME CONSTANTS - SUMMARY OF RESULTS 115
TABLE 6-8 CALCULATED TIME CONSTANT FOR CYLINDRICAL PEEK CAPSULE USING VARYING AMOUNTS OF DESICCANT 119
TABLE 7-1 TIME CONSTANTS OF TI COATED (CAD) PEEK PACKAGES 131
TABLE 7-2 TIME CONSTANTS (IN DAYS) FOR PACKAGES COATED WITH 3UM TITANIUM (WITH AND WITHOUT COATING AT JOINT) 134
TABLE 7-3 TIME CONSTANTS OF AR SPUTTERING PVD COATED PEEK PACKAGES (AL, TI, CR – 0.5 MM) 144
TABLE 7-4 TIME CONSTANTS PVD COATED PEEK PACKAGES (TI+AU, CR+AU - 0.5 MM, NICR – 2 MM) 146
TABLE 7-5 TIME CONSTANTS OF UNCOATED AND ALD PEEK PACKAGES, COATED PEEK PACKAGES, AND TITANIUM PACKAGES 151
TABLE 7-6 COATINGS - SUMMARY OF RESULTS 158
TABLE 8-1 CALCULATED TIME CONSTANT FOR CYLINDRICAL PEEK CAPSULE USING VARYING AMOUNTS OF DESICCANT AND A THIN FILM COATING 164

List of figures

FIGURE 2.1 MOLECULAR STRUCTURE OF PEEK 20
FIGURE 2.2 CLASSIFICATION OF FUSION BONDING TECHNIQUES FOR THERMOPLASTICS 24
FIGURE 2.3 HEALING OF A POLYMER-POLYMER INTERFACE 25
FIGURE 2.4 HOT PLATE WELDING 25
FIGURE 2.5 INFRARED WELDING 25
FIGURE 2.6 TRANSMISSION LASER WELDING (TLW) 26
FIGURE 2.7 DIRECT LASER WELDING, JOINT DESIGN 27
FIGURE 2.8 FRICTION WELDING 27
FIGURE 2.9 SPIN WELDING 27
FIGURE 2.10 ULTRASOINC WELDING 28
FIGURE 2.11 RESISTANCE WELDING 28
FIGURE 3.1 MOISTURE INGRESS INTO ENCLOSURE 38
FIGURE 3.2 DESCRIPTION OF THE PEEK CAPSULE 39
FIGURE 3.3 WATER PERMEATION THROUGH A 1MM THICK WALL – TRANSIENT MODEL 40
FIGURE 3.4 DIFFUSION – CASE OF A VERY LARGE VOLUME 41
FIGURE 3.5 DIFFUSION – CASE OF A VERY SMALL VOLUME 42
FIGURE 3.6 TENCER MODEL AND ITS COMPONENTS 42
FIGURE 3.7 COMPARISON BETWEEN THE 'QSS' MODEL (DASHED LINE) AND THE FULL TRANSIENT SOLUTION 43
FIGURE 3.8 MOISTURE INGRESS THROUGH A POROUS WALL INTO AN ENCLOSURE, ELECTRICAL ANALOGY 44
FIGURE 3.9 MOISTURE INGRESS INTO AN ENCLOSURE WITH WALLS OF VARYING PROPERTIES, ELECTRICAL ANALOGY 45
FIGURE 3.10 EQUIVALENT SYSTEM 46
FIGURE 3.11 CONDUCTANCE (LEFT) AND CAPACITANCE (RIGHT) OF PACKAGE ELEMENTS 47
FIGURE 3.12 HUMIDITY SENSOR ACCURACY 48
FIGURE 4.1 CIRCUIT DIAGRAM OF THE TELEMETRY SYSTEM 51
FIGURE 4.2 CIRCUIT DIAGRAM OF THE RECEIVER SIDE 52
FIGURE 4.3 CIRCUIT DIAGRAM OF THE TRANSMITTER SIDE 53
FIGURE 4.4 OSCILLOGRAM SHOWING THE TRANSMITTER CARRIER (CHANNEL 1 – YELLOW), THE OUTPUT OF THE DEMODULATOR (CHANNEL 2 – BLUE) AND THE RECEIVER CARRIER (CHANNEL 3 – PINK) 54
FIGURE 4.5 SKIN DEPTH AS A FUNCTION OF FREQUENCY FOR TITANIUM 55
FIGURE 4.6 SKIN DEPTH AS A FUNCTION OF FREQUENCY 56
FIGURE 4.7 FIELD MAGNITUDE VS. DEPTH 56
FIGURE 4.8 HUMIDITY SENSOR DIAGRAM 58
FIGURE 4.9 ACCURACY OF THE SENSOR 59
FIGURE 4.10 PIC MICROCONTROLLER 60
FIGURE 4.11 OUTPUT VOLTAGE GENERATED BY THE MICROCONTROLLER 60
FIGURE 4.12 FINAL DESIGN 61
FIGURE 4.13 BREADBOARD DESIGN 62
FIGURE 4.14 PROTOTYPE TESTING 1 62

FIGURE 4.15 PROTOTYPE TESTING 2 62
FIGURE 4.16 SCHEMATIC OF THE RECEIVER CIRCUIT 63
FIGURE 4.17 PCB LAYOUT OF THE RECEIVER 63
FIGURE 4.18 IMPLANT SIZED HUMIDITY SENSING CIRCUIT 64
FIGURE 4.19 TESTING OF HUMIDITY SENSING CIRCUIT 64
FIGURE 4.20 TRANSMITTER - DIAGRAM 66
FIGURE 4.21 TRANSMITTER 67
FIGURE 4.22 GRID TO HOLD PEEK CAPSULES 68
FIGURE 4.23 EXPERIMENTAL SET UP – WATER TANK 68
FIGURE 4.24 EXPERIMENTAL SET UP 68
FIGURE 5.1 IONIC BOND 72
FIGURE 5.2 NORMAL COVALENT BOND 72
FIGURE 5.3 DATIVE COVALENT BOND 72
FIGURE 5.4 SURFACE TENSION 75
FIGURE 5.5 CONTACT ANGLE AND SURFACE FREE ENERGY COMPONENTS 76
FIGURE 5.6 RH LEVEL IN PEEK CAPSULE JOINED WITH CYANOACRYLATE 81
FIGURE 5.7 EXTRACTION OF THE EXPERIMENTAL TIME CONSTANT 81
FIGURE 5.8 COMPARISON EXPERIMENT VS. TIME CONSTANT FOUND THROUGH LINEARISATION AND REGRESSION 82
FIGURE 5.9 MOISTURE INGRESS INTO PEEK PACKAGE WITH SILICONE, CYANOACRYLATE, AND EPOXY SEAL 82
FIGURE 5.10 EFFECTIVENESS OF SEALANT MATERIALS - FROM (TRAEGER 2002) 83
FIGURE 5.11 MASS GAIN OF ADHESIVELY JOINED PEEK CAPSULES IN WATER 84
FIGURE 5.12 TITANIUM CAPSULE 85
FIGURE 5.13 TITANIUM CAPSULES IN WATER 85
FIGURE 5.14 EVOLUTION OF RH WITH TIME FOR TI CAPSULES 85
FIGURE 5.15 BRASS CAPSULE 87
FIGURE 5.16 EVOLUTION OF RH WITH TIME FOR BRASS CAPSULE WITH CA SEAL 87
FIGURE 5.17 DESIGN THE GRIPS FOR LAP SHEAR TEST 88
FIGURE 5.18 LAP SHEAR TEST 89
FIGURE 5.19 SHEAR STRENGTH OF ADHESIVELY JOINED TI SQUARES IN BOILING WATER 90
FIGURE 5.20 FAILURE OF ADHESIVE JOINT 91
FIGURE 5.21 RH LEVEL IN PEEK CAPSULES JOINED WITH CYANOACRYLATE AND POLYEFIN PRIMER 93
FIGURE 5.22 RH LEVEL IN TITANIUM CAPSULE JOINED WITH CYANOACYLATE AND POLYEFIN PRIMER 93
FIGURE 5.23 SHEAR STRENGTH OF ADHESIVELY JOINED TI SQUARES IN BOILING WATER WHEN A PRIMER IS USED 94
FIGURE 5.24 CYLINDRICAL ENCLOSURE OF CONSTANT WALL THICKNESS D - SECTION 95
FIGURE 5.25 INFLUENCE OF WALL THICKNESS AND CAVITY VOLUME ON THE TIME CONSTANT FOR A CYLINDRICAL PACKAGE 96
FIGURE 6.1 MOLECULAR DIMENSIONS AND ZEOLITE PORE SIZE (FROM (BRECK 1974)) 101
FIGURE 6.2 ADSORPTION ISOTHERMS FOR MOLECULAR SIEVE AND SILICA GEL AT 25^{O}C - FROM (DESICCARE INC. 2010) 102
FIGURE 6.3 THE FIVE TYPES OF ADSORPTION ISOTHERMS 103
FIGURE 6.4 WATER ADSORPTION VS. TIME AT 21^{O}C AND 50%RH 108

FIGURE 6.5 ADSORPTION ISOTHERM AT 25^{O}C FOR SILICA GEL, MOLECULAR SIEVE AND THIRSTY VYCOR DESICCANTS 108
FIGURE 6.6 ISOTHERM DATA FOR TYPE 3A SILICA GEL - FROM (NG 2001) 110
FIGURE 6.7 ISOTHERM DATA FOR 3A SILICA GEL AS A FUNCTION FROM THE RELATIVE HUMIDITY (DATA FROM (NG 2001)) 110
FIGURE 6.8 MOISTURE INGRESS THROUGH A PEEK PACKAGE CONTAINING DESICCANT - ELECTRICAL ANALOGY 112
FIGURE 6.9 WATER MASS GAIN FROM PACKAGES 113
FIGURE 6.10 MOLECULAR SIEVE (TOP) AND SILICA GEL (BOTTOM) DESICCANT IN PEEK CAPSULES 114
FIGURE 6.11 RH LEVEL IN PEEK CAPSULE WITH MOLECULAR SIEVE DESICCANT 114
FIGURE 6.12 RH LEVEL IN PEEK CAPSULE WITH SILICA GEL DESICCANT 115
FIGURE 6.13 INFLUENCE OF DESICCANT TYPE ON RH LEVEL 116
FIGURE 6.14 INFLUENCE OF THE USE OF SILICA GEL DESICCANT (10% OF CAVITY VOLUME) ON THE TIME CONSTANT FOR A CYLINDRICAL ENCLOSURE 118
FIGURE 6.15 INFLUENCE OF WALL THICKNESS AND AMOUNT OF DESICCANT ON THE TIME CONSTANT 119
FIGURE 7.1 QUASI-EQUILIBRIUM EVAPORATION SOURCE - THE EFFUSION CELL 121
FIGURE 7.3 ION BEAM ASSISTED DEPOSITION (IBAD) 123
FIGURE 7.2 NON EQUILIBRIUM EVAPORATIVE SOURCES: (A) CRUCIBLE SOURCE, (B) BOAT SOURCE, (C) HOT FILAMENT EVAPORATOR, (D) ELECTRON BEAM SOURCE (CROSS SECTION) 123
FIGURE 7.4 DC SPUTTERING 126
FIGURE 7.5 ION BEAM SPUTTERING 127
FIGURE 7.6 PEEK CAPSULE WITH 3 M TI COATING (CAD) 131
FIGURE 7.7 EVOLUTION OF THE RH LEVEL IN PEEK CAPSULE WITH AND WITHOUT TI COATING, FOR TWO TYPES OF ADHESIVE JOINTS 131
FIGURE 7.8 MODEL OF DIFFUSION FRONT NEAR THE METAL/POLYMER TRANSITION (FROM (ZANNI-DEFFARGES 1995)) 132
FIGURE 7.9 EFFECT OF METALLISED JOINT ON PEEK PACKAGE ADHESIVELY JOINED WITH CYANOACRYLATE 133
FIGURE 7.10 EFFECT OF METALLISED JOINT ON PEEK PACKAGE ADHESIVELY JOINED WITH EPOXY 134
FIGURE 7.11 DEGRADATION OF A 135
FIGURE 7.12 DEGRADATION OF E 136
FIGURE 7.14 SAMPLE B 136
FIGURE 7.13 DEGRADATION OF D 136
FIGURE 7.15 SEM IMAGE OF PEEK CAPSULE SURFACE (X1400) 138
FIGURE 7.16 SEM IMAGE (BACKSCATTERED E^{-}) OF TI COATED CAPSULE (CAD) (X1400) 138
FIGURE 7.17 SEM IMAGE OF TI COATED CAPSULE (CAD) (X1400) 138
FIGURE 7.18 SEM IMAGE OF TI COATED CAPSULE (CAD) (X10,000) 139
FIGURE 7.19 PEEK CAPSULES WITH EVAPORATION DEPOSITED ALUMINIUM THIN FILM - WITH (BOTTOM) AND WITHOUT (TOP) BASE LACQUER APPLIED BEFOREHAND AND STOVED 140
FIGURE 7.20 EVOLUTION OF RH IN EVAPORATION PVD COATED CAPSULES (AL -3 MM) 140
FIGURE 7.21 SEM IMAGE OF AL COATED CAPSULE (EVAPORATION) WITHOUT BASE LACQUER (X100) 141
FIGURE 7.22 SEM IMAGE OF AL COATED CAPSULE (EVAPORATION) WITH BASE LACQUER (X200) 141

FIGURE 7.23 SEM IMAGE OF AL COATED CAPSULE (EVAPORATION) WITH BASE LACQUER (X1,000) 142
FIGURE 7.24 EVOLUTION OF RH IN MAGNETRON SPUTTERING PVD COATED CAPSULES (ZR – 1.9 MM) 142
FIGURE 7.25 ZR COATED PEEK CAPSULE (MAGNETRON SPUTTERING) - BLISTERING OF THE FILM 143
FIGURE 7.26 AR SPUTTERING OF PEEK CAPSULES WITH (FROM LEFT TO RIGHT): AL, TI, AND CR (500NM THICKNESS) 143
FIGURE 7.27 RH IN AR SPUTTERING PVD COATED PEEK CAPSULES (AL, TI, CR – 0.5 MM) 144
FIGURE 7.28 SEM IMAGE OF TI COATED CAPSULE (SPUTTERING) (X20,000) 145
FIGURE 7.29 AR SPUTTERING OF PEEK CAPSULES WITH (FROM LEFT TO RIGHT): TI+AU AND CR+AU (500 NM THICKNESS) 145
FIGURE 7.30 RH LEVEL IN AR SPUTTERING PVD COATED PEEK CAPSULES (TI+AU, CR+AU - 0.5 MM, NICR – 2 MM) 146
FIGURE 7.31 SEM IMAGE OF TI-AU COATED CAPSULE (SPUTTERING) (X20,000) 147
FIGURE 7.32 PEEK CAPSULE COATED WITH SIOX BY PACVD (1 MM THICKNESS) 148
FIGURE 7.33 RH LEVEL IN PACVD COATED PEEK CAPSULES - TI (1 MM)+DLC (2 MM), SIOX (1 MM) 148
FIGURE 7.34 DLC COATING PEELING OFF 149
FIGURE 7.35 SEM IMAGE OF SIOX COATED CAPSULE (PACVD) (X100, X20,000) 149
FIGURE 7.36 CROSS SECTION OF CYLINDRICAL PEEK CAPSULES USED FOR PVD/PACVD TESTS (TYPE A - LEFT) AND ALD TESTS (TYPE B - RIGHT) 151
FIGURE 7.37 EVOLUTION OF THE RH LEVEL IN ADHESIVELY JOINED TITANIUM AND PEEK CAPSULES (WITH AND WITHOUT ALD COATING) 151
FIGURE 7.38 PEEK CAPSULE ELECTROPLATED WITH COPPER 153
FIGURE 7.39 DEPOSITION OF TITANIA THIN FILMS BY SOL-GEL DIP COATING PREPARATION 154
FIGURE 7.40 RH LEVEL IN TIO_2 COATED PEEK CAPSULES 155
FIGURE 7.41 MICROSCOPE VIEW OF THE TITANIA COATING FOR SAMPLE (3) (SCALE IN MM) 155
FIGURE 7.42 RH LEVEL IN CERAMIC COATED PEEK CAPSULES 156
FIGURE 7.43 MASS GAIN OF CERAMIC COATING IN WATER 157

Nomenclature

Symbol	Description	Unit
A	surface area	cm^2
A_C	External surface area of cylinder	cm^2
ADRES	value of the A/D conversion stored in the register	8 bit number
c	water concentration	$g.cm^{-3}$
C	capacitance	F
c_a	moisture concentration outside the package	$g.cm^{-3}$
C_D	capacitance of desiccant	cm^3
C_P	capacitance of a porous material	cm^3
C_V	capacitance of a cavity	cm^3
D	diffusion coefficient	$cm^2.s^{-1}$
d	thickness of the wall	cm
d_{CM}	thickness of the solid	cm
E	amplitude of the magnetic field	fraction of the original
F	rate of transport of the substance	$g.s^{-1}$
f	frequency	Hz
F_{RC}	flow rate through coating	$g.day^{-1}$
h	thickness of sample	m
K	permeation constant: combination of D and S	$cm^2.s^{-1}$
L	inductance of coil	H
L_x	'true' or 'standard' leak rate of gas x	$cm^3.s^{-1}$
μ	electrical permeability	$H.m^{-1}$
M	molecular mass	$g.mol^{-1}$
m	mass	g
m*	mass of dry desiccant	g
m_{lim}	maximum amount of water allowed in the package	g
m_{limD}	limit of moisture a desiccant can adsorb	g
$m_{POLYMER}$	mass of polymer	g
M_S	water saturation level of polymer	g
M_t	water absorption by polymer	g
n	amount of substance	moles
P	pressure of the gas under consideration	Pa
P_x	number of atm. of gas x in the package	atm
Q	Partial pressure of water inside the package cavity at time t	atm or Pa
Q_{ini}	partial pressure of water inside the package cavity at time t=0	atm or Pa
Qin_p	quantity of gas entering the package in time t	atm
R	measured leak rate: quantity of gas permeating through a solid	$atm.cm^3.s^{-1}$
R	universal gas constant	$J.mol^{-1}.K^{-1}$
RH_a	relative humidity outside of the package	%
RH_i	relative humidity at t=0	%
RH_t	relative humidity at time t	%
R_P	resistance of a porous material to the flow of water vapour	$s.cm^{-3}$
S	solubility of gas in the polymer	dimensionless(cm^3/ cm^3

		at 1 atm)
S_D	'solubility' of gas in the desiccant	dimensionless(cm^3/ cm^3 at 1 atm)
T	temperature	^oC or K
T_d	lifetime of desiccant	hours or days
t_{LC}	lifetime of coated capsule	days
t_{LDC}	lifetime of coated capsule with desiccant	days
V	volume of the cavity in the package	m^3 or cm^3
V_C	Internal cavity volume of cylinder	cm^3
V_D	volume occupied by the desiccant in the cavity in the package	cm^3
V_{DD}	supply voltage	V
$V_{polymer}$	volume of polymer	cm^3
V_{SO}	voltage fed to the microcontroller	V
$V_{WATERvapour}$	volume of water vapour	cm^3
z	depth of the conductor	μm
δ	skin depth	μm
ΔP	difference in partial pressure between outside and inside the package	atm or Pa
ΔP_{ATM}	partial pressure difference of the gas under consideration between inside and outside the solid	atm
Δ_{Pi}	initial partial pressure difference between outside and inside the package	atm
Δ_{Pt}	partial pressure difference between outside and inside the package at time t	atm
$\varrho_{POLYMER}$	density of polymer	$g.cm^{-3}$
σ	electrical conductivity	$\Omega^{-1}.m^{-1}$
τ	time constant of exponential relaxation process	s
τ_e	experimental time constant associated with PEEK package	s

Chapter 1 Introductory summary

High-reliability electronic implants such as pacemakers have 'hermetic' enclosures with the electronic components in dry gas. This type of package, generally made of titanium alloy, or alumina, guarantees a very long lifetime but is stiff, which may not be an advantage for implants; also these materials and methods used to seal them can be expensive. For applications which only require a more limited lifetime (less than two years), it may be possible to use a polymeric material instead. For reference, Table 1-1 provides example applications depending on their lifetime.

Lifetime	Application/examples
2 days – a few weeks	Prototyping – animal testing (9 days in (Lexell et al. 1992)
2 months – 3 years	Animal models – clinical trials (Borton et al. 2013; Wang et al. 2012) Instrumented orthopaedic implants (e.g. 9 months in (Faroug et al. 2011)) Veterinary/ patient monitoring – neuromuscular stimulators (e.g. gastric stimulator for obesity which may only need to be used until the patient has learned to adapt the food intake - http://www.ulb.ac.be/rech/inventaire/projets/5/PR4375.html)
3 – 5 years	Pacemaker (Forde 2006) - ICD (Duffin 2006) : for these two applications, the whole device must be swapped after 3-5 years because of the battery, monitoring devices
5 – 20 years	Neurostimulators (Dai Jiang et al. 2011) - Artificial vision prosthesis (Weiland et al. 2005)
20+ years	Cochlear implants (McDermott 1989) – Neurostimulators (Loeb 2001; Nonclercq et al. 2010) : these devices are recharged by induction

Table 1-1 Electronic implant applications and their lifetimes

Polyetheretherketone (PEEK) is a polymer that is used in orthopaedic implants because of its favourable mechanical properties and its biocompatibility. It can be easily machined or injection-moulded, making it an attractive material for implant manufacturers. Novel designs made from PEEK based on established material properties may be used in some applications and provide a cheaper alternative to established materials, making them more widely available. One significant advantage of a polymer over a metal for housing electrically isolated instrumentation is that power can be induced, and telemetry can be achieved, without eddy current loss. PEEK, like all polymers, absorbs water. This work investigates the lifetimes which are achievable using PEEK packages for electronic implants, including means to extend this lifetime.

Chapter 2 provides an introduction to PEEK and its main properties. It lists existing joining technologies applicable to this type of thermoplastic polymer, which could also be used for the packaging seal. The subject of water permeation through polymers is also introduced, and the main calculation methods for water diffusion are reviewed from

literature. Although an in vivo environment contains many elements which can interact with an implanted material, this study does not focus on biocompatibility (which is already proved for PEEK) and is concerned only with water permeation. This is explained in more details in Chapter 2.

In Chapter 3, the main objectives of this work are presented in more detail, and the subject of water diffusion is analysed further. The two main calculation methods introduced in chapter 2 are compared. An original method which builds upon one of them is proposed. The validity of this model is assessed experimentally. It proves to provides a good approximation of moisture ingress into polymer packages which are made of different materials or have complex geometries (Dahan et al. 2012).

In order to evaluate the evolution of water permeation experimentally, an inductive telemetry system is used to measure wirelessly the humidity inside sealed immersed PEEK packages. The methods and experimental set up used are outlined in Chapter 4, which provides a detailed description of the humidity sensing circuit design and the telemetry system.

In Chapter 5, a literature review of adhesive bonding theory is included before the first experimental results. This chapter deals primarily with the lifetime of unmodified adhesively sealed PEEK packages. Different types of adhesives and their effectiveness are tested, and the influence of water diffusion through the seal vs. the package body is investigated. The effect of wall thickness on the lifetime is also assessed, using the calculation method we have presented.

Ameliorative or preventative measures can be used against moisture ingress. Chapter 6 starts with a presentation of the theory of desiccants, following which the calculation method presented in Chapter 3 is further developed to include the case where desiccant is used. Different types of desiccants are compared, and their effect on the lifetime of the packages is assessed experimentally (Dahan et al. 2013). This work validates the calculation method, which is then used to predict the impact of varying amounts of desiccant on the lifetime of different types of packages, and provide a guideline of achievable lifetimes.

Chapter 7 looks into thin film coatings as a way to reduce the rate of moisture ingress. Physical Vapour (PVD) and Chemical Vapour (CVD) Deposition techniques are first reviewed, before a range of methods and thin film materials are tested experimentally. Different types of evaporation and sputtering PVD techniques are used for metallisation, while plasma enhanced CVD is used to deposit other types of materials. Other coating techniques are also investigated, including Atomic Layer Deposition, which proves to be the most effective. The thesis concludes with Chapter 8 which summarises and discusses the findings of this study in order to answer our research question. Finally, topics for future research are highlighted.

Chapter 2 PEEK, hermeticity, and moisture ingress – an introduction

2.1 Introduction

PEEK is already widely used as a biomaterial, but this study's goal is to establish whether it can be used for implants incorporating electronics and sensors, by getting a useful lifetime for this type of package, and exploring ways to prolong this lifetime.

2.2 PEEK as a material, properties

It is interesting to first have a look at the properties of PEEK.

2.2.1 Chemical structure and properties

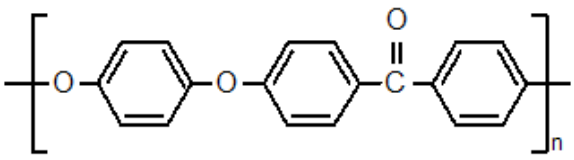

PEEK or Polyetheretherketone is a polyaromatic semi-crystalline thermoplastic polymer of basic formula (-C_6H_4-O-C_6H_4-O-C_6H_4-CO-).

Figure 2.1 Molecular structure of PEEK

Typically, crystallinity ranges from 25-35%. Its melting temperature is ~340°C and its glass transition temperature is ~145°C. It can be readily melted by extrusion and injection moulding with conventional methods. Its chemical structure makes it stable at temperatures exceeding 300°C and resistant to chemical and radiation damage (Tavakoli et al. 2004; Ha, Kirch, et al. 1997) . After polymerization, PEEK is inert and apart from 98% sulphuric acid, it is not soluble in conventional solvents at room temperature (Kurtz & Devine 2007) .

2.2.2 Barrier properties

PEEK membranes exhibit good resistance to the permeation of gases such as oxygen and helium (permeability coefficients respectively $1.57x10^3$ and 76 $cm^3.m^{-2}.day^{-1}$) and low water vapour permeation (3.9 $g.m^{-2}.day^{-1}$). PEEK can also be metallised or coated with other materials in order to further reduce permeability, as will be investigated during this thesis. [Data for permeability coefficients provided by Invibio Ltd. for a film thickness of 100μm, 37°C, 1 bar pressure and 90% RH]

2.2.3 Joining technology

PEEK can be welded with various methods (fusion, laser, ultrasonic) and adhesively joined, either to itself or to metallic substrates such as titanium alloy and Co-Cr alloy,

which are both implantable. This can be done effectively using adhesives such as silicones, epoxies and acrylics (Tavakoli et al. 2004).

2.2.4 Mechanical properties

PEEK is compatible with many reinforcing agents, including glass and carbon fibres, and then has a specific strength (strength/material density) higher than some metals such as steel (Kurtz & Devine 2007). As a composite material, it is available with a wide range of mechanical properties which can be tailored to the application. For instance, the tensile strength of unfilled polyetheretherketone is ~100 MPa but this can be extended to 2000 MPa as a composite. Similarly, unfilled PEEK has a Young's modulus of about 4 GPa but can be reinforced to match cortical bone (18 GPa) or titanium alloy (110 GPa) by varying the size and orientation of fibres in the composite (Kurtz & Devine 2007) . Matching bone modulus can be important in order to minimize stress shielding (Tavakoli et al. 2004). In the context of this PhD, this is a very interesting property to design implants in a field such as orthopaedics. Another interesting feature in this framework is that carbon fibre reinforced (CFR) PEEK composites' mechanical properties are hardly affected by exposure to high temperature saline environments.

2.2.5 Surface activation and coating of PEEK

As a biocompatible material, PEEK has been increasingly used as a biomaterial for implants since the 1980s, in fields such as orthopaedic, trauma and spinal implants (Kurtz & Devine 2007). In order to improve implant fixation with bone, researchers have been investigating ways to make PEEK bioactive (i.e. with the capacity to interact with a living tissue or system; in this case, to improve the strength of the bone-implant interface), employing Hydroxyapatite (HA) to coat the polymer surface or as a composite filler and stimulate bone apposition for orthopaedic applications where a load is applied, e.g. non cemented hip stems (Ha, Kirch, et al. 1997; Ha, Eckert, et al. 1997).

Hydroxyapatite is a naturally occurring mineral form of calcium apatite which is part of the mineral phase of the extracellular matrix of bones. It can be synthetically produced and is considered to be osteoconductive (Ha, Kirch, et al. 1997) (osteoconduction is the passive process by which bone grows on a surface).

PEEK-HA composites have been tested and bioactivity was improved. However, problems regarding the mechanical affinity between HA and the PEEK matrix have been identified, resulting in reduced strength and toughness of the material (Kurtz & Devine 2007) . To avoid this problem and therefore extend the range of applications of PEEK for implants, coating with HA by precipitation or thermal plasma can be employed and it has been found to influence positively its bone-bonding properties (Kurtz & Devine 2007; Ha, Kirch, et al. 1997).

It is also possible to dual coat PEEK with titanium and HA. Titanium, as a well-proven biocompatible implant surface, is still present after HA has been absorbed in vivo, avoiding potential mild tissue reactions occurring around PEEK implants (Kurtz & Devine 2007; Ha, Eckert, et al. 1997). Vacuum Plasma Spray (VPS) is a suitable, highly reproducible and economically efficient process to realise this, granting good interlocking between all layers (Ha, Gisep, et al. 1997).

2.2.6 Benefits of PEEK

PEEK has many advantages which make it attractive as an implant material. As we have just seen, it has very good mechanical properties. Unfilled, it is one of the strongest polymers available, has a better strength to weight ratio than its metallic counterparts, as well as resistance to fatigue (Ramakrishna 2001). Its mechanical properties can also be tailored to the application by reinforcing it with carbon fibres. Furthermore, PEEK is inert, biocompatible, radiation/chemical resistant, and has a low heat conductivity. It can be injection moulded, 3D printed, and machined. Finally, as a polymer, it has high resistivity, low permeability, and does not attenuate RF electromagnetic fields, which makes it useful for implant applications which require telemetry or power induction.

2.3 Encapsulation and hermetic packages

Looking at electronic implants, it is important that electronic components are protected from humidity and from liquid water coming from the surrounding body fluids. This permeation can occur through the material itself, through the seals, and feedthroughs depending on the nature of the enclosure.

2.3.1 Encapsulation

To protect the electronic function of the implants, electronics can be either encapsulated, or placed in a hermetic package. The functions of these are quite different, as explained in (Donaldson 1992) :

"The encapsulant is not intended to be a barrier to moisture but, by adhering to the device surfaces and filling the spaces between conductors, it prevents water from condensing, which would permit ionic conduction and thus, perhaps after some time, failure (by leakage currents, gas evolution, corrosion, etc)."

Encapsulation in waxes, epoxy resins or silicone rubbers can provide protection lasting more than ten years (Donaldson & Sayer 1981a; Donaldson 1988; Sinnadurai 1996). However, any failure of adhesion between the encapsulant and the components can create a void where water vapour can condense, with the consequences mentioned in the quoted paragraph above (Donaldson & Sayer 1981a). Rules are given in order to avoid such failure by optimizing component shape as well as the choice of encapsulant, insulator, and conductor (Donaldson & Sayer 1981a; Donaldson & Sayer 1981b). Plastic

encapsulation using junction coatings can also provide very high protection of semi conductor devices (Sinnadurai 1996).

2.3.2 Hermetic packages

Although it is possible to protect integrated circuits by means of encapsulation, the efficiency of encapsulation is very often unknown because of the variety of ICs available as well as the constant evolution of IC technology. Moreover, manufacturers do not test their ICs at 100% RH and under bias. It is therefore prudent to use hermetic packages which act as moisture barriers. Nevertheless, encapsulants must still be used to insulate the junction of the cables to the leadouts (Donaldson 1992). The best way to achieve long term protection is with hermetic packages made of glass, ceramic or metal (Schneider 1988), although these are expensive and complicated solutions. This thesis will investigate the hermeticity of PEEK packages in order to assess their longevity, as this would provide a cheaper and easily manufactured type of hermetic enclosure for implants.

This type of package however is never 100% impermeable. Gases inside and outside can travel using cracks, capillaries, faults in the seal or through the material itself if it is permeable, as is the case for polymers such as PEEK. However, **the package will be considered sufficiently 'hermetic' if it prevents these gases (especially water vapour) reaching a potentially harmful level within its expected lifetime**.

2.3.3 The importance of sealing

In order to be effective, hermetic packages must be appropriately sealed. Poor seals can lead to damage of the electronics by condensation of water vapour, leading to corrosion, electromigration, or high current leakage (Traeger 2002). It has been shown that polymeric lid sealants, although processed at low temperature, inexpensive, and easy to rework, do not provide sufficient protection against water vapour permeation (Traeger 2002). Seals made of metals are therefore preferred and processed by welding or soldering in order to limit the electronics' exposure to high temperatures (Donaldson 1992). However, it is also possible to realise effective composite seals for ceramic packages (Donaldson 1988). Irrespective of the process, it is important to prevent moisture from penetrating the cavity during sealing. This can happen from the substrate, the inert gas filling, the polymer materials or the sealant itself (Schneider 1988).

"As the temperature drops below the dew point the enclosed vapour condenses creating a thin water film on one of the inner surfaces of the package. With the different contaminations from die surfaces, polymers, flux residuals, and so on, the initially harmless water vapour becomes an electrolyte which can give start to various chemical and electrochemical reactions." (Schneider 1988)

2.4 Joining technologies for thermoplastic polymers and the case of PEEK and implanted electronic devices

In order to study the application of PEEK to implanted electronic devices, we must identify a way to join PEEK to itself or other polymeric materials, as this will be required either to seal a PEEK package containing electronic components, or to join parts while forming a structurally strong bond. There are many methods available for joining thermoplastic polymers. The ideal technology for sealing a PEEK package would be simple, cheap and ensure that the electronics are protected from excessive heat and vibrations at all times without affecting the hermeticity. The joining methods for thermoplastics which will be discussed here can be divided into 3 main categories: mechanical fastening, fusion bonding, and adhesive bonding (Amanat, James, et al. 2010). Mechanical fastening uses means such as clipping, clamping, riveting or screwing in order to join two parts. However, this cannot be used for hermetic implanted packages, as hermeticity can by no means be guaranteed by any of these methods. We will then review the other two techniques.

2.4.1 Fusion bonding

In fusion bonding, the principle is to generate heat at the joint interface to bring the material to melt locally and ensure that parts form a strong bond, which can approach the bulk properties of the adherents (Stokes 1989; Grimm 1995). The different joining techniques can then be classified according to the method used for heat generation, as shown on Figure 2.2 below.

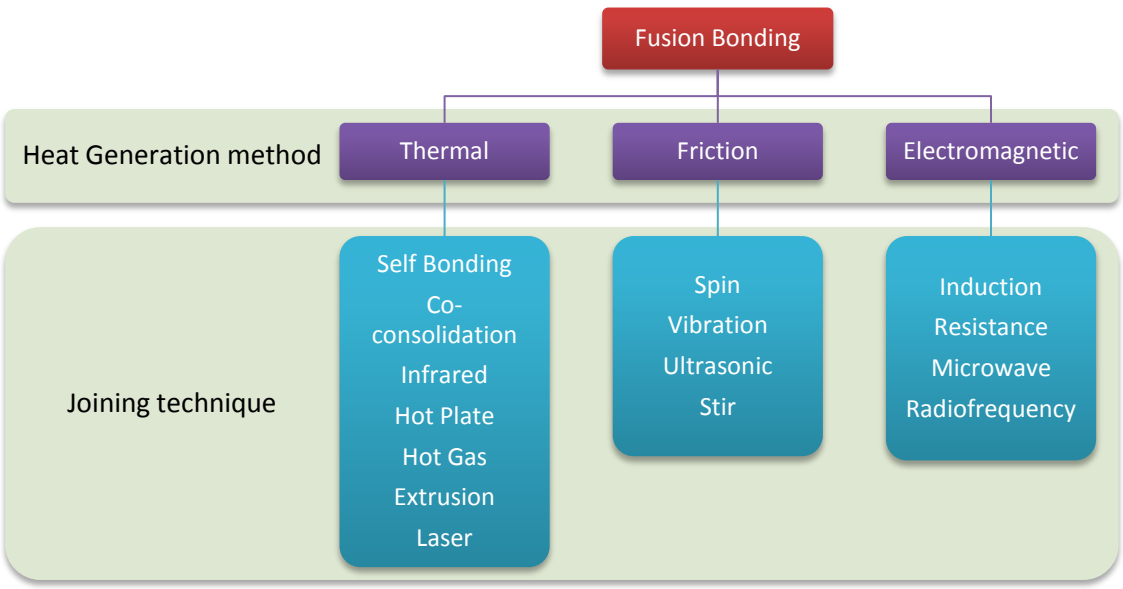

Figure 2.2 Classification of fusion bonding techniques for thermoplastics

2.4.1.1 Thermal bonding

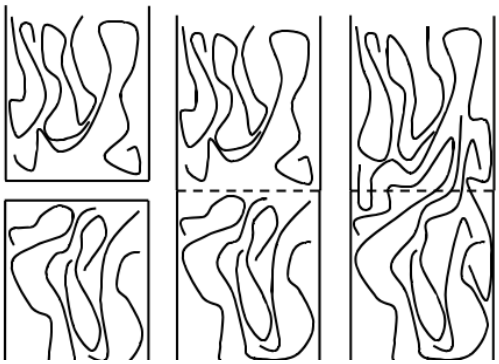

Figure 2.3 Healing of a polymer-polymer interface

Thermal bonding consists in heating the surfaces to be joined and applying pressure until the joint cools and consolidation occurs. Various techniques can be used to bring heat.

Autoclaving or compression moulding can be used for **co-consolidation,** where the entire part is brought to melt temperature (340°C in the case of PEEK). This, however, requires expensive processes and complex tooling to ensure that pressure is maintained on the entire part to prevent de-consolidation (Ageorges et al. 2001).

In **self bonding** the whole part is also heated up, but without reaching the melting point. Pressure is applied to promote chain interdiffusion. Above the glass transition temperature (143°C), a 'healing' process takes place at the interface through 5 steps (Kim & Wool 1983), and its mechanical strength develops: surface rearrangement, surface approach, wetting, diffusion and randomisation.

However, the presence of potentially heat sensitive internal components in the case of this study forbids the use of both previously described techniques, where the amount of heat to provide would damage the electronics. We then look at techniques where the application of heat is more localised.

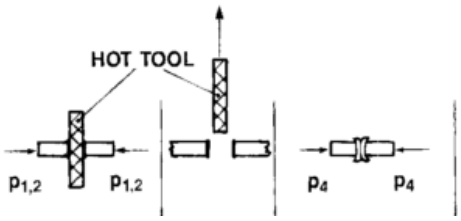

Figure 2.4 Hot plate welding

Hot plate welding for instance is a 2 stage process in which both surfaces are put in contact with a hot surface which brings them to melting temperature, before being pressed together and allowed to cool down. Besides the relatively long weld times, the two main disadvantages of this technique are the severe deformation occurring with higher temperatures, as well as the melt residue adhering to the hot plate surface (Amanat, James, et al. 2010), particularly for high melting temperature polymers such as PEEK.

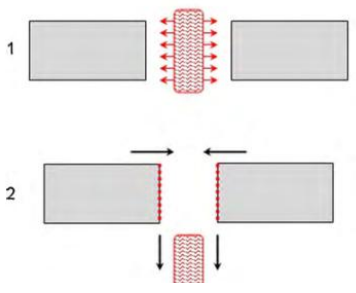

Figure 2.5 Infrared welding

Infrared welding is very similar to the previous process, with the added advantage that the infrared source of heat is not in contact with the surfaces to bond. However, in most cases this technique will require pigmentation of the substrates, and there is a risk of cooling down between the two phases of the process

which could decrease the bond strength.

Hot gas and **Extrusion welding** are manual methods which both use a stream of hot gas to heat the surfaces to be joined. The difference lies in the fact that the former technique uses a thermoplastic filler rod between the two adjoining surfaces, whereas molten polymer is extruded into the joint with the latter.

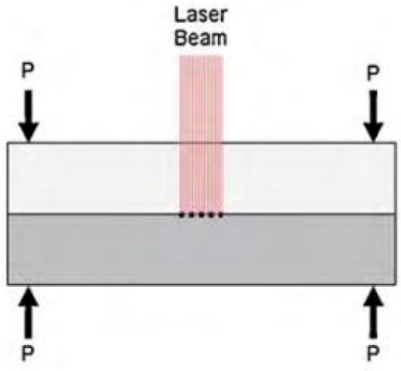

Figure 2.6 Transmission Laser Welding (TLW)

In the context of implanted electronic devices, none of these methods can be used as the excessive heat produced would damage the electronics. There is however one thermal bonding technique which could be used, as the heat affected zone (HAZ) is extremely localized, guaranteeing the protection of the electronic components: **laser welding**.

In **Transmission Laser Welding (TLW)**, a near infrared laser beam goes through a laser transparent top part and onto a laser absorbing bottom layer. This could be either a carbon black pigmented part or a non absorbing part with a coating which absorbs laser energy in the laser wavelength range, e.g. Clearweld (Amanat, Chaminade, et al. 2010). When absorption occurs on the bottom part, it causes melting of the polymer at the bond interface. Upon cooling, the interface solidifies and creates a fused seal.

This technique offers the advantage of a highly localised HAZ (more so than any other technique). However, its main limitation (besides the high cost) is the thickness of polymer which can be bonded. In the case of PEEK, the crystallinity scatters the laser light, and as a result of this loss of energy this technique is not suitable for parts thicker than 1.0 mm. Ideally, the parts to be bonded should not exceed 0.5 mm thickness.

Direct Laser Welding provides a way to bond slightly thicker parts of up to 3 mm by introducing a clever design for the joint (cf. Figure 2.7 below) where the laser beam irradiates the joint directly, and the joint is designed to collapse during welding (Warwick & Green 2008). Nevertheless, even though the parts to be bonded can have thicker walls, the actual layer of PEEK which is melted is still limited to 1 mm, and therefore this method is not necessarily a great improvement in terms of hermeticity.

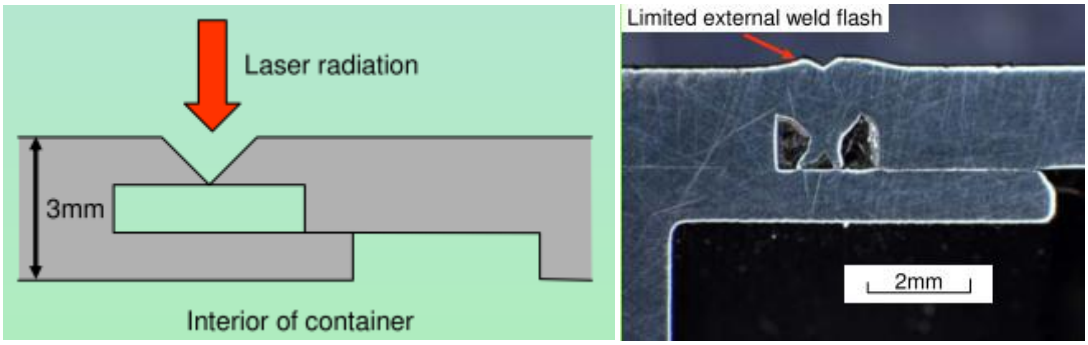

Figure 2.7 Direct Laser welding, joint design

To summarise, most thermal bonding techniques are not suitable for PEEK in the context of implanted electronic devices, as the heat produced would damage the electronics contained within the enclosure. Laser welding could be a suitable alternative in this respect, but the limitations linked to the thickness of parts to be bonded would be a problem in terms of hermeticity of a package. However, if there was a way to make the external or internal surface of the package less permeable, with the use of a suitable coating for instance, then laser welding could prove appropriate for this type of applications.

2.4.1.2 Friction welding

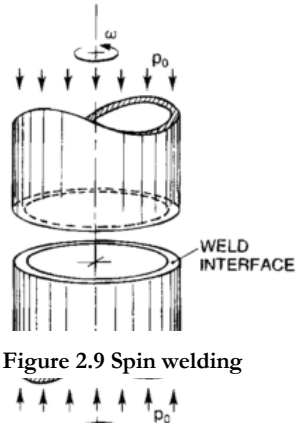

Figure 2.9 Spin welding

In friction welding, heat is generated by rubbing the two surfaces to be bonded together under an applied pressure (see Figure 2.8). As with other thermal bonding techniques, the joint then consolidates and fuses upon cooling down, while the parts are still held under pressure.

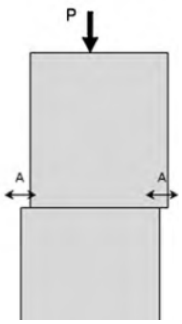

Figure 2.8 Friction welding

When components have symmetrical and circular cross sections for instance, **spin welding** can be used (see Figure 2.9). The parts to be bonded are pressed together and rubbed while in rotation relative to each other, with one fixed part and one spinning. The friction heat melts the polymer at the interface, and the molten film solidifies under pressure when the motion stops, creating a weld.

For large parts with flat mating surfaces, a very similar technique is used: **vibration welding**. The principle is exactly the same as for spin welding, except that instead of spinning one of the parts, it is vibrated parallel to the weld line at a certain frequency and amplitude.

Stir welding consists in using the head pin of a metallic rotating tool to stir and mix the polymer at the joint interface (Amanat, James, et al. 2010). This method results in an exit hole when the tool is removed, which would induce stress concentrations and hermeticity loss, even when filled.

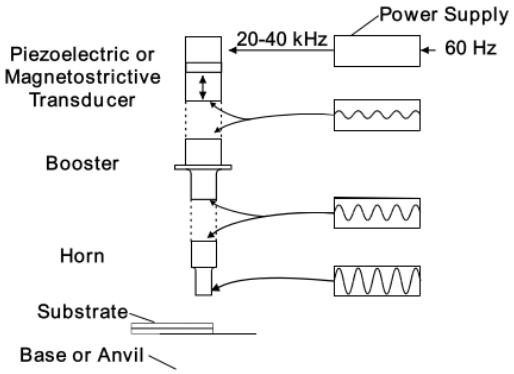

Figure 2.10 Ultrasoinc welding

Finally, **ultrasonic welding** allows the melting of the interface by transmitting ultrasonic vibrations through the material. By a combination of surface and intermolecular friction (Stokes 1989), melting occurs at 'energy directors', which are irregularities at the interface. It is necessary to design the part to incorporate these energy directors, as not enough friction would occur with flat parallel surfaces.

The main drawback associated with friction welding techniques is the amount of vibrations generated, which may be incompatible with the presence of electronics in the package/implant.

2.4.1.3 Electromagnetic welding

Induction welding consists in producing a field by a coil in order to induce heating in a conductive material implanted in the plastic at the seal interface. An obvious limitation to this technique is its use when electronic components are included, especially if telemetry with a coil is already in use.

Similarly, in **microwave welding**, a layer of electromagnetic absorbent material is placed at the interface and is heated using microwave power. The surrounding polymer then melts and a seal can be formed. This technique has the same limitations as induction welding and cannot be used for implanted electronic devices.

Radiofrequency welding is used for polymers with polar groups in their structure, and melts the polymer at the interface with an intense electromagnetic field, applied by pressing electrodes on the sides of the parts to be joined. However, it only works with thin films and sheets and is not compatible with high melting temperature polymers such as PEEK, which does not have polar groups anyway.

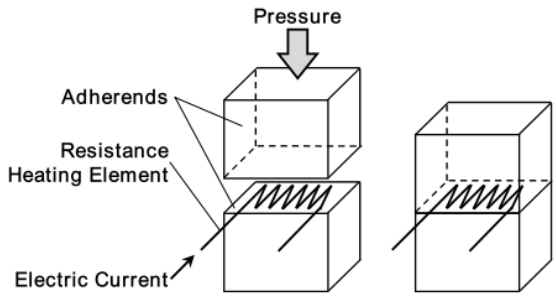

Figure 2.11 Resistance welding

The only type of electromagnetic welding which could potentially be used with PEEK in this study is **resistance welding**, where an electrically resistant material is trapped between the two parts to be joined and heated by the passage of an electrical current. This causes the surrounding polymer to melt and weld upon subsequent cooling. The use of this technique for PEEK packages containing

electronics depends on the proximity of these components with the heated wire, as well as how localised the application of heat is. Other limiting factors include a potential increase in permeability due to the presence of this wire, or a weak structure at the joint. Moreover, this technique is mostly applied for composites, where a layer of conductive mesh is trapped at the interface, in order to provide uniform temperature. There is no guarantee that this would work with a single wire on a smaller surface, e.g. seal of PEEK capsule.

2.4.2 Adhesive bonding

Adhesive bonding can potentially join any two materials. It can be achieved either with a two component system which are mixed before use or with a single component bonding agent. The main drawbacks associated with this technique are the high permeability and the structural weakness of some adhesives. However, it is a cheap and simple technique which could be suitable to seal PEEK packages containing electronics if the required lifetime is limited. This lifetime is currently unknown and should be investigated in order to assess whether adhesive bonding is an appropriate process.

2.5 Flow of gas in and out of sealed packages

Having reviewed the properties of PEEK, as well as ways to seal a package made with this material, we now look at how moisture can permeate implant packages.

2.5.1 Viscous, molecular and diffusive flow

The flow of gases can be of three kinds, depending on the mean free path (mfp) of the gas under consideration (i.e. the average distance travelled by a molecule before it collides with another one). The flow will be viscous (or Poiseuille flow) if the collisions between molecules dominate (as opposed to collisions with the walls of the enclosure) and there is a difference in total pressure across the interface. This occurs for pressures larger than 10^{-3} atm. When the pressure is less than 10^{-5} atm., collisions with the walls dominate, and the flow is described as molecular (or Knudsen flow). In between, when both types of collisions are common, the flow is said to be diffusive (or transitional) (Greenhouse 2000; Davy 1975) .

2.5.2 Origin

Water inside a package can have three origins, besides the potential presence of water in the sealing chamber when the package was sealed.

a) It can leak into the package from the outside environment through various faults in the material or sealing.
b) Outgassing can take place from the package walls or from components or materials inside it, the extent of which depends on the kind of material, their

preparation as well as the preseal treatment. '*Most of the outgassing occurs during burn-in or high temperature operation'* (Greenhouse 2000) .

c) There is a possibility for the gaseous hydrogen and oxygen inside the enclosure to combine directly into water. However, this reaction has a very slow rate so that no significant amount of water could be produced in years, although '*a suitable catalyst could cause the reaction to take place'* (Greenhouse 2000) .

2.5.3 Consequences

Water inside a package can lead to dendritic growth between interconnects of opposite polarities (Meyer 2007), ionic conduction, leakage currents, short circuits and various chemical and electrochemical reactions (Kornilov & Barinova 1996; Donaldson 1992) such as corrosion, often enhanced by electrical current in the circuit (Sedlak & Donaldson 1993). Provided that the pH is not between 4.5 and 7.5, positive and negative ion corrosion (respectively acidic and basic) can occur (Greenhouse 2000). Two examples of corrosive chemical reactions are:

$$3Al + 3Cl^- + 6H_20 = AlCl_3 + 2Al(OH)_3 + 3H_2 + 3e^-$$

$$3Al + Na^+ + 7H_20 = Al(OH)_3 + NaOH + 3H_2 + 3e^-$$

Eventually, these various reactions will lead to failure of the electronic components. Failure will occur according to how fast these reactions occur and, although the presence of water is necessary for them to happen in the first place, trying to correlate moisture with failure rates can be inconclusive if the contaminant levels are not controlled as well (Greenhouse 2000) .

2.5.4 Failure criteria

There is no consensus on what the failure criterion should be (Vanhoestenberghe & Donaldson 2011). For instance, one criterion would be to use 99% RH. Condensation theoretically occurs at 100% RH, so any level below this should be acceptable. However it has been demonstrated in the literature that condensation could be promoted below that level due to impurities around which nucleation can occur. The presence of salts for instance can promote condensation at an earlier stage (Tencer 1994). At the opposite extreme, using that principle, some very conservative approaches are taken for long term hermetic packages, using criteria such as 10% RH, 5000 ppm, or 3 monolayers of water. The latter is the amount of liquid water theoretically necessary to promote corrosion. Nevertheless, this limit represents only the amount of liquid water condensed, and does not account for saturation of the air before condensation. Similarly, the 5000 ppm limit corresponds to the dew point of water vapour just below the freezing mark (-2°C). At that temperature, ice would form before any water could condense. It is also equivalent to 3 monolayers of water.

These limits have been defined for long term devices which are meant to last many decades in a wide range of environments and temperatures (often for military applications). For implant applications however, temperature is more or less constant around 37°C. Therefore a dew point (or condensation) temperature of -2°C would never occur, and such conservative limits do not apply. Using the same reasoning as the 5000 ppm criterion, temperature is not expected to drop below 35°C for an implant, and using this as a dew point temperature corresponds to a limit well in excess of 50,000 ppm, more than ten times the value of the 'military' criterion.

It must also be noted that this study attempts to understand and predict the ingress of water vapour through PEEK, and therefore focuses on water vapour only. It has been proved that a saline environment only has a very limited effect on the mechanical properties of PEEK (Kurtz & Devine 2007). Exposure to saline is not expected to modify the solubility or diffusion coefficients of the adhesive either (Chin et al. 1999). Moreover, the saturated vapour pressure of water vapour in equilibrium with salt water is slightly less than above water; therefore the gradient of pressure which is driving moisture ingress is also less. Silicone rubber has been proved to act as a semi permeable membrane which lets water vapour through, but through which most metal compounds do not diffuse at a significant rate (Donaldson et al. 2012). As a porous polymer, PEEK is expected to exhibit the same type of behaviour, although we have not measured the rate at which other molecules will go through. (Dahan et al. 2013)

2.5.5 Helium leak tests

For a 'traditional' package, made of metal or ceramic, the material of the package itself is often considered to be completely impermeable to water. However, practically, defects in the form of very fine leak channels can exist, whether in the material or the seal, meaning that gases can travel between the inside and outside. As mentioned previously, the package will be considered hermetic if it prevents gases (especially water vapour) from reaching a potentially harmful level within its expected lifetime. The most common method for studying fine leaks consists in detecting helium leaks using a mass spectrometer. To that end, the package is filled with helium using one of these two methods:

- **Bombing:** the package under test is placed in a high pressure helium chamber for a set time, hence forcing helium into it, before being transferred rapidly to the mass spectrometer chamber for detection.
- **Backfilling:** the package is sealed in a helium chamber at known pressure and tested quickly afterwards.

2.5.6 Formulas for the flow of gases and leak rates

Through a leak channel, the measured leak rate is

$$R = F\sqrt{\frac{T}{M}}(P_1 - P_2) \tag{2.5}$$

where M is the molecular mass of the gas considered, T is the temperature and F is the conductance of the leak channel. This formula is valid for molecular flow. For viscous or combined flow, other equations are available (Greenhouse 2000) (Davy 1975).

A difference must be acknowledged between the measured leak rate R and the 'standard' or 'true' leak rate L produced by a reference pressure of 1 atm, which is used in equations to determine the quantity of gas leaking in or out of a package.

$$L_x = \frac{R_x}{P_x} \tag{2.6}$$

where P_x is the number of atm. of gas x in the package.

Leak rates are different for different gases through the same leak channel because of the gases' different density and molecular size. However a simple relationship exists to derive the true leak rate of a gas if the true leak rate of another gas is known. This is easily found by combining Equations (2.5) and (2.6):

$$L_1 = L_2\sqrt{\frac{Molecular\ mass\ of\ gas\ 1}{Molecular\ mass\ of\ gas\ 2}} \tag{2.7}$$

The quantity of gas entering the package in time t is

$$Qin_p = \Delta p_i.(1 - e^{-\frac{Lt}{V}}) \tag{2.8}$$

where Δp_i is the initial partial pressure difference, L is the true leak rate and V the internal volume of the package.

We can then easily derive the time it would take for a given amount to leak in or the leak rate.

$$t = -\frac{V}{L}\ln(1 - \frac{Qin_p}{\Delta p_i}) \tag{2.9}$$

$$L = -\frac{V}{t}\ln(1 - \frac{Qin_p}{\Delta p_i}) \tag{2.10}$$

And the total quantity of gas in a package is the quantity that has leaked in, plus the amount that was there initially, minus that which has leaked out. These equations apply to all gases independently.

2.5.7 The case of permeation through a solid

It is usual manufacturing practice to determine the permeation rate by means of helium detection using equation (2.7) (Meyer 2007) (Kornilov & Barinova 1996). Bubble and fine leak tests (after bombing or backfilling) are used and these two detection methods together can detect almost the whole range of leak rate (Tencer 1994) (Lin et al. 2007). In this case, $L_{H20} = 0.471\ L_{He}$.

However, in the case of permeable solids such as PEEK, moisture ingress does not only occur through leak channels, but also through the solid itself, as well as the seal in the case of adhesive bonding. The diffusion rate of a gas through this solid depends on many factors such as the porosity of the material and the gas molecule size and affinity with the material (Greenhouse 2000).

It is therefore not beneficial to predict the moisture ingress rate into a package made of a permeable material from a Helium leak detection test using Equation (2.7), although a correspondence could be found *a posteriori*, by treating permeation as a leak rate. This however would require finding the permeation rate through other means. In our case, humidity will be measured directly using humidity sensors, as detailed further in the next chapters.

2.6 Expected lifetime of a polymer package

If the enclosure material, such as PEEK, is permeable to the gas under scrutiny (i.e. water vapour), the passage through it is possible, via a two phase process (Greenhouse 2000) .

a) Adsorption of the gas on the surface of the solid.
b) Diffusion of the gas through the solid, due to leak channels in the solid, an internal porous structure, and the chemical affinity of the gas for the solid.

It is essential to review how to evaluate the lifetime of a polymer enclosure before trying to obtain it experimentally.

2.6.1 Full transient model – Analogy with heat conduction problem

The process of moisture diffusion through polymers follows Fick's diffusion laws (Crank 1975). The first law relates the diffusive flux and the gradient of concentration. It states that moisture goes from the region of high concentration to the region of low concentration. The rate of transport is then

$$F = -D\,\frac{\partial c}{\partial x} \tag{2.11}$$

where F is the amount of water c transported through a unit cross section (per unit of time). c can be expressed as a density of water vapour, or as an absolute pressure. D is

the diffusion constant for a given temperature T. Fick's second law describes the concentration of the gas in the polymer at a particular position and time.

$$\frac{\partial c}{\partial t} = D\frac{\partial^2 c}{\partial^2 x} \tag{2.12}$$

The case of diffusion into a container with a finite volume is analogous to the heat conduction problem of a slab in contact with a perfect conductor or a well stirred fluid, for which a solution was given by Carslaw and Jaeger (Carslaw & Jaeger 1959) and adapted to the diffusion problem (Paul & DiBenedetto 1965) to give an expression of c. If the temperature T is constant, c is also directly equivalent to the relative humidity, which is the ratio of the absolute pressure of water vapour c over the saturation vapour pressure (as it is constant for a given T). The solution is given by (2.13).

$$RH_t = RH_i + (RH_a - RH_i)\left[1 - \sum_k \frac{2(\beta_k^2 + \eta^2)\sin\beta_k}{\beta_k(\beta_k^2 + \eta^2 + \eta)} e^{-\frac{-\beta_k^2 Dt}{d^2}}\right] \tag{2.13}$$

where η=dAS/V and the β_k are the roots of the following equation

$$\beta \tan\beta = \eta \tag{2.14}$$

and RH_i = relative humidity in % at t=0
RH_t = relative humidity in % at time t
RH_a = relative humidity in % outside of the package
D = diffusion constant in $cm^2.s^{-1}$
V = volume of the cavity in the package in cm^3
d = thickness of the wall in cm
A = surface area in cm^2
S = solubility coefficient (dimensionless)

There is no general analytical solution for the equation above. We must therefore solve this equation numerically for our specific case in order to get values to feed into Equation (2.13). It is not necessary to go beyond the tenth term of the sum, as the terms in the exponential become vanishingly small, and therefore so does the contribution of the subsequent terms of the sum.

2.6.2 Tencer's approximation

Tencer developed a simpler model (Tencer 1994) to calculate the moisture ingress in the cavity. The solution he finds is a typical exponential relaxation process:

$$RH_t = RH_i + (RH_a - RH_i)\left[1 - e^{-\frac{t}{\tau}}\right] \tag{2.15}$$

with the time constant defined as

$$\tau = \frac{Vd}{KA} + \frac{d^2}{2D} = \frac{2DVd + KAd^2}{2KAD} \tag{2.16}$$

where K=S.D is the permeation constant for the package in $cm^2.s^{-1}$. The two terms in the time constant represent the two physical phenomena taken into consideration in the process:

The first term corresponds to the diffusion through a non absorbing membrane, which in the full transient model corresponds to the case of a very large volume V. We then have $\eta=0$ and $\beta_k=k\pi$ and it can be proven that the situation reduces to the flow through a membrane (Paul & DiBenedetto 1965) and that the process will be described by Equation (2.15) with the time constant reduced to

$$\tau = \frac{Vd}{KA} \tag{2.17}$$

The second term of Tencer's time constant is related to the diffusion of water inside the body of the polymer, which corresponds to the other extreme, i.e. when $V \rightarrow 0$. In this case, $\eta = \infty$ and $\beta_k=(k+1/2)\pi$, the problem reduces to the case of diffusion into a slab (Tencer 1994), and Equation (2.13) reduces to the following (for convenience of calculation we assume there is no water in the package at t=0):

$$RH_t = RH_a \left[1 - \frac{4}{\pi} \sum_{n=0}^{\infty} \frac{(-1)^n}{2n+1} e^{-\frac{-D(2n+1)^2\pi^2 t}{4L^2}} \right] \tag{2.18}$$

A 'time constant' can then be defined (even though this is a sum of exponentials) as the time after which water at the interface achieves 1-1/e of the ambient value, which means that

$$\frac{RH_t}{RH_a} = \left[1 - \frac{4}{\pi} \sum_{n=0}^{\infty} \frac{(-1)^n}{2n+1} e^{-\frac{-D(2n+1)^2\pi^2 t}{4L^2}} \right] = 1 - e^{-1} \tag{2.19}$$

Solving this equation gives $Dt/d^2=0.505$ (Tencer 1994). Therefore the time constant can be estimated as:

$$\tau = \frac{d^2}{2D} \tag{2.20}$$

The time to reach any humidity level can therefore be calculated by solving Equation (2.15) for time:

$$t = -\frac{(2DVd + KAd^2)ln\left(1 - \frac{RH_t - RH_i}{RH_a - RH_i}\right)}{KA2D} \quad (2.21)$$

2.7 Difference between the solubility (S), diffusion (D) and permeation (K) constants

Polymers can absorb significant amounts of water. PEEK for instance has a water absorption at saturation corresponding to 0.5% of its mass (fractional mass gain). S is called the solubility and corresponds to the amount of water per unit of volume which can be absorbed and stored into the porous wall. S is dimensionless, but often expressed in cm^3/cm^3 at a pressure of 1 atm (it is then equivalent to a Henry's law constant (Yasuda 1975) – see Equation (2.23)). The solubility for metals is zero, and ranges from 0.001 for the least absorbent glasses and ceramics, to 400 for the most absorbing polymers (Greenhouse 2000). It can be calculated using the water absorption (fractional mass gain) of the material.

$$S = \frac{V_{WATER}}{V_{POLYMER}} = \frac{\rho_{POLYMER} \times \substack{fractional \\ mass\ gain} \times \substack{molar \\ volume\ at\ T}}{\substack{molar \\ weight}} \quad (2.22)$$

where the molar volume is 22.4 $l.mol^{-1}$ at 0^0C and converted for T using the ideal gas equation (Yasuda 1975; Burnett et al. 1996).

The permeation constant K is different from the diffusion constant D; as well as the diffusion of water through the solid, it takes into consideration the adsorption of water on the surface of the material and subsequent storage in the bulk material.

$$K = S.D \quad (2.23)$$

2.8 Conclusion

In this chapter, we have reviewed the main characteristics and properties of PEEK, the difference between encapsulation and hermetic packages, joining technologies for thermoplastic polymers which can be used to seal a package, as well as the theory behind water permeation through leak channels and polymer walls. After covering this background, the next chapter will focus on comparing existing calculation methods for water permeation through polymers and developing our own.

Chapter 3 Moisture ingress in an adhesively joined polymer packages - theoretical considerations and a novel calculation method

3.1 Objectives and failure mechanisms

The aim of this project is to develop the science of Smart Implanted Devices using the Polyetheretherketone (PEEK) polymer, which has attractive properties for many types of implants, with potential applications in orthopaedics, neuroprosthetics, veterinary and patient monitoring. The useful lifetime for an implantable package made of PEEK which contains electronic components must first be defined. We will then define the objectives, as well as the various modes of failure, in order to clearly identify the parameters which influence the lifetime.

3.1.1 Useful lifetime and objectives

The first task is to define what a useful lifetime is. In the context of this project, it can be defined as the time that the implant can sustain the function exerted by the electronics before the risk of failure appears. This function may be the primary purpose of the implant, but not necessarily. For example, it would be the main function for a nerve stimulation device, but not for a tibial nail with a force sensor. For the latter, the primary purpose of the implant is to replace the bone, whereas the function of the electronics is to monitor the strains in bone. The implant will still fulfil its main purpose of replacing the bone/promoting healing, etc. even if the electronics fails. Therefore, for that type of applications the useful lifetime corresponds to the definition given previously.

For the tibial nail for instance, a useful lifetime for the electronics could be of about 9 months. For some clinical applications however, the implant function can be needed for as little as one or two weeks (e.g. animal experiment). In this case a cheaper form of packaging would be highly beneficial. There is therefore a wide range of lifetimes for which a PEEK package can potentially be used. On the other hand, the more we can extend this lifetime, the more types of application we can reach.

The objectives of this project can then be summarised as follows:

- Design of a package of similar size as traditional implants
- Monitor humidity level inside the package
- Establish lifetime
- Identify the parameters which affect the lifetime and their influence
- How can the lifetime be maximised in order to broaden the range of potential applications?

3.1.2 Failure mechanisms and criterion

As we have seen previously, the criterion for failure corresponds to the risk of malfunction of the electronics due to the presence of water, and different standards are used throughout the literature (see 2.5.4 Failure criteria). Working with a polymer package for relatively short lifetimes, a reasonable level to work with is 60-65 %RH. This does not mean that failure will occur at these levels, but keeping the water vapour below this will not jeopardise the safety of the electronics sealed inside the package. For simplicity purposes, we can then assimilate lifetime and time constant, as the latter corresponds to the time to reach 63.2% RH (exponential decay $1-e^{-t/\tau}$, with τ the time constant; when $t = \tau$, the relative humidity is $1-e^{-1}=0.632$ of its initial value).

The sequence of events during failure is as follows: diffusion of water vapour, condensation, corrosion. After that, corrosion products may start diffusing out. By fixing a limit situated before the condensation stage, the lifetime considered here also takes into account this risk of diffusion of toxic elements. Furthermore, it is expected that even after corrosion, '*likely corrosion products permeate through [..] at a low rate and seem unlikely to cause toxic effects'* (Donaldson et al. 2012).'

Although this limit is just as 'arbitrary' as the others, it offers the advantage of being flexible. By defining the time constant every time, one does not have to agree to the RH limit we define, but can use it to calculate water diffusion at whichever level they feel comfortable. For this reason, all the data will also be presented in graphs showing the evolution of the relative humidity with time.

Figure 3.1 shows the schematic of a generic hermetic enclosure for an active implantable device (Amanat, James, et al. 2010) as well as the three ways moisture can penetrate inside the package and compromise the electronics.

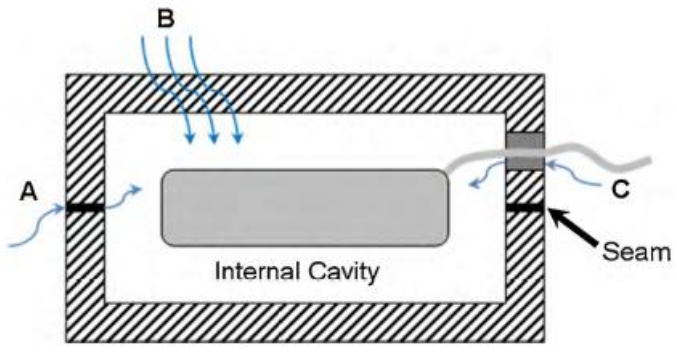

Figure 3.1 Moisture ingress into enclosure

Moisture ingress can occur through:

A. The seal, especially if we want to assess the viability of adhesive bonding
B. The body of the capsule

C. The feedthrough when it exists. In order to eliminate this possibility, power and data can sometimes be transmitted by means of telemetry.

If telemetry is used, we are therefore left with moisture penetrating through the seal and the body of the capsules, and we can focus on these two parameters.

3.1.3 Description of the package

A package has been designed in which the relative humidity will be monitored in order to get a useful lifetime for this type of enclosure. Before the experiment, we can try to evaluate what this lifetime would be by means of calculation.

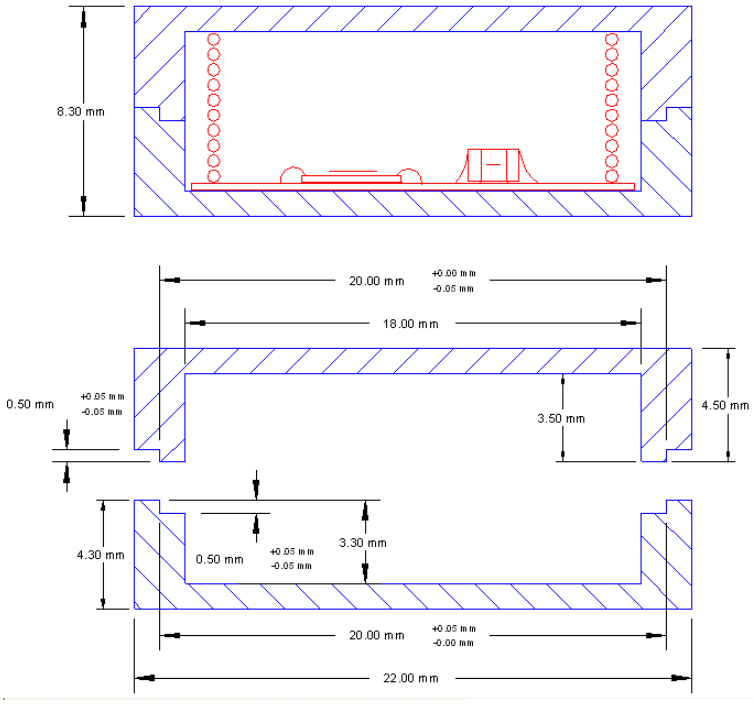

Figure 3.2 Description of the PEEK capsule

The PEEK package is a cylindrical capsule of outer diameter $Ø_{out}$=22.0 mm and height h_{out}=8.3 mm. The inside diameter is $Ø_{in}$=18.0 mm and the height inside is h_{in}=6.3 mm. The wall thickness is 1 mm on the top and the bottom of the capsule. This area represents 5.09 cm^2. The thickness is 2 mm on the side of the cylinder. This area is 3.56 cm^2. The total surface area is S_A=8.65 cm^2 and the internal volume is V_{in}=1.603 cm^3.

3.2 Is the Tencer approximation a good representation of the full transient model?

The previous chapter has presented two methods to evaluate water diffusion. We can now look at both models to assess whether they are in good agreement with each other. The full transient model is presumably more accurate, but is difficult to evaluate, whereas the Tencer approximation is supposedly less accurate but allows easy calculation of the lifetime. The question is therefore: how good is the approximation?

3.2.1 Transient model

First of all, it is important to note that there is no general analytical solution for Equation (2.13), representing the transient model (Paul & DiBenedetto 1965). We must therefore solve this equation numerically for our specific case in order to get values to feed into Equation (2.13). It is not necessary to go beyond the tenth term of the sum, as the terms in the exponential becomes vanishingly small, and therefore so does the contribution of the subsequent terms of the sum.

For our comparison, if we take the case of the PEEK capsule, we consider the case of permeation through the top and bottom side of the capsule only. These sides have the same thickness of 0.1 cm, as opposed to the lateral sides which are twice as thick. Much less permeation would occur through these anyway, as all diffusion equations are functions of the square value of the thickness. The result is plotted on Figure 3.3.

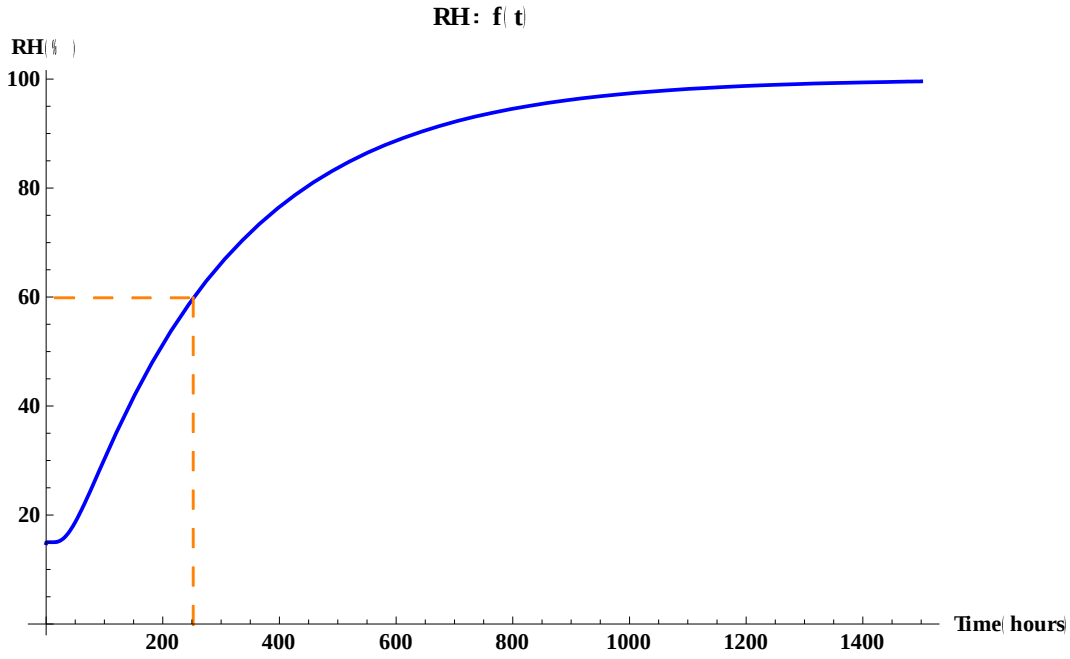

Figure 3.3 Water permeation through a 1mm thick wall – transient model

We can observe three phases on this plot. In the first hours, the humidity level in the cavity does not rise, as moisture has to penetrate the thickness of polymer. There is then a quasi linear diffusion, which gradually slows down as the partial pressure difference diminishes. The expected time to reach 60% RH is around 250 hours, which is equivalent to 10.4 days.

3.2.2 Tencer's approximation

Tencer's approximation, on the other hand considers a single exponential relaxation process (see Equation (2.15)) with the following time constant (see Equation (2.16)):

$$\tau = \frac{Vd}{KA} + \frac{d^2}{2D}$$

Where the two terms in the time constant represent the two physical phenomenon taken into consideration in the process:

The first term corresponds to the diffusion through a non absorbing membrane, which in the full transient model corresponds to the case of a very large volume V. This solution is plotted on Figure 3.4, corresponding to equations (2.15) and (2.17) as repeated below.

$$RH_t = RH_i + (RH_a - RH_i)\left[1 - e^{-\frac{t}{\tau}}\right] \text{ where } \tau = \frac{Vd}{KA}.$$

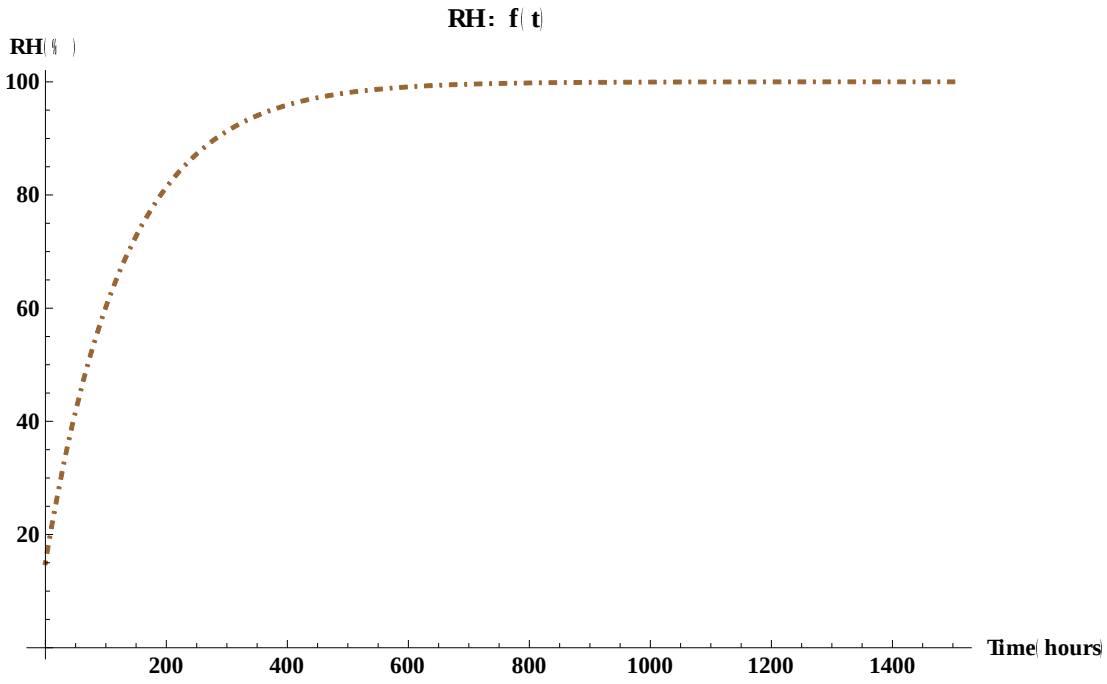

Figure 3.4 Diffusion – case of a very large volume

The second term of Tencer's time constant is related to the diffusion of water inside the body of the polymer, which corresponds to the other extreme, i.e. when V→0. The result is plotted on Figure 3.5, corresponding to equation (2.18) as repeated below.

$$RH_t = RH_a\left[1 - \frac{4}{\pi}\sum_{n=0}^{\infty}\frac{(-1)^n}{2n+1}e^{-\frac{-D(2n+1)^2\pi^2 t}{4L^2}}\right]$$

In terms of profile, this looks very similar to the full transient model.

Finally, Tencer's approximation is plotted with both contributions on Figure 3.6. It gives a time to reach 60% RH of 10.1 days.

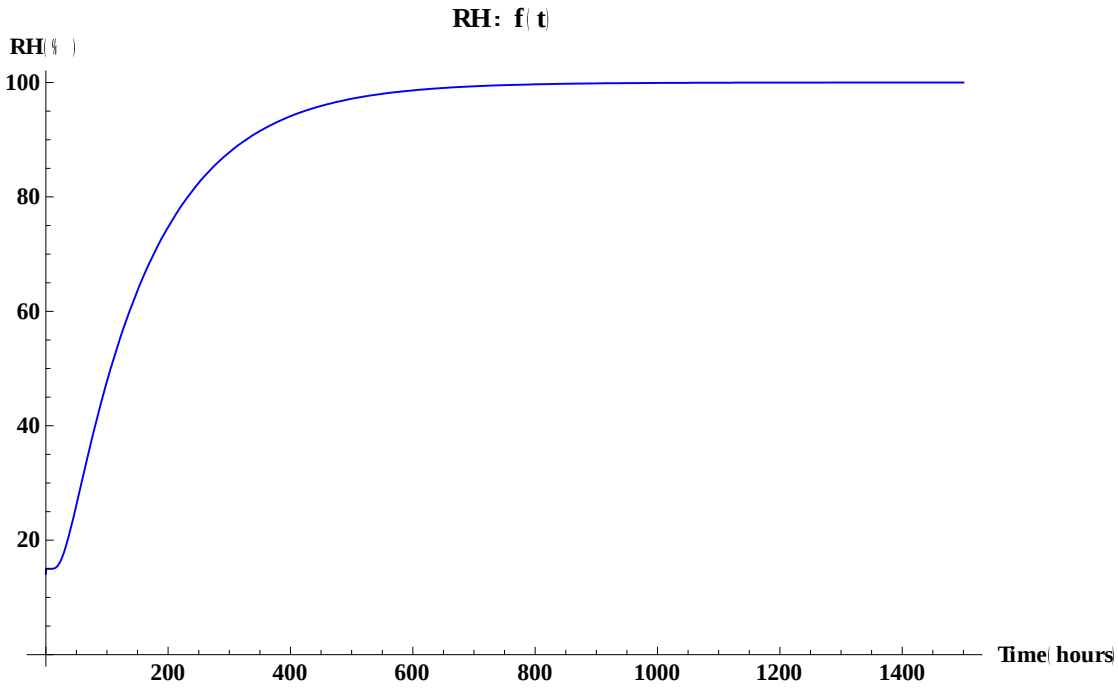

Figure 3.5 Diffusion – Case of a very small volume

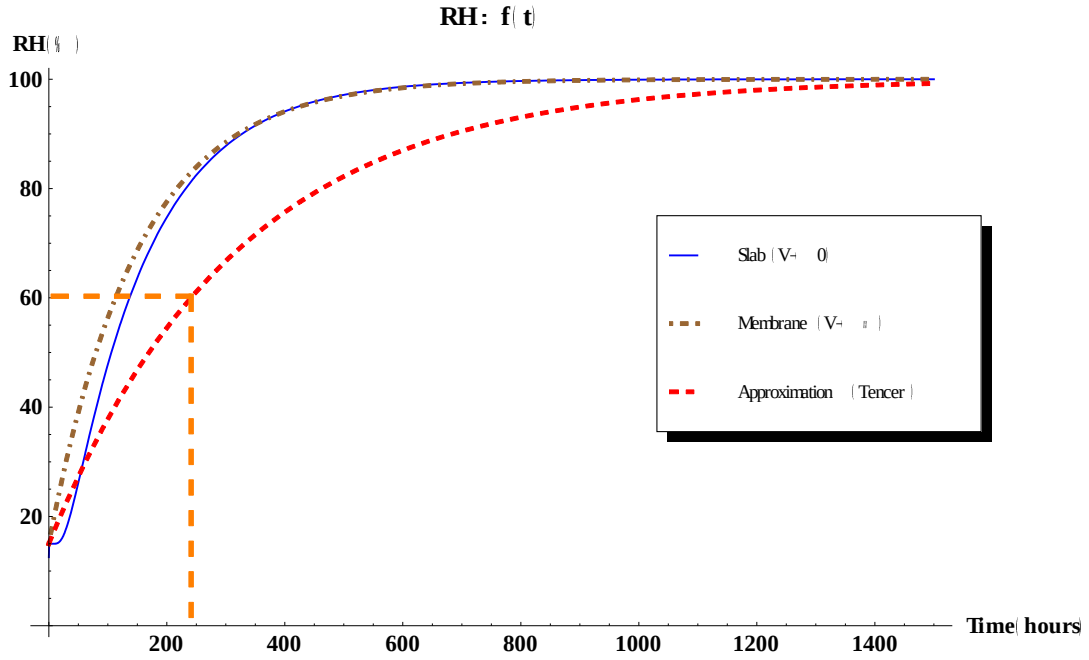

Figure 3.6 Tencer model and its components

3.2.3 Comparison of the two models

The two models are presented on Figure 3.7. We can see that the Tencer model provides a very good approximation of the full transient model (analytical solution, see Equation (2.13)) when predicting the lifetime (respectively 10.4 and 10.1 days), which is the value

we are interested in. However, the single exponential equation does not represent very well the humidity/time profile, especially in the beginning.

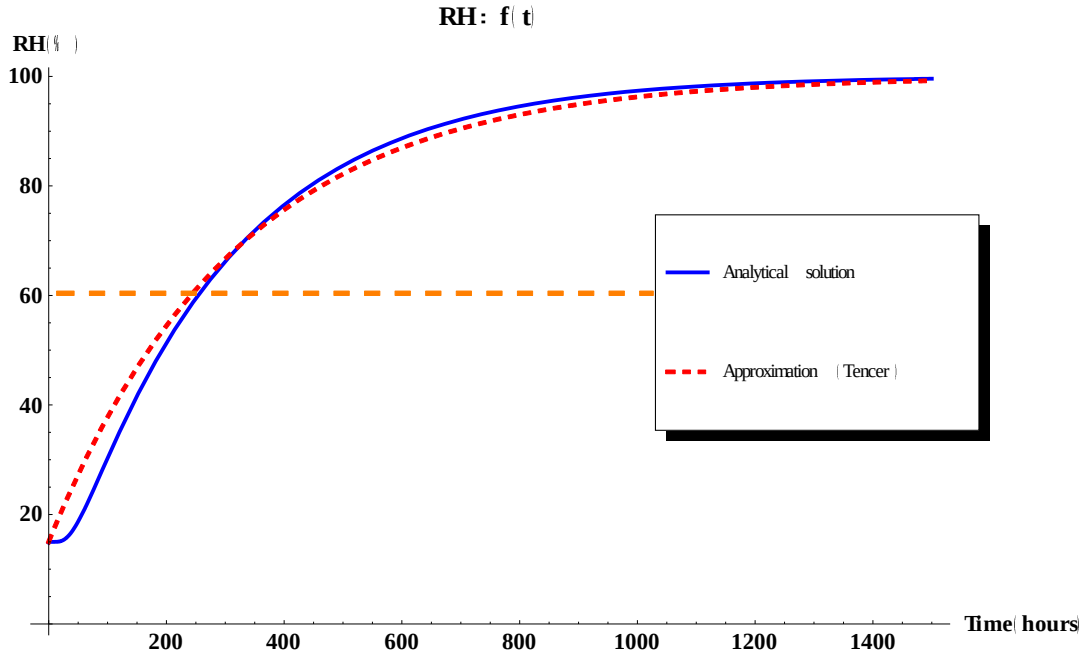

Figure 3.7 Comparison between the 'QSS' model (dashed line) and the full transient solution

3.3 A new calculation method for polymer packages with walls of varying thickness/properties.

NB. This section is mainly extracted from (Dahan et al. 2012)*: which was published during the course of this study:*

Dahan, N., Vanhoestenberghe, A. & Donaldson, N., 2012. Moisture Ingress into Packages With Walls of Varying Thickness and/or Properties: A Simple Calculation Method. IEEE Transactions on Components, Packaging and Manufacturing Technology, 2(11), pp.1796–1801.

The Tencer model is a good approximation of the full transient solution, which is convenient and simple to use. Nevertheless, like the full solution, it can only be used if the package has a single 'porous' wall or, alternatively, if all the walls are made of the same material and have the same thickness. If this is not the case, how do you use Tencer's formula, and how are the contributions of the different walls added up? In this section, the model will be adapted to this specific case. Using an electrical analogy, the various components making up the time constant will be identified, and simple calculations allowing to consider walls of different thicknesses or materials will be described.

3.3.1 Electrical analogy, making sense of the time constant

To sum up the contributions from different walls, it is important to understand how to identify the terms making up Tencer's time constant, given by equation (2.16). An electrical analogy is proposed as drawn on Figure 3.8, where the voltage H is equivalent to the external relative humidity (RH_a), the current i represents the rate of diffusion of water molecules (these molecules represent the charge Q), and the resistance R_P is analogous to the resistance of the porous wall to the flow of water vapour. Finally, the capacitances C_V and C_P are equivalent to the ability to store water molecules by the volume of the cavity and the porous wall respectively. When both capacitors are charged, they reach the same potential H. We are then interested in characterising the evolution of H_C (i.e. the humidity in the cavity of the package) over time. As will be discussed later in this chapter, this model is not meant to be the most physically accurate, but the one that best fits Tencer's (see 3.3.4 and 6.5.3 for more detailed discussions).

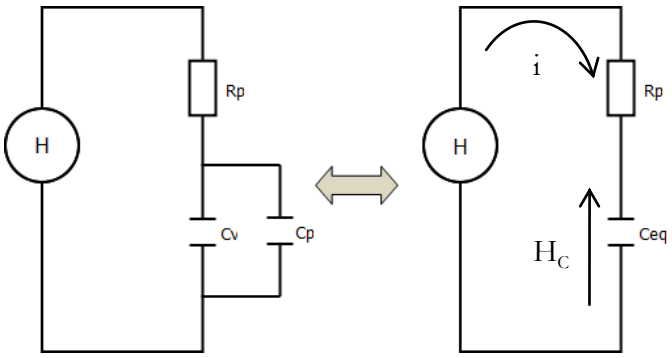

Figure 3.8 Moisture ingress through a porous wall into an enclosure, electrical analogy

As shown on Figure 3.8, $C_{eq} = C_P + C_V$. Let H_C be the voltage across C_V. Using Kirchhoff's voltage law:

$$H = iR_P + H_c \tag{3.1}$$

By differentiation, this expression becomes:

$$\frac{dH}{dt} = 0 = R_P \frac{di}{dt} + \frac{dH_C}{dt} \tag{3.2}$$

Since

$$i = C_{eq} \frac{dH_C}{dt} \tag{3.3}$$

We obtain the first order differential equation:

$$\frac{di}{dt} + \frac{1}{R_p C_{eq}} i = 0 \tag{3.4}$$

At t=0, $i = (H - H_{CO})/R_P$, with H_{C0} the amount of moisture already present in the package when it is sealed. The solution is given by:

$$H_C = H - (H - H_{co})e^{\frac{-t}{\tau}} \tag{3.5}$$

with the time constant $$\tau = R_P C_{eq} = R_P C_V + R_P C_P \tag{3.6}$$

This is exactly equivalent to the exponential relaxation process described by Tencer in equation (2.15), and we can identify the expressions (3.6) and (2.16) in order to obtain the correct form of R_P, C_V and C_P. We already know by definition that C_V corresponds to the volume V of the cavity.

$$C_V = V \tag{3.7}$$

From the first term of the time constant in (2.16), we obtain:

$$R_P = \frac{d}{KA} \tag{3.8}$$

And from the second term, C_P can be identified:

$$C_P = \frac{ASd}{2} \tag{3.9}$$

3.3.2 Calculation method for package made with walls of different properties

The example of a cylindrical package which is adhesively sealed is taken (as presented in section 3.1.3). The electrical analogy previously described then becomes as shown on Figure 3.9.

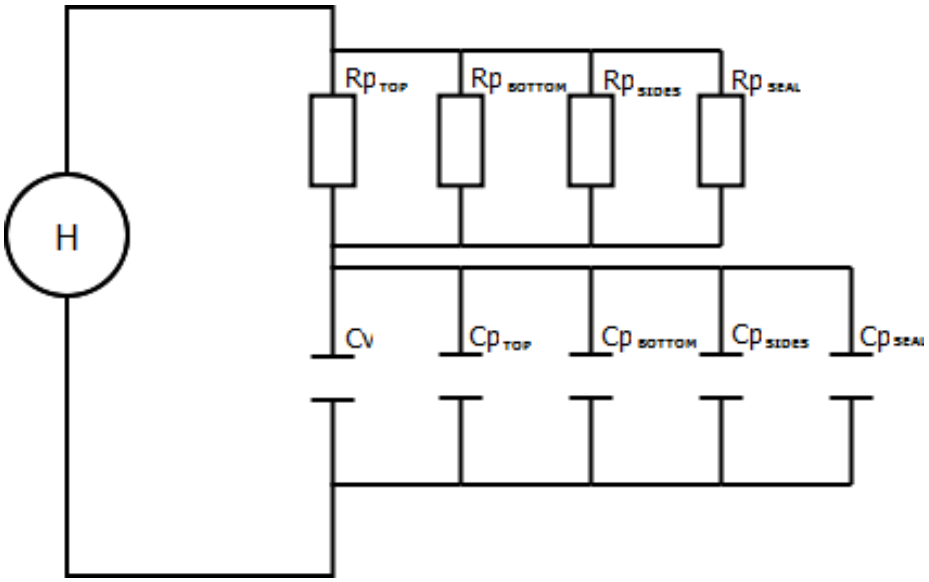

Figure 3.9 Moisture ingress into an enclosure with walls of varying properties, electrical analogy

Each wall has a capacitive and a resistive component. There are three R_P elements corresponding to the resistance to the flow of moisture offered respectively by the top and bottom, side polymer walls, as well as the seal, which may be made of a different material. The walls themselves can have different thicknesses. Similarly, there are three capacitive elements corresponding to the ability of these walls and seal to store a small amount of water, as well as one for the volume of the cavity.

The resistances are arranged in parallel, hence the total resistance of the package decreases as resistive elements are added, and so does the time constant. The capacitors are also arranged in parallel, with the opposite effect. As all elements can store water, increasing their number will increase the total capacity of the package, as well as the value of the time constant associated with it.

Regardless of the number of elements, it is then always possible to reduce the system to a simple equivalent as shown on

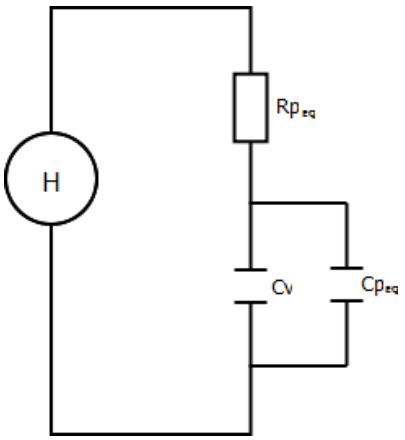

Figure 3.10 Equivalent system

C_V remains unchanged and equal to the volume V of the cavity, and we have:

$$R_{P\,eq} = 1/\sum_i \frac{1}{R_{P_i}} \tag{3.10}$$

and

$$C_{P\,eq} = \sum_i C_{P\,i} \tag{3.11}$$

The calculation method is therefore as follows.

(1) For each element (wall, seal, etc.), calculate the R_P and C_P components using equations (3.8) and (3.9).
(2) Find the equivalent R_P and C_P for the package using equations (3.10) and (3.11).
(3) Calculate the time constant of the system with equation (3.6)
(4) Calculate the RH level in the cavity at any time t using equation (2.15).

3.3.3 Experimental results

In order to test the applicability of this calculation model, the implant size package described in section 3.1.3 is fitted with a humidity sensor (see Chapter 4 for the detailed method), and the experimental time constant is compared with the calculated one.

Package Element	Top +Bottom	Sides	Seal
Material	PEEK OPTIMA	PEEK OPTIMA	Cyanoacrylate (Loctite 4061)
Thickness d (cm)	0.10	0.20	0.23
Surface area A (cm^2)	5.09	3.56	0.03
Solubility S (cm^3/cm^3)	9.17	9.17	32.4
Diffusion D ($cm^2.s^{-1}$)	[a]$8.20x10^{-9}$	[a] $8.20x10^{-9}$	[b]$1.08x10^{-8}$
Permeation K ($cm^2.s^{-1}$)	$7.52x10^{-8}$	$7.52x10^{-8}$	$3.50x10^{-7}$
C_V (cm^3)	----------1.60----------		
C_P (cm^3)	2.33	3.27	0.13
R_P ($s.cm^{-3}$)	$2.62x10^5$	$7.47x10^5$	$1.9x10^7$

Values for the solubility coefficients were calculated using the water absorption and the density of the material (Greenhouse 2000). Values for the diffusion coefficients were taken from the literature for similar materials ([a](Grayson & Wolf 1987) and [b](Braden 1964)) but are not specific to the materials we used, as those values were not available.

Table 3-1 Calculations

The value of the time constant for this enclosure is calculated using the method outlined in the previous section. The values for the various other parameters are calculated and presented in Table 3-1. Looking at these values, it is interesting to notice the predicted contributions of the various package elements (top & bottom, sides, seal). Figure 3.11 shows these contributions to the total 'conductance' ($1/R_p$ – how well it lets water through) and 'capacitance' (C_p and C_v – how much water can be stored) of the package respectively. In terms of conductance, the top and bottom parts are the most 'conductive' by far (73% of the total conductance). This is because they are only 1mm thick, compared to the sides which are twice as thick. As for the capacitance, the sides, which are thicker, are expectedly the most absorbing element. In both cases, the contribution of the seal is expected to be negligible (1 and 2% respectively).

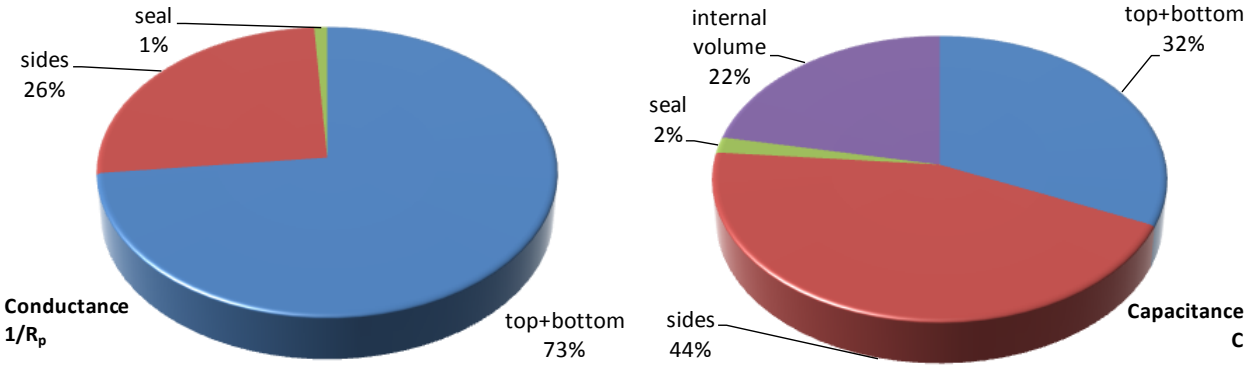

Figure 3.11 Conductance (left) and capacitance (right) of package elements

The calculated time constant is $\tau = 15.9$ *days*. This can be compared with the experimental time constant of 16.3 days (see '5.2.2 Preliminary experiment' for detail), which matches the calculated one with an accuracy of $\frac{\tau - \tau_e}{\tau} = 2.4\%$. This difference may be due to the accuracy of the sensor (see Figure 3.12), as well as the expected discrepancy between the diffusion coefficients used in calculations and the actual coefficients for PEEK and the adhesive used (Loctite 4061). Similarly, we also get an excellent approximation when using a capsule of uniform thickness 2 mm. The calculated time constant (33.8 days) is almost equal to the experimental one (34 days) (0.5% error).

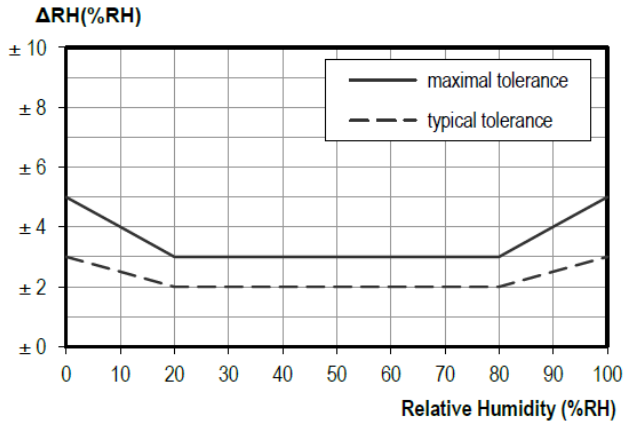

Figure 3.12 Humidity sensor accuracy

3.3.4 Discussion

Our model is based on the 'QSS' ('quasi steady state') model (Tencer 1994), which is itself an approximation of the full transient solution. This is illustrated by Figure 3.7 which plots the calculated evolution of the RH level in the capsule cavity if moisture ingress was exclusively occurring though the top and bottom walls of the package. We can see that the QSS model (dashed line – Equation (2.15)) provides a very good approximation of the full transient model (full line, (2.13) solved numerically) when predicting the time constant or the lifetime of the package.

However, the single exponential equation does not represent very well the humidity/time profile, especially in the beginning. Our model therefore has the same limitations and advantages.

It is important to realise that the proposed electrical analogy is not meant to be the most accurate possible description of the actual physical diffusion process, but a reasonable fit for the 'QSS model'. Indeed, the aim was to be able to identify the values of the capacitive and resistive elements with the time constant formula provided by Tencer. A consequence for instance is that instead of showing a slight initial delay in the increase of

RH in the cavity (corresponding to the time needed for moisture to go through the wall), the RH level rises immediately, as the 'capacitor' C_V starts charging immediately.

Our analogy will remain valid until condensation, as a step change in the capacitance of the cavity volume (C_V) is then likely to occur. Nevertheless this is acceptable when using this method to determine the lifetime of a package, as the criterion used is the risk of condensation appearing.

Finally, this model does not account for the moisture storage capacitance of the items enclosed in the package. This would simply be another capacitor element in parallel with the existing one, which capacitance value may or may not be negligible, depending on each case. However, this aspect may be difficult to evaluate, and neglecting it in any case makes the model more conservative, as any C element added would only prolong the lifetime of the package.

Nevertheless, this method allowed us to find a way to combine the capacitive and resistive elements associated with each type of porous wall. The experimental results in the previous section showed that our model is appropriate to predict the lifetime of packages made of porous walls when their thickness or material properties vary, and does so with an excellent accuracy.

3.4 Interpreting experimental results

3.4.1 Normalising the lifetime

When placing the sensing circuits within the capsules, it is unlikely that the external conditions will stay the same from one experiment to the other. However, as can be seen from the exponential relaxation equation (2.15), the lifetime will depend on RH_i, which corresponds to the initial level of moisture present when closing the capsule. In order to compare the results, we can therefore 'normalise' the lifetime by determining experimentally the time constant, which itself depends exclusively on the package characteristics (material, thickness, etc.) and not on the initial conditions. This time constant can then be fed back into the exponential relaxation equation, and the time needed to reach any humidity level can be calculated. For simplicity purposes, the experimental time constant can be used as a reference to compare the various experimental parameters.

3.4.2 Determining the experimental time constant

The experimental plot of the evolution of the RH level within the capsule versus time assumes an exponential shape. In order to extract the experimental time constant τ, a linearization of Equation (2.15) must be performed.

$$RH_t = RH_i + (RH_a - RH_i)\left[1 - e^{-\frac{t}{\tau}}\right]$$

This equation can be rearranged:

$$\frac{RH_a - RH_t}{RH_a - RH_i} = e^{-\frac{t}{\tau}} \tag{3.12}$$

And by taking the logarithm of this expression, the linearisation is obtained:

$$\ln(RH_a - RH_t) = -\frac{t}{\tau} + \ln\,(RH_a - RH_i) \tag{3.13}$$

Therefore, by plotting $\ln(RH_a\text{-}RH_t)$ as a function of time, a linear regression can be performed and the regression equation y=ax+b (with y the dependant variable and x the explanatory variable) obtained so that we can identify:

$$\tau = -\frac{1}{a} \tag{3.14}$$

The validity of the linearisation can be checked by looking at the R^2 coefficient. This is the square of the Pearson correlation coefficient, which measures the linear association between the two variables. The value of R^2 corresponds to the percentage of the variation in y which can be accounted for by its relationship with x. For instance, if R=0.9, it then means that 90% of the variation in y happens because of a variation in x, and 10% has to be accounted for by another reason. When convinced that this degree of association between the two variables is strong enough, the regression provides the best fit possible describing this relationship. The method used is that of ordinary least squares, where the squares of the residuals (real value of y – value of y expected if following the regression) are summed and the regression providing the smallest value for this sum is kept as the best fitting line.

3.5 Conclusion

This chapter started by defining what a useful lifetime is for our type of package. The Tencer 'QSS' model has been compared to the full transient solution of Fick's equations applied to the problem of diffusion. Furthermore, we have built an original, simple model based on Tencer's, which allows predicting accurately the lifetime of a polymer package with walls of varying thickness and properties. Finally, the method used to extract the time constant from an experimental plot has been presented. The next chapter will then present the rest of the experimental methods used in this study, including the design of a humidity sensing circuit.

Chapter 4 Measuring the humidity inside the capsule: method and set up

In this chapter, a telemetry system for measurement of the relative humidity inside a PEEK capsule is designed, using the method of passive signalling. The influence of a metal coating on the power/data transfer is also discussed, and it is recommended to limit the thickness of such a coating to a few microns in order to limit eddy current losses.

4.1 Telemetry using electromagnetic inductive coupling

As discussed in section 3.1.2, it is advantageous to use telemetry as it removes a source of water permeation into the package, also allowing a better differentiation and understanding of diffusion through walls and seal.

4.1.1 How does it work?

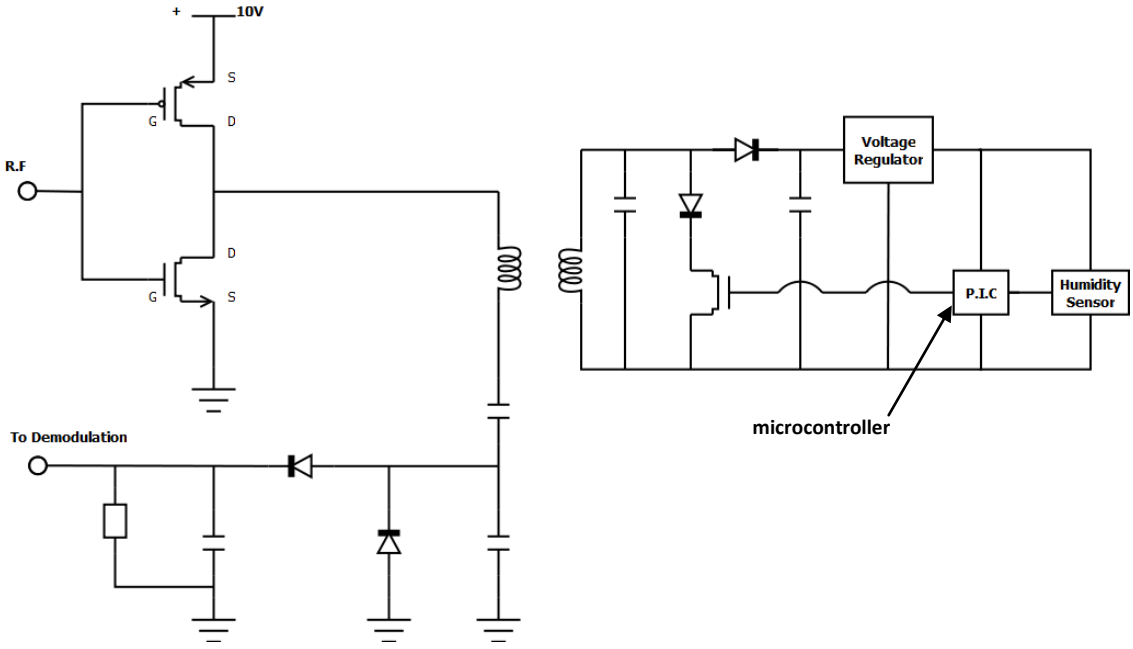

Figure 4.1 Circuit diagram of the telemetry system

In order to provide power and data to the electronic components enclosed in an implant, it is possible to use inductive coupling with the advantage of powering the implant externally from batteries housed within a small external package worn by the patient (Taylor et al. 1997). Signals can also pass in both directions through skin for telemetry purposes (Donaldson & Perkins 1983; Donaldson 1986). One coil pair is necessary, with each coil alternately used as a transmitter (of energy) and a receiver. This method of 'passive signalling' is achieved by modulating the impedance of the receiver (Donaldson 1986). This system has been successfully used for years, e.g. Telemetry of forces in

implants (Taylor et al. 1997; Taylor & Walker 2001; Lu et al. 1997), and will be used throughout this study.

The focus is on establishing useful lifetimes from enclosures made of PEEK. This can done by measuring the humidity levels inside capsules, using the telemetry system mentioned above (see Figure 4.1). The functioning of this passive signalling system will be described in more detail in this chapter (Donaldson & Perkins 1983; Donaldson 1986; Taylor 1996; Donaldson 1990) .

4.1.2 Description of the receiver side (implant) of the telemetry system

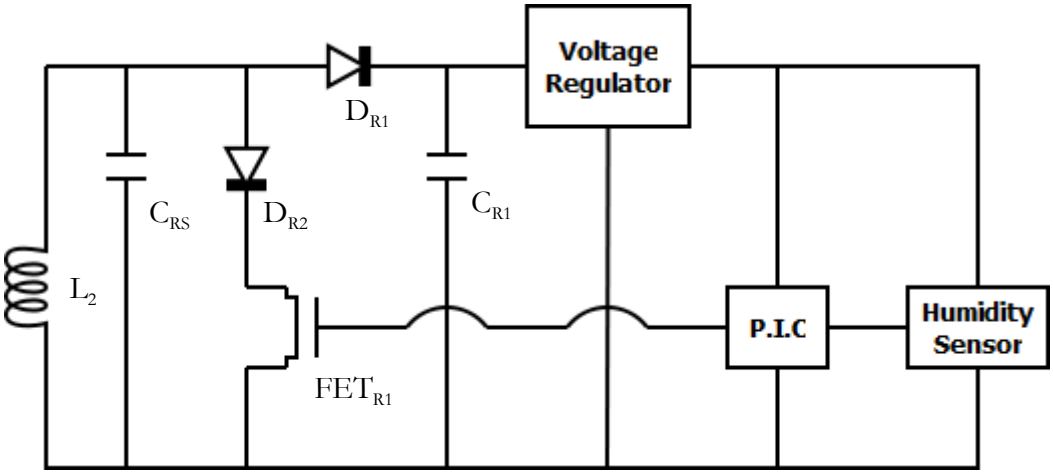

Figure 4.2 Circuit diagram of the receiver side

Power is transmitted to the capsule by an inductive link (see Figure 4.1). Figure 4.2 presents a schematic of the humidity sensing circuit placed in the PEEK package. An updated and completed design will be presented later in this thesis.

The coil L_2 is shunt-tuned with capacitor C_{RS}, which increases the output voltage of the coil and gives the shunt-tuned receiver a low output impedance (Donaldson 1990). Diode D_{R1} and capacitor C_{R1} form a peak rectifier with an output voltage slightly less than the peak voltage across L_2C_{RS}. As mentioned before, the impedance on this side is modulated by short-circuiting the coil through FET_{R1}.

The humidity sensor sends a signal via the PIC microcontroller with a certain period, to which corresponds a certain relative humidity level. This switches on the field effect transistor FET_{R1}, which short-circuits the receiver coil. As a result, this changes the coupled impedance seen by the transmitter. This mirrored change in impedance is detected by the transmitter and can be demodulated to extract the RH level. In practice, the power flow is broken by brief signal pulses, which can be modulated with the signal. The short-circuiting pulses are short, so power flow to the implant is not much affected, and the voltage on C_{R1} is maintained during the short-circuit pulses.

4.1.3 Description of the transmitter side of the telemetry system

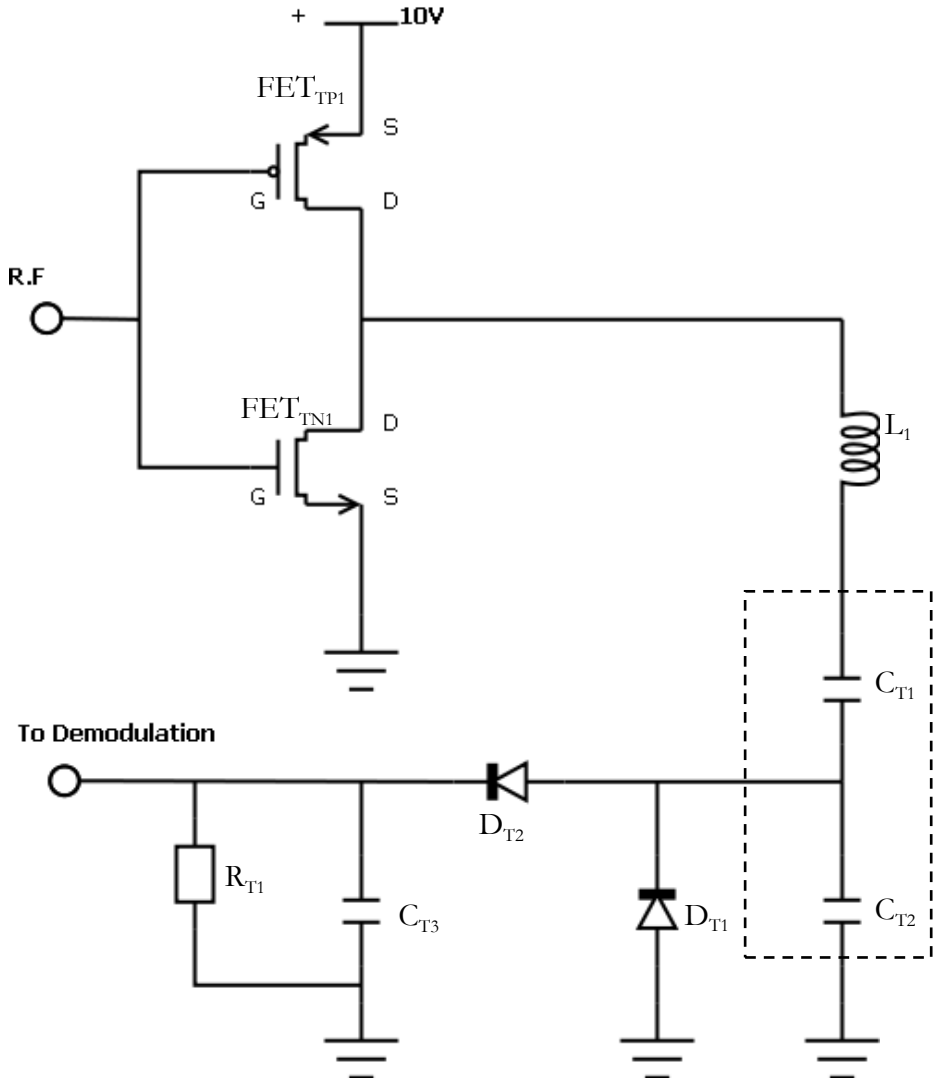

Figure 4.3 Circuit diagram of the transmitter side

On the transmitter side, a frequency generator drives two FETs which are a current amplifying stage driving the series-tuned coil (L_1, C_{T1}, C_{T2}), and power and carrier are sent to the receiver side via the coil L_1. L_1 is series tuned using C_{T1} and C_{T2} (with $C_{T1} << C_{T2}$) as tuning capacitors. The circuit (D_{T1}, D_{T2}, C_{T3}, R_{T1}) is a demodulator, as we measure a sinusoidal signal which is rectified by D_{T2} and smoothed by C_{T3} and R_{T1}. D_{T1} recharges C_{T2} on the negative half cycle. The envelope of that signal has a constant amplitude, and as the impedance on the receiver side is modified, this is reflected on the transmitter side, as a peak or drop, according to the configuration. This is demodulated, amplified, and the period of that signal can be measured. This period has a correspondence with the level measured by the humidity sensor, so we measure the RH inside the PEEK packages. Heat dissipation on the receiver side is limited by the short time to take a measurement (four to five seconds on average).

Figure 4.4 shows an oscillogram of the transmitter and receiver carriers as well as the output of the demodulator for the built system (see following sections). As described previously, the receiver carrier (channel 3 – pink) shows the shorting of the receiver circuit at regular intervals, here with a period of 460 µs. The reflected changes in impedance can be seen on the transmitter carrier (channel 1 – yellow) as amplitude peaks with the same period. Finally, the output of the demodulator is displayed on channel 2 (blue), once again showing the same inter-pulse interval, which corresponds to 38% RH.

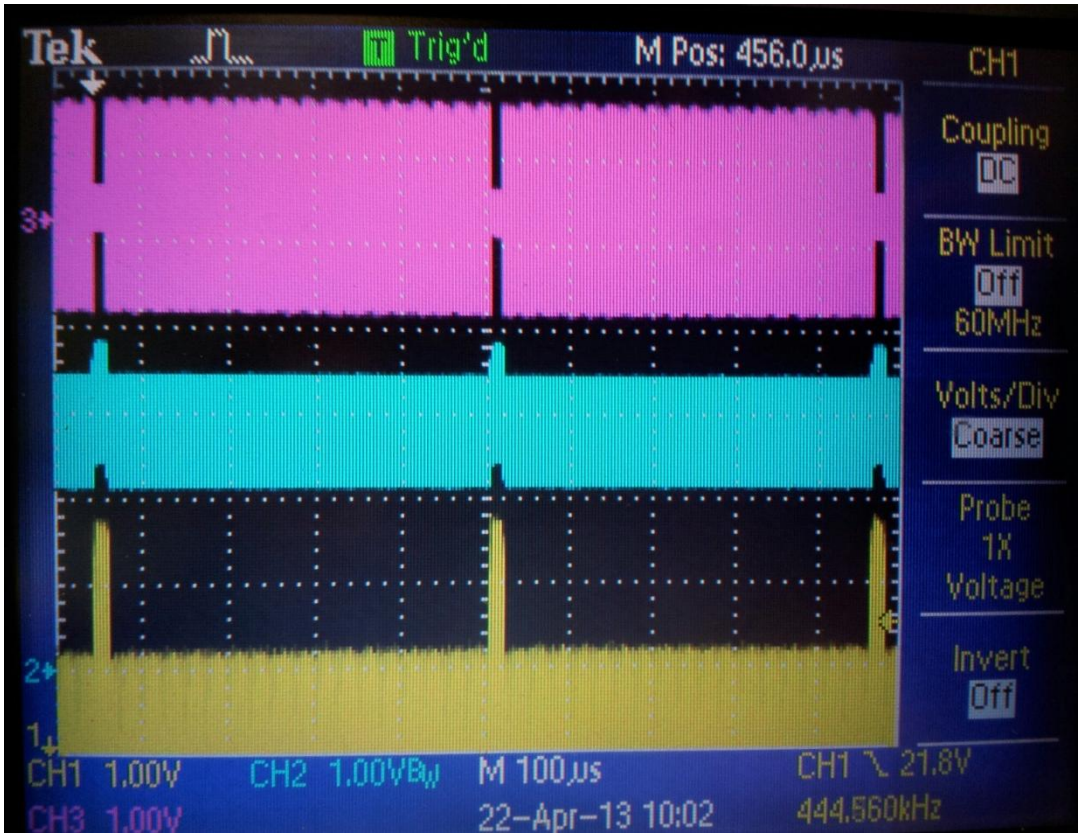

Figure 4.4 Oscillogram showing the transmitter carrier (channel 1 – yellow), the output of the demodulator (channel 2 – blue) and the receiver carrier (channel 3 – pink)

4.1.4 Attenuation issues

Hermetic enclosures made of metal or ceramic generally use a metal seal, which then becomes an electrically conductive ring. Placed in the radio-frequency magnetic field, this ring can become a 'short-circuited turn' by allowing eddy currents to circulate, which will affect the performance of the inductive link (Donaldson 1992). Potentially, a similar issue could appear due to any internal metal coating of PEEK deposited to reduce permeation.

4.1.4.1 Skin depth

Electrical currents that oscillate at radio frequency (in the range of about 30 kHz to 300 GHz) are confined to a layer below the surface, the thickness of which depends on the frequency. This is known as the 'skin effect'. The depth to which electromagnetic radiation can penetrate a conducting surface decreases as the conductivity and the frequency increase. This is characterized by the skin depth δ, expressed for a good conductor as

$$\delta = \frac{1}{\sqrt{\pi f \mu \sigma}} \tag{4.1}$$

where f is the frequency of the incident electromagnetic wave, σ is the electrical conductivity of the material and μ its permeability. In our case the signal is transmitted at a frequency of 13.56 MHz. For titanium for instance, $\sigma=1.8.10^{-6}\ \Omega^{-1}.m^{-1}$ and $\mu=4\pi.10^{-7}$ $H.m^{-1}$ so $\delta=102\ \mu m$.

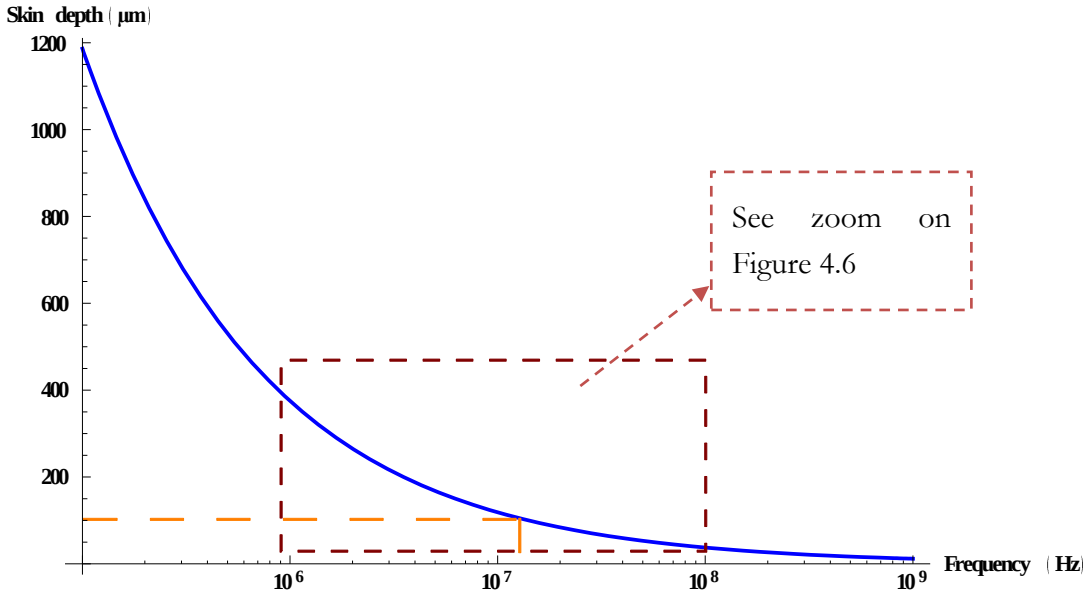

Figure 4.5 Skin depth as a function of frequency for titanium

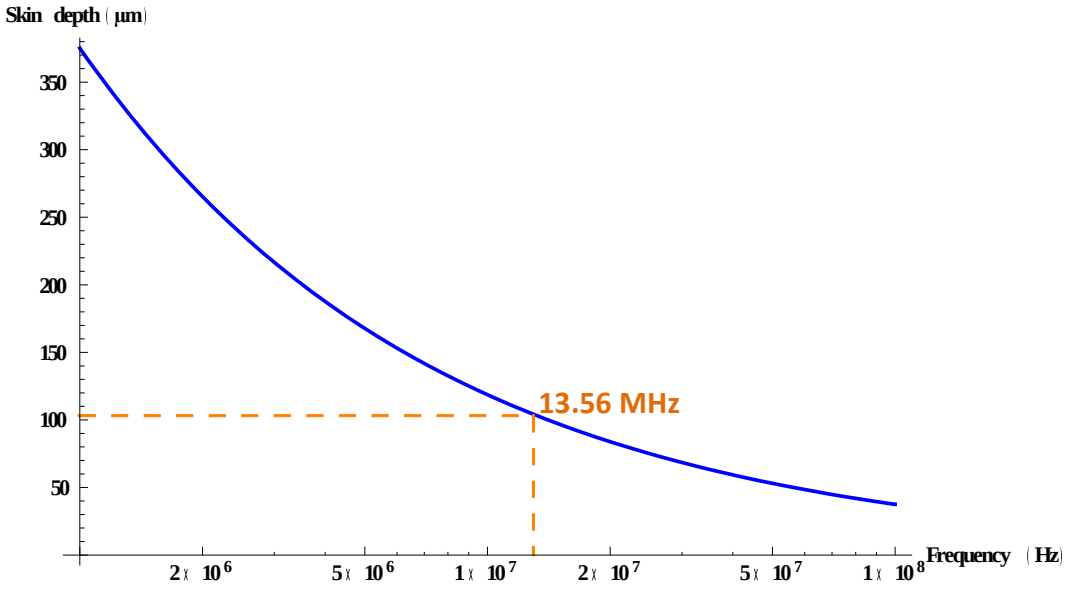

Figure 4.6 Skin depth as a function of frequency

Figure 4.5 and Figure 4.6 show that there is a trade off between high frequency and skin depth. As shown by the log scale, skin depth increases slowly with decreasing frequency.

If we consider a field at the surface of a titanium sheet, located at z=0, at depth z in the titanium the magnitude of the field is

$$|E| = Ke^{-\frac{z}{\delta}} \tag{4.2}$$

where the constant K represents the magnitude of the field at the surface. The field drops off exponentially with depth as shown in Figure 4.7, and higher frequencies are more attenuated.

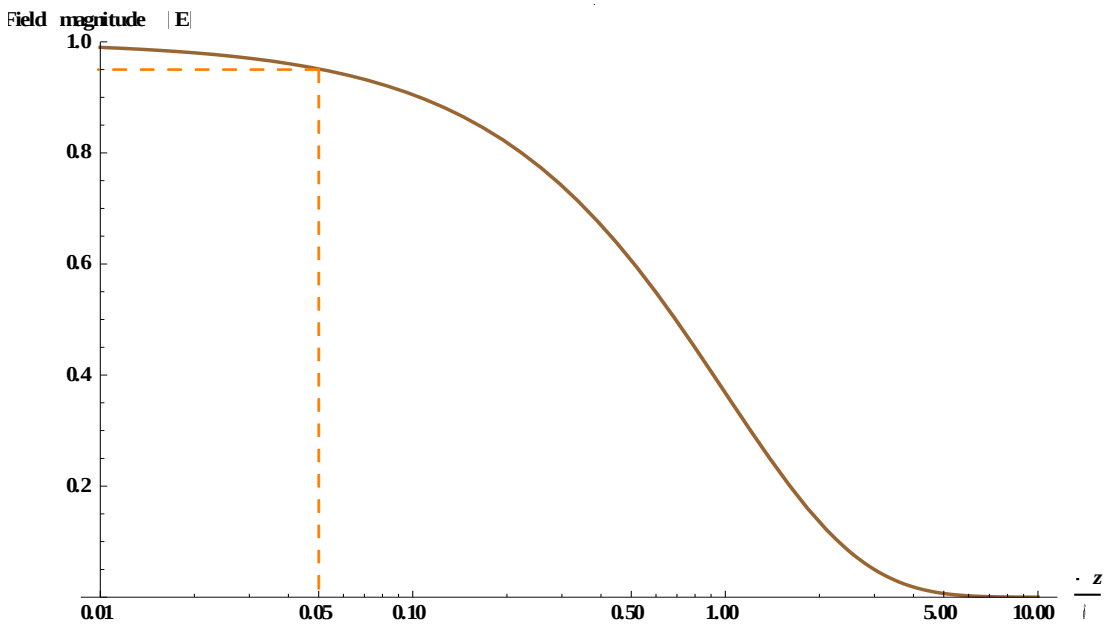

Figure 4.7 Field magnitude vs. depth

At a single skin depth, the magnitude of the field is 36.8% of its incident value. At five skin depths it is 0.67%. Titanium has a skin depth of 102 μm at 13.56 MHz. A 5 μm thick coating for example is very small compared with the skin depth of titanium at this frequency. The magnitude of the field in this case would be 95% of its incident value (see Figure 4.7) and there should be little transmission issues due to attenuation by the Ti coating by skin effect only. However this illustrates the importance of limiting the thickness of coatings deposited in order not to affect the quality of the inductive link.

4.1.4.2 Eddy current losses

The skin effect we have just described is caused by self induced eddy currents. We have shown that a thickness of 5 μm should have a limited effect on the inductive link according to this effect alone. However, eddy currents can also induce efficiency losses which may be much more significant. As a first observation, we can see that the signal through a 3 μm Ti coated PEEK capsule cannot be picked up at the output of the demodulator as there are too much losses. This shows that this effect is very much present. It is however still possible to detect the signal by placing the oscilloscope probe at the transmitter coil instead (see trace 1 in Figure 4.4). We can then assess the extent of losses experimentally by looking at the amplitude of the peak coming from the reflected change in impedance at the transmitter coil, when thin film coatings are applied. The following coatings are tested:

1. 0.5 μm aluminium (sputtered)
2. 0.5 μm titanium (sputtered)
3. 2 μm nichrome (sputtered)

An uncoated PEEK capsule is used as control. The transmitter coil is placed at 1 cm from the receiver (humidity sensing) circuit. The uncoated capsule (control) presents a peak of 1.9 V (amplitude from the top of the carrier envelope to the peak of amplitude coming from the reflected change in impedance seen by the transmitter – e.g. Figure 4.4). results are summarised in Table 4-1. From these results we can see that there are significant losses due to the metal coatings. A 2 μm nichrome coating presents more than 40 % of losses compared to the unattenuated signal. It is therefore important when testing coatings with this system to limit the thickness of the deposited material, and to stay within a 3-4 μm thickness range.

Coating	Amplitude of peak at transmitter (V)	Attenuation
Uncoated PEEK capsule	1.9	--
0.5 μm aluminium	1.2	37 %
0.5 μm titanium	1.6	16 %
2 μm nichrome	1.1	42 %

Table 4-1 Attenuation of signal due to metal coating

4.2 Measuring the humidity level inside the PEEK capsule

In order to determine the useful lifetime of a PEEK enclosure, it is necessary to examine the evolution of the humidity level in such a package. The principle of data transmission with passive signalling has just been explained. We can now see how to measure humidity and convert the signal in a way that can be transmitted and read appropriately.

4.2.1 The humidity sensor

The relative humidity inside the PEEK capsule is measured by a sensor from Sensirion (www.sensirion.com). The **SHT21S** is a capacitive type humidity sensor of small size: 3x3x1mm. It is a smaller version of the SHT15, which has been reported as the sensor of choice for implant applications (Schuettler et al. 2011).

The sensor provides calibrated, linearized signals, thanks to the 4C COMSens® technology which allows the chip to contain an amplifier, an A/D converter, intelligence for linearization and temperature compensation, as well as memory to hold calibration data.

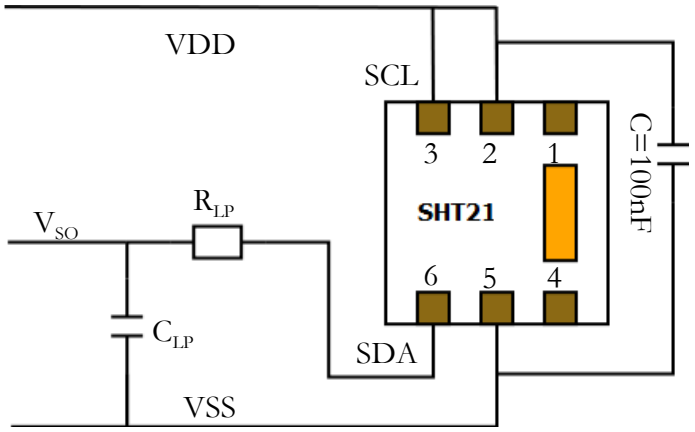

Figure 4.8 Humidity sensor diagram

It is powered using V_{DD} and V_{SS} on pins 2 and 5 respectively (see Figure 4.8). The recommended supply voltage is 3.0 V. V_{DD} and V_{SS} must be decoupled with a 100 nF capacitor, placed as close to the sensor as possible.

SCL on pin 3 is pulled high (to V_{DD}) to tell the sensor to measure the relative humidity (as opposed to the temperature if SCL is pulled low). The sensor output on pin 6 (SDA) produces a 0-5 V rectangular wave output with a duty cycle proportional to the signal, which can then be converted into an analog voltage output V_{SO} with a low pass filter. The recommended values for the low pass filter are R_{LP}=100 kΩ and C_{LP}=220 nF, resulting in a cut-off frequency of 7 Hz. V_{SO} as a proportion of V_{DD} is then converted into an analog voltage. The sensor measures the relative humidity once per second and its value is then obtained with the following equation

$$RH = -6 + 125 \cdot \frac{V_{SO}}{V_{DD}} \tag{4.3}$$

So when RH varies from 0 to 100 %, V_{SO} varies from 0.144 to 2.544 V (if V_{DD} is 3.0V). It is important to note the following instruction from the SHT21S datasheet:

'IMPORTANT: After soldering, the devices should be stored at >75 % RH for at least 12h to allow the sensor element to rehydrate. Otherwise the sensor may read an offset that slowly disappears if exposed to ambient conditions. Alternatively, the re-hydration process may be performed at ambient conditions (> 40% RH) during more than 5 days'

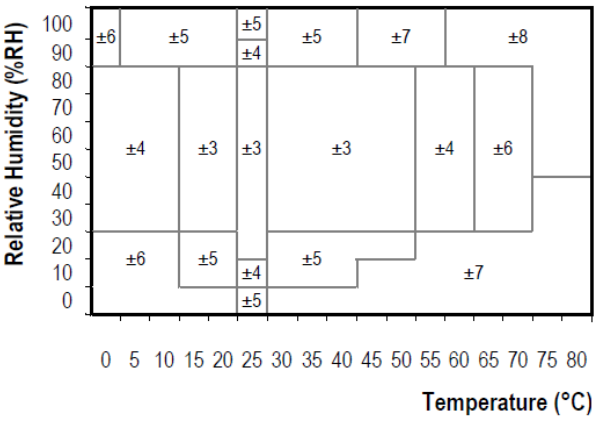

Figure 4.9 Accuracy of the sensor

In terms of accuracy, Sensirion provide maximal tolerances against a high precision reference such as a dew point mirror. Typical deviation are at ±2%RH where maximal tolerance is ±3%RH and about half the maximum tolerance at other values. These values are detailed in Figure 4.9 (Sensirion datasheet).

At 37°C, the tolerance is ±7% RH between 0 and 10% RH, ±5% RH between 10 and 30% RH and ±3% RH between 30 and 90% RH, to which the typical deviation must be added.

4.2.2 The PIC Microcontroller and the program

The principle of the telemetry system has been described previously: a signal is sent to a field effect transistor which, by short circuiting the coil, changes the coupled impedance seen by the transmitter side of the telemetry system. This is managed by a microcontroller, which reads the variable voltage V_{SO} produced by the humidity sensor with an A-D input, converts it to a digital signal, and outputs a 3V signal with variable frequency F, activating the transistor with the same frequency.

The microcontroller used is the **PIC10F222** from Microchip (www.microchip.com). The PIC10F222 is an 8-bit microcontroller with six pins (see Figure 4.10). The assembler programming language is explained by (Smith 2006) .

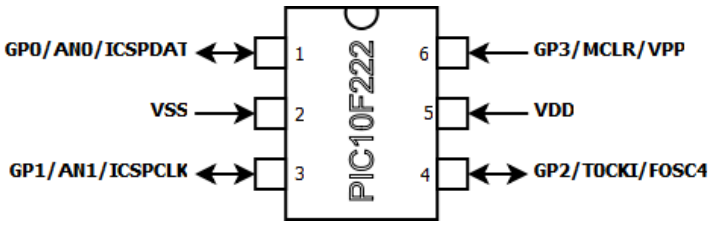

Figure 4.10 PIC microcontroller

Pins 5 and 2 are used to supply power to the microcontroller as V_{DD} (3.0 V) and V_{SS} respectively. V_{SO} is applied to Pin 1 (GP0) as an analogue input, and GP1 on pin 3 is a digital output, producing a 3.0 V signal with a variable frequency. The structure of its program should be as follows:

Start
Initialize
1s delay to make sure that a signal is sent from the humidity sensor
Read GP0
Analogue/Digital Conversion. Result stored in ADRES.
Begin Loop
Set GP1 high
Fixed delay(15μS)
Set GP1 low
Small fixed delay of 85 μS
Variable delay according to ADRES
Go to Loop
END

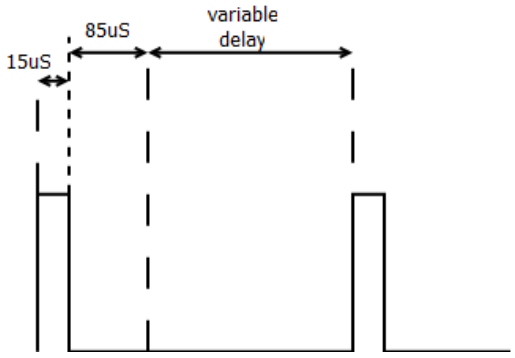

Figure 4.11 output voltage generated by the microcontroller

The result of the A/D conversion is stored in a register called ADRES, which is an 8-bit number. It can therefore take values between 0 and 255. As it is expressed as a function of V_{DD} (3.0 V), each unit of ADRES represents 11.7 mV (=3/256). Therefore equation (4.3) can be rewritten as follows:

$$RH = -6 + 0.488 \cdot ADRES \tag{4.4}$$

Effectively, when RH varies from 0% (0.144V) to 100% (0.2544V), ADRES ranges from 12 to 217. As shown by the program structure and Figure 4.11, the signal is high for 15μs, then low for 85μs plus a variable delay, which is chosen to be 4 times the value of ADRES. This was chosen in order to have a signal period ranging from about 150 - 1000μS (about 1 - 6.5 kHz). The period of the signal can then be expressed as:

$$T = 100 + 4 \cdot ADRES \tag{4.5}$$

And at the demodulation end, using equations (4.4) and (4.5), RH can be expressed directly as a function of the period T:

$$RH(\%) = -18.2 + 0.122 \cdot T \tag{4.6}$$

The program in Assembler language is reported in Appendix 1.

4.3 Circuit design

4.3.1 The receiver

4.3.1.1 Updated receiver

Now that the details of the humidity sensor and microcontroller are known, the circuit diagram of the receiver circuit can be redrawn (Figure 4.12), including a few additional components.

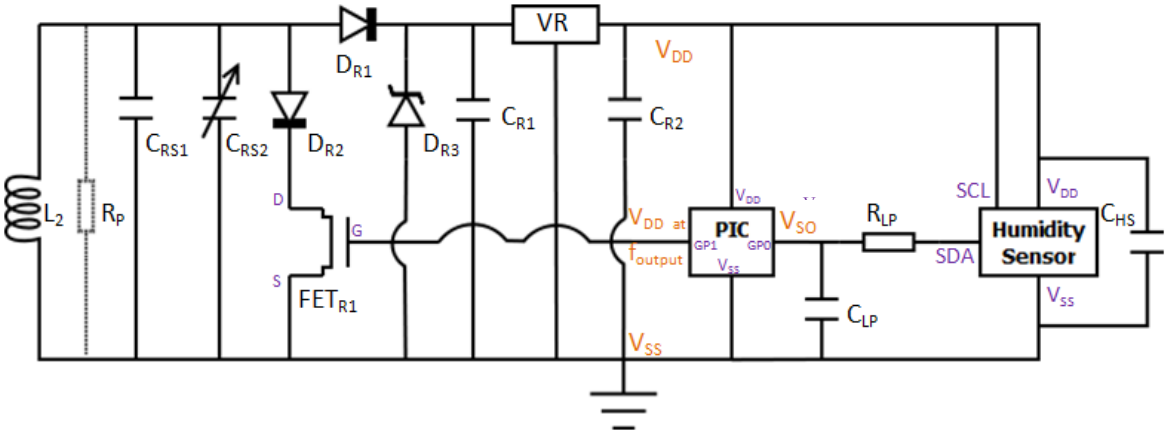

Figure 4.12 Final design

The coil characteristics are as follows: Ø16 mm, wire is Ø0.315 mm, 8 turns, L=1.559 µH. The coil has a shunt resistance R_P=15.08 kΩ, drawn on the schematic, although not physically present in the circuit. As explained before, C_{RS} is used to tune the coil. In theory, $C=1/\omega^2 L=88.33$ pF. However, the actual coil characteristics cannot be known exactly, so C_{RS1} and C_{RS2} are used, where C_{RS1}=50 pF and C_{RS2} is a 100 pF variable capacitor. D_{R3} is a 15 V Zener diode. D_{R1} and D_{R2} are Schottky diodes with 0.4 V forward drop. C_{R1} is a 6.8 µF capacitor, and C_{R2} is a 2.2 µF capacitor for stability. A list of all components is available in Appendix 2.

4.3.1.2 Prototype

A prototype on breadboard, as shown in Figure 4.13, has been built in order to check that the circuit behaves as it should.

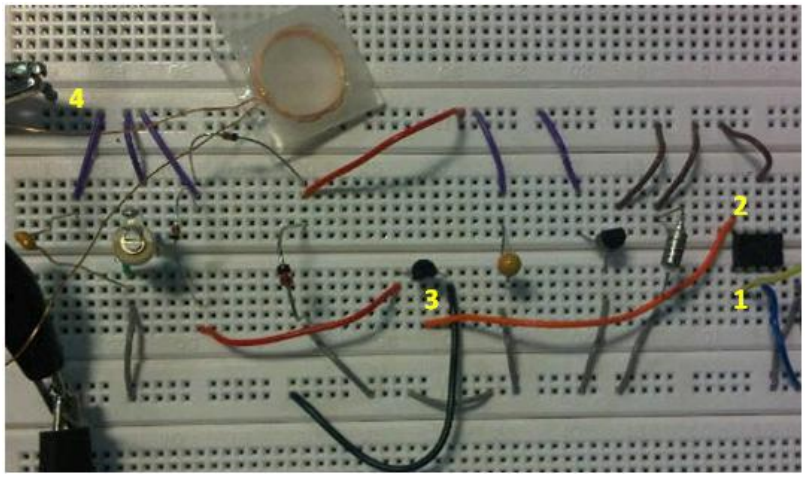

Figure 4.13 Breadboard design

The coil here is replaced by a power supply and a resistor, and the microcontroller gets a set voltage from another power supply as an input (V_{SO}), on **1** on Figure 4.13, to simulate the humidity sensor.

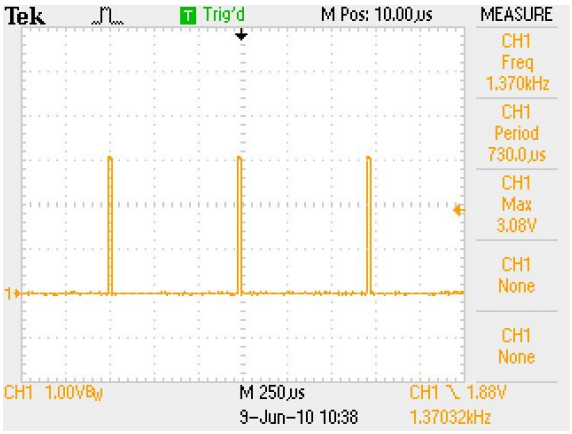

Figure 4.14 Prototype testing 1

This input signal applied on **1** is V_{SO}=1.88 V, which should produce a 3 V output signal on **2** with a period of 730 µS. As shown on Figure 4.14 the signal does indeed have a period of 730 µS and behaves as described in the previous section.

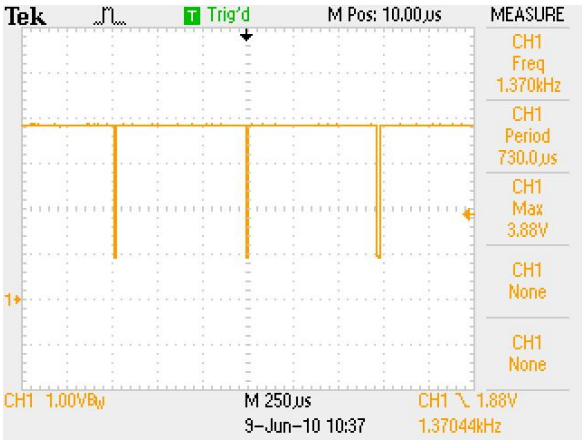

Figure 4.15 Prototype testing 2

The output signal is then applied to the gate of FET_{R1} on **3** which shorts the coil and affects the impedance of the circuit with the same period, as shown on Figure 4.15 (signal measured at **4** on Figure 4.13).

4.3.1.3 PCB Design

For the PCB design, C_{RS1}=75 pF, while C_{RS2} is a 5-20 pF variable capacitor. It should be kept in mind that the final aggregate value of C_{RS1} + C_{RS2} should be around 88pF. We also want to have these as low loss capacitors. C0G (NP0) type capacitors should allow a high Q at high frequency.

The schematic for this circuit is shown on Figure 4.16. The printed circuit board layout is presented on Figure 4.17 and a picture of the circuit once built is presented on Figure 4.18.

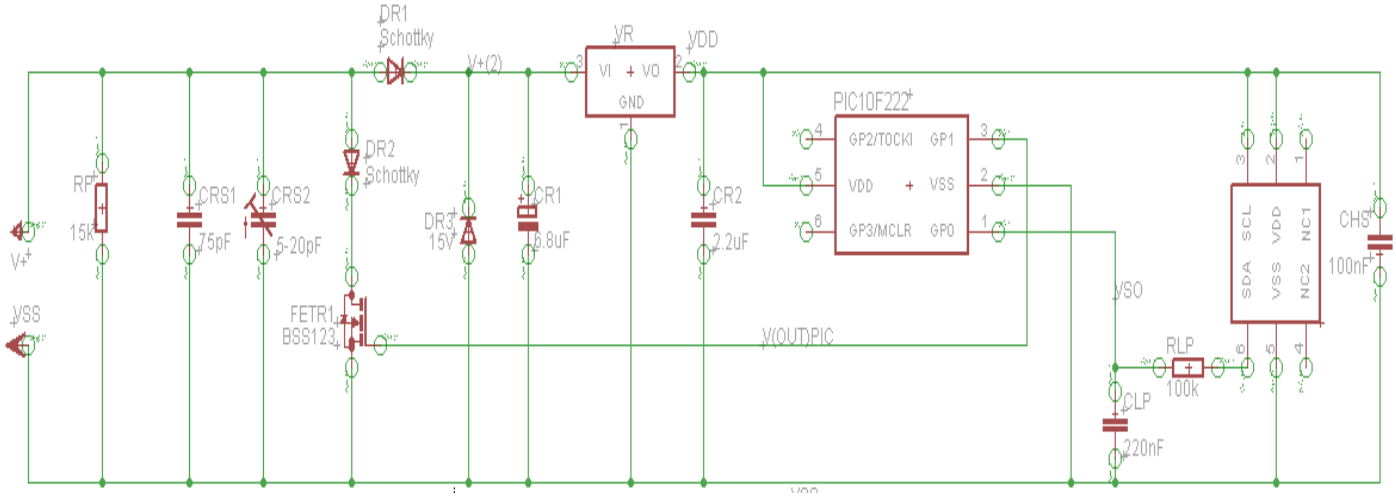

Figure 4.16 Schematic of the receiver circuit

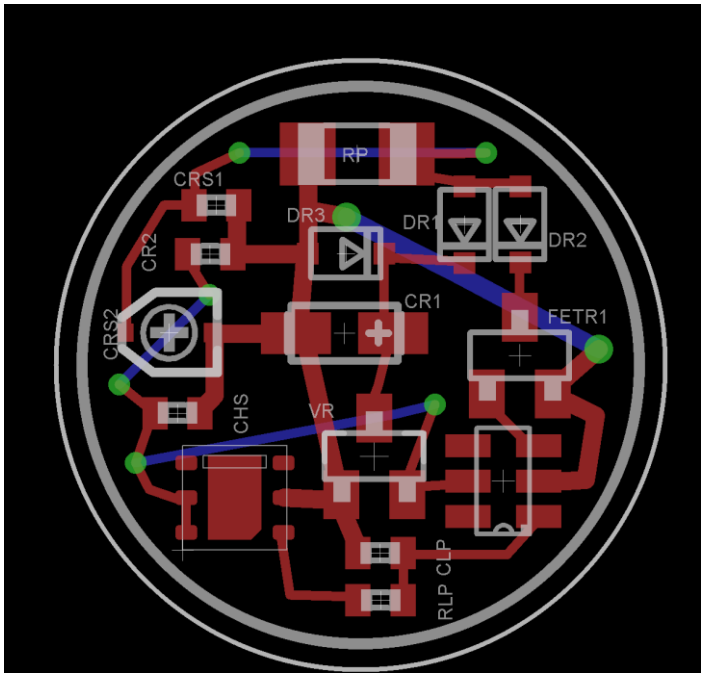

Figure 4.17 PCB layout of the receiver

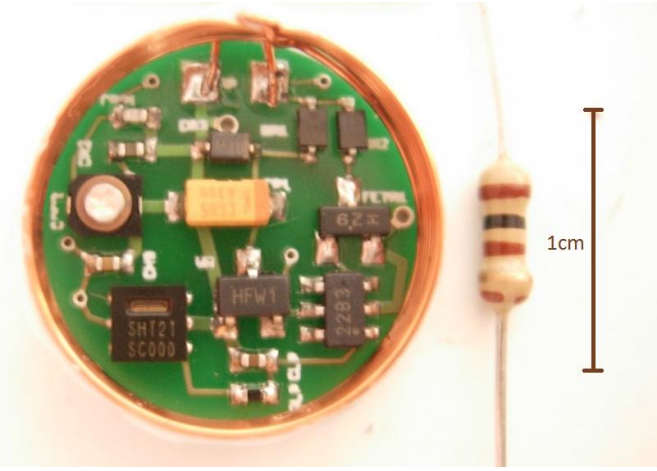

Figure 4.18 Implant sized humidity sensing circuit

A test of the PCB, similarly to what was done previously, shows that the circuit is behaving as it should. Figure 4.19 below shows that the period of the measured signal is 550 μS, corresponding to a relative humidity of 49.5% at room temperature (≈ 21°C), as derived from Equation (4.6) .

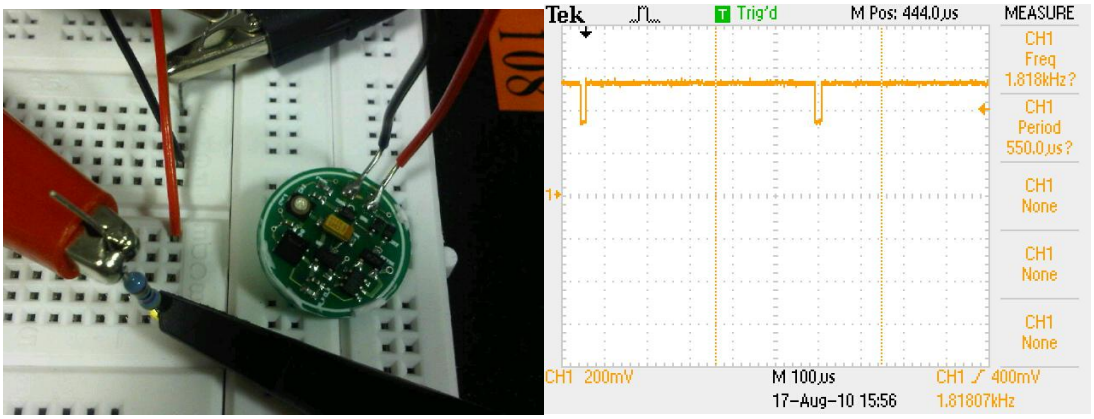

Figure 4.19 Testing of humidity sensing circuit

4.3.1.4 Tuning the coil

In order to obtain the best performance, the coil has to be tuned for the frequency that will be used, using C_{RS1} and C_{RS2} as described previously. This is done with the help of a coil in impedance analyzer and inductive link, which shows a drop in impedance for the tuned frequency. The aim is therefore to match this drop with the desired frequency, in this case 13.56 MHz, by changing the tuning capacitance.

When doing so, the analyzer showed that with the capacitance that we have, we were out of range, as the maximum reachable frequency was 11.6 MHz, for a tuning capacitance of 80 pF (C_{RS1}=75 pF and C_{RS2}=5 pF). Without the trimming capacitor, the frequency was 12.16 MHz, for a capacitance of 75 pF, so still out of range. This difference between

the expected and real values is due to the fact that the coil is not ideal. Moreover, several factors, such as the presence of the board, tracks, conducting components, and gaps between the board and the coil are likely to affect the flux. The tuning capacitance therefore has to be lowered further. The expected value can be calculated, by first reevaluating the true inductance of the coils:

$$L = \frac{1}{\omega^2 . C} = \frac{1}{(2\pi f)^2 . C} \tag{4.7}$$

In this case, f=12.16 MHz and C=75 pF, so **L=2.3 µH**. Feeding this back into Equation (4.7), the expected tuning capacitance can be calculated for the desired tuning frequency (f=13.56 MHz): $\mathbf{C_{tuning}=60\ pF}$. As a result, C_{RS1} has to be changed for a 47 pF capacitor, and C_{tuning} is reached with the help of the variable capacitor C_{RS2} which remains unchanged (5-20pF).

4.3.2 The transmitter

The principle of the transmitter was explained in section 4.1.3. Our circuit is a simplified version of a more complex circuit designed by Dominik Cirmirakis from the Electrical Engineering Department at UCL (cf. Figure 4.20 for the schematic).

The corresponding board is then built (cf. Figure 4.21) using a black mask on a PCB with UV-sensitive photo resist. Developer is used, and the circuit is etched to define the tracks. Holes are drilled and the components are soldered onto the board. The next step is then to tune the coil by choice capacitors C6-C11 as well as trimming capacitor C5. A list of all components is available in Appendix 2.

The circuit is tested and shows that the signal is picked up at demodulation as described previously in Section 4.1.3. The period measured in Figure 4.4 is 460 µS, corresponding to a relative humidity level of 37.9% according to Equation (4.6).

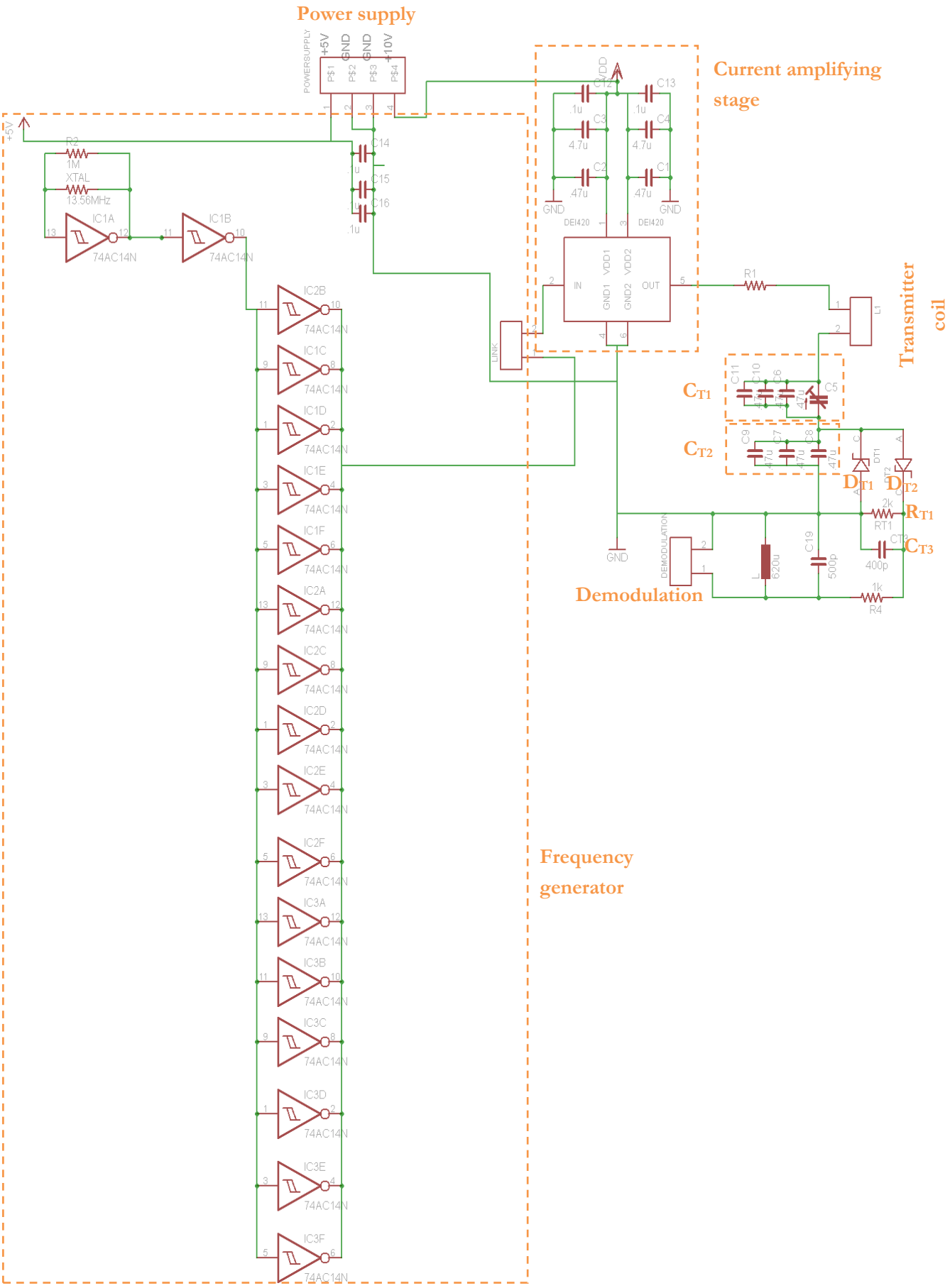

Figure 4.20 Transmitter - diagram

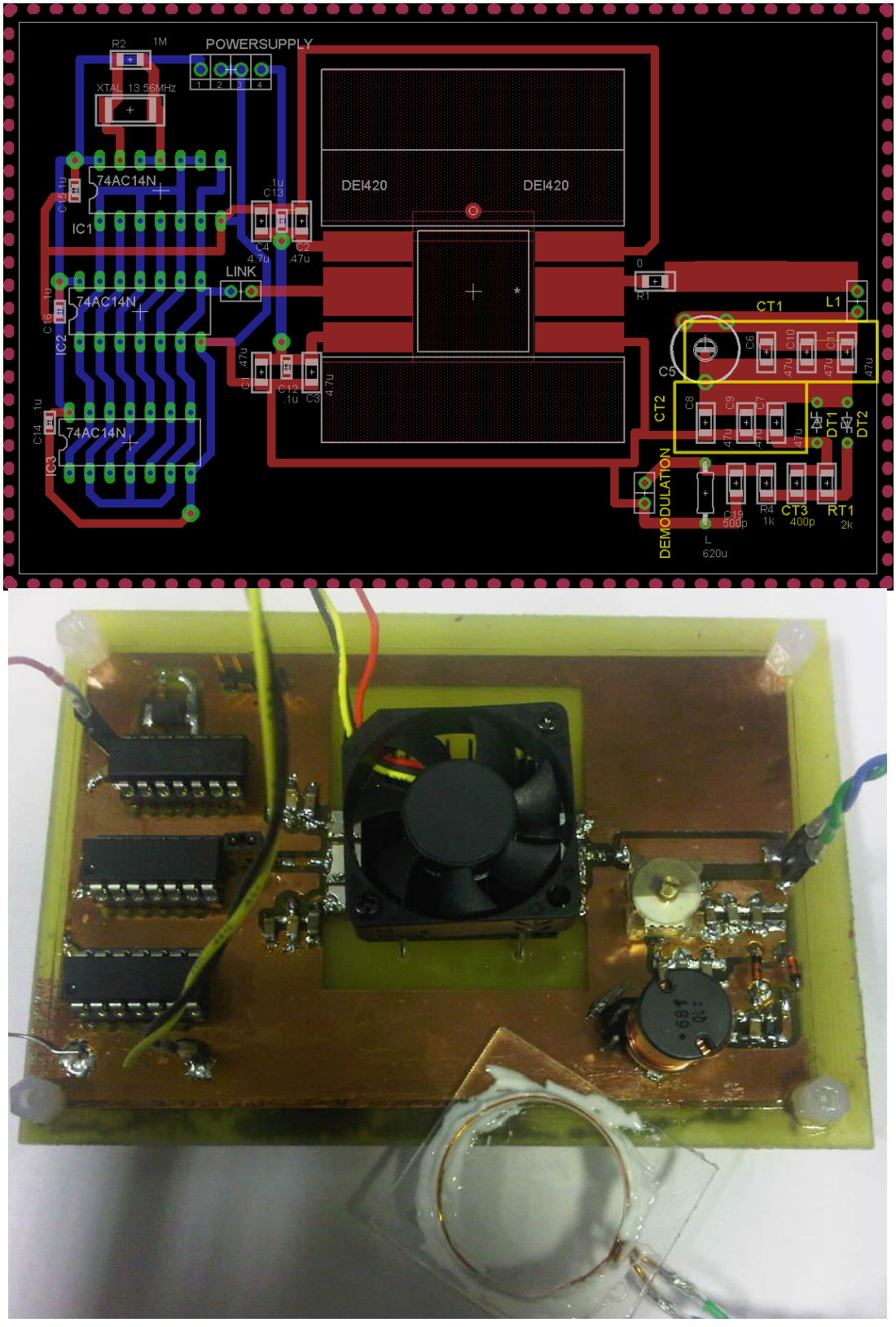

Figure 4.21 Transmitter

4.4 Experimental set up

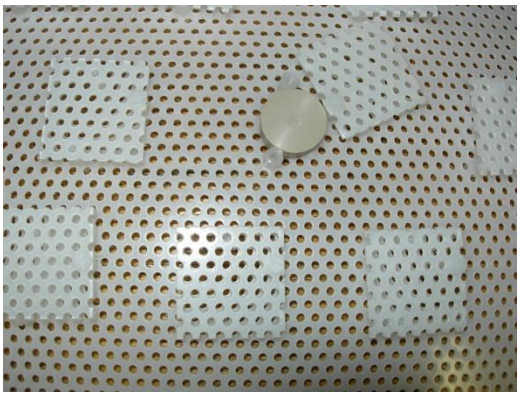

Figure 4.22 Grid to hold PEEK capsules

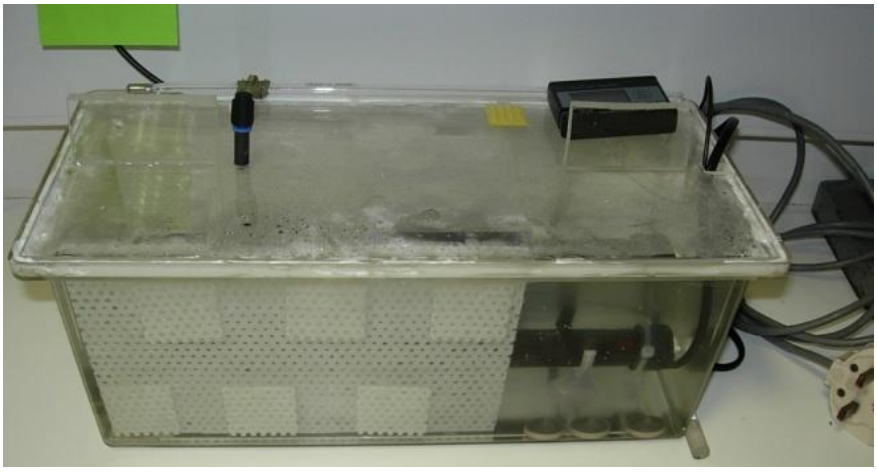

Figure 4.23 Experimental set up – water tank

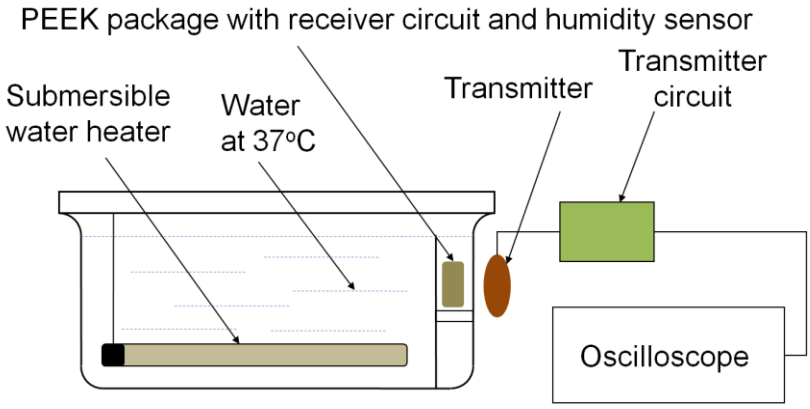

Figure 4.24 Experimental set up

In order to evaluate the lifetime of our PEEK packages, capsules are placed on a perforated plastic grid (cf. Figure 4.22), which is in turn placed in a water tank where water is heated to 37°C by a 150 W submersible heater equipped with a thermostat (cf. Figure 4.23).

The packages are sealed by applying adhesive on the joint area and keeping pressure between the two sides using metal clips during curing. They are then placed on the grid and data is read through the side of the tank by placing the transmitter's coil facing the corresponding capsule (see Figure 4.24).

4.5 Sample size

Each capsule tested contains one of the humidity sensing circuits described in this chapter. For time and resources considerations, I decided to test three samples for each experimental parameter (n=3). Another reason for this decision is that we are trying to find large improvement in lifetimes. Small improvements are discarded in the face of the additional cost they incur compared with the benefit they provide.

Retrospectively, it is also possible to justify this choice with a power calculation, using some of our experiments as pilot studies. The data used for the power calculation is summarised in Table 4-2.

	Experiment	Average time constant (days)	Standard deviation σ (days)	P-value from two sample t-test with control
Control	PEEK-Ep seal	17.99	0.73	N/A
Chapter 5	PEEK-CA seal	15.88	0.26	0.00900
Chapter 5	Ti-Ep seal	472	119	0.00272
Chapter 6	PEEK-Silica gel-Ep seal	73.7	6.05	0.00009
Chapter 7	PEEK-lacquer-Al coating-Ep seal	41.64	4.10	0.00060

Table 4-2 Data for power calculation

The power calculation is used to provide the sample size needed to be able to reject the null hypothesis that the population means of the experimental and control groups are equal with probability (power) 0.8 in this case. The Type I error probability associated with this test of this null hypothesis is 0.05 (probability of rejecting the null hypothesis when it is true).

Comparing each pilot study in the table above with the control returns an optimal sample size of n=1. Normally, an a priori power calculation would not return n=1 as it is impossible to do comparative statistics with just one sample. Moreover n=1 is not a valid result as you need a standard deviation to do the power calculation, which you cannot have if n=1.

However in our case we are doing a retrospective calculation, and we already have a standard deviation value that we can use. Furthermore, we are trying to measure large differences with a relatively small standard deviations, so there is no overlap of

distributions, and it makes sense that the power calculation returns n=1. Therefore the conclusion is that using n=3 for our experiments is sufficient.

4.6 Conclusion

In this chapter, we presented the telemetry system used, including the design of the receiver and transmitter, as well as the programming of the microcontroller and the experimental set up. In the next three chapters, experiments with PEEK capsules, metal coatings and desiccants are detailed, in order to assess the lifetime achievable by PEEK packages. In this study, more than 140 capsules have been tested. This experimental set up has proved to be robust, reliable and convenient, with each measurement taking four to five seconds maximum. The receiver circuits did go off-tune after a while, but re-tuning was only needed very occasionally (every 10 months or so). Overall, this has been an extremely satisfactory method.

Chapter 5 Moisture ingress in adhesively joined PEEK capsules: experimental work

This chapter begins with a literature review of adhesive bonding, followed by the experimental investigation of the lifetime of adhesively joined PEEK packages. Moisture ingress through the seal vs. the walls is differentiated using solid metal capsules, which only let water through the adhesive joint. The durability of adhesive joints under water is also tested using lap shear tests, and a guideline graph is provided to evaluate the time constant depending on the wall thickness and cavity size.

5.1 Adhesive bonding – Literature review

> *'The forces involved in holding adhesives and sealants to their substrates or in holding adhesives and sealants together as a bulk material arise from the same origins. These same forces are all around us in nature.* ***To understand what is happening in an adhesive or sealant joint, we must first understand the forces that bind atoms and molecules together***' (Petrie 2000).

As an introduction, we will therefore first briefly review the forces which attract molecules to each other (intermolecular forces). These must be differentiated from intramolecular forces, which hold atoms together in a molecule. Having this full picture will then enable us to better understand how adhesive bonding works. This background information, although of a very basic level, will also prove useful in Chapter 6 to understand how desiccants and the adsorption process work.

5.1.1 Intramolecular forces

Intramolecular forces, also called primary forces, are those which attract atoms to each other to form a molecule. There are three types of primary or chemical bonds: ionic, covalent and metallic. The source of these interactions is the electrostatic force of attraction or repulsion between electrically charged particles (Coulomb force – proportional to the charge of the particles under consideration and inversely proportional to the square of their distance). They all involve the valence electrons, as there is a tendency of atoms to have a stable electron structure and fill the outermost electron shell (Malone 2003).

1. Atoms can transfer electrons to each other and form ions. These oppositely charged ions can then form an ***ionic bond*** to create a stable compound. A typical example of this is sodium chloride (NaCl), in which an electron from a sodium atom is transferred to a chlorine atom. The two ions Na^+ and Cl^- can then form an ionic bond to create NaCl (see Figure 5.1). Ionic bonding is always found in compounds composed of both metallic and non metallic elements, as the former easily give up

their valence electrons to the latter due to the difference in electronegativity (Callister & Rethwisch 2008).

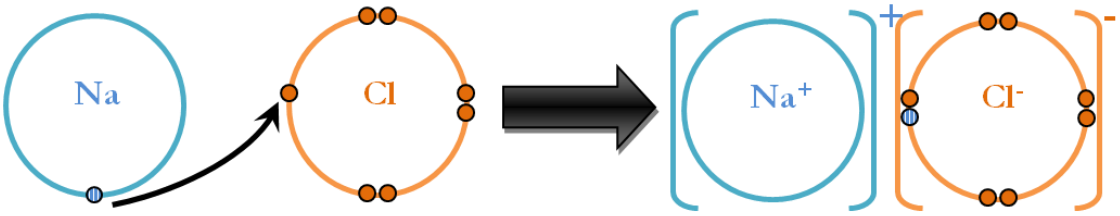

Figure 5.1 Ionic bond

2. When two atoms share a pair of electron, they form a **covalent bond**. It is a normal covalent bond if each atom provides one of the electrons in the bond, as shown by the example of water in Figure 5.2.

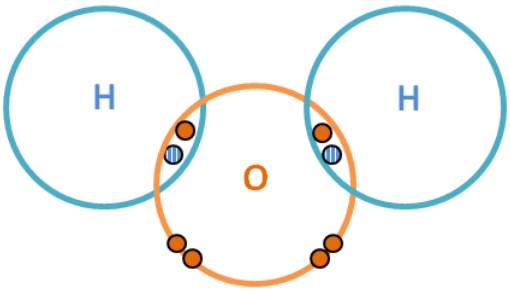

Figure 5.2 Normal covalent bond

If one of the atoms provides both electrons, it is a dative covalent bond (also called dipolar or co-ordinate bond). This happens because electrons are more stable when attracted to two nuclei rather than one. An example of dative covalent bond can be found with the ammonium ion, as a hydrogen ion is transferred from hydrogen chloride to the lone pair of electrons of an ammonia molecule (see Figure 5.3).

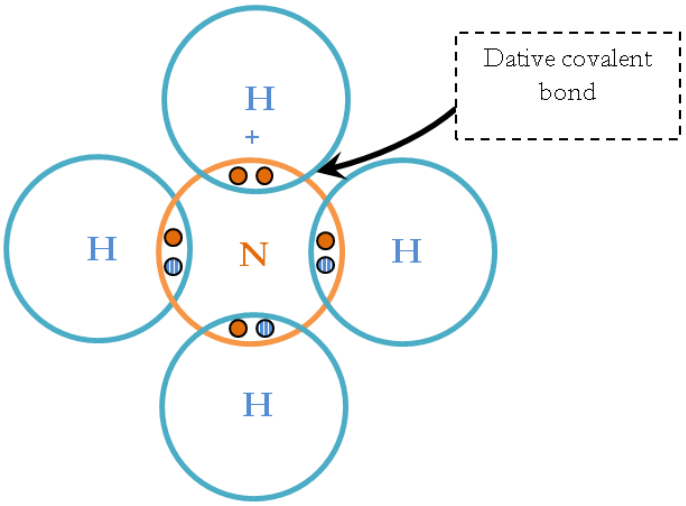

Figure 5.3 Dative covalent bond

3. In the case of **metallic bonding**, atoms lose electrons, and the resulting cations are attracted to the resulting 'sea of electrons'. These electrons are not attached to a particular atom but are free to move between the 'ion cores' (Callister & Rethwisch 2008). They are said to be delocalized. The strength of these bonds is summarised in Table 5-1 (Petrie 2000).

Type of intramolecular bond	Bond energy (kJ/mol)
Ionic	600 - 1000
Covalent	60 - 700
Metallic	100 - 350

Table 5-1 Types of intramolecular bonds

The type of bond formed depends mainly on the electronegativity (capacity to attract electrons in a covalent bond) of the elements under consideration (Malone 2003). Electronegativities vary from 0.7 to 4.0 and are relative to the most electronegative element (F - 4.0). Electronegativities can then be used to predict how much ionic or metallic character a covalent bond will have, as very few components exhibit pure ionic or covalent bonding (Callister & Rethwisch 2008).

If both atoms have a similar electronegativity, the electrons will be equally attracted to each element and will remain between the two. However, if one element is more electronegative than the other, the electrons will tend to be more attracted to it and on average will be closer to it. Its side of the molecule will have a slight surplus of electrons and a slight negative charge (δ^-) (the opposite is true for the other element). In this case the bond is said to be **polar covalent**, and it is possible that the molecule as a whole will be polar as well, depending on its geometry and the elements under consideration.

If the difference in electronegativity is large, then the bond is ionic: the electrons have a much stronger attraction towards the more electronegative element, which becomes negatively charged, whereas the more electropositive element becomes positively charged. In reality, most bonds are covalent with more or less of an ionic or metallic character (Malone 2003).

Identical atoms have no difference in electronegativity, and the bond will be either covalent, or metallic if both elements are electropositive (neither can strongly attract electrons, which are then free to move).

Although the forces presented here are called intramolecular forces, they can also sometimes be found between molecules. This is the case for example within a crystalline structure, which can have covalent or ionic bonds for instance. When that is the case the terms 'primary forces' or 'chemical bonds' is used instead of 'intramolecular' in order to avoid confusions. Crystalline structures can also have Van der Waals bonds, which are weaker and are the most general type of intermolecular forces.

5.1.2 Intermolecular forces

Intermolecular forces, also called Van der Waals forces and physical bonds, are those which generally attract molecules to each other. They are the forces which must be overcome when a substance is melted or boiled, as these bonds must be broken for molecules to be free to move with respect to each other, and therefore make the substance liquid or gaseous. These forces are of three types.

1. **Dispersion forces,** also known as London forces, are the electrostatic forces of attraction between a temporary and an induced dipole. In a molecule, electrons are not static, but in constant movement. As a result, at a given time, it is possible that most electrons are on one side of the molecule, and this side becomes slightly negatively charged (δ^-). Conversely the other side is slightly positively charged (δ^+). The molecule is then a *temporary dipole*, as this state lasts for a very short time only. A nearby molecule, as a result, will see its electrons repelled by the negative part of the dipole, and that side will become δ^+, making the molecule an *induced dipole*, which is attracted to the temporary dipole. The polarities of the molecules are constantly fluctuating, but do so in a synchronised manner if they are close enough to each other. The strength of dispersion forces is affected by the molecular size and shape (Malone 2003).
2. As seen previously, some molecules can be permanent dipoles, due to the ionic character of the intramolecular bonds. They are said to be polar. NaCl is a good example of this (Figure 5.1). In addition to dispersion forces, such molecules therefore also experience **dipole-dipole bonding** (or polar bonding). As a result, compounds which are attracted to each other by dipole-dipole bonding generally have a higher boiling point than those which only experience dispersion forces.
3. However, the difference of bond strength provided when a permanent dipole is involved is generally not of great magnitude, with the notable exception of **hydrogen bonding**: If a hydrogen atom is bonded to a very electronegative element such as N, O or F, its only electron will be on average much closer to this other element. The permanent dipole will then be able to form a strong dipole-dipole bond with adjacent elements if these are highly electronegative. Hydrogen bonding is basically a stronger form of polar bonding, and has a significant effect on the properties of a compound (Malone 2003).

Type of Van der Waals bond	Bond energy (kJ/mol)
Dispersion	0.1 - 40
Polar	4 - 20
Hydrogen	Up to 40

Table 5-2 Types of Van der Waals bonds

The strength of these secondary bonds is summarised in Table 5-2 (Petrie 2000). These forces are much weaker than the primary forces shown in Table 5-1.

5.1.3 Surface energy

We have seen the types of cohesion forces which hold the bulk of a material together. Let us now look at the boundary between the bulk and the environment: the surface of the material. The surface atoms are not bonded to the maximum number of neighbours, and therefore they are in a higher energy state than the bulk atoms. This excess of energy at the surface is called the surface energy γ (in mJ/m^2).

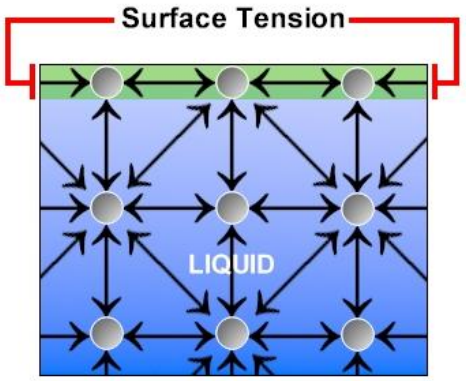

Figure 5.4 Surface tension

If the material under consideration is a liquid, a molecule within the body of this liquid is equally attracted in all directions. The molecules on the surface however are only pulled downwards and sideways, not upwards. The tendency to minimize energy therefore means that the surface area will be minimized too. This is why liquid water droplets are spherical (minimum surface area per volume) (Callister & Rethwisch 2008). Still in the case of a liquid, the surface energy γ is equivalent to the surface tension γ_{LV} (in $mN.m^{-1}$), which is effectively the energy necessary to break through the surface (see Figure 5.4). The surface tension of water at 20°C is 73 $mN.m^{-1}$ (Adamson & Gast 1997). For silicone and cyanoacrylate, the values are respectively 24 $mN.m^{-1}$ (Petrie 2000) and 34 $mN.m^{-1}$ (source: cyanobond.de).

In the case of a solid however, the material cannot freely change shape, but can try to reduce the surface energy by creating bonds with liquid substances for instance. If the surface energy of the solid is higher than the surface energy of the liquid, then the best option for the liquid to reduce its excess energy is not anymore by assuming a spherical shape, but by wetting the solid.

Traditionally, solids are divided into high energy or low energy solids, and the surface energy depends on the strength of the molecular interactions within the bulk of the material. Metals, ceramics and glasses are high energy solids, as the bonds within the bulk are very strong (primary forces). Conversely, if the intermolecular forces are weak (Van der Waals forces), the solid has a low surface energy (fluorocarbons, hydrocarbons, polymers, etc). The surface free energy for PEEK and Titanium are respectively 38 $mJ.m^{-2}$ (Blundell & Osborn 1983) and 1588 mJ/m^{-2} (Adamson & Gast 1997).

When a drop of liquid is placed on an ideal solid surface, a characteristic angle θ is formed (see Figure 5.5), and the force balance between the three phases' surface tensions is described by Young's equation (Young 1805):

$$\gamma_{SV} = \gamma_{LV} \cos\theta + \gamma_{SL} \tag{5.1}$$

where γ_{SV}, γ_{LV} and γ_{SL} are respectively the solid-vapour, liquid-vapour and solid-liquid interfacial tensions.

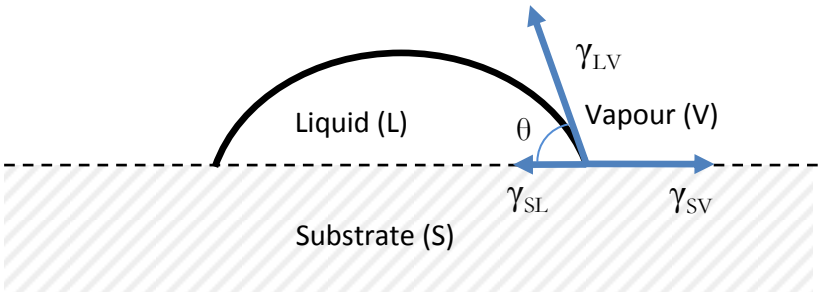

Figure 5.5 Contact angle and surface free energy components

The wettability is deemed to be high if the contact angle θ is less than 90°. The criterion of 'perfect wetting' (θ=0°) is used to define the *critical surface tension* of the solid γ_C. This is the threshold for the surface tension of a liquid under which this liquid will perfectly wet the substrate. As a result, a liquid with a surface tension $\gamma_{LV}<\gamma_C$ will perfectly wet this solid (provided it is an ideal surface – perfectly flat, clean, smooth, etc.)

5.1.4 Work of cohesion and work of adhesion

For a truly cohesive failure in the bulk of a material, the work of cohesion corresponds to the energy necessary to create two new surfaces from the bulk material:

$$W_C = 2\gamma \tag{5.2}$$

In the case of an adhesive and a surface, we can similarly define the work of adhesion. However, in this case, the interfacial energy must be added as there are intermolecular forces existing between the two materials. This yields the Dupré equation (Dupré 1869) which defines the work of adhesion:

$$W_A = \gamma_{LV} + \gamma_{SV} - \gamma_{SL} \tag{5.3}$$

Equations (5.1) and (5.3) can then be combined into the Young-Dupre equation:

$$W_A = \gamma_{LV}(1 + cos\theta) \tag{5.4}$$

And if there is prefect wetting (i.e. cosθ=1), then $W_A=W_C$, the adhesive bond is as strong as the bulk of the adhesive (Petrie 2000).

5.1.5 Theories of adhesion

All the interactions between the adhesive and the adherend cannot be modelled on a single, comprehensive, unifying theory of adhesion. Instead, there are several theories which can be applied depending on the nature of the joint and how it is used in service. These theories can help understand why adhesive joints fail or succeed. The most common ones are '*adsorption, mechanical interlocking, diffusion, electrostatic interaction, and weak-boundary layers'* (Petrie 2000).

1. According to the **adsorption theory**, adhesion occurs as adhesive molecules are adsorbed onto the surface of the substrate. Most of the time, it is a case of 'physisorption' with weak Van der Waals forces. In more rare cases, 'chemisorption' can occur. In this case the bonds are either covalent or ionic, and both adhesive and substrate structures are changed (Oura et al. 2003). In both cases, it is necessary to establish a continuous contact between adhesive and adherend, hence the importance of good 'wetting', which, as we have seen before, is determined by the difference between γ_{LV} and γ_C. For good wetting, we need $\gamma_{ADHESIVE}<\gamma_{C\ SUBSTRATE}$. This is one of the reasons why some polymeric adhesive (with relatively low surface tension) will work very well with high energy surface materials such as metals and ceramics, but might not offer as strong a bond with lower energy surfaces such as some polymers. After wetting is achieved, permanent adhesion (after curing of the adhesive) results mainly from primary and Van der Waals forces (Petrie 2000).
2. Another aspect of the adhesion process relates to the **mechanical theory**, as there is always a degree of roughness associated with a surface. According to this theory, the surface roughness helps by providing more surface area for adhesive forces to develop. Moreover, it allows mechanical interlocking with the adhesive, provided that '*the adhesive can penetrate the cavities on the surface, displace the trapped air, and lock on mechanically to the surface*' (Petrie 2000). Under standard conditions of pressure, this is controlled mainly by the viscosity of the liquid adhesive.
3. Bikerman first described the **weak boundary layer theory**, explaining that even when it seems that there is purely adhesive failure, it is in reality most of the time cohesive failure of a weak boundary layer very near the interface (Bikerman 1961). These layers can occur during application, setting, or service, if there is concentration of impurities near the bonding surface. They can be caused by air, constituents of the adhesive itself or water (as they easily adsorb on the substrate surface), metallic oxides, or a chemical reaction by-product of the curing reaction for instance. During service, moisture can also favour the formation of a weak boundary layer as it diffuses through the adhesive or the substrate and locates at the interface (Petrie 2000).

For a limited number of applications, the electrostatic and the diffusion theories can also be appropriate. However, these theories are generally not as favoured as the first two (Petrie 2000).

4. The **electrostatic theory** states that electrostatic forces form at the adhesive-adherend interface, under the form of an electrical double layer, and account for the bond strength. This theory arose from observing electrical discharges when peeling an adhesive from a substrate.
5. When both adhesive and adherend are polymeric, the **diffusion theory** explains that the cause of adhesion is inter-diffusion of molecules, provided that both substances have compatible long-chain molecules capable of movement. This theory can be applied for solvent or heat welding of thermoplastics for instance.

All these theories have been reported in the literature to provide a good explanation of experimental observations. However none of them can be applied to all cases. As we will see later in this chapter, the adsorption, mechanical and weak boundary layer theories are the most relevant to the case of adhesive bonding to PEEK.

5.1.6 Effect of moisture on an adhesive joint

In a high relative humidity environment, moisture is a major threat to the stability of adhesive joints, due to the polar nature of water and the fact that polymers are permeable to it. Moisture can indeed degrade the properties of the bulk adhesive itself or the adhesion properties at the interface. It can also potentially degrade the properties of some adherends and cause dimensional changes (Petrie 2000; Lee 1987).

As water permeates the bulk of the adhesive, it can induce cracks, or reduce the glass transition temperature of the adhesive by reducing intermolecular forces. Water will also generally lower tensile strength and Young's modulus, although these changes are generally reversible upon drying. Furthermore water can degrade the adhesive by hydrolysis, causing the adhesive to lose hardness and strength. The chemical reaction involved here consists in degrading the long polymer chains into smaller molecules, causing the reduction of strength. This in turn will cause cohesive failure. However, a swelling of the adhesive may occur before then, and may cause deformation and bond failure before hydrolysis.

Another even more common problem caused by moisture is that water permeating the adhesive can migrate to the interface and cause a loss of adhesion by displacing the adhesive at the bond interface. This displacement results from the competition between water and adhesive for surface sites: as water permeates the adhesive and migrates to the interface, its molecules occupy surface sites and 'chase away' the adhesive, causing adhesive failure.

In the case of a metal, water can promote the formation of metal oxides, forming a weak boundary layer with the adhesive which is therefore more likely to fail (Bikerman 1961). It is however possible to reduce the effect of water and improve the quality of the bond by various means.

5.1.7 Promoting adhesion

In order to obtain a stronger bond, there are several ways to prepare the surface.

1 Applying a surface treatment in order to remove the weak boundary layers (passive process) which could increase the chances of bond failure. Another aim of surface treatment could be to increase the surface energy of this surface (active process) to improve wetting. Common surface treatments include degreasing (solvent or vapour), mechanical abrasion (added roughening effect for mechanical interlocking), plasma, chemical etching, etc. (Petrie 2000). The type of surface treatment to apply, if any, depends highly on the materials used and on the application (structural, hermetic, etc.).
2 Whether in addition, or in place of surface treatment, the application of primers and coupling agents can help form a stronger bond and improve resistance to moisture. This is especially helpful when the substrate has a low surface energy, or if it is porous and allows moisture to migrate to the interface. The principle is to add an intermediate layer which bonds very well to both the substrate and the adhesive by chemisorption. As a result, the new covalent bonds formed are stronger than the bulk of the adhesive (Petrie 2000). Coupling agents can either be incorporated into the formulation of the adhesive, or added as a very thin coating (ideally one monolayer).

5.2 Lifetime of adhesively joined PEEK packages – experimental work

5.2.1 Selection of adhesives

Joining technologies have been investigated in section 2.4 'Joining technologies for thermoplastic polymers and the case of PEEK and implanted electronic devices'. Adhesive bonding has been selected as the method of choice to seal packages in the context of this study for three reasons:

- It is a very easy method to seal a large number of packages with virtually no extra equipment. It also makes the retrieval of humidity sensing circuits simpler, which is important as they are to be reused throughout this study.
- Other sealing methods involve an amount of vibrations or heat which may be detrimental to the electronics (particularly the humidity sensor, which is a very sensitive component), or to the integrity and porosity of the PEEK package. Laser welding involves highly localized heating, but can only bond parts with a

maximum thickness of 1mm, which is counterproductive when looking at limiting moisture diffusion through the walls.

- It is expected (because of the dimensions involved) that diffusion through the seal is negligible compared to diffusion through the bulk of the PEEK capsule, so using adhesive bonding should not be detrimental. This hypothesis will be tested in the following section of this study.

In order to select appropriate adhesives, I chose to follow the work done by TWI Ltd., which assessed the adhesive bonding of PEEK for medical device applications (Tavakoli et al. 2004). Among the adhesives used, which are all certified for use with medical devices, I selected three types of adhesives:

1. **Silicone**: NuSil MED3-4013. Silicone, although not as strong as other types of adhesives, is widely used for encapsulation of electronics, thanks its durability when exposed to water.
2. **Cyanoacrylate**: Loctite 4061. Cyanoacrylate has a very low viscosity and surface tension, which helps form strong bonds with most materials. It also offers the benefit of curing very quickly at room temperature
3. **Epoxy**: Loctite Hysol M31-CL. Epoxy is a strong structural adhesive with a good durability when exposed to water (although not as good as for silicones).

In Tavakoli's paper, these types of cyanoacrylate and epoxy adhesives presented the strongest bonds to PEEK.

5.2.2 Preliminary experiment

We can begin by going through the process used in experiments throughout this thesis. In the previous chapter, the PEEK capsule, the humidity sensing circuit, as well as the experimental set up, have been described in detail. For the first experiment, a PEEK capsule is adhesively joined with Loctite 4061 (cyanoacrylate) and placed in water at 37°C (n=3). The relative humidity is recorded and its evolution with time is plotted in Figure 5.6. It can be noticed that the three capsules tested give extremely similar results, and the shape of the rise in humidity follows expectations, as presented in Chapter 3.

Following the method presented in the section '3.4 Interpreting experimental results', a linearization of Equation (2.15) is performed in order to extract the experimental time constant τ. This is done by plotting $\ln(RH_a\text{-}RH)$ as a function of time for the plot of average values for this experiment. The results are presented in Figure 5.7, and the time constant is found to be 15.9 days. Figure 5.8 shows that using the exponential model and finding the experimental constant this way provides an excellent approximation of the real, experimental behaviour.

The method just described will be used throughout this work to calculate the experimental time constants. For clarity purposes, only the plot of average values will be presented for each experiment, and the time constants will be given without showing the regression plot. **Unless it is stated otherwise, the reader should assume that for each parameter, the plotted results represent the average for three samples every time (n=3).** Error bars showing the standard deviation will be displayed for each graph.

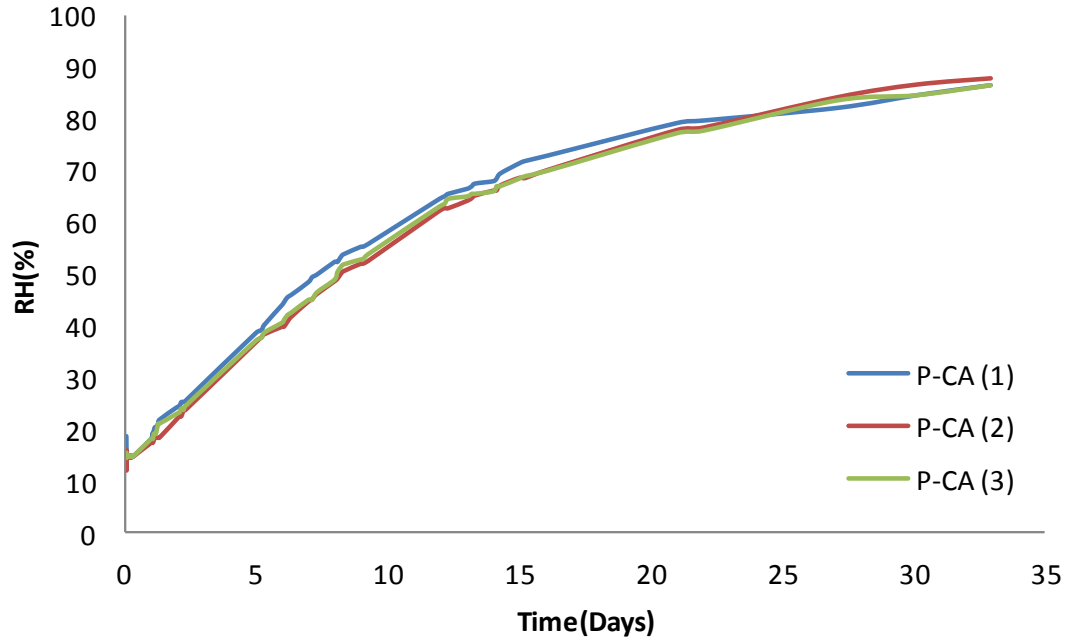

Figure 5.6 RH level in PEEK capsule joined with cyanoacrylate

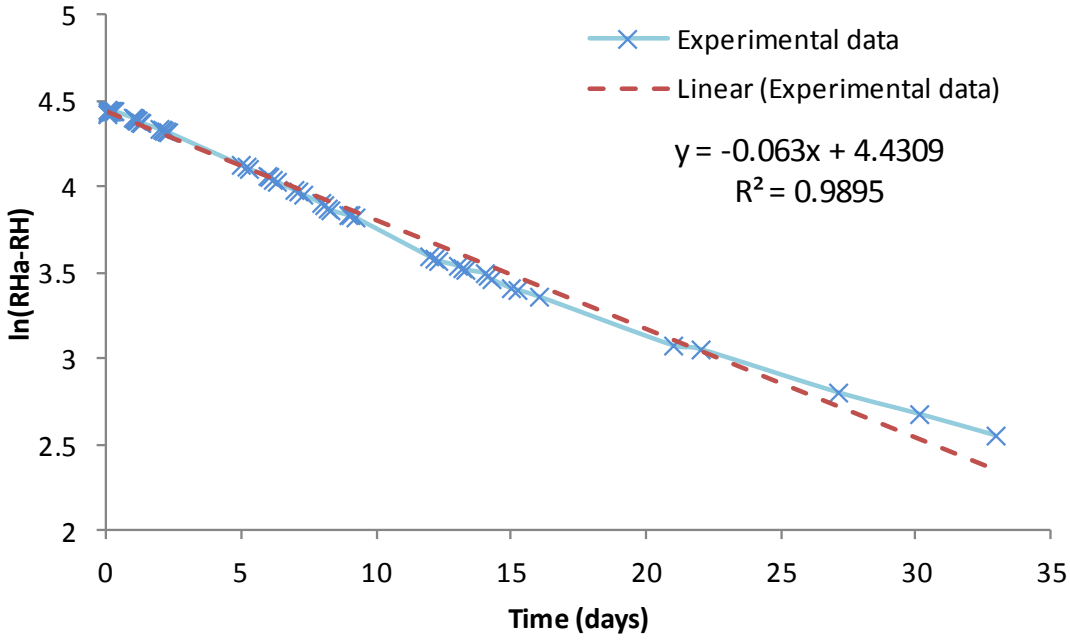

Figure 5.7 Extraction of the experimental time constant

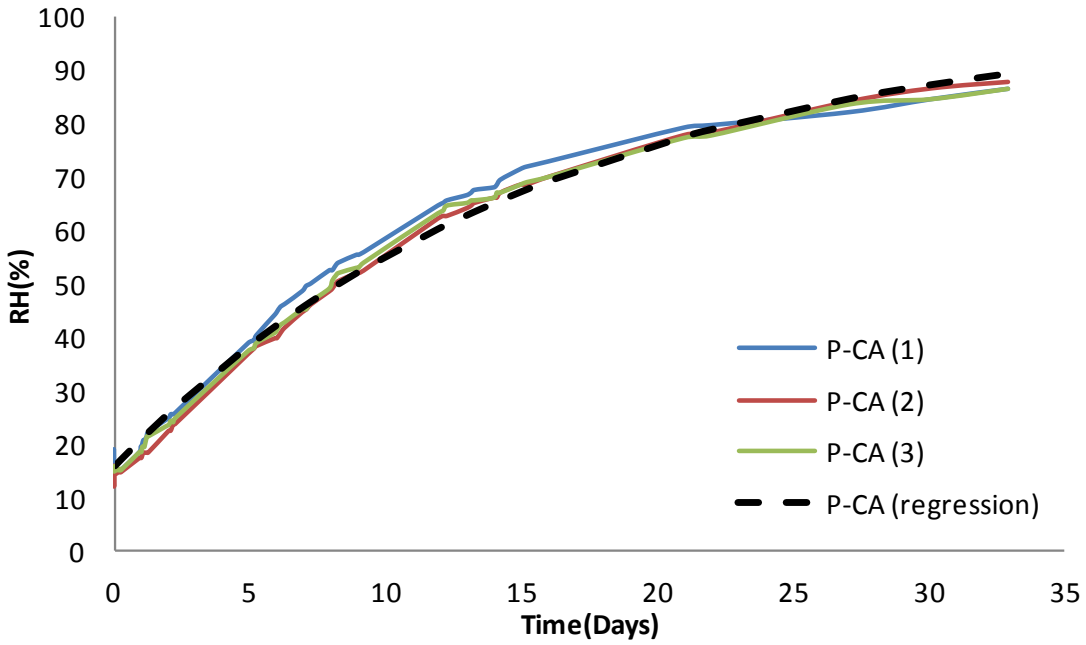

Figure 5.8 Comparison experiment vs. time constant found through linearisation and regression

5.2.3 Lifetime of adhesively joined PEEK packages

5.2.3.1 Moisture ingress into adhesively joined PEEK packages

We now compare moisture ingress in the PEEK capsule for the three different types of adhesive seals.

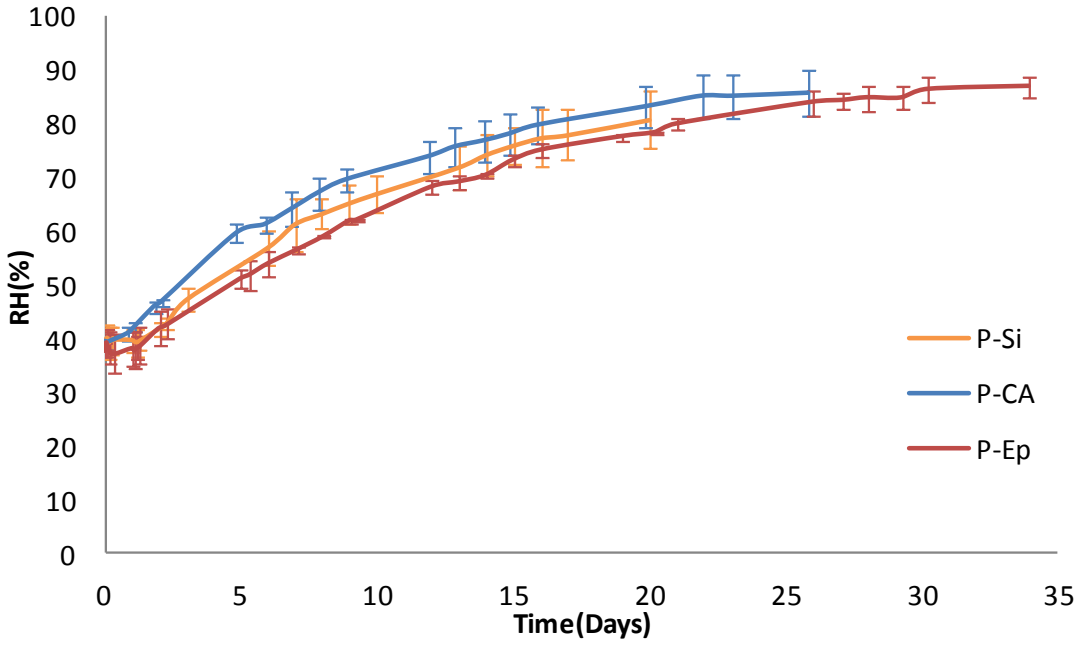

Figure 5.9 Moisture ingress into PEEK package with silicone, cyanoacrylate, and epoxy seal

Parameters	P-Si	P-CA	P-Ep
Time constant(days)	16.0	16.3	18.0

Table 5-3 Time constants for different types of seal

Figure 5.9 shows the evolution of RH for packages sealed with MED3-4013 (silicone), Loctite 4061 (cyanoacrylate), and Loctite Hysol M31-CL (epoxy). The time constants are presented in Table 5-3. They are 16, 16.3, and 18 days respectively. Even though some of the adhesives are in theory much more permeable than PEEK, those time constants are actually very similar, which suggests that, diffusion through the seal has a very limited effect on the overall diffusion. This is because the area available for diffusion through the seal is much smaller than the area available for diffusion through the bulk of the capsule. However, there is still a difference of 12-13% between the time constant of silicone and cyanoacrylate on one side, and epoxy on the other. This is because epoxies are several order of magnitude less permeable than silicones, as can be seen in Figure 5.10 from (Traeger 2002), which shows the permeability values for different types of materials.

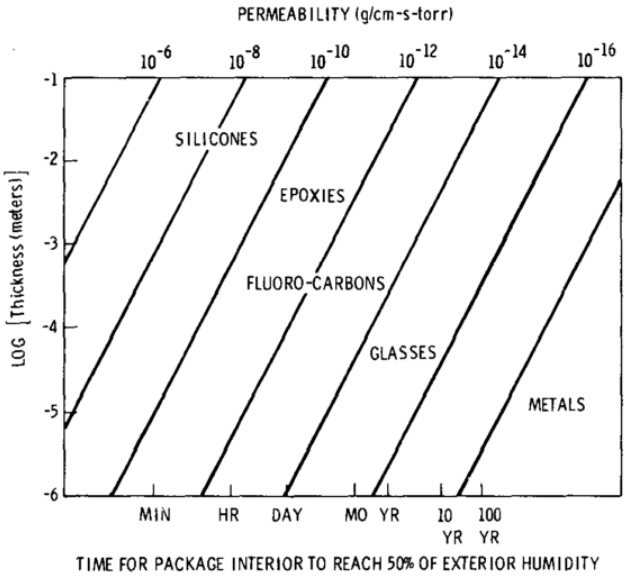

Figure 5.10 Effectiveness of sealant materials - from (Traeger 2002)

We can also evaluate the total amount of water which permeates through the package, including any moisture contained within the package walls, by placing capsules in a water bath at 37°C and weighing them periodically with a precision balance (Sartorius BP211D – Precision 10^{-5} g). The results for PEEK capsules joined with Loctite 4061 (cyanoacrylate) and Loctite Hysol M31-CL (epoxy) can be observed in Figure 5.11.

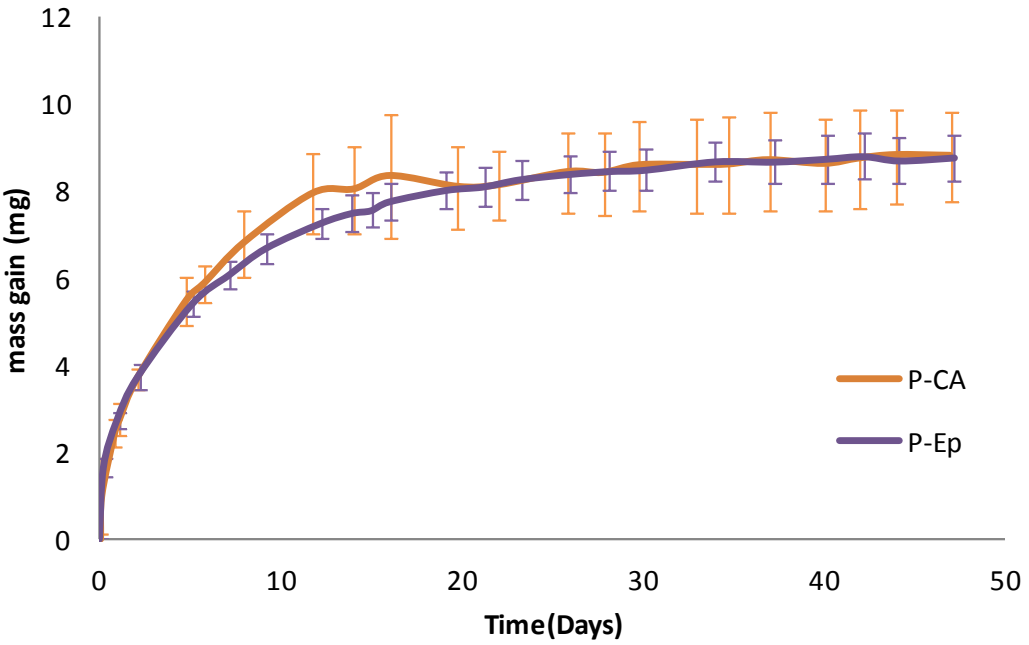

Figure 5.11 Mass gain of adhesively joined PEEK capsules in water

This figure shows that the amount of water absorbed by the capsule is exactly the same whether an epoxy or a cyanoacrylate seal is used. This is because the amount of water which permeates into the seal is negligible compared to the amount absorbed by the body of the capsule.

5.2.3.2 Water diffusion through the joint only – Metal capsules

In order to assess how much water actually diffuses through the seal, we can use 'hermetic' capsules, which will not let water through the body of the capsule. To this end, titanium capsules are used, which have dimensions exactly the same as the previously-tested PEEK capsules. Because the capsule is metallic, it is impermeable to water, but cannot be used with our telemetry system. A feedthrough is therefore necessary for power supply and data transfer. Detailed views and dimensions for both the capsule and the feedthrough are shown in 'Appendix 3. Solid Titanium capsule and feedthrough'. The feedthrough is laser welded to a holder, which is in turn laser welded to the capsule in order to guarantee hermeticity (see Figure 5.12). A wire is crimped with the feedthrough using a piece of gold tube (inside diameter 0.7 mm, 0.15 mm thickness). The body of the capsule is glued with silver filled epoxy to another wire and grounded. The base of these wires is encapsulated in silicone rubber to prevent leakage currents.

The capsules are then sealed with silicone (MED3-4013), cyanoacrylate (Loctite 4061) and epoxy (loctite Hysol M31-CL) adhesives (n=3 for each), and placed in water at 37°C (see Figure 5.13).

Figure 5.12 Titanium capsule

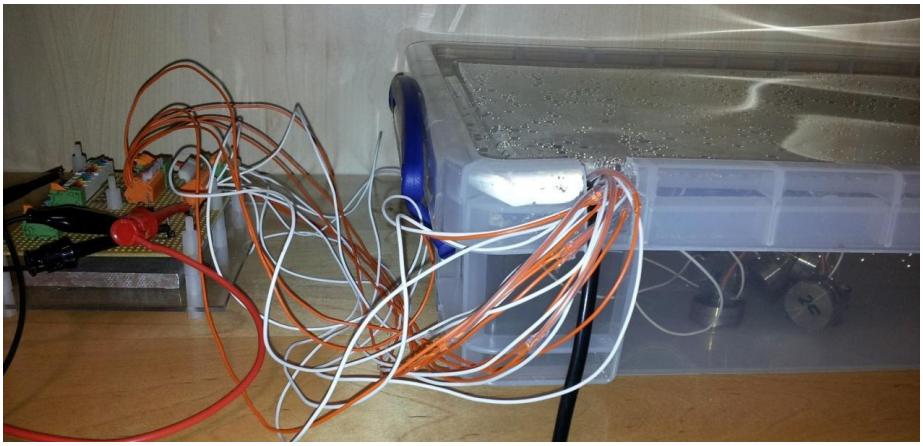

Figure 5.13 Titanium capsules in water

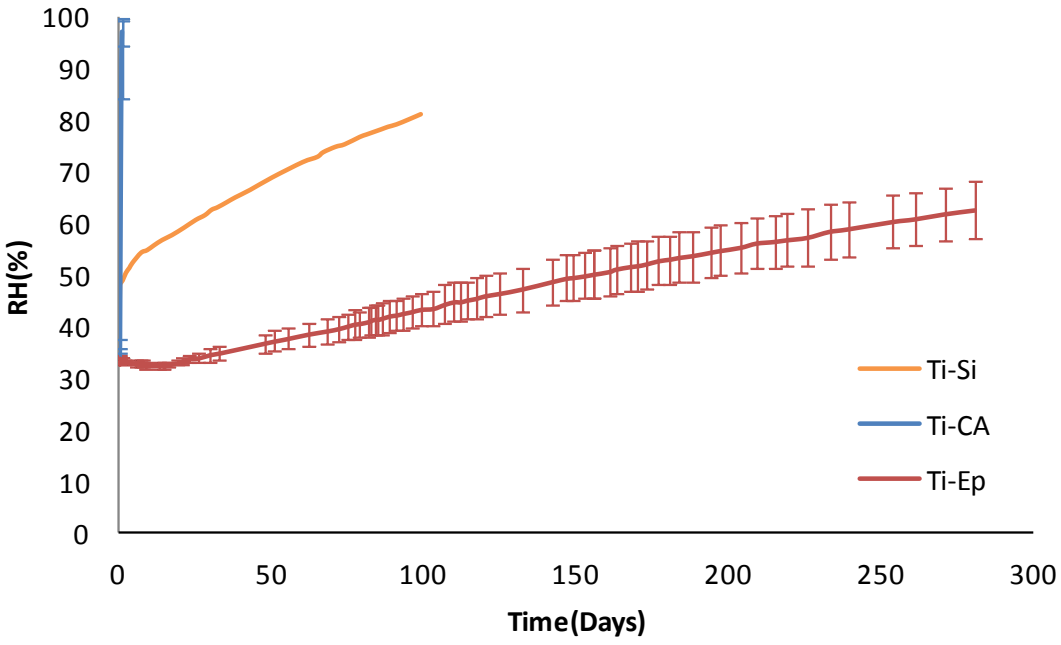

Figure 5.14 Evolution of RH with time for Ti capsules

The evolution of the relative humidity with time is plotted in Figure 5.14. In this instance, we find that the time constants vary greatly, from a few hours to a few hundred days. The time constants for the package with the silicone and epoxy seal are 102 days and 405 days respectively. This is very much in line with expectations, as can be seen from Figure 5.10, and confirms that diffusion through the seal alone is negligible compared with diffusion through the bulk of the PEEK capsule.

It is the result with cyanoacrylate which is unusual and unexpected, as it is much shorter than what was obtained with the PEEK capsule (0.4 days for the Ti capsule, 16.3 days for the PEEK package). This suggests that it cannot be due only to diffusion through the adhesive seal, but that there was adhesive failure which provided a path for moisture to penetrate at a much faster rate than it should. The most likely explanation is failure between titanium and the weak boundary layer covering it (oxide layer promoted by the presence of water – see 5.1.6).

Testing a cyanoacrylate seal with a capsule made of brass instead of titanium shows interesting results. The brass capsule is fitted with a welded feedthrough, and a ground wire is welded using low temperature solder wire in order to avoid re melting the feedthrough solder. The brass package is shown in Figure 5.15 and results of the experiment are plotted in Figure 5.16.

These results show that a similar phenomenon is happening. The moisture ingress is slow and steady before a point when it starts rising more abruptly. This tends to confirm that at some point failure of the joint occurs and affects the rate at which water vapour permeates the enclosure. For sample B, this inflexion occurs after only 18 days, whereas it takes 65 days for sample A and 75 days for sample C. Nevertheless, we can still evaluate and compare the rate of diffusion through cyanoacrylate by looking at the portion of plots for samples A and C before failure of the adhesive seal. Using the same method as previously, we find a time constant of 200 days, which is longer than for silicone, but shorter than the time constant associated with the epoxy seal. This results also highlights the obvious fact that the seal properties are different depending on the materials used (brass and titanium and PEEK). Whereas the PEEK/cyanoacrylate was very durable, the bond with titanium and brass was clearly affected by the presence of water.

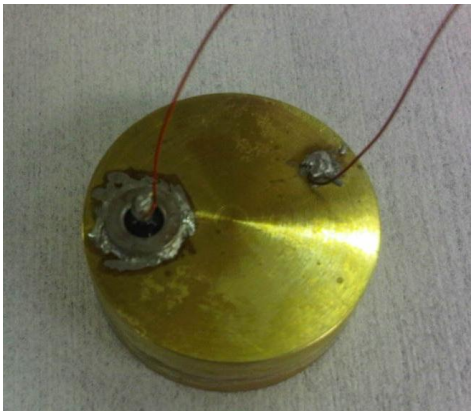

Figure 5.15 Brass capsule

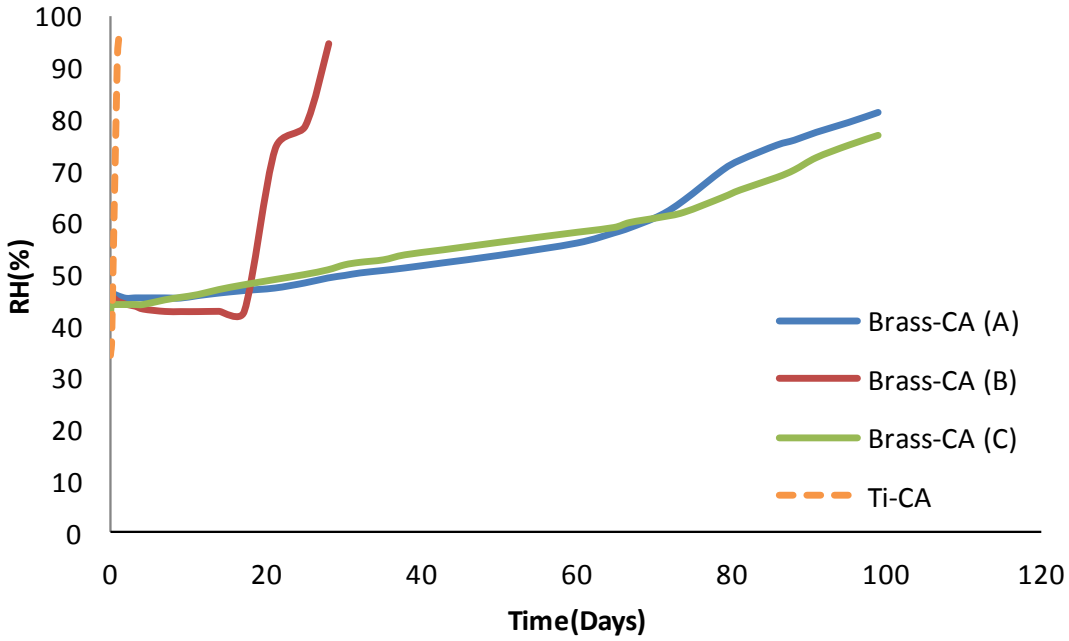

Figure 5.16 Evolution of RH with time for brass capsule with CA seal

5.2.3.3 Permeability coefficient of the seal materials

Now that we have determined the time constants of adhesively sealed packages with impermeable walls (i.e. diffusion is only occurring though the seal material), it is possible to find the associated experimental permeability coefficient K. Equation (3.6) gave the time constant as:

$$\tau = R_P(C_V + C_P)$$

Here, we can make the assumption that the amount of water absorbed in the seal is negligible compared to the amount of water in the cavity, as seen in Figure 3.11. We therefore neglect the capacitance C_p of the seal, and the time constant is now $\tau = R_p.C_V$; we are in the case of diffusion through a non absorbing membrane (see 3.2.2). According to equation (3.8), the permeability coefficient is therefore:

$$K = \frac{Vd}{\tau A} \tag{5.5}$$

We have found the time constants for the metal packages with silicone, cyanoacrylate and epoxy to be respectively 102, 200 and 458 days. The corresponding permeability coefficients are then 11.9×10^{-7} $cm^2.s^{-1}$, 6.1×10^{-7} $cm^2.s^{-1}$, and 2.7×10^{-7} $cm^2.s^{-1}$ respectively, using values in Table 6-6 for V, d, and A. However, it must be kept in mind that due to the assumption we made, these values are only approximations to give an idea of orders of magnitude, especially for silicone and epoxy which actually tend to absorb quite a bit of water. Nevertheless, our assumption is still correct as long as there is only a very thin thickness of adhesive present.

5.2.3.4 Durability of adhesive joints exposed to water

The durability of cyanoacrylate and epoxy joints with titanium in the presence of water can be evaluated by testing their shear strength before and after continuous exposure to water at 37°C. The geometry of the joint to test must be carefully thought through in order to avoid cleavage or peel stress. This can occur for instance if the bonded adherends are too thin or flexible, especially if the pulling is not in the line of the joint. To avoid or minimize this effect, there are different joint geometries which can be used, such as beveled, joggle laps, or strap joints (Petrie 2000, p.107). I decided instead to use a classic single lap joint geometry, but to design custom made grips which ensure that the pulling is done exactly in the line of the joint, and therefore that only shear stress is applied. The grip design is shown in Figure 5.17.

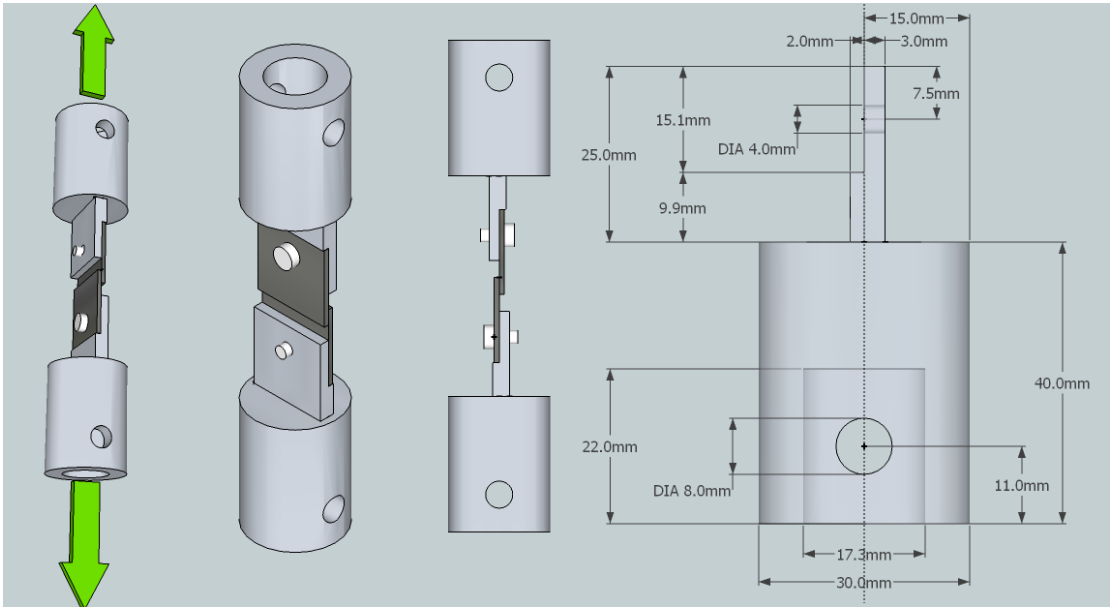

Figure 5.17 Design the grips for lap shear test

The pull test machine used is a Hounsfield OS11 Model H5k5, fitted with a 2.5kN strain gauge transducer. The set up is shown in Figure 5.18.

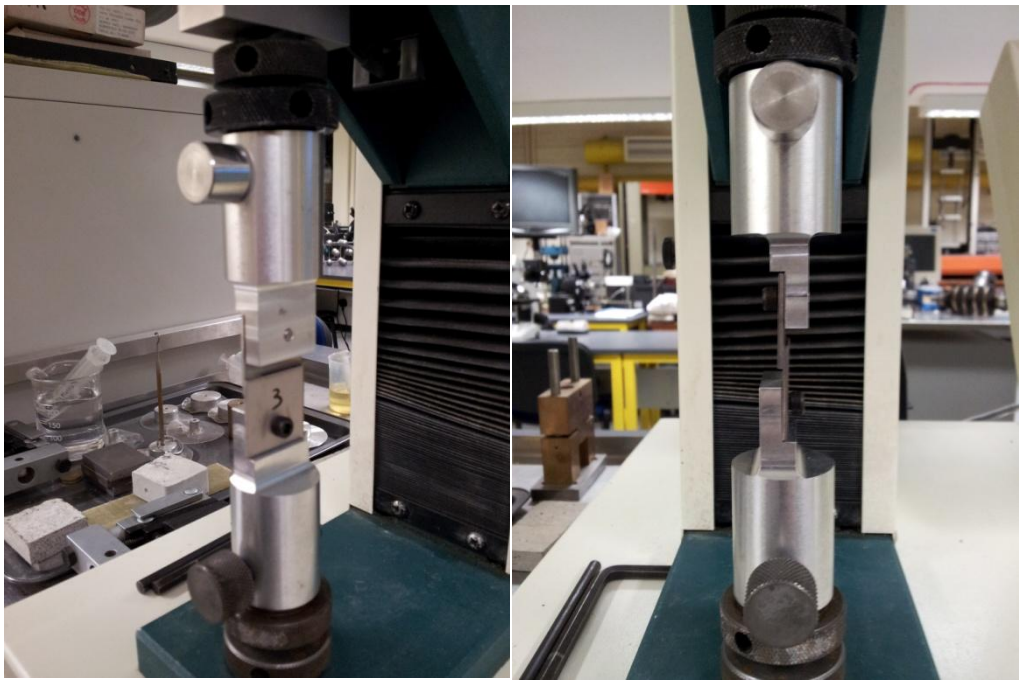

Figure 5.18 Lap shear test

In order to accelerate the ageing of the samples, they are placed in boiling water for different amounts of time and the effect of exposure to water on the bond strength is observed. The '10°C rule', commonly used in the literature, can be applied here to get an equivalent time at 37°C. This rule is based on a conservative approximation of an Arrhenius behavior, which assumes that the rate k of a chemical degradation process (in our case, hydrolysis of the joint by water) is proportional to $e^{(-Ea/RT)}$, with Ea the activation energy, R the gas constant, and T the absolute temperature. In that case, this '10°C rule' states that the rate of the chemical reaction will double for every 10°C increase in temperature (Hemmerich 1998). If t_1 is the time of exposure to the 'accelerated' temperature T_1, and t_2 the equivalent time of exposure at temperature T_2, we have the following equation:

$$t_2 = t_1 \times 2^{\frac{T_1 - T_2}{10}} \tag{5.6}$$

Using this equation, we find that the acceleration factor when T_1=100°C and T_2=37°C is 79. This means that 1 and 2 weeks exposure at 100°C is equivalent to 1.5 and 3 years respectively at 37°C. It is important however to notice that this should be used as a guideline only, as our acceleration factor was based on an Arrhenius model, which in our case is only an assumption, although this is commonly used and shown to be true in the literature for some epoxies on metal (Broughton & Mera 1997; Kinloch 1995; Schuettler

et al. 2011). Moreover, for every 10°C, we also double the error originally introduced by the assumptions linked to this model (Hemmerich 1998), which can lead to significant uncertainty on the final result.

25x25mm titanium squares are adhesively joined with either cyanoacrylate or epoxy, and placed in boiling water. The joint area measures 25x5mm. Their shear strength is then tested using the pull test machine. The results are summarized in Figure 5.19.

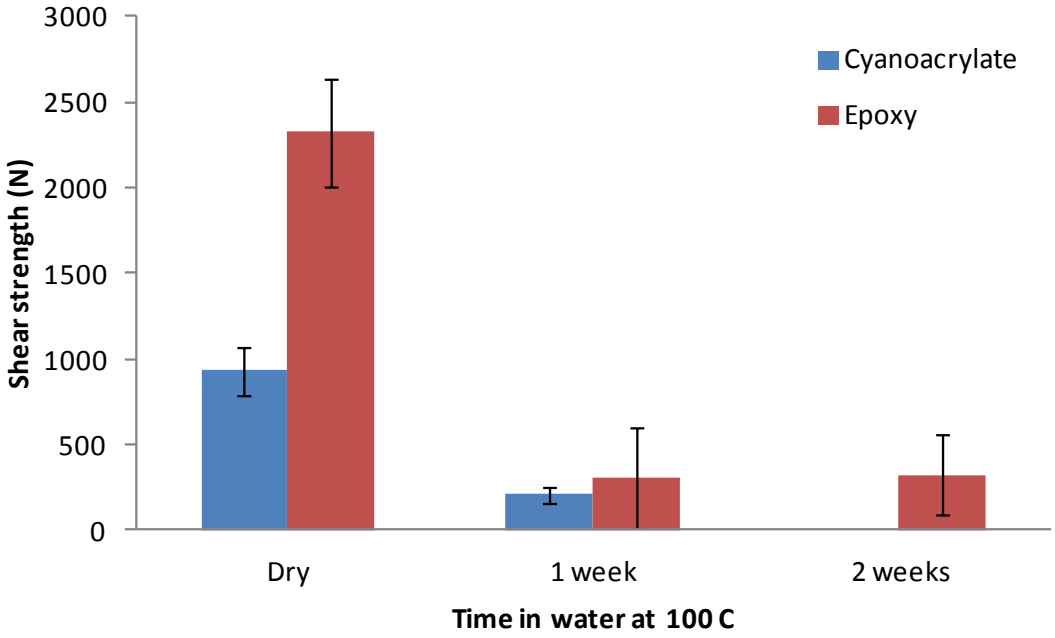

Figure 5.19 Shear strength of adhesively joined Ti squares in boiling water

For each time/adhesive combination, 3 samples were tested (n=3). Figure 5.19 shows the mean value for each. The standard deviation for each series is also displayed as error bars. When dry, the force applied leading to failure is 930 N and 2320 N for cyanoacrylate and epoxy respectively. After one week in boiling water (corresponding to 1.5 year to water at 37°C), the forces to failure are then 211 N and 306 N respectively. However, as shown by the error bars, there is a very large uncertainty on the 'epoxy' result. After two weeks, the samples joined with cyanoacrylate fail spontaneously, whereas the ones joined with epoxy fail at an average pulling force of 325 N. It is therefore interesting to notice that a fair amount of force is still required to pull the epoxy joined samples. This means that even after three years in water at 37°C, we do not expect the joint to fail spontaneously (i.e. with no stress applied to it). As for the cyanoacrylate joint, we have seen previously that their adhesion to titanium is compromised when exposed to water. For all the samples, failure was purely adhesive, which means that even though the cohesive strength of the joint is expected to drop, the adhesive strength is affected to a greater degree.

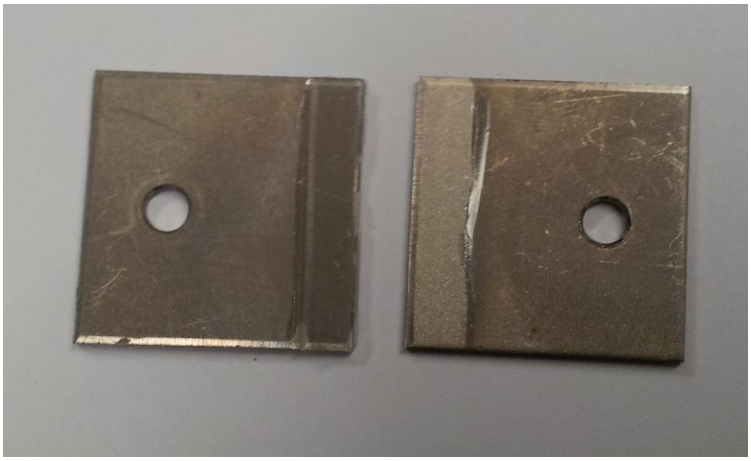

Figure 5.20 Failure of adhesive joint

Figure 5.20 shows the adhesive failure on the surface of one titanium sample. It is very interesting here to notice the colour difference between the titanium square and the area where the adhesive has failed. Here the cyanoacrylate adhesive very visibly removed the oxide layer from the surface of the substrate (see bright patch). This confirms that the failure of the cyanoacrylate joint of the metal capsules is due to a weak boundary layer of oxide, which is promoted by the presence of water and the action of the adhesive itself. It is therefore not an adhesive failure, but cohesive failure of the weak boundary oxide layer. It is also possible that the solvent in the cyanoacrylate adhesive affected the oxide layer on the surface of the titanium substrate in a way that precipitated its failure when exposed to water.

Adhesion to PEEK has obviously not shown the same problem, and it is expected from this experiment that spontaneous adhesive failure of the PEEK capsule adhesive joint should not occur within the lifetime of the package.

This phenomenon has been reported in the literature previously for metal/polymeric adhesive joints (Molitor et al. 2001), and surface treatments of the metal surface are recommended in order to improve mechanical interlocking (by increasing the surface roughness) and/or remove/replace the weak boundary oxide layer by a different type of layer which would form strong bonds with the adhesive while not being as susceptible to displacement by water.

5.2.3.5 Failure of adhesive joints - explanation

Exposure to moisture results in degradation of polymeric material primarily by hydrolysis, which affects the cross link density of the polymer (Broughton & Mera 1997). Looking at adhesive joints, water first accumulates to a critical concentration in the interfacial region, and hydrolysis in the long term causes failure of interfacial bonds (both primary and secondary), leading to loss of adhesive strength (Kinloch 1995; Gledhill et al. 1980). If the adhesive becomes detached, it then provides a path for increased

permeation, as we have seen in the case of adhesively joined metallic capsules. The critical concentration of water necessary for this to happen depends on the material temperature and stress (Davis 2003), and may not be reached within the lifetime of the joint, as seems to be the case for the PEEK capsule.

In the case of metallic substrates, water also weakens the oxide layer. This is because metal oxide surfaces are polar and attract water molecules which break the Van der Waals bonds between that surface and the substrate surface (Davis 2003; Drain et al. 1985). The Dupre relation represented by Equation (5.3) can be adapted to define the work of adhesion W_A in the presence of water as a function of the interfacial free energy adhesive/water γ_{AW}, substrate/water γ_{SW}, and adhesive/substrate γ_{AS} (Kinloch 1987):

$$W_A = \gamma_{AW} + \gamma_{SW} - \gamma_{AS} \tag{5.7}$$

When no water is present, $W_A>0$ and the bond is stable. In the presence of water however, W_A may become negative and the interface unstable. This weak boundary layer is then the cause of the adhesive failure, as it was the case for the metal capsules and the lap shear tests performed.

However, we have established that, when exposed to water at 37°C, the unstressed adhesively joined PEEK package does not experience adhesive failure over the course of its lifetime. Besides not having a weak oxide layer like metallic adherends, polymeric adherends have sometimes also been proved to dissolve into the uncured adhesive monomer, which results in a system with no true 'interface', therefore less subject to the effects of moisture (Drain et al. 1985).

5.2.3.6 Use of a polyefin primer

As mentioned in section 5.1.7, primers can sometimes be used to promote adhesion to low energy surfaces by adhering well both to the substrate and the adhesive. Instead of forming dispersive bonds, they can sometimes form covalent bonds, which are less susceptible to displacement by water. We can investigate whether the use of a primer with cyanoacrylate influences the rate of moisture ingress. The adhesive manufacturer recommends the use of a polyefin primer (Loctite 770) with the cyanoacrylate adhesive used (Loctite 4061). This type of primer has been proved very effective in producing strong bonds with dry samples (Tavakoli et al. 2004). PEEK capsules adhesively joined with Loctite 4061 + polyefin primer Loctite 770 were tested and results are presented in Figure 5.21.

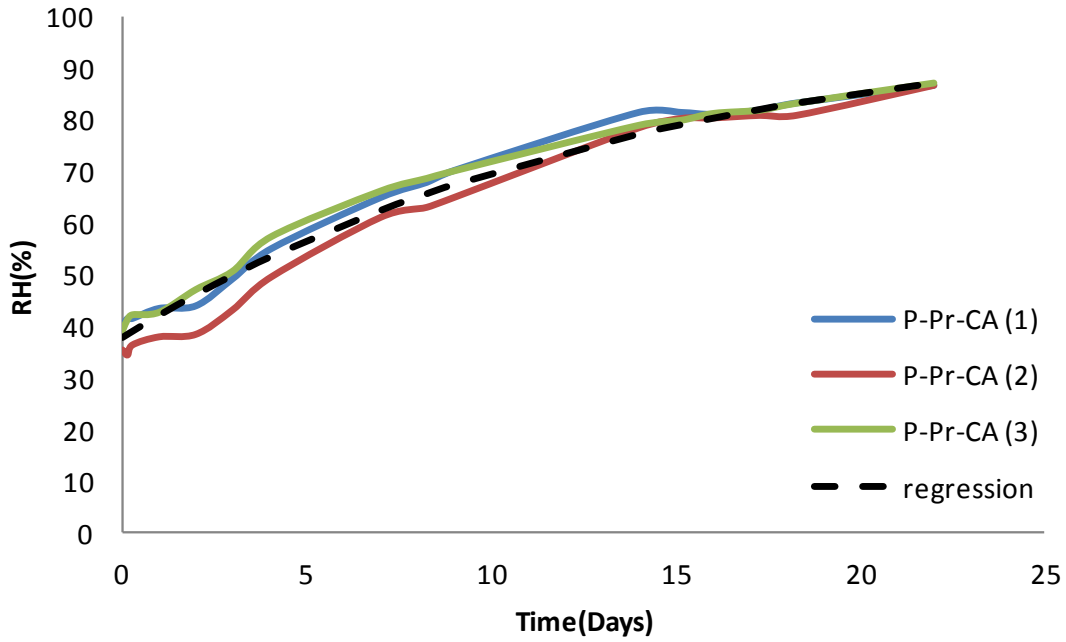

Figure 5.21 RH level in PEEK capsules joined with cyanoacrylate and polyefin primer

The average time constant associated with this bond is 13.6 days, which is actually less than the time constant when no primer is used (16.3 days). The same primer and adhesive are used with a titanium capsule such as described in section 5.2.3.2. The results are plotted in Figure 5.22, and show very similar results to those obtained without primer (see Figure 5.14 and Figure 5.16).

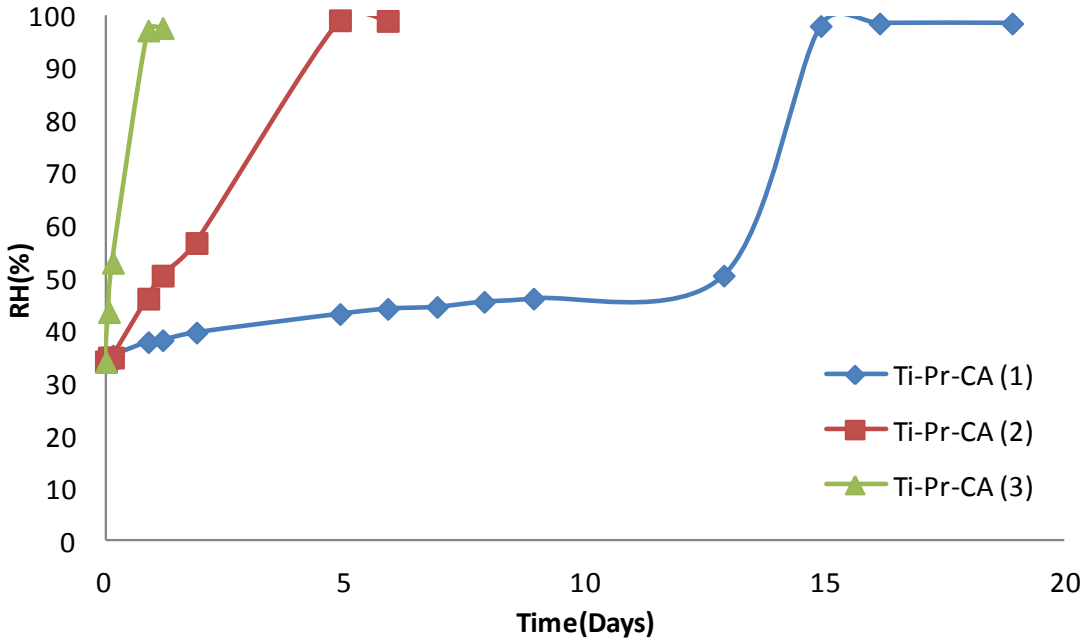

Figure 5.22 RH level in titanium capsule joined with cyanoacylate and polyefin primer

For two of the samples (2 and 3), there is almost immediate adhesive failure leading to very fast moisture ingress. The third sample shows a much slower moisture permeation

rate for a while, until its joint fails as well, allowing the water vapour content inside the package cavity to rise sharply. Moreover, the diffusion rate of the 'flat' part is actually once again faster than when no primer is used (time constant associated is 48 days, against 200 days for the adhesively joined brass capsule with no primer).

The ineffectiveness of the primer is confirmed when looking at the shear strength of adhesively joined titanium squares exposed to water, as presented in Figure 5.23. This result is not surprising: as we have seen, the reason adhesively joined metal substrates do not resist very well in water is because of the weak oxide boundary layer, so trying to improve the bond between the adhesive and the oxide layer cannot improve the adhesion between the substrate surface and the oxide layer, or the cohesive strength of that same layer. But as previously stated, this does not affect the bond between PEEK substrates. Nevertheless, we have seen that using this primer actually has an adverse effect on the resistance to water, which explains why the time constant is less than when no primer is used.

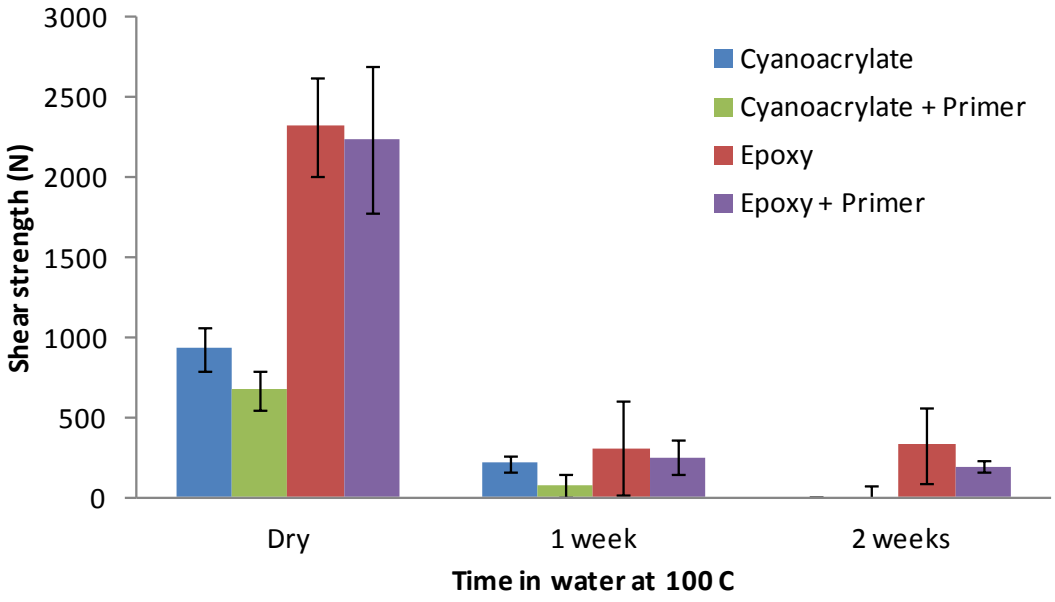

Figure 5.23 Shear strength of adhesively joined Ti squares in boiling water when a primer is used

5.3 Influence of the wall thickness on the lifetime

NB: Parts of this section are extracted from (Dahan et al. 2013), which was published during the course of this project.

So far we have established that our calculation model fits the experimental results very well, and that an adhesively joined PEEK capsule has a lifetime varying between 16 and 18 days, depending of the type of adhesive joint used. Using this calculation method, it is

then possible to establish the influence of the wall thickness and the size of the implant cavity on the package lifetime.

We can examine the influence of the wall thickness on the time constant, by looking at the theoretical case of a cylindrical PEEK enclosure of constant thickness d (see Figure 5.24). We can use either Tencer's model (equation (2.16)) or ours (equation (3.6)). They are exactly equivalent in this case because of the geometry considered (uniform thickness).

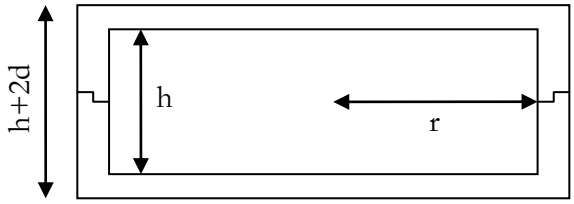

Figure 5.24 Cylindrical enclosure of constant wall thickness d - section

For ease of calculation, the cylindrical package considered is such that the internal height h of the cavity is equal to its internal radius r. This radius can then be expressed as a function of the internal cavity volume V_C:

$$r = \sqrt[3]{\frac{V_C}{\pi}} \tag{5.8}$$

The external surface area A_C of this enclosure is:

$$\begin{aligned} A_C &= 2\pi(r+d)^2 + 2\pi(r+d)\cdot(r+2d) \\ &= 2\pi(r+d)\cdot(2r+3d) \end{aligned} \tag{5.9}$$

And therefore the internal cavity volume of this cylinder and its external surface area can be related:

$$A_C = 2\pi\left(\sqrt[3]{\frac{V_C}{\pi}} + d\right)\left(2\cdot\sqrt[3]{\frac{V_C}{\pi}} + 3d\right) \tag{5.10}$$

The formula for the time constant then becomes:

$$\tau = \frac{V_C.d}{K\times 2\pi\left(\sqrt[3]{\frac{V_C}{\pi}} + d\right)\left(2\cdot\sqrt[3]{\frac{V_C}{\pi}} + 3d\right)} + \frac{d^2}{2D} \tag{5.11}$$

Using this formula, we can calculate the predicted time constant for packages of varying cavity volume and wall thickness. The results are plotted in Figure 5.25.

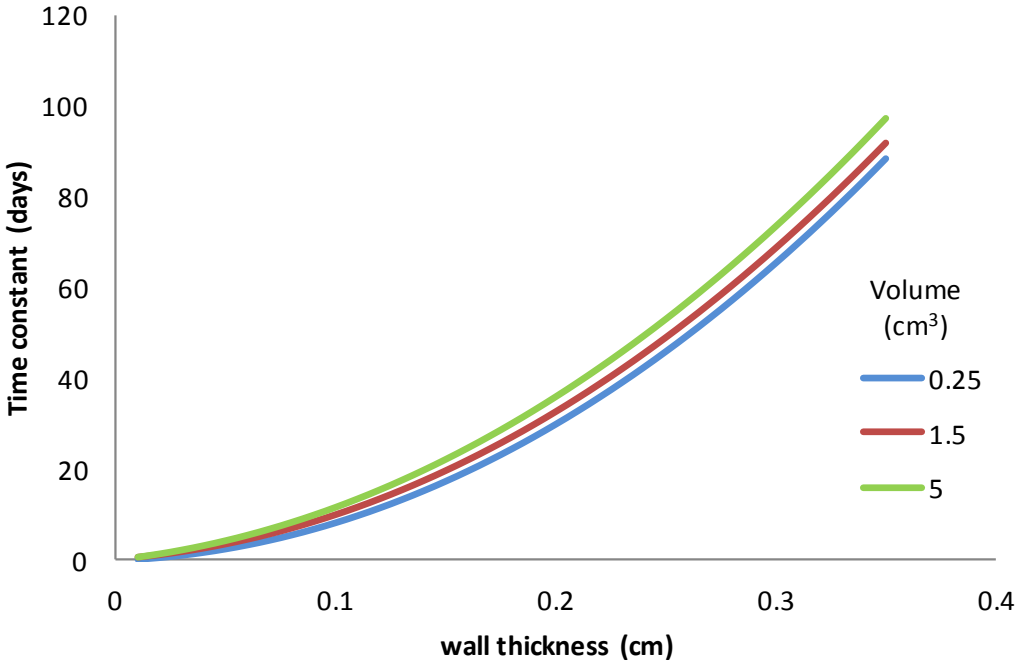

Figure 5.25 Influence of wall thickness and cavity volume on the time constant for a cylindrical package

It can be noted that the cavity volume has very little influence on the time constant. This is because, as the cavity volume increases, so does the external surface area. The package is made of a porous material, so the effect of increasing cavity volume V_C is compensated by an increase of surface area A.

The wall thickness however has a major impact on the time constant (quadratic function for d large – see equation (5.11)). By pushing the thickness of the package wall to 3 mm, we can obtain a maximum time constant of nearly 69 days, for a package with a 1.5 cm^3 cavity volume (same order as our PEEK capsule).

5.4 Summary and conclusion

In this chapter we have compared three types of adhesives to be used as sealing materials for the PEEK package. The results of these tests are summarized in Table 5-4 (10 experiments – n=3 – so 30 capsules were tested overall). We have found that although none of the adhesive joints are likely to fail if unstressed within the lifetime of the capsule, due to the action of water, the epoxy adhesive has proved to be the most durable and least permeable option.

However, we have seen that the chosen adhesive only has a limited impact on the time constant of the package (up to 10%) when looking at such short lifetimes (less than a month). Experiments with adhesively joined metal capsules showed that the amount of water diffusing through the seal is 20 times less than the amount of water permeating the

adhesively joined PEEK capsule. It is therefore perfectly acceptable to use adhesive bonding to seal the packages, and other more complex and expensive fusion welding methods are not necessary.

Nevertheless, it must be kept in mind that if a method was found, that significantly reduces the amount of water diffusing through the body of the PEEK capsule, then the amount of water diffusing through the seal would be a greater proportion. The metal capsule experiments also demonstrated that the cyanoacrylate/metal interface fails very quickly when exposed to water, and therefore it should be avoided unless the metal is treated appropriately by removing weak boundary layers, promoting strong chemical bonds and mechanical interlocking. Alternatively, epoxy/metal interfaces proved to be very durable.

Finally, using our calculation method, we produced a guideline graph which can be used to quickly assess the time constant of PEEK packages of various size and thickness. In the next two chapters, we will investigate the use of desiccants and metal coatings with the aim of prolonging this lifetime.

Parameters	Time constant (days)	Comments
PEEK + Cyanoacrylate seal (Loctite 4061)	15.9	--
PEEK + Cyanoacrylate seal	16.3	--
PEEK + Epoxy seal (Loctite Hysol M-31CL)	18.0	--
PEEK + Silicone seal (NuSil MED3-4013)	16	--
Ti + Cyanoacrylate seal	N/A	Immediate failure
Ti + Epoxy seal	405	--
Ti + Silicone seal	102	--
Brass + Cyanoacrylate seal	Variable	Time constant before failure of joint is 200 days
PEEK + Polyefin primer (Loctite 770) + Cyanoacrylate seal	13.6	--
Ti + Polyefin primer (Loctite 770) + Cyanoacrylate seal	Variable	Quick failure of adhesive joint

Table 5-4 Summary of results

Chapter 6 Prolonging the lifetime using a desiccant

This chapter assesses the extent to which the lifetime of a PEEK package can be extended using desiccant. The theory of adsorbents and desiccants is first studied, following which silica gel and molecular sieve are selected as the best types of desiccant for our application. The calculation model developed in Chapter 3 is expanded to the use of desiccant and tested experimentally. It is found that it provides a very good approximation of the time constant when silica gel is used, but that it is not applicable to molecular sieve. This result is linked to the type of isotherm of those desiccants. Finally, guideline graphs and tables are provided to evaluate the time constant of PEEK packages of various sizes, wall thickness, cavity volume, and desiccant content.

6.1 Desiccants and adsorption – Literature review

6.1.1 Introduction on adsorbents

In order to prolong the lifetime of electronics within a package, one method is the use of a desiccant which will adsorb water and therefore increase the maximum amount of water which can penetrate the enclosure before presenting a threat. Let us first review the different types of desiccants and the processes involved in the adsorption of moisture.

Adsorption technology is used in a wide range of applications in order to separate and purify gases and liquids (See Table 6-1 for a list of separation made by adsorption). Adsorbents can be used for instance to remove smells or moisture from air, or to refine oils and fat. In our case, we are only interested in adsorbents which help remove moisture from air. These particular types of adsorbents, which have a special affinity for water, are referred to as desiccants.

6.1.2 Types of desiccant

As for all types of adsorbents, desiccants use adsorption to attract and retain moisture. It is a surface phenomenon, and therefore the high capacity of an adsorbent depends on the high internal surface area per unit of mass. These can range from 100 $m^2.g^{-1}$ to 3000 $m^2.g^{-1}$ (Crittenden & Thomas 1998).

The capacity and selectivity of an adsorbent depends on its pores size (see 6.1.3 Adsorption equilibrium). While some adsorbents such as zeolitic molecular sieves have uniform pore sizes, others show a range of pore sizes organised in interconnected networks (silica gels, aluminas). There are three types of pores: micropores which are smaller than 2 nm, mesopores which have diameters ranging from 2 to 50 nm, and macropores which are in excess of 50 nm (Crittenden & Thomas 1998). As we will see

later, this plays a great part in determining the isotherm type of the adsorbent (see 6.1.3.1).

As explained in a previous section on adhesive bonding (see 5.1.5 Theories of adhesion), adsorption can be of two types, physisorption or chemisorption. However, almost all adsorptive separation processes depend on physical adsorption rather than chemisorption (Ruthven 1984, p.30), and therefore water bonds to the surface of the adsorbent by physisorption only (especially Hydrogen bonding). As a result, the secondary bonds (dispersion forces, dipole and hydrogen bonds) can be broken easily by heat, the desiccant can be regenerated, and its potential for adsorption restored.

Separation[A]	Adsorbent
Gas Bulk Separations	
Normal paraffins, isoparaffins, aromatics	Zeolite
N_2/O_2	Zeolite
O_2/ N_2	Carbon molecular sieve
CO, CH_4, CO_2, N_2, A, NH_3/ H_2	Zeolite, activated carbon
Acetone/vent streams	Activated carbon
C_2H_4/vent streams	Activated carbon
H_2O/ethanol	Zeolite
Gas Purifications[C]	
H_2O/ air, olefin-containing cracked gas, natural gas, synthesis gas, etc.	**Silica, alumina, zeolite**
CO_2/C_2H_4, natural gas, etc.	Zeolite
Organics/vent streams	Activated carbons, others
Sulfur compounds/natural gas, hydrogen, liquefied petroleum gas (LPG), etc.	Zeolite
Solvents/air	Activated carbon
Odours/air	Activated carbon
NO_X/N_2	Zeolite
SO_2/vent streams	Zeolite
Hg/chlor-alkali cell gas effluent	Zeolite
Liquid Bulk Separations[B]	
Normal paraffins, isoparaffins, aromatics	Zeolite
p-Xylene/*o*-xylene, *m*-xylene	Zeolite
Detergent-range olefins/paraffins	Zeolite
p-Diethyl benzene/isomer mixture	Zeolite
Fructose/glucose	Zeolite
Liquid Purifications[C]	
H_2O/organics, oxygenated organics, chlorinated organics, etc.	Silica, alumina, zeolite
Organics, oxygenated organics chlorinated organics, etc./H_2O	Activated carbon
Odour, taste bodies/drinking H_2O	Activated carbon
Sulfur compounds/organics	Zeolite, others
Various fermentation products/fermentor effluent	Activated carbon
Decolorizing petroleum fractions, sugar syrups, vegetable oils, etc.	Activated carbon
[A] Adsorbates listed first. *[B] Adsorbate concentrations of about 10 wt. % or higher in the feed.* *[C] Adsorbate concentrations generally less than about 3 wt.% in the feed.*	

Table 6-1 Representative Commercial Adsorption Separations - From (Keller II 1987)

Adsorption of water is always accompanied by an increase in heat (exothermic process), '*the extent of which depends mainly on the magnitude of the Van der Waals forces involved, phase change, electrostatic energies and chemical bonds*' (Srivastava 1998).

We can review the main types of desiccants and their properties:

6.1.2.1 Molecular Sieve Zeolites

Zeolites are alluminosilicates of crystalline porous structure. This structure constitutes the 'pores' of the adsorbent which the adsorbate penetrates. Because of this natural crystal form, there is no distribution of pore size. The lattice is uniform and the size of its channels determines which products it will adsorb. This feature is what distinguishes zeolites from other types of microporous adsorbents. Zeolites are also polar by nature. SiO_4 and AlO_4 tetrahedra assemble to form the zeolite framework in various regular arrangements through the sharing of oxygen atoms (Ruthven 1984). Differences based on molecular size, shape and other properties such as polarity are the differences on which the process of adsorption is based (Crittenden & Thomas 1998). A zeolite structure is represented by the crystal unit cell of formula:

$$M_{x/n}[(AlO_2)_x(SiO_2)_y] \cdot wH_2O$$

where n is the valence of the cation M, w is the number of water molecules per unit cell and x and y are the total number of tetrahedra per unit cell (Keller II 1987). The cation M balances the negative charge introduced by the aluminium atom, because of the 2/1 ratio oxygen to aluminium, with respectively 2 negative and 3 positive charges each. The type and position of this exchangeable cation determine the channel size and therefore the properties of the zeolite (Crittenden & Thomas 1998).

There are more than 150 types of synthetic zeolites known, and some typical commercially available molecular sieve zeolites and properties are presented in Table 6-2.

Zeolite Type	Designation	Cation	Pore Size (nm)	Bulk Density ($kg.m^{-3}$)
A	3A	K	0.3	670 -740
	4A	Na	0.4	660 - 720
	5A	Ca	0.5	670 - 720
X	13X	Na	0.8	610 - 710
Mordenite, small port	Zeolon-300	Na + mixed cations	0.3 - 0.4	720 - 800
Chabazite	AW-300	Mixed cations	0.4 -0.5	640 - 720

Table 6-2 Commercial Molecular Sieve adsorbents and properties - From (Keller II 1987)

The choice for zeolite type depends on the application and the substance to be adsorbed and hence on the pore size. For water adsorption, types 3A and 4A are used as desiccants, as their small pore sizes (respectively 0.3 and 0.4nm) only allow water and very few other small molecules to be adsorbed (see Figure 6.1). They use respectively

potassium and sodium as cations, and their formulas are $K_{12}[(AlO_2)_{12}(SiO_2)_{12}]$ and $Na_{12}[(AlO_2)_{12}(SiO_2)_{12}]$ (Ruthven 1984).

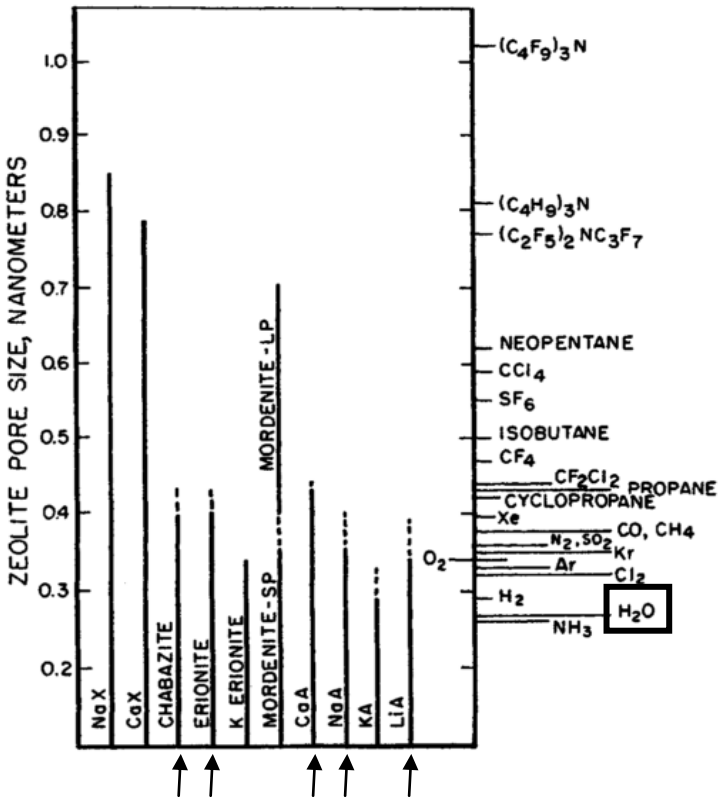

Figure 6.1 Molecular dimensions and zeolite pore size (From (Breck 1974))

6.1.2.2 Silica gels

Silica gel, of formula $SiO_2.nH_2O$, is a partially dehydrated form of polymeric colloidal silicic acid. It is amorphous, chemically inert, and polar. During manufacturing, chains and nets of linked SiO_4 tetrahedra aggregate to form spherical particles. They agglomerate upon drying and treatment, and their size mainly determines the pore size of the microporous structure formed (Ruthven 1984). As a result, there is a large distribution of pore size, which varies from 1 to 40 nm (see Table 6-3) and influences the adsorption capacity of the desiccant (Yang 2003).

	Physical Properties
Surface area ($m^2.g^{-1}$)	830
Density ($kg.m^{-3}$)	720
Reactivation temperature (°C)	130-280
Pore volume (% of total)	50-55
Pore size (nm)	1-40
Pore volume ($cm^3.g^{-1}$)	0.42
Adsorption Properties	**Percent per weight**
H_2O capacity at 4.6 mm Hg, 25°C (19.3% RH)	11
H_2O capacity at 17.5 mm Hg, 25°C (73.6% RH)	35

Table 6-3 Typical Properties of Adsorbent-Grade Silica Gel (From (Keller II 1987))

Hydroxyl groups are present on the surface and confer it a degree of polarity, which favours the adsorption of polar molecules such as water by hydrogen bonding. Silica gel can exhibit surface areas of over 800 $cm^2.g^{-1}$.

6.1.2.3 Activated aluminas

Activated alumina is a porous high-area form of aluminium oxide Al_2O_3. Like silica gel, it has a range of pore sizes (although not as wide) which means that its capacity is strongly dependent on the ambient relative humidity. However, as shown on Table 6-4, the adsorption capacity ultimately is not as great as silica gel, which would therefore be a better choice of desiccant.

	Physical Properties
Surface area ($m^2.g^{-1}$)	320
Density ($kg.m^{-1}$)	800
Reactivation temperature (°C)	150-315
Pore volume (% of total)	50
Pore size (nm)	1-7.5
Pore volume ($cm^3.g^{-1}$)	0.40
Adsorption Properties	Percent per weight
H_2O capacity at 4.6 mm Hg, 25°C (19.3% RH)	7
H_2O capacity at 17.5 mm Hg, 25°C (73.6% RH)	16

Table 6-4 Typical Properties of Adsorbent-Grade Activated Alumina - From (Keller II 1987)

6.1.2.4 Isotherms and comparison of molecular sieve and silica gel

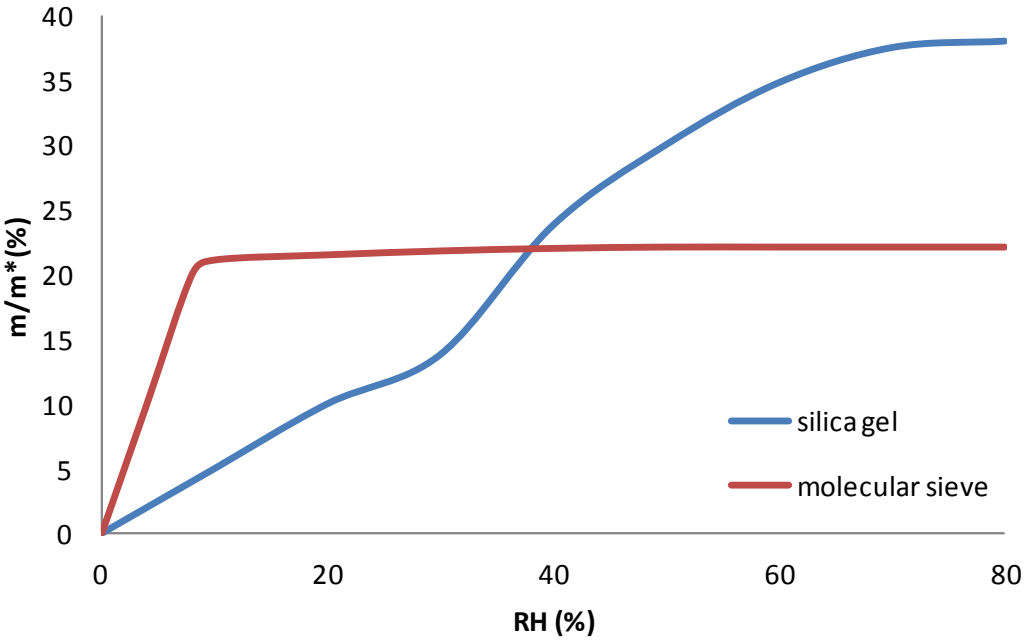

Figure 6.2 Adsorption isotherms for molecular sieve and silica gel at 25°C - From (Desiccare Inc. 2010)

Figure 6.2 shows the adsorption isotherms of silica gel and molecular sieve, i.e. the evolution of the adsorption capacity (represented here by the ratio *mass of water adsorbed/dry mass of desiccant)* vs. the partial pressure of water in the air to dry (which is equivalent to the relative humidity for a constant temperature).

The isotherm of silica gel shows that the capacity rises constantly with RH, due to the distribution of pore sizes, and will reach its maximum value at high humidities. Conversely, molecular sieve desiccant reaches its full capacity at much lower RH, as the pores all have the same size. As a result, molecular sieve is much more effective at low RH. However, when reaching high humidities, silica gel offers a greater capacity. The use of one or the other will hence depend on the application, and it is important to keep these properties in mind when selecting a desiccant.

6.1.3 Adsorption equilibrium

6.1.3.1 The five types of experimental adsorption isotherms

As we have seen previously, the isotherm is the function relating the quantity of gas q adsorbed and the steady state equilibrium partial pressure p at constant temperature (Crittenden & Thomas 1998). To allow a comparison of different materials, the quantity adsorbed is generally normalised by the dry mass of the adsorbent, which then gives the capacity of the adsorbent as a percentage of its dry mass.

The isotherms for physical adsorption have been divided into the five main classes experimentally observed (Brunauer et al. 1940), which are represented in Figure 6.3.

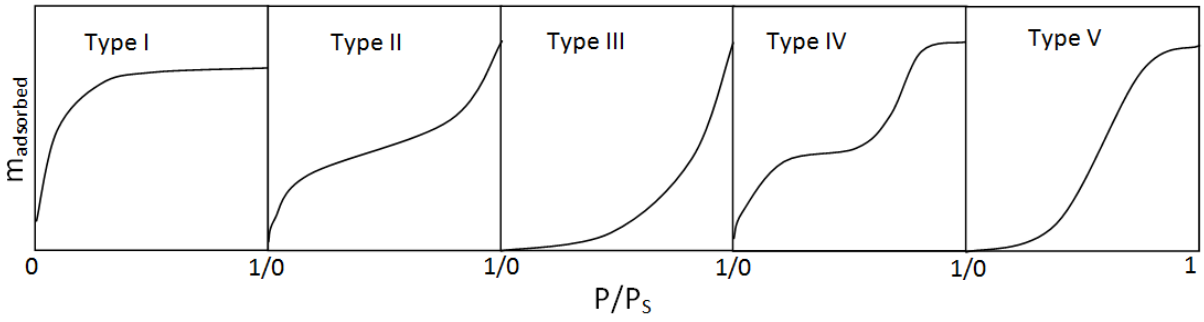

Figure 6.3 The five types of adsorption isotherms

Among these, the most common are by far types I, II and IV (Crittenden & Thomas 1998).

- Type I characterises adsorption when it is limited to one monolayer of adsorbate at the adsorbent surface. It is valid for true microporous adsorbents, as the pore size is of the same order as the size of the molecule to adsorb. When the micropores are filled, which corresponds to the completion of a molecular layer, a saturation limit is reached. This type of isotherm is therefore observed for molecular sieve (see Figure 6.2), which has a uniform pore size.

- On type II isotherms, the completion of a monolayer corresponds to the inflexion of the curve (see Figure 6.3). After this, adsorption occurs in indefinite successive layers, and then in capillary condensation as the diameter of the pores increases with the pressure. As a result, there is no saturation limit exhibited by these adsorbents. This is due to the large distribution pore sizes within the material.
- Similarly, adsorbents which exhibit the type III behaviour also have a wide pore size range. In this case however there is a steady increase in adsorption as the vapour pressure rises
- Type IV isotherms are similar to type II isotherms at low vapour pressure, but a saturation limit is reached as the pressure increases. This suggests that there is a finite number of multi layers, which corresponds to complete filling of the capillaries. This is the type of isotherm which matches the behaviour of silica gel (see Figure 6.2).
- Finally, an isotherm of type V is observed when there are large intermolecular attraction effects. They are similar to type III isotherms, except for the fact that it exhibits a saturation limit when the vapour pressure increases.

6.1.3.2 Adsorption equilibrium theories

There is a variety of different isotherm equations and theories which attempt to describe the adsorption equilibrium of adsorbents. Two of the main models will be described here, corresponding respectively to monolayer and multilayer adsorption.

6.1.3.2.1 The Langmuir and Langmuir-Freundlich isotherms

Langmuir developed the simplest theoretical model for monolayer adsorption as he tried to represent chemisorption on localised sites (Langmuir 1916). This corresponds to the type I model of the Brunauer classification (Figure 6.3), and is based on the following assumptions:

- All molecules are adsorbed through the same mechanism, at a fixed number of defined localised sites.
- All the adsorption sites are energetically equivalent
- There is no interaction between adsorbed molecules
- Each site can only adsorb one molecule. Therefore there is only one monolayer formed at most.

If θ represents the fraction of the adsorption sites occupied

$$\theta = \frac{q}{q_m} \tag{6.1}$$

where q_m is the quantity q of adsorbate adsorbed in one monolayer.

Langmuir defined the rate of adsorption as being proportional to the partial pressure P of the gas and the fraction (1-θ). This fraction represents the surface still available for adsorption sites. Similarly, he supposed that the rate of desorption was directly proportional to the fractional surface coverage θ. At equilibrium, the rate of adsorption onto the bare surface and the rate of evaporation from the first layer of adsorbate are equal, which yields the following equation:

$$k_a P(1-\theta) = k_d \theta \tag{6.2}$$

where k_a and k_d are respectively the rate constants for adsorption and desorption, and P is the partial pressure of the adsorbate (gas). This equation can be rearranged and the adsorption equilibrium constant K (also called Langmuir constant) is defined such as:

$$\frac{\theta}{1-\theta} = \frac{k_a}{k_d} P = KP \tag{6.3}$$

The commonly quoted form of the Langmuir isotherm is then:

$$\theta = \frac{q}{q_m} = \frac{KP}{1+KP} \tag{6.4}$$

The Langmuir model is a good fit for Type I isotherms which are characteristic of true microporous adsorbents such as molecular sieve. At low pressures, this isotherm can be reduced to a linear form (or Henry's law form):

$$\theta = \frac{q}{q_m} = KP \tag{6.5}$$

6.1.3.2.2 The BET equation

The four assumptions on which the Langmuir model is based are not always correct. This is especially true when it comes to limiting adsorption to one monolayer of adsorbate. Indeed, for non microporous surfaces (e.g. silica gel), a large proportion of pores can accommodate more than one molecule. In this case, multilayer adsorption is occurring and the formation of layers n>1 starts well before the completion of the first monolayer. This can be seen for instance on isotherms of type II and IV (Figure 6.3), where the point of inflexion corresponds to the filling of the first monolayer.

The problem of multilayer adsorption is addressed by the BET isotherm (Brunauer 1938), which most useful form is

$$\frac{P}{q(P_S - P)} = \frac{1}{q_m c} + \frac{(c-1)}{q_m c} \cdot \frac{P}{P_S} \tag{6.6}$$

where P_S is the saturation vapour pressure of the adsorbate, and c is the BET equivalent of the constant K we used in the Langmuir equation. It represents for each layer the ratio of rate constants for adsorption and desorption. The BET theory assumes that c is constant across layers for a given temperature. Like the Langmuir theory, it also assumes that there is no interaction between neighbouring molecules of adsorbate.

This expression has the general form of a type II isotherm (Ruthven 1984), but c and q_m can be chosen so that it can fit any of the isotherms types II to V included (Crittenden & Thomas 1998).

6.1.4 Rate of adsorption

As mentioned previously, water adsorption by desiccants is done by physisorption. The Van der Waals forces occurring have very small energy barriers to overcome. The bonding should therefore normally be extremely rapid. However it has been noted that different types of transport resistances limit this rate significantly. These different types, inter and intraparticle, occur in series (Crittenden & Thomas 1998).

The main resistance identified is the limit imposed to the transport of gas to the surface available for bonding within the porous structure of the adsorbent. This type of intraparticular transport resistance corresponds to diffusion in the porous material. It includes the following which, when present, occur in parallel.

1. Depending on whether the mean free path of the water molecules is smaller or larger than the pores diameter, the diffusion through these pores is either Knudsen diffusion (molecular flow) or bulk diffusion (viscous flow) respectively. As many desiccants present a range of micro and mesopores (e.g. silica gel), both types of transport processes occur, and together they can be described by Fick's laws of diffusion. For Silica gel for instance, the effective diffusion coefficient, representing the empirical net diffusion coefficient of the porous medium (Crittenden & Thomas 1998), was reported to be in the region of $4x10^{-7}$ $m^2.s^{-1}$ (Aristov et al. 2006) which is about 10^5 larger than the diffusion coefficient of PEEK. This shows that we are still looking at a very fast process.
2. When molecules are adsorbed, they may also move over the internal surface towards other adsorption sites. This surface diffusion phenomenon occurs especially within high area adsorbents which have narrow pores, and the magnitude of the effective diffusion coefficient is in the range 10^{-7} to 10^{-10} $m^2.s^{-1}$ (Crittenden & Thomas 1998).
3. Diffusion in molecular sieve materials such as zeolites is relatively slow, as the adsorbate penetrates the material and its internal channels through molecular sized apertures which significantly restrict the entry rate. The associated effective diffusion coefficients are in the range 10^{-13} to 10^{-15} $m^2.s^{-1}$ (Crittenden & Thomas 1998).

There is also interparticular resistance occurring and restricting the physical adsorption of the adsorbate to the adsorbent. This type of resistance is present in series with intraparticular resistance.

Each of the solid particles of adsorbent is surrounded by a layer of stagnant fluid. This thin fluid boundary layer acts as a transport resistance to the attachment of the adsorbate. Differences in concentration and temperature between the external surface of the particle and the bulk fluid are the driving forces which then define the rate of adsorption. For this reason, this phenomenon is referred to as interparticle mass and heat transport (Crittenden & Thomas 1998)

NB: Parts of the following sections have been published in (Dahan et al. 2013)

6.2 Selection of an appropriate desiccant

In order to select the most appropriate desiccant to use in an implant cavity, the water adsorption of three types of desiccants was recorded over time. The desiccants tested were silica gel, molecular sieve, and 'Thirsty Vycor' porous glass (composed of 96% silica). These were dried under vacuum (70 mbar) according to manufacturers' specifications:

Type of desiccant	Manufacturer's designation	Regeneration method
Silica gel	BDH® Silica Gel Prod. 30063	2 hours at 130°C
4A Molecular sieve	Multisorb Technologies Skavenger™ Preform	1 hour at 130°C + 1 hour at 250°C
Porous Glass	Vycor® Brand Porous Glass no. 7930	Cleaning with Hydrogen Peroxide at 90°C + 1 hour at 60°C + 1 hour at 180°C

Table 6-5 Regeneration conditions for desiccants

It must be noted that different conditions of drying were also tested (shorter times, or higher temperatures than specified) and impacted negatively on the adsorption capacity. It is therefore important to stay in that range of parameters when drying the desiccants.

After drying, the desiccants were placed at ambient conditions (21°C, ca. 45% RH) on a precision balance (Sartorius BP211D – Precision 10^{-5} g) and their weight was measured over time. The results can be observed on Figure 6.4, showing the water adsorption (the ratio 'mass of water adsorbed/mass of dry desiccant') over time.

As can be seen on the graph, for these particular conditions of pressure and temperature, Thirsty Vycor adsorbs up to 5% of its dry weight, molecular sieve 17% and silica gel more than 26%. These results can be compared to the theoretical isotherms for these types of desiccant as shown on Figure 6.5 (data found on literature (Desiccare Inc. 2010), not specific to these particular brands of desiccants, apart from Thirsty Vycor). According to these adsorption isotherms, at 45% RH, Thirsty Vycor should adsorb around 10% of its dry weight in water, molecular sieve up to 22%, and silica gel 27%.

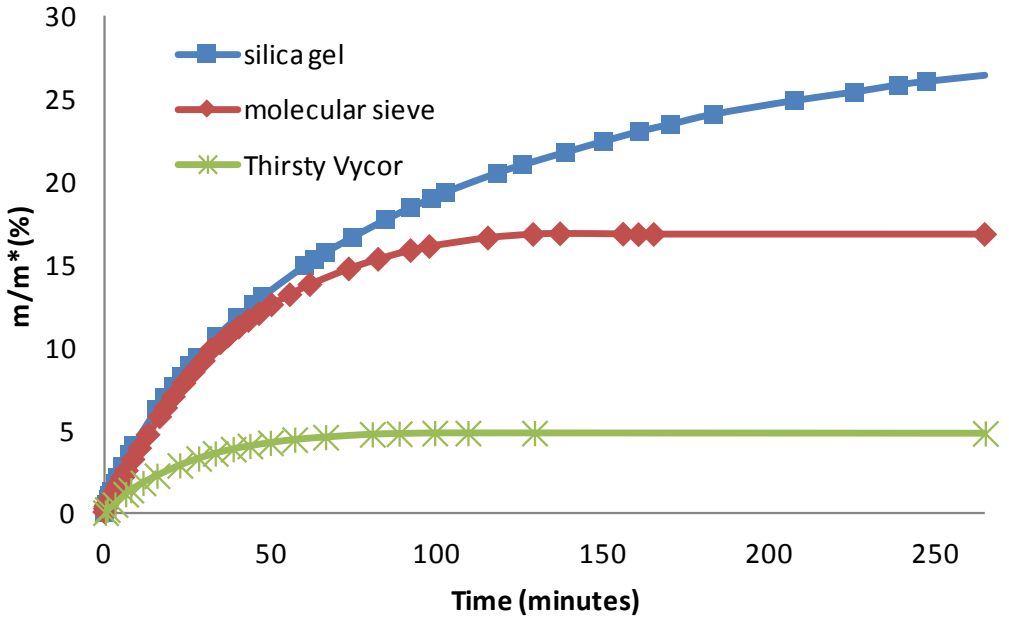

Figure 6.4 Water adsorption vs. time at 21ºC and 50%RH

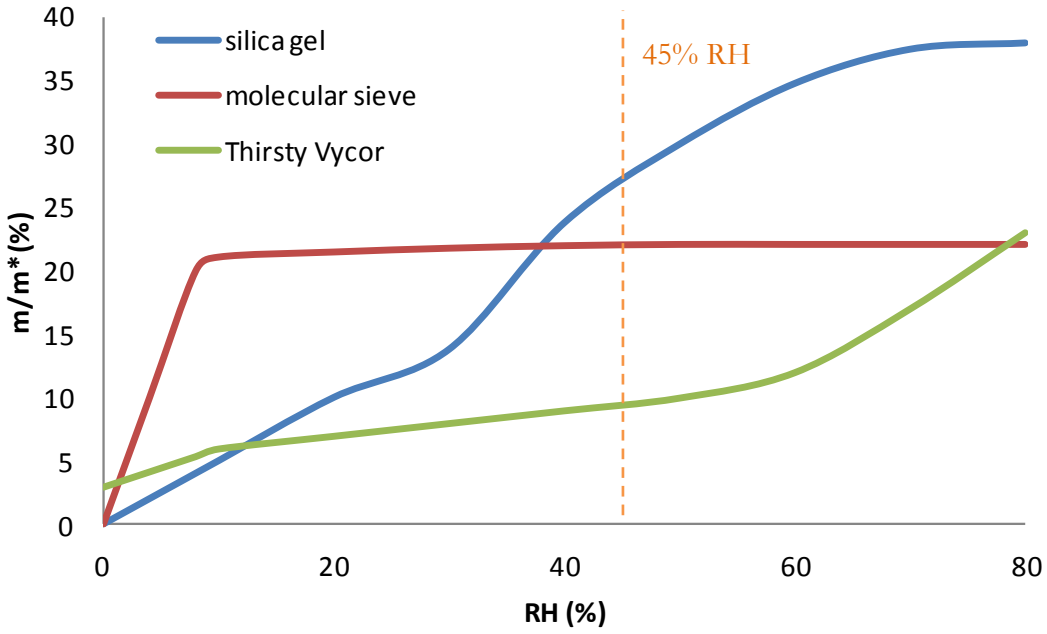

Figure 6.5 Adsorption isotherm at 25ºC for silica gel, molecular sieve and Thirsty Vycor desiccants

For silica gel, the results are therefore in very good accordance with the data shown on Figure 6.5. The values for molecular sieve and Thirsty Vycor are below expectations, which could be due to their short time constant. The time used to transfer the sample from the vacuum oven and starting recording the data (ca. 1-2 minutes) could see the desiccant adsorbing the missing amount of water. Other causes could include incomplete drying, or samples not performing as well as generic specifications. Adsorption sites destroyed by heat could be another explanation.

At any rate, it is clear that silica gel is the best desiccant for this application, as it can theoretically adsorb up to 33% of its dry weight in water at 60% RH and 25°C. The previous experiment shows that the performance is in good accordance with the theory, and that the cavity should be closed as soon as the desiccant is dry. The desiccant would otherwise very quickly adsorb significant amounts of water from the surrounding air and its capacity to keep the cavity dry would be reduced.

Molecular sieve could also be a suitable desiccant for this application, although its capacity is not as large as for silica gel. Thirsty Vycor however has a very limited capacity and will only start adsorbing significant amounts of water (around 25% of dry weight) between 60 and 100% RH, which makes it unsuitable for our application.

6.3 Influence of the temperature on the adsorption capacity

The tests and isotherms we have looked at so far were performed at 21°C and 25°C, but we need to look at how the desiccant will behave at higher temperatures. There has been extensive testing of silica gel desiccants in the literature, and we can use this data to see whether the temperature influences the adsorption capacity of our desiccant.

Figure 6.6 is reproduced from (Ng 2001) and plots the water adsorption by the desiccant as a function of the absolute pressure of water vapour.

This shows that for a given water vapour pressure, the water adsorption is highly dependent on the temperature. Data can be extracted from this graph to plot the evolution of the water adsorption as a function of the relative humidity. This is plotted in Figure 6.7 and shows that the temperature has in fact a negligible influence on the water adsorption by silica gel for a given relative humidity level. We can therefore use the isotherms obtained in the previous section (around 20-25°C) in further experiments at higher temperature (37°C).

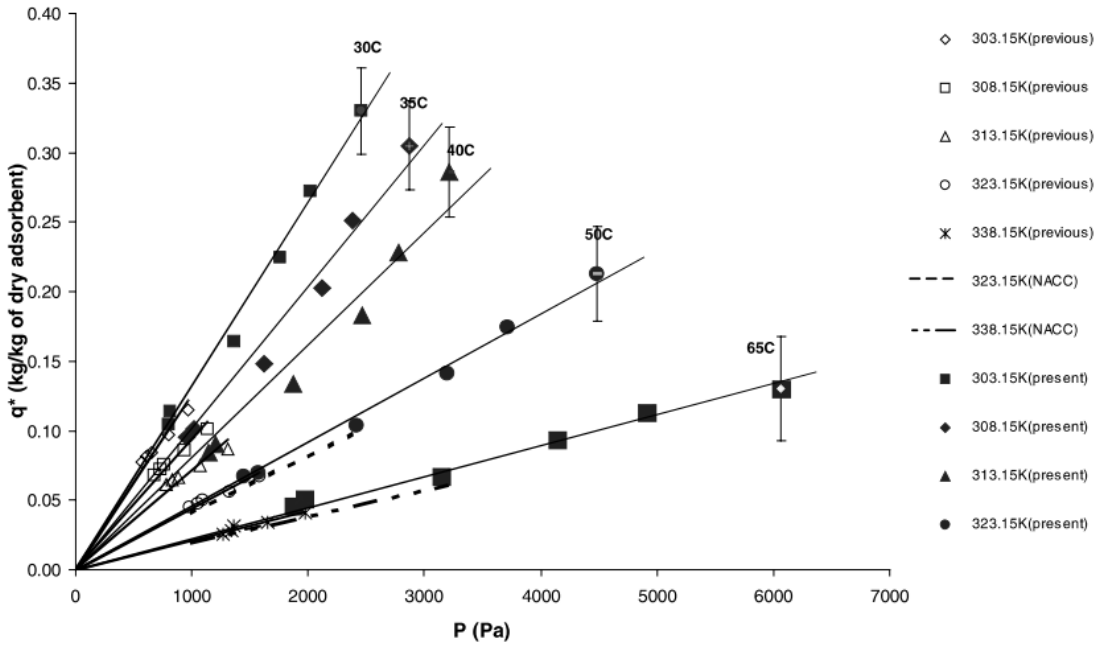

Figure 6.6 Isotherm data for Type 3A silica gel - from (Ng 2001)

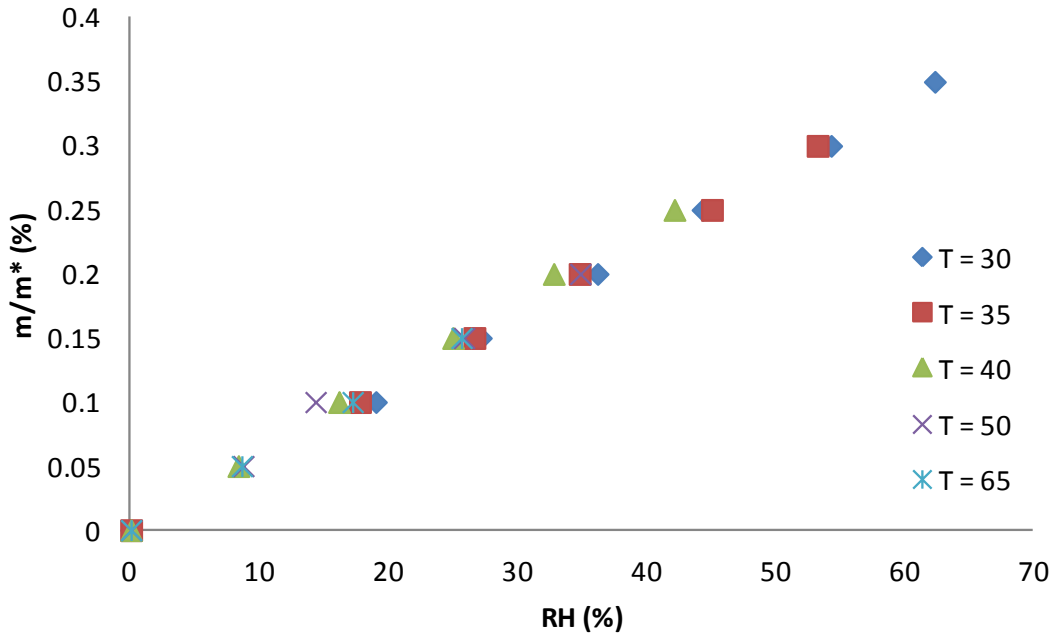

Figure 6.7 Isotherm data for 3A silica gel as a function from the relative humidity (data from (Ng 2001))

6.4 Lifetime calculations and preliminary experiments

6.4.1 Calculation method

For traditional packages made of metal or ceramic, the enclosure material is not porous. The only way water can permeate the package is through leak channels, often in the seal (see section 2.5 Flow of gas in and out of sealed packages). Unlike polymers such as PEEK, the walls of these packages cannot store water. The RH level in the cavity is therefore a direct result of the difference in humidity between both sides of the walls.

When using a desiccant, the lifetime of these packages can be calculated by multiplying the lifetime of the package without desiccant by the ratio $\frac{amount\ of\ water\ which\ can\ be\ stored\ in\ desiccant}{acceptable\ amount\ of\ water\ in\ cavity\ with\ no\ desiccant}$ which can reach up to 5000 (Singh et al. 2001).

However this method cannot be used in the case of a polymer package. This is because the humidity level in the cavity will only rise when it is inferior to the level in the PEEK walls and the desiccant. As long as these elements can absorb and adsorb water respectively, they keep the RH level in the cavity low. We can also understand from here that the effect of a desiccant in this type of 'porous' package is less than in traditional packages, which are much less permeable and have walls that cannot store water.

It is possible to calculate the lifetime of the package incorporating desiccant using the method described in section 3.3 (A new calculation method for polymer packages with walls of varying thickness/properties.), which is repeated here, with a slight change to account for the presence of the desiccant. This desiccant is accounted for by the presence of another capacitance, C_D, placed in parallel with the capacitance C_V representing the package cavity (see Figure 6.8).

(1) For each element (wall, seal, etc.), we calculate the R_P and C_P components using equations (3.8) and (3.9), $R_P = \frac{d}{KA}$ and $C_P = \frac{ASd}{2}$ respectively.

(2) The equivalent R_P and C_P for the package can be found using equations (3.10) and (3.11), $R_{P_{eq}} = 1/\sum_i \frac{1}{R_{P_i}}$ and $C_{P_{eq}} = \sum_i C_{P_i}$ respectively.

(3) The time constant of the system is calculated with the following equation:

$$\tau = R_{P_{eq}} \times \left(C_V + C_{P_{eq}} + C_D\right) \tag{6.7}$$

where C_D is the 'capacitance' associated with the desiccant.

(4) Finally, the RH level in the cavity at any time t is found using equation (2.15),

$$RH_t = RH_i + (RH_a - RH_i)\left[1 - e^{-\frac{t}{\tau}}\right]$$

To find the capacitance of the desiccant C_D, we first establish the solubility of water vapour into the desiccant S_D, the same way we do with any type of porous material (see Equation (2.22)).

$$S_D = \frac{V_{WATER}}{V_{DESICCANT}} = \frac{\rho_{DESICCANT} \times \frac{adsorption}{capacity} \times \frac{molar}{volume\ at\ T}}{\frac{molar}{weight}} \tag{6.8}$$

and the capacitance C_D is:

$$C_D = S_D \times V_D \tag{6.9}$$

where V_D is the volume of the desiccant. C_D then corresponds to the volume of water which can be stored in the desiccant at 1 bar. As we will see later, the use of this method is highly dependent on the type of desiccant used (i.e. constant capacitance? Linear/non-linear?) and it is not to be expected to be valid for all types of adsorbents.

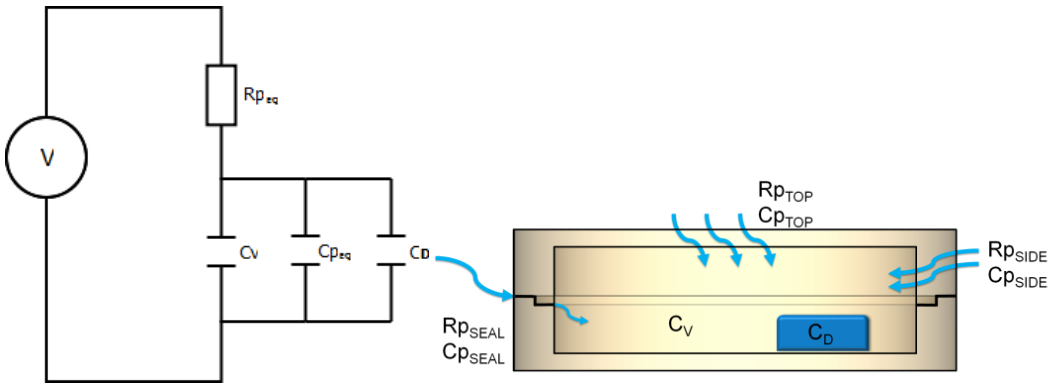

Figure 6.8 moisture ingress through a PEEK package containing desiccant - Electrical analogy

6.4.2 Preliminary experiment – amount of water adsorbed by silica gel at high humidity levels

Unlike molecular sieve, which adsorption capacity does not evolve past 8 – 10% RH (see Figure 6.5), the adsorption capacity of silica gel is strongly dependent on the surrounding humidity level. Preliminary experiments were led to assess the amount of water ab/adsorbed in the body of a PEEK capsule and the silica gel desiccant respectively. These PEEK capsules were placed in water at 37°C, and then weighed periodically with a 10^{-5} g accuracy and the weight gain was averaged for each set of tests (n=3).

The first batch of capsules contains no desiccant. The other set contains 87 mg of silica gel desiccant, which, when dried, comes down to 70 mg (20% adsorption capacity at ambient conditions – see Figure 6.5). This amount of desiccant occupies ca. 6% of the volume cavity.

The water vapour mass gain from each package is presented in Figure 6.9, which shows that the package without desiccant absorbs about 9 mg of water at saturation, whereas the package with desiccant gains 28 mg. The amount of water in the cavity is expected to be negligible (ca. 0.05 mg), and therefore it can be deduced that the desiccant adsorbs up to 19 mg of water at saturation. This corresponds to 27% of its dry weight, which is less than expected from the isotherm in Figure 6.5. This could be due to any of the reasons mentioned in section 6.2 - Selection of an appropriate desiccant.

As the true value for water adsorption by the desiccant, it will be the one used for the calculation of the predicted time constant and validation of the model.

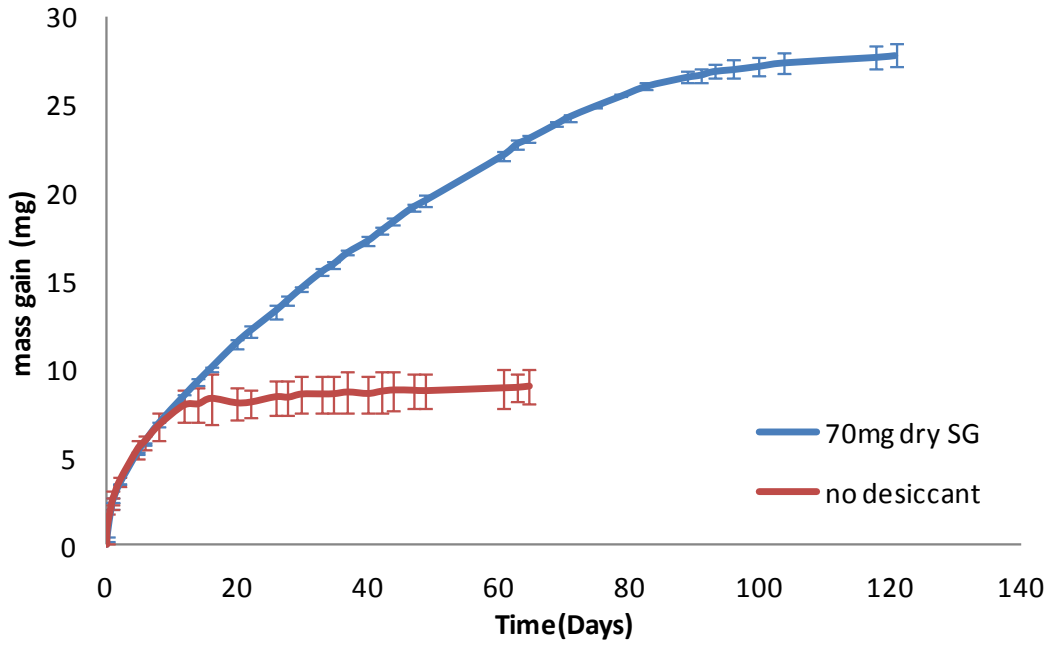

Figure 6.9 Water mass gain from packages

6.4.3 Calculated lifetime

When using molecular sieve or silica gel desiccant, values for S_D and C_D can be found using Equations (6.8) and (6.9). For 70 mg of dry silica gel and an adsorption capacity of 27%, we find S_D = 274 and C_D = 26.6 cm^3. Using these values as well as those previously calculated in Table 3-1, which are reported in Table 6-6, we find a **predicted time constant of 75.5 days**. Similarly, for 4A molecular sieve desiccant, S_D= 149, and C_D=16.5 cm^3. The predicted time constant for this package is then 48.6 days.

Package Element	Top +Bottom	Sides	Seal	Desiccant
Material	PEEK OPTIMA	PEEK OPTIMA	Cyanoacrylate (Loctite 4061)	Silica Gel
Thickness d (cm)	0.10	0.20	0.23	N/A
Surface area A (cm^2)	5.09	3.56	0.03	N/A
Solubility S (cm^3/cm^3)	9.17	9.17	32.4	356
Diffusion D ($cm^2.s^{-1}$)	[a]8.20×10^{-9}	[a] 8.20×10^{-9}	[b]1.08×10^{-8}	N/A
Permeation K ($cm^2.s^{-1}$)	7.52×10^{-8}	7.52×10^{-8}	3.50×10^{-7}	N/A
C_V (cm^3)	----------1.60----------			
C_P (cm^3)	2.33	3.27	0.13	C_D= 34.5
R_P ($s.cm^{-3}$)	2.62×10^{5}	7.47×10^{5}	1.9×10^{7}	N/A

Values for the solubility coefficients were calculated using the water absorption and the density of the material (Greenhouse 2000). Values for the diffusion coefficients were taken from the literature for similar materials ([a](Grayson & Wolf 1987) and [b](Braden 1964)) but are not specific to the materials we used, as those values were not available.

Table 6-6 Values used for calculation of moisture ingress

6.5 Experimental results

Two sets of capsules (n=3) with desiccant were placed in water at 37°C and the RH level is recorded over time. Two types of desiccant are used: molecular sieve and silica gel (see Figure 6.10). The quantities of desiccant are those described in the calculations section.

Figure 6.10 Molecular sieve (top) and silica gel (bottom) desiccant in PEEK capsules

6.5.1 Using molecular sieve desiccant

The results for the experiment with molecular sieve are presented in Figure 6.11.

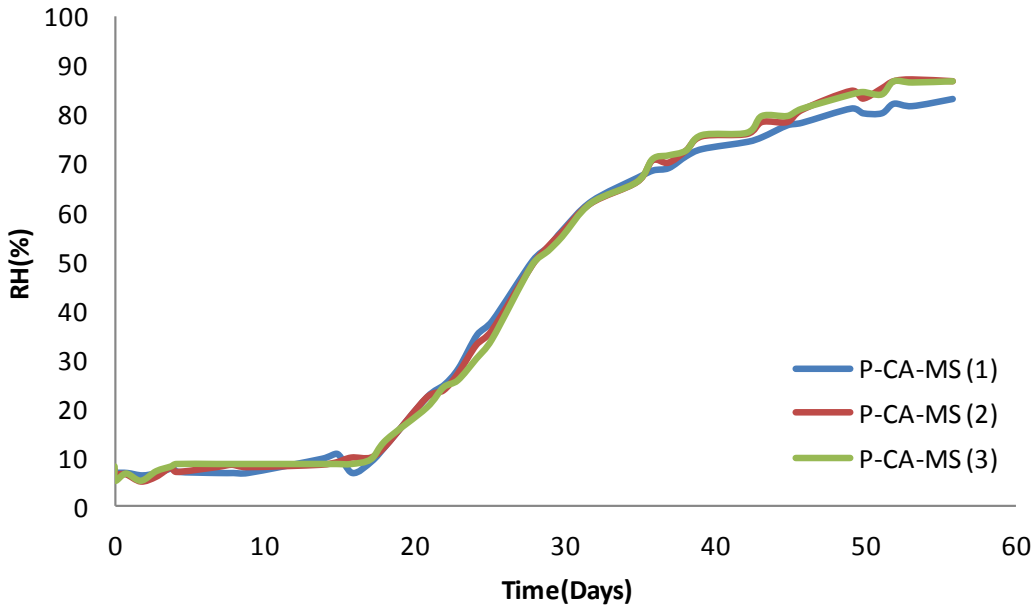

Figure 6.11 RH level in PEEK capsule with molecular sieve desiccant

From this graph we can see that it takes 33 days for the RH level to rise to 63%. The progression follows what is expected from the isotherm. Molecular sieve has a high capacity at low humidity (see Figure 6.5), and therefore the RH level remains low as long as the desiccant has not reached its maximum capacity. After this, the humidity rises normally in the cavity. However, the actual lifetime (33 days to reach 63% RH) is quite

far off the lifetime prediction of 48 days (32% accuracy). Because of the shape of the increase, we can also see that it is not appropriate to talk about 'time constant' in this case.

6.5.2 Using silica gel desiccant

The results are presented in Figure 6.12.

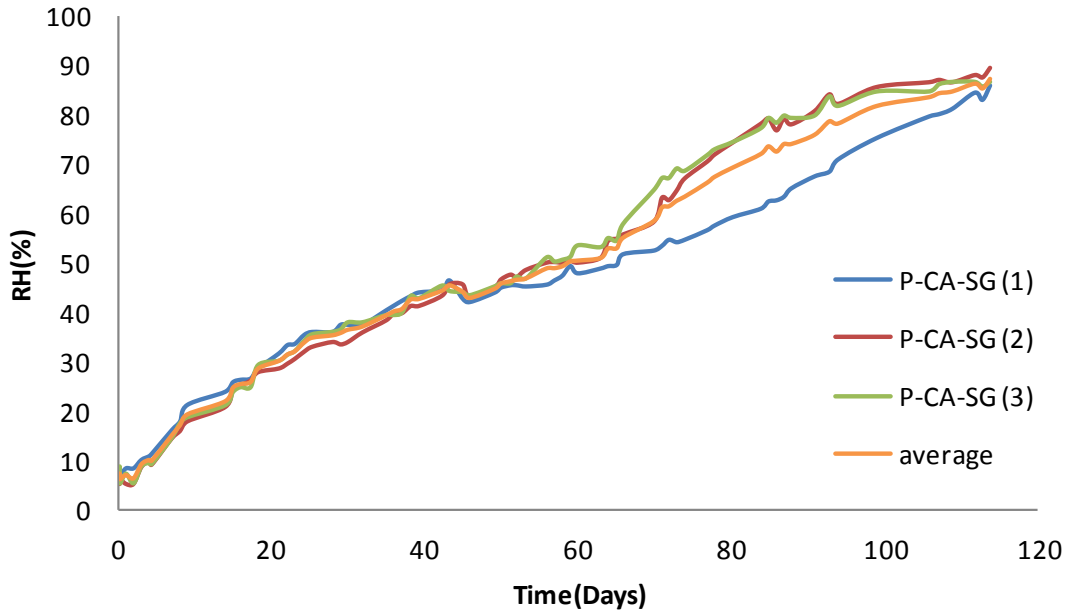

Figure 6.12 RH level in PEEK capsule with silica gel desiccant

For silica gel, the plot looks very different. The adsorption capacity is highly dependent on the humidity level (see Figure 6.5), so the RH is constantly rising, but at a slower rate. The experimental lifetime obtained is 73.5 days, which was very well approximated by calculation (75.6 days – 2.8% accuracy).

6.5.3 Comparison and validity of the calculation method

The influence of desiccant on the humidity rise in the package can be observed and compared on Figure 6.13, which displays results for molecular sieve, silica gel, and a regular capsule without desiccant. The results are summarised in Table 6-7.

Parameters	Predicted time constant	Real time constant	Accuracy of prediction
No desiccant	16.3 days	15.9 days	2.4%
4A molecular sieve (73 mg dry)	48.6 days	33 days	32%
Silica gel (70 mg dry)	75.6 days	73.5 days	2.8%

Table 6-7 Time constants - summary of results

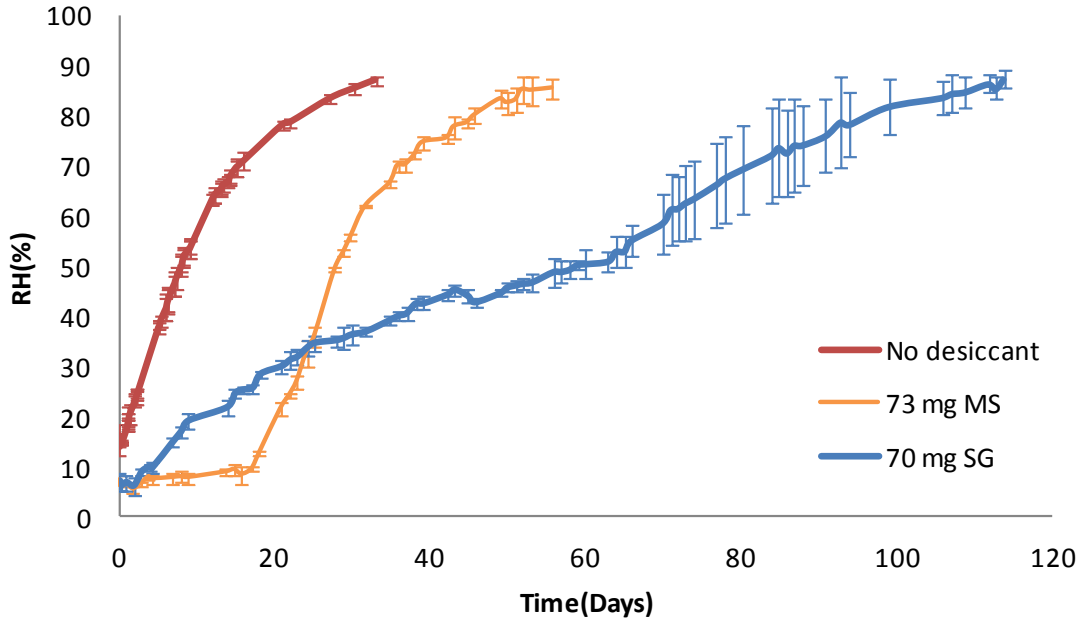

Figure 6.13 Influence of desiccant type on RH level

As mentioned previously, we can see that when using molecular sieve, the humidity remains low until full capacity is reached, as after this the RH level increases at the same rate as for the capsule without desiccant. The lifetime prediction however turned out to be not very accurate (32%). At best it predicted the order of magnitude of the lifetime. When using silica gel, we obtained a more linear response, with a more accurate lifetime prediction (2.8% accuracy).

These results show that the validity of this calculation method is highly dependent on the type of desiccant used and the isotherm type. The model is relatively appropriate for isotherm types II to V, but not really for type I isotherm (see Figure 6.3), unless you want an indication of the order of magnitude of the lifetime, which it can still provide. The model still uses the correct adsorption capacity; it is the way it considers the RH rise which does not correspond to reality, especially for desiccant exhibiting a type I isotherm behaviour such as 4A molecular sieve.

Indeed, the calculation model supposes an inverse exponential increase of the RH level inside the cavity (following equation (2.15)), as it is the case when no desiccant is present. However, the shape of this increase is highly dependent on the type of desiccant used. A molecular sieve desiccant for instance, which exhibits high adsorption at low RH level, would keep the RH level low until it has reached full adsorption capacity, and would then allow the RH level to rise as if no desiccant was present. So if we look at the electrical analogy (see Figure 6.8), C_V only starts charging once C_D is fully charged, which is a different, more complicated model altogether. This model would be similar to that of a battery charger, where current flows to the battery to be charged (C_D) until it is full, after which the current is switched to another path, C_V.

Silica gel on the other hand, has increased capacity at higher RH level. In that sense the model we use is also inaccurate. In this case C_D really is a capacitor with a non linear capacitance (ability to store water depends on the RH level), which would be dependent on the voltage across C_V (i.e. the humidity in the cavity). However, because this is much closer to the model we use and the capacity of the desiccant evolves without latency, it still provides a very good estimation of the lifetime.

6.6 Maximum lifetime achievable using a desiccant

We can see from Figure 6.13 that using a desiccant offers a significant improvement in lifetime: 3-fold for molecular sieve, and 7-fold for silica gel. The maximum lifetime obtained of 73 days corresponds, as mentioned in a previous section, to an arbitrary limit at which we consider the risk of failure starts appearing. In practice our humidity sensing circuit enclosed in the package was still working after 120 days when we stopped the experiment. This has been true of every capsule experiment conducted in this study. Out of the 140+ capsules tested in this study, there has been no failure of humidity sensing circuits due to exposure to moisture. This tends to prove that any electronics enclosed in such a package is actually extremely likely to survive way beyond the designated 'lifetime'. However, this is a safe, conservative working limit, and 73 days is already a useful lifetime for a number of clinical and test applications.

We can now wonder how far this lifetime can be pushed using desiccant and increasing the thickness of wall enclosures. Our calculation method can be used to evaluate the lifetime of various capsule geometries containing a certain amount of desiccant. For ease of calculation, we can compare the time constants, which are very close to our definition of the lifetime, as it corresponds to the time it take to reach $1\text{-}e^{-1}$=63% of the final value, i.e. 63% RH.

In section 5.3, we looked at the influence of the wall thickness on the lifetime of a PEEK package. We can now conduct the same analysis with the case of desiccant. What is the maximum achievable lifetime when using desiccant?

So far in the previous tests, the silica gel desiccant tested was occupying ca. 6% of the cavity volume. It is however reasonable to assume that 10% of an implant cavity can be filled with desiccant. Using this number, we can look at the influence of desiccant on the time constant for the theoretical case of a spherical package, using equation (5.11), which becomes:

$$\tau = \frac{(V_C + C_D) \cdot d}{K \times 2\pi \left(\sqrt[3]{\frac{V_C}{\pi}} + d \right) \left(2 \cdot \sqrt[3]{\frac{V_C}{\pi}} + 3d \right)} + \frac{d^2}{2D} \qquad (6.10)$$

The results of these calculations are presented in Figure 6.14.

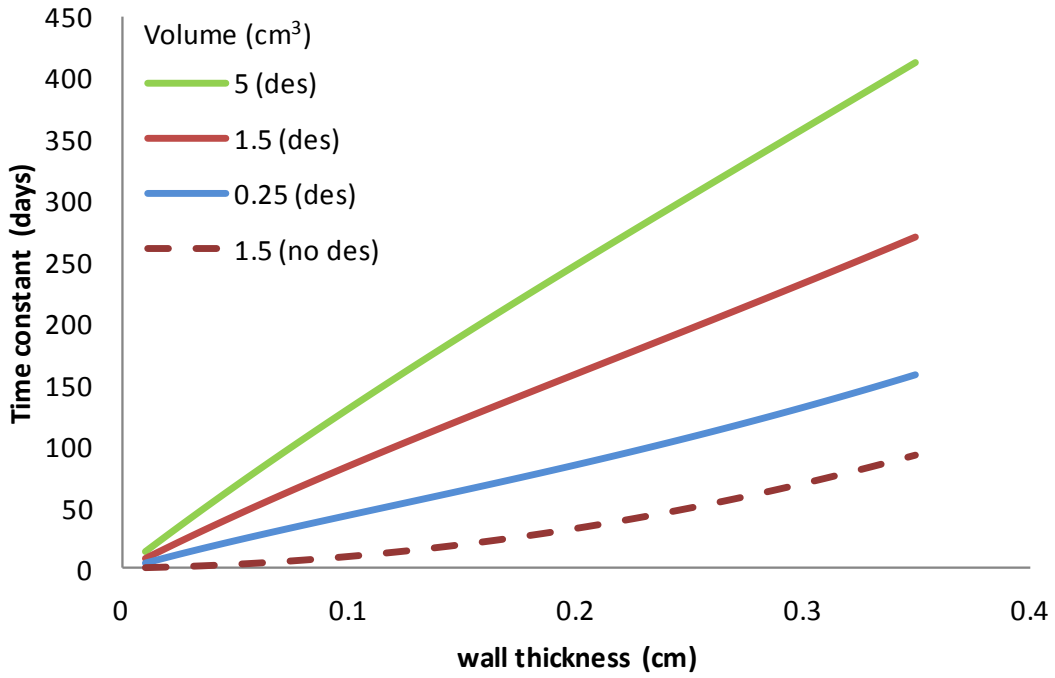

Figure 6.14 Influence of the use of silica gel desiccant (10% of cavity volume) on the time constant for a cylindrical enclosure

The first thing to notice is that, unlike the previous case (no desiccant), the cavity volume has a major influence on the time constant. This is because the quantity of desiccant depends directly on V (10%).

For a typical implant size cavity V=1.5 cm^3, and a constant wall thickness of 3 mm, the time constant goes from 69 days when no desiccant is used to 233 days with silica gel desiccant.

When the cavity volume increases further, as more desiccant can be fitted, the time constant rises, to 357 days when V=5 cm^3 for instance.

These calculations have used a basis of 10% of the cavity filled with desiccant. However, depending on the application, there may be much more space available for desiccant in the cavity. Figure 6.15 shows the effect of different amounts of desiccant for a fixed internal volume of 1.5 cm^3.

When filling 10% of the volume with silica gel, we have seen that the time constant can reach 7.6 months for a 3 mm thick cylindrical enclosure with 1.5 cm^3 cavity volume. This value goes up to 13 months when using 20% desiccant, and 18.5 months with 30%, which would be sufficient for many applications. Some results are presented in Table 6-8.

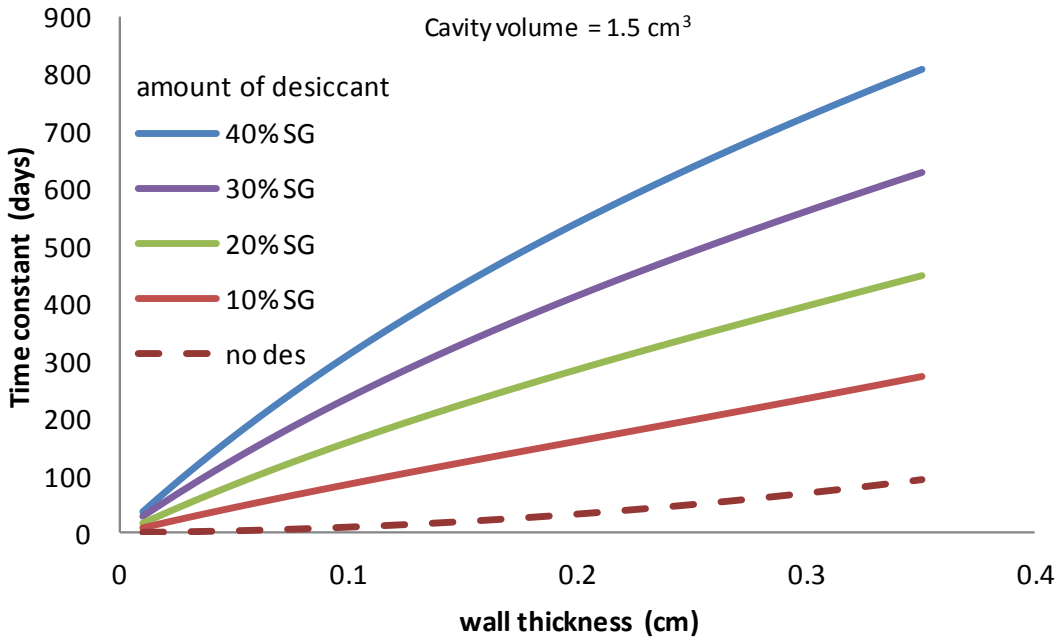

Figure 6.15 Influence of wall thickness and amount of desiccant on the time constant

Amount of desiccant used	V=1.5 cm^3 - d= 2 mm	V=1.5 cm^3 - d= 3 mm
No desiccant	33.9 days	81 days
10%	5.3 months	7.6 months
20%	9.4 months	13 months
30%	13.6 months	18.5 months

Table 6-8 Calculated time constant for cylindrical PEEK capsule using varying amounts of desiccant

6.7 Conclusion

To summarise, we have seen that the lifetime of a PEEK package highly depends on the thickness of its walls, as well as whether or not desiccant is used. The lifetime must therefore be calculated for each case using the method provided in 6.4.1. However Figure 6.14 and Figure 6.15 can be used as a guideline or a first approximation of what is achievable. Time constants varying from a couple of months to 1.5 year can be obtained using the right combination of wall thickness and silica gel desiccant. This provides a useful lifetime for a number of applications which could benefit from cheaper packaging options.

Chapter 7 Prolonging the lifetime using a thin film coating

In this final experimental chapter, the main vacuum deposition techniques are first reviewed, before a range of coating techniques and materials are tested. It is found that most PVD films fail due to high residual stress and the growth of a porous morphology, which can be alleviated to some extent by the use of a lacquer prior to deposition. ALD also proves to be effective in reducing moisture permeation by a factor of 2.3.

7.1 Vacuum deposition techniques – Literature review

Coatings are generally used to improve the surface properties of materials, such as biocompatibility, water wettability, adhesion properties (using high surface energy coatings), corrosion resistance, wear and scratch resistance. They can also be used to give new properties to the substrate on which they are applied, such as photo sensitivity or electrical conduction. A method to reduce the water permeability of PEEK could be to apply a coating to its surface.

Coating PEEK with hydroxyapatite and/or titanium has been investigated and applied successfully previously for orthopaedic implants (Ha, Kirch, et al. 1997; Kurtz & Devine 2007; Ha, Eckert, et al. 1997). This was done using particulate deposition techniques such as vacuum plasma spray (VPS), which produces 10-50 μm thick porous coatings (Pawlowski 2009), in order to improve osteoconductivity. In our case, porosity is obviously to be avoided. On top of producing porous coatings, VPS has been reported to increase the porosity of PEEK, as overheating PEEK can lead to formation of holes and voids due to viscous flowing above the glass transition temperature (oral presentation by Eurocoatings S.P.A. at the 2012 World Biomaterials Conference in Chengdu, China).

There is a very wide range of coating processes available, depending on the application and the materials involved. Because of the telemetry system used in our experiments, having too thick a coating may affect power and data transfer (see 4.1.4 Attenuation issues), so our investigation will be limited to thin films of less than 5 μm thick. The following section provides an overview of the main thin film vacuum coating techniques which may be useful to improve the barrier properties of our material.

7.1.1 Physical vapour deposition (PVD)

In physical vapour deposition (PVD), the material to be deposited is vaporised, then transported while in gas phase, and deposits on the substrate by condensing on its cold surface, regaining a solid form. There are no chemical reactions involved in PVD (unlike in the case of reactive sputtering). This is a purely physical process, hence its name. There are many ways to vaporise the deposition material, which determine the type of

PVD. In these methods, the coating material is vaporised either by evaporation or sputtering. We can briefly review the main PVD techniques available.

7.1.1.1 Evaporation sources

Before the vaporised atoms can be deposited on a substrate, they have to be removed from a source. When the removal process consists in thermally heating the source material, we talk of evaporation. This is used for instance to metallise large polymer films (crisps bags, helium balloons, etc.). Evaporation is generally realised under high (10^{-9} bar) or ultra high (10^{-12} bar) vacuum, in order to minimise the probability of the evaporated atoms to collide with other particles before condensing at the surface of the substrate to be coated. It is a 'line-of-sight' process (Mattox 1998). If they did not have this long mean free path, the particles would lose energy by scattering and the deposition rate would drop significantly. The other purpose of the vacuum is to avoid any reaction between the species to deposit and potential contaminants, except in the case of '**reactive evaporation**' which can be used to form compound films and deposit oxides or nitrides for instance (reaction of the deposition material with oxygen and nitrogen respectively).

Evaporative sources can be separated into two categories: The first category regroups the methods in which the gas phase generated is in quasi equilibrium with its source, and the second describes the sources which are not (Mahan 2000, p.115).

The **effusion (or Knudsen) cell**, as shown in Figure 7.1, is a source in which the coating material is heated inside a closed container. The evaporated material is then in equilibrium with the liquid phase, and is emitted into the coating chamber (which is under a high vacuum) via a small orifice at the top of the container. This allows the particles produced to escape the chamber without collisions and with a long mean free path (much greater than the orifice diameter). The flow generated is therefore 'molecular' (see 2.5.1 Viscous, molecular and diffusive flow), and is called 'molecular beam'. This gave the name to the PVD technique called '**molecular beam epitaxy**'.

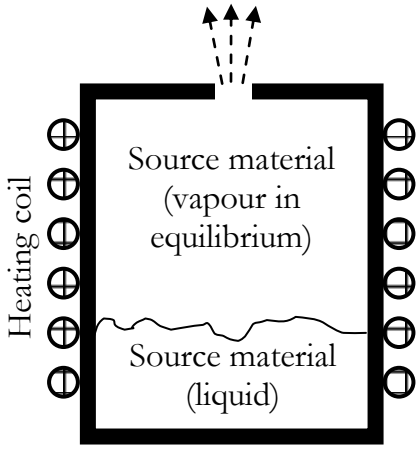

Figure 7.1 Quasi-equilibrium evaporation source - The effusion cell

The second category of evaporative sources, non equilibrium sources, is much broader, and describes those sources where the liquid evaporant is in a large, low pressure volume and there is therefore no separation between the source and the coating chamber. Examples of nonequilibrium sources are presented in Figure 7.2 (a), (b), (c), and (d).

The **crucible source** (a) is typically a ceramic cup which is heated by a resistive coil or wire. The **boat source** (b) is usually made of a refractory metal such as tantalum or tungsten. A large current is passed through 'the boat' and heats it up to allow evaporation of the coating material. These last two sources are generally used at low temperature, as at high temperature the crucible or boat material might react chemically with the evaporant (Spear 1976; Rossnagel 2003). (c) is a simple **hot filament source** which is heated and melts the source material attached to it, emitting particles in all directions. (d) represents the **electron beam source (EBPVD -** also called E-gun evaporator): A electron beam is generated by passing a high current through a hot filament (cf. (c)), accelerated, and bent at 270^{o} using a magnetic field in order not to interfere with the emitted flow of particles. The kinetic energy of the electrons produced is then converted into thermal energy and used to locally heat up only the top part of the evaporant contained in a water cooled crucible, thus avoiding the potential issue of chemical reactions with the container material as described for sources (a) and (b) . The type of heating used generally depends on the vaporisation temperature of the source material, with resistive heating used mostly below 1500^{o}C, and EBPVD above that temperature (Mattox 1998), for the reason described previously.

Irrespective of the source type, the substrate to be coated is placed in a line of sight of the emitted particles, generally between 10 and 100 cm away from the source, and '*it is desired that the mean free path of the evaporant flux exceed the distance to the sample. This reduces in-flight scattering with the background gas, which can lead to reduced deposition rates'* (Rossnagel 2003). In the case of reactive evaporation, where chemical reactions between the evaporated species and the background gas are sought, a low vacuum is applied instead of a high vacuum.

There are also variations of reactive evaporation, such as **activated reactive evaporation (ARE)** or **partially ionized beam (PIB),** where the deposition is altered by using a plasma and some ionization respectively. Another form, **ion beam assisted deposition (IBAD)**, is shown in Figure 7.3. These techniques offer the added benefit of accelerated rates in the compound formation by providing extra energy.

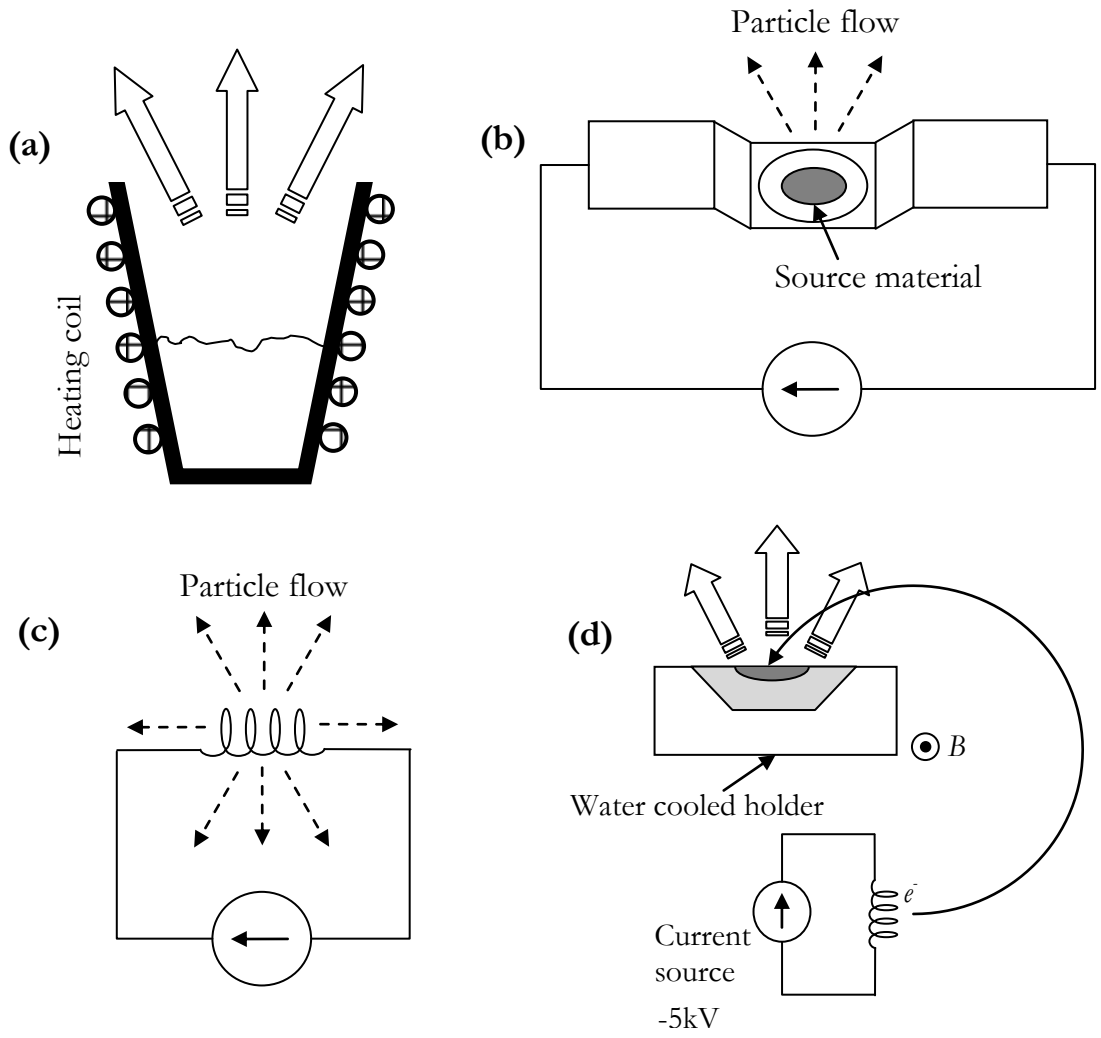

Figure 7.2 Non equilibrium evaporative sources: (a) crucible source, (b) boat source, (c) hot filament evaporator, (d) electron beam source (cross section)

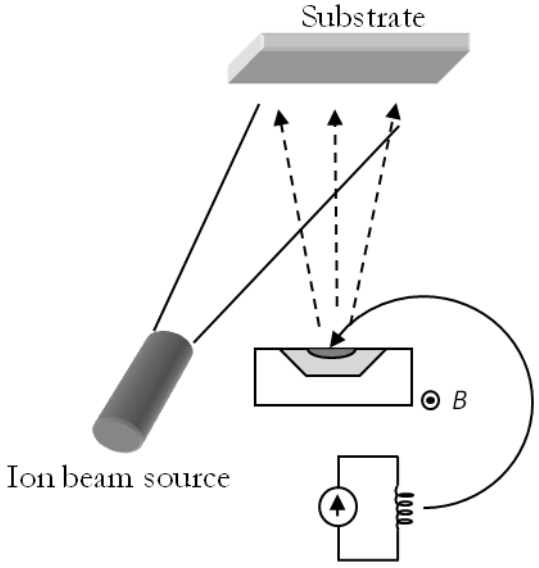

Figure 7.3 Ion beam assisted deposition (IBAD)

The last two main evaporation techniques are **pulsed laser deposition (PLD)** and **cathodic arc deposition (CAD)**. PLD is a 'flash evaporation' method which consists in bombarding the source material with photons in order to evaporate it. This is done using a laser which vaporises the top 100 nm of the material surface and creates a plasma plume containing the source material under various forms such as ions, molecules, atoms, molten globules and clusters (Hubler & Chrisey 1994). The main advantage of PLD is its versatility when it comes to the form of source material used. It can be under the form of a liquid, solid, powder or as ceramic pellets. However, this technique is not suitable for deposition on large areas and its energetic inefficiency restrains its use mostly to research purposes (Rossnagel 2003).

In CAD, the source material is used as a cathode and struck with a very high current, low voltage arc. The very high energy present at the point of impact is used to vaporise the source material (Martin 1996). Similarly to EBPVD, the arc is bent using a transverse magnetic field to avoid interactions with the emitted flux. Cathodic arc deposition can be used to form thin ceramic, metallic and composite films.

Evaporation may however present several problems: film properties may be affected by the temperature difference between the hot source and the cooler substrate. A thin film is deposited in thermal equilibrium with the substrate, but can then be subject to issues related to '*wetting, nucleation, cluster formation and agglomeration'* (Rossnagel 2003). In contrast, this is much less of an issue with sputtering techniques, as the sputtered atoms benefit from their large kinetic energy to bond more readily with the substrate surface.

In cathodic arc deposition, microparticles can be emitted from the source material due to the violent nature of the arc, and deposit under the form of droplets, which would affect the properties of the film by making it 'underdense and bumpy' (Rossnagel 2003). There is also a risk in PVD techniques linked to high temperatures, and electron beams tend to produce X-Rays which may damage the substrate. Furthermore, if the substrate surface is hot, the film can present internal tensile stress because of the difference in thermal expansion coefficient between the film material and the substrate material (Birkholz et al. 2004). The other potential problem comes from the long mean free path of the particles and therefore the very directional coverage. Although this guarantees that the deposition rate does not drop excessively, it also means that the material may deposit non-uniformly on a rough surface, or present shadowing if there are steps in the geometry of the substrate.

7.1.1.2 Sputter deposition techniques

Sputtering techniques consist in bombarding a target material (the source) with particles to dislodge kinetically some of its surface atoms. These atoms are then responsible for a 'cascade effect' by dislodging more atoms deeper below the surface, which will then do

the same until all residual energy is not sufficient to dislodge more atoms. The ejected atoms are those which are emitted from the target material as a result of this multi-collision process. These sputtered particles once vaporised can then deposit on the substrate. Although the bombarding particles can theoretically be anything (atoms, ions, molecules, photon), they are usually an inert gas ion such as argon ions. This is because it is easier to create a large flux of ions, and because noble gases have a full outer shell of valence electrons, and therefore are less likely to react chemically with other species (the ion will be neutralised before hitting the surface (Rossnagel 2003)). Sputtering is typically performed under low to moderate vacuum (10^{-4} to 10^{-7} bar). The sputtered atoms tend to have a shorter mean free path than with evaporation techniques, and as a result sputtering generally results in better step coverage. Another important advantage of sputtering techniques is that they can sputter very high temperature metals which may be difficult to evaporate. The deposition systems typically use either a plasma or an ion beam to bombard the target material.

In **diode sputtering**, the plasma is created from the gas atoms present (generally argon) by applying a voltage across a cathode (the target material) which attracts the positive ions and an anode which attracts the electrons in that volume. The plasma thus generated, called a diode, contains electrons and ions in the same proportion, as well as neutral gas which has a density which is one to three times that of the ions and electrons (Rossnagel 2003). Near the cathode target, the ions present in the plasma can be accelerated and bombarded onto it, triggering the sputtering process as previously described. There are different types of diode sputtering arrangements, the fundamental ones using either a DC, an RF, or an RF discharge and a magnetron (Mahan 2000, p.153). The DC arrangement uses a DC discharge (current flowing through the low pressure plasma). The substrate is the anode and the target is the cathode, as presented in Figure 7.5. The typical physical separation between the anode and cathode is a few centimetres. RF sputtering uses an RF discharge instead and presents the advantage of using lower voltages and pressures, with higher deposition rates.

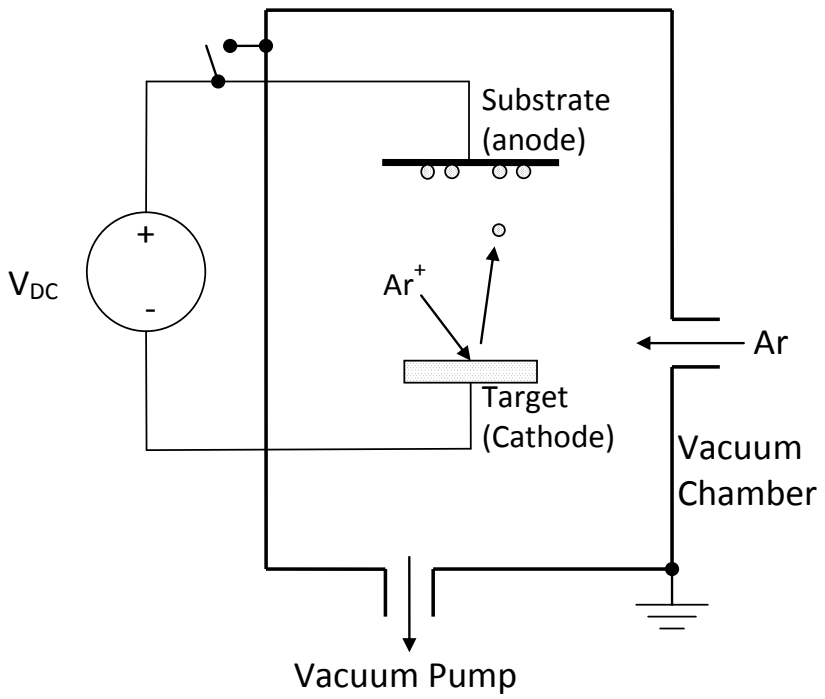

Figure 7.4 DC sputtering

A **magnetron** can be used to increase the plasma density by creating a magnetic field B perpendicular to the existing electric field E. This magnetic field is therefore parallel to the target surface, increases the path length of the electrons in the near cathode region and traps them in a closed loop (Hall Effect), which in turn augments the number of collisions with the background gas. This results in increased ionisation, higher plasma density, as well as enhanced bombardment and deposition rates.

Another improvement consists in ionising some of the sputtered metal atoms before they deposit on the substrate, and therefore deposit metal ions in the film alongside neutral atoms (Rossnagel 1998). This is known as **Ionised PVD (I-PVD)**, and is done in order to collimate the directional distribution of the metal atoms.

Although it is possible to coat the substrate by placing it directly within the plasma, the geometry (size) of the substrate can be a limiting factor. Moreover, direct exposure to plasma can cause damage, for instance by exposing the substrate to high temperatures. A solution consists in keeping the plasma within a contained volume (Kaufman 1986), and accelerating an ion beam to bombard the substrate within the coating chamber. This is known as **ion beam sputtering** (see Figure 7.5). However this technique presents lower deposition rates than magnetron sputtering because the ion beam has a lower power density (Rossnagel 2003). As with previous methods, a vacuum (low vacuum – less than 10^{-6} bar) is used to increase the mean free path of both the beam ions and the sputtered particles, making ion beam sputtering a line-of sight process. As a result, bombarding atoms can trigger resputtering of previously deposited particles on the substrate

(Hoffman 1990; Bauer 1994). This a general problem linked to sputtering methods though, and not just to ion beam sputtering.

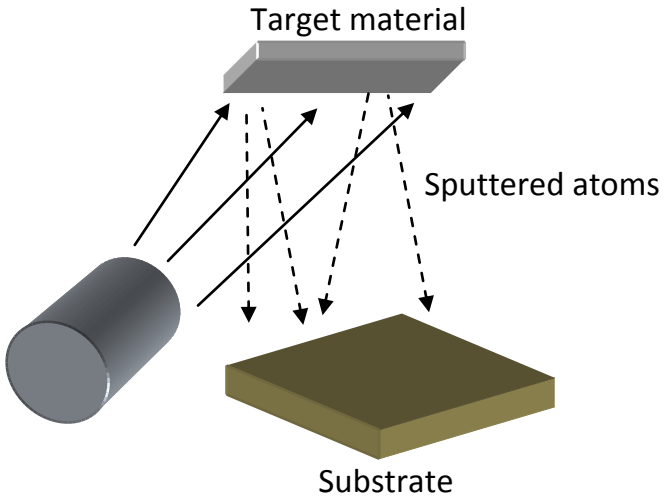

Figure 7.5 Ion beam sputtering

Similarly to evaporation, it is also possible to have **reactive sputter deposition** by introducing in the chamber a species (such as oxygen or nitrogen for example) which will react with either or both the target material and the thin film deposited on the substrate.

7.1.2 Chemical vapour deposition (CVD)

Chemical vapour deposition (**CVD**) is another widely used thin film vacuum deposition technique. Unlike PVD, the source of depositing material for chemical vapour deposition is a gas, as opposed to a solid or a liquid. The gaseous precursors are either reduced or decomposed at the substrate surface to deposit the desired atoms or molecules, generally forming chemical bond at high temperature (Morosanu 1990; Pierson 1999). As a result, the deposited atoms form a stronger bond than those deposited by PVD. There are many CVD deposition techniques available, and there is also a wide range of thin film materials which can be deposited using CVD. Graphene for instance has been reported to be completely impermeable to gases (Bunch et al. 2008; Novoselov et al. 2012). Diamond films could also be used for this purpose. However, because of the elevated temperatures used (typically between 600 °C and 950°C), CVD of these materials is not suitable for deposition on PEEK (Davis 1993; Singh Raman et al. 2012). Nevertheless, there is a variation of CVD which uses plasma to 'activate' gaseous precursors and enhance the decomposition and reaction, allowing the overall temperature to be lowered significantly. Plasma Enhanced CVD (also designated as **PCVD, PeCVD or PaCVD**) may therefore be used to deposit a thin film on a polymer substrate provided the required temperature is low enough. In order to reach temperatures which would be low enough to use with PEEK, a combination of CVD and PVD should be used, and the substrate should not be placed directly in the plasma discharge zone.

7.1.3 Film growth and properties

The growth of the deposited film and its properties can be affected by a variety of causes, such as particulate contamination (which can generate pinholes), angle of incidence of the depositing atoms, as well as outgassing for instance (which can have an adverse effect on adhesion and nucleation) (Mattox 1998, p.474). The process of film growth can be divided into five stages (Venables et al. 1984; Stowell 1974; Reichelt 1988; Mattox 1998):

A. ***Condensation and nucleation***: The atoms which have reached the substrate surface but not yet condensed are called 'adatoms', and are mobile on this surface until they condense. The substrate temperature, its surface interaction with adatoms (bonding) and the energy of the atoms affect this mobility. When they lose energy, they can bond to other atoms and condense. This loss of energy can be due to collisions with other atoms, chemical reaction with surface atoms, or when they find nucleation sites such as impurities or discontinuities for instance. In order to obtain a dense film, a high nucleation density (number of nuclei/unit area) is sought. The nucleation density can be improved by various means, such as changing the deposition temperature or rate for example.

B. ***Growth of nuclei***: The growth occurs when more atoms collide with an existing nucleus or are directed towards it.

C. ***Formation of interface***: When the depositing atoms diffuse and react with the substrate, there is formation of an interface, which properties influence the adhesion and characteristics of the film. Interfacial regions can be qualified as: abrupt, diffusion, compound, pseudo diffusion, reactively graded, or any combination of these categories.

Abrupt interfaces generally occur when there is little or no diffusion into the bulk material, as well as a low nucleation density. As a result, a thick film is necessary to ensure continuity, and interfacial voids are often present which leads to low adhesion.

When the film and the substrate materials can, and do, diffuse into each other, there is formation of a **diffusion interface,** which is highly dependent on time and temperature**.** This produces a graded interface which generally promotes adhesion, provided there are no contaminants on the surface (Williams et al. 1986). Diffusion interfaces are mostly formed in metallic systems, although there is diffusion of metals into polymers during the early stages of the deposition process (Zaporojtchenko et al. 2000; Faupel F. et al. 1998). However, different materials have different diffusion rates, which can cause porosity at the interface and can lead to poor adhesion (Mattox 1998, p.490). **Compound interfaces** are formed when chemical reactions occur at the surface alongside diffusion. When more than one material is deposited, the deposition of one can start before the deposition of the previous begins, which forms a **graded interface**.

D. *Film growth*: As nucleation continues, the film is allowed to grow as new material is deposited. Film properties such as grain size, surface morphology and film density are dependent on this growth.

E. *Changes occurring after deposition*: More changes can occur after the deposition due to 'natural' causes: adhesion of the film can change because of residual stress (the relief of residual stress can promote the formation of voids), moisture or corrosion for instance. Chemical reactions with the ambient gas can also affect the film properties. Post treatments of the film surface, whether it is under the form of thermal, chemical, mechanical treatments, as well as topcoats, can also be used to modify the film after deposition.

7.1.4 Adhesion and loss of adhesion

As we have just seen, film adhesion is very closely linked with those properties which influence film growth, namely '*nucleation, interface formation, film growth, as well as the properties of the interfacial materials*' (Mattox 1998, p.651). The loss of adhesion can occur near the interface region (either in the substrate or the film) by cohesive failure or in the interfacial region by adhesive failure. Depending on the scale, de-adhesion can cause pinholes or delamination, and its origin can be mechanical, thermal or chemical (as well as electro chemical). There are several factors which influence the quality of adhesion of the film to the substrate:

- The film **density** and **morphology** are highly dependent on the way the film grows. The columnar morphology is very common with PVD and CVD coatings (Mattox 1998, p.497), and may promote or degrade the adhesion properties depending on the case. However, the 'columns' even when well bonded to the substrate, often attach to each other poorly, which makes for a porous coating, and should be avoided when trying to improve barrier properties (Prater & Moss 1983). This is the case for example with some evaporation techniques where the incident atoms have very little energy and mobility, which results in 'self shadowing', columnar growth, low density, and porosity of the film (Rossnagel 2003). This effect of directionality is also reinforced with surface roughness (more showing), as well as when the deposition is 'line of sight', which is mostly the case of evaporative techniques. Conversely, sputtering techniques, which operate at higher pressure, often within a plasma, tend to minimise this effect.
- **Residual film stress**, whether compressive or tensile, finds its origins in the difference in thermal coefficient between the film and the substrate materials. When it is close to the fracture stress, or when an external load is applied, residual film stress leads to buckling and is relieved by producing blisters and voids in the case of compressive stress (Gille & Rau 1984). Residual internal tensile stress on the other hand produces cracks and/or peeling of the film. The highest stresses are generated by high modulus materials such as Tungsten (411 GPa) or Chromium (279 GPa) for example, and can

cause spontaneous loss of adhesion (Mattox 1998, p.625). This is because these materials tend to not deform under stress and therefore 'store' it instead.

- **Porosity and pinholes**, which are closely related to the columnar morphology and particulate contamination, facilitate the diffusion of water or other corrosive substances which will in turn affect the adhesion of the film to the substrate.
- The columnar morphology is not the only one which promotes pinholes and porosity. Granular morphology also contributes to the formation of voids, and therefore allows de-adhesion to occur (Carcia et al. 2007).
- Molten droplets deposited can also be preferential sites for the growth of discontinuities (nodules). These **nodules**, which have a poor adherence to the substrate can easily give way to pinholes (Spalvins 1974).

7.2 PVD coating on PEEK

After reviewing the different types of existing vacuum deposition techniques. We can evaluate some of them experimentally in order to gain a better understanding of their effect as a moisture barrier, as well as to investigate whether they can be helpful in prolonging the lifetime of a package.

7.2.1 Evaporation coating

We first coat PEEK with a thin layer of titanium using a PVD technique, and observe the influence on moisture permeation. PEEK capsules, as described in previous chapters, were coated with a 3 μm titanium thin film using cathodic arc deposition, which is an evaporation technique. The result is shown in Figure 7.6. As previously, a humidity sensing circuit inside the capsule records the evolution the he relative humidity (n=3). The result (averaged) is compared to the result without coating, for two types of adhesive joints. The four experiments presented in Figure 7.7 are:

1. PEEK capsule adhesively joined with Loctite 4061 (Medical grade cyanoacrylate)
2. PEEK capsule adhesively joined with Loctite Hysol M31-CL (Medical grade epoxy)
3. PEEK capsule with 3 μm thick Ti coating deposited with Cathodic arc deposition PVD system (evaporation), adhesively joined with Loctite 4061 (Medical grade cyanoacrylate)
4. PEEK capsule with 3μm thick Ti coating deposited with Cathodic arc deposition PVD system (evaporation), adhesively joined with Loctite Hysol M31-CL (Medical grade epoxy)

Figure 7.6 PEEK Capsule with 3 m Ti coating (CAD)

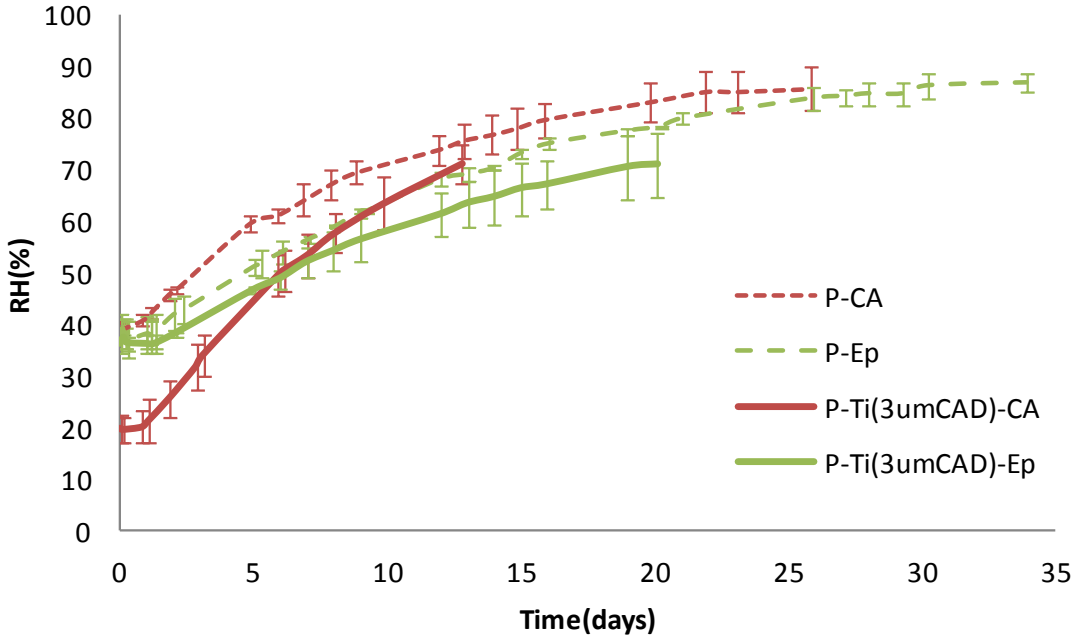

Figure 7.7 Evolution of the RH level in PEEK capsule with and without Ti coating, for two types of adhesive joints

The associated time constants are calculated by performing a regression on a linearised version of each curve (see 3.4.2 Determining the experimental time constant) and summarised in Table 7-1.

Parameters	P-CA	P-Ep	P-Ti(3µmCAD)-CA	P-Ti(3µmCAD)-Ep
Time constant (days)	16.3	18	11.4	23.5
Change coated/uncoated	-	-	-30%	+30%

Table 7-1 Time constants of Ti coated (CAD) PEEK packages

The main thing to note here is that the titanium coating produced only a very slight improvement in lifetime in one case (+30% when using the epoxy adhesive), and a reduction of lifetime in the other (-30% when using cyanoacrylate), which prompts two categories of questions:

- Why does the coating provide barely any improvement? Is it defective or is it all the fault of moisture ingress at the joint?
- Why is there a difference between the cyanoacrylate and the epoxy? Can this account for the reduction in lifetime?

We can first look at what happens at the joint. The experiment with the cyanoacrylate joint suggests that there is increased diffusion at the joint. Indeed, even if the coating was completely porous, the lifetime should be identical to that of the uncoated package. As it is shorter, the most likely explanation is that there is more moisture ingress at the joint.

This phenomenon has been previously observed when Zanni-Deffarges studied the diffusion of water in bulk and in joints (Zanni-Deffarges 1995), and based his findings on a study of moisture ingress in composite materials (Bonniau & Bunsell 1981), where it is shown that '*water enters the system along the interface between matrix* and fibre'. On this basis, he offers a possible explanation for this enhanced diffusion, where two mechanisms favour water ingress:

1. 'Regular' diffusion though the thickness of the adhesive
2. Water '*seeps or spread close to the interface and may then, in turn, diffuse towards the bulk of the glue line*'

A phenomenon of 'capillary diffusion' is suggested, where the interface region allows water to enter the system by seepage. Zanni-Deffarges imagines the diffusion near the metal (Ti coating)/polymer (Epoxy adhesive) transition to be analogous to a wetting triple line (see Figure 7.8).

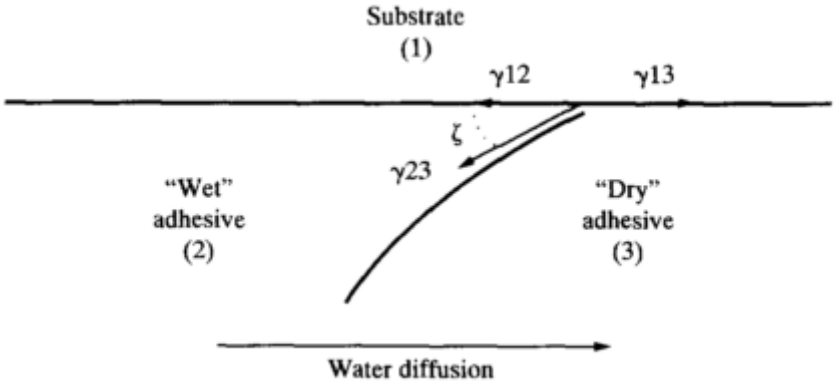

Figure 7.8 Model of diffusion front near the metal/polymer transition (from (Zanni-Deffarges 1995)**)**

The Ti coating is a relatively high energy surface, and the free energy could be quite large at the metal (oxides)/'dry' adhesive interface. As a result, a large interfacial tension could favour the water diffusion front progression by 'pulling' it. A good analogy given for this phenomenon is the wetting front of a liquid spreading on a high energy surface, where the surface tension powers the motion. We can test this hypothesis by looking at diffusion of moisture into coated capsules where the joint remains uncoated. This is presented in Figure 7.9.

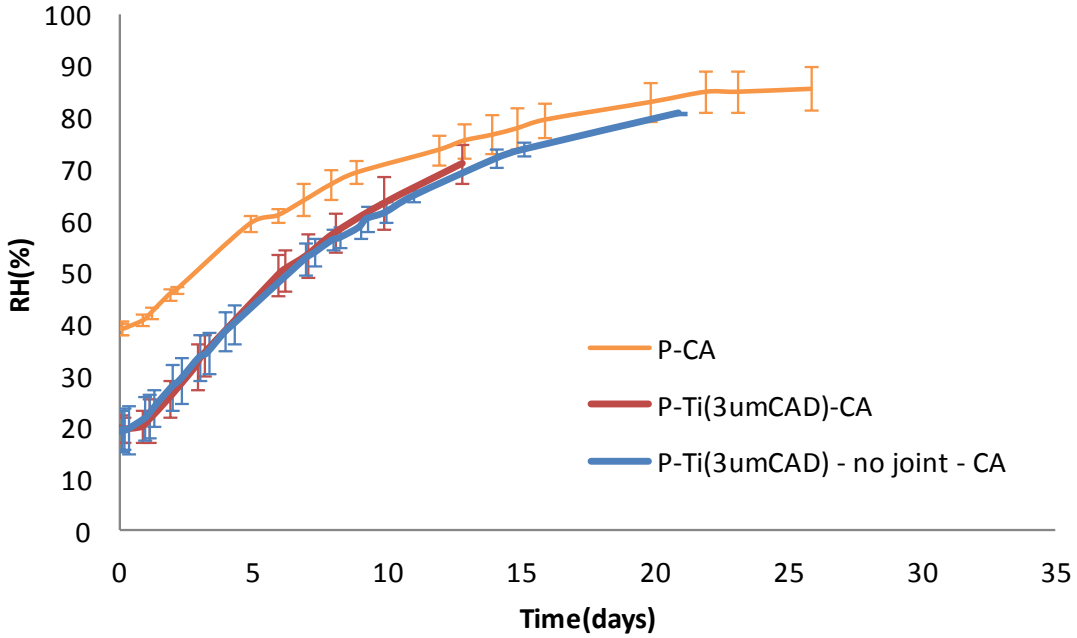

Figure 7.9 Effect of metallised joint on PEEK package adhesively joined with cyanoacrylate

It is very clear here that metalizing the joint area or not has little effect on moisture ingress. Looking at time constants, we find 11.4 days for the capsule coated everywhere versus 13.4 days for the capsule which is not coated at the joint. Moreover, the coated packages actually present a smaller time constant than the uncoated one. These facts suggest that there is indeed increased diffusion at the joint, although its effect is fairly limited. However, if we look at Figure 7.10 which presents results for the same experiment, but with an epoxy adhesive instead of cyanoacrylate, we can refine this analysis further.

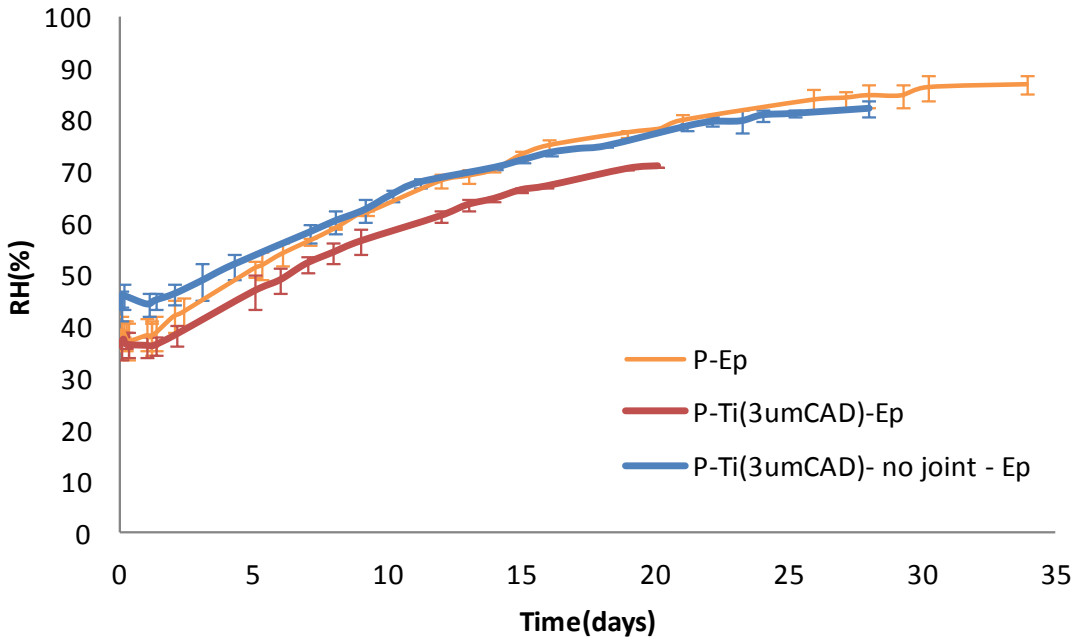

Figure 7.10 Effect of metallised joint on PEEK package adhesively joined with epoxy

Results are summarised in Table 7-2.

P-CA	16.3	**P-Ep**	18
P-Ti-CA	11.4	**P-Ti-Ep**	23.5
P-Ti-no joint-CA	13.4	**P-Ti-no joint-Ep**	22.3

Table 7-2 Time constants (in days) for packages coated with 3um titanium (with and without coating at joint)

When an epoxy adhesive is used, we can see that there is very little difference in time constants whether the joint remains uncoated or not. Moreover, the time constant of the coated capsules in this case (23.5 days) is slightly increased compared to the uncoated one (18 days). Nevertheless, the increase linked to the titanium coating remains small (30%), and the coating is mostly ineffective as a barrier against moisture. This experiment however shows no evidence that the theory of increased 'capillary diffusion' is true, and that it certainly is not applicable in this case. The lesser time constant observed in coated capsules joined with cyanoacrylate (11.4 and 13.4 days) compared with the uncoated one (16.3 days), demonstrates that there is increased diffusion at the joint in that case though. This can be explained by the metal capsule and lap shear test experiments led in Chapter 5, which established that titanium joints with cyanoacrylate are degraded very quickly in water (see section 5.2.3 for more details). For this reason, future experiments with metal coatings will only use epoxy as an adhesive.

7.2.2 Reasons for failure

We can now try to understand why this titanium coating is not effective in reducing diffusion of water through the walls. It could be that the coating is inherently porous, or that the interface PEEK/metal is degraded by the presence of water for instance. Water can degrade the bulk properties (chemical, physical and mechanical) of the adhesive, as well as the interfacial adhesive properties. It can also induce dimensional changes which may in turn result in additional stress in the deposited film.

We can first look at the effect of water by placing half capsules directly in water and observe the effect on the integrity of the film. Six half capsules (three top and three bottom parts) are placed open in water at 37°C to allow direct observation of potential delamination. The six parts, coded A, B, C, D, E and F, show various levels of resistance for the coating. The first signs of degradation appear on A after 6 days, and then gradually develop through time as shown in Figure 7.11.

Figure 7.11 Degradation of A

A similar phenomenon is observed with sample E (see Figure 7.12). It is interesting to note that the coating here is still present and the titanium does not peel away. Instead, it seems that water induces a lack of adhesion between the PEEK and the thin and dense Ti layer.

Figure 7.12 Degradation of E

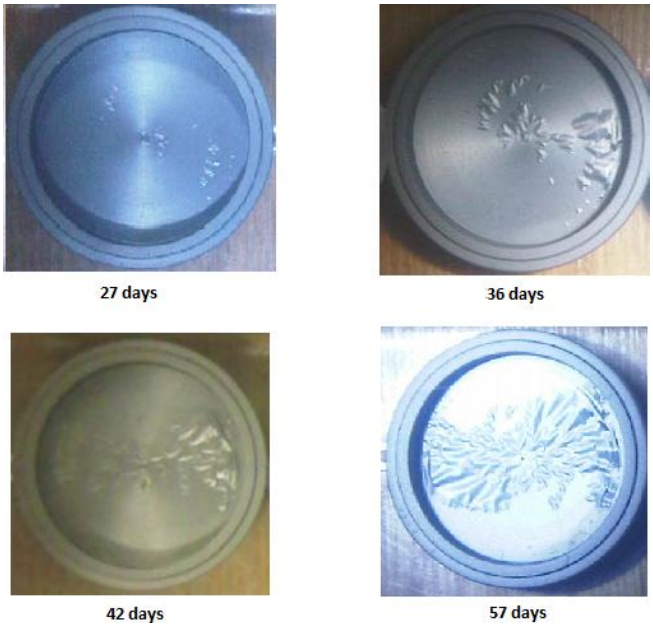

Sample D starts to be degraded only after 27 days, but in a similar fashion to the previous two samples (see Figure 7.13). Here again, there is still cohesion of the Ti layer, but lack of adhesion between the Ti layer and the PEEK body.

The other three samples, however, stay completely intact after two months in water (e.g. sample B in Figure 7.14).

Figure 7.13 Degradation of D

Figure 7.14 Sample B

As we have seen in 7.1.4 'Adhesion and loss of adhesion', internal tensile strength in the film can result in de-adhesion of the film. Blistering at the surface occurs by buckling when there is high residual compressive stress in the film which is relieved. Voids can subsequently be formed, as was observed. If there were residual tensile stress, we would have seen cracking or peeling of the film instead. The magnitude of the total stress depends on the film material and thickness. We obviously look for a thick coating to act as a barrier to moisture but it must be kept in mind that there is a trade off as increasing the thickness is likely to also increase the internal residual force.

This effect is enhanced by the presence of water. Water vapour diffusion has been reported to degrade the adhesive properties at the interface between a polymer material and a metallic film (Venables 1984). After diffusing to the interface, water can hydrolyse and destroy the Van der Waals bonds between the film and the substrate. Furthermore, we know that the diffusion barrier properties of the substrate material are important. '*For example, one mode of failure of aluminium metallised plastic film is diffusion of water from the unmetallised side of the polymer surface'* (Mattox 1998, p.627). It is this loss of adhesion which relieves the residual stress in the film and causes blistering and potentially rupture of the film. The apparent loss of adhesion might also be due to '*incomplete contact of the film with the substrate surface, or growth effects such as voids'* (Mattox 1998, p.327) during formation of the film, which could be caused by shadowing effects (because of machining of the surface for instance).

PVD evaporative coatings in general have been reported to produce 'non-optimal film properties' such as 'pinholes, less than bulk density, columnar morphology, high residual film stress' (Mattox 1998, p.326). We looked at the surface of the film with an field emission electron scanning microscope (SEM – JEOL JSM7401F) to see if these non desirable properties can be spotted. For reference, an SEM view of the uncoated PEEK package surface is displayed in Figure 7.15, with a x1400 magnification.

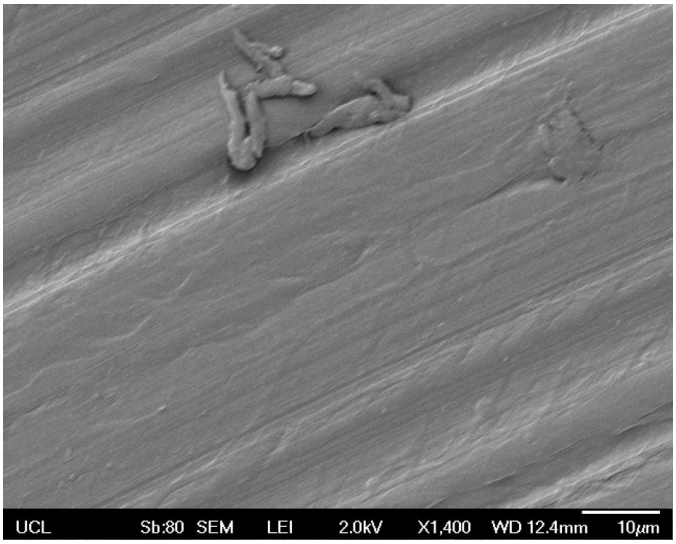

Figure 7.15 SEM image of PEEK capsule surface (x1400)

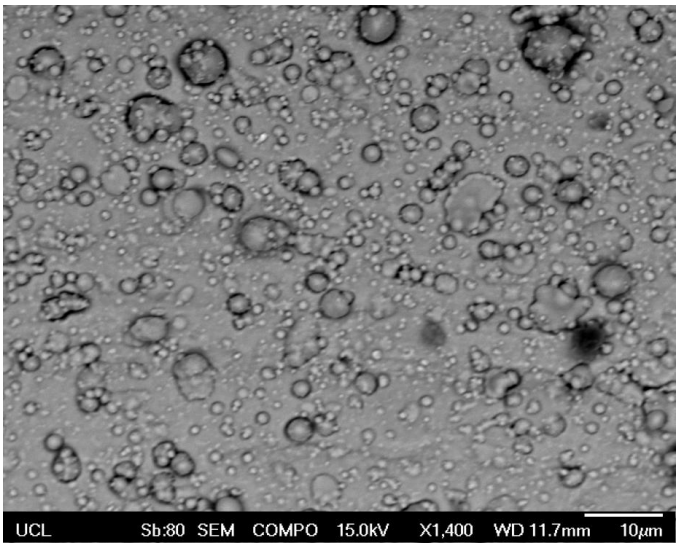

Figure 7.16 SEM image (backscattered e^-) of Ti coated capsule (CAD) (x1400)

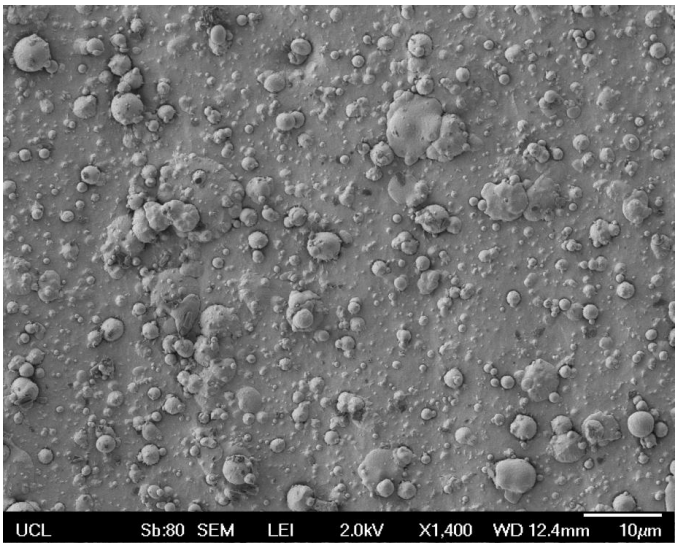

Figure 7.17 SEM image of Ti coated capsule (CAD) (x1400)

Figure 7.16 and Figure 7.17 show similar views of the surface of the Ti coated capsule we have tested. These views clearly confirm the presence of nodules. Molten droplets ('spits') deposited generally exhibit poor adhesion with the substrate and can easily give way to pinholes (see dark zones around nodules).

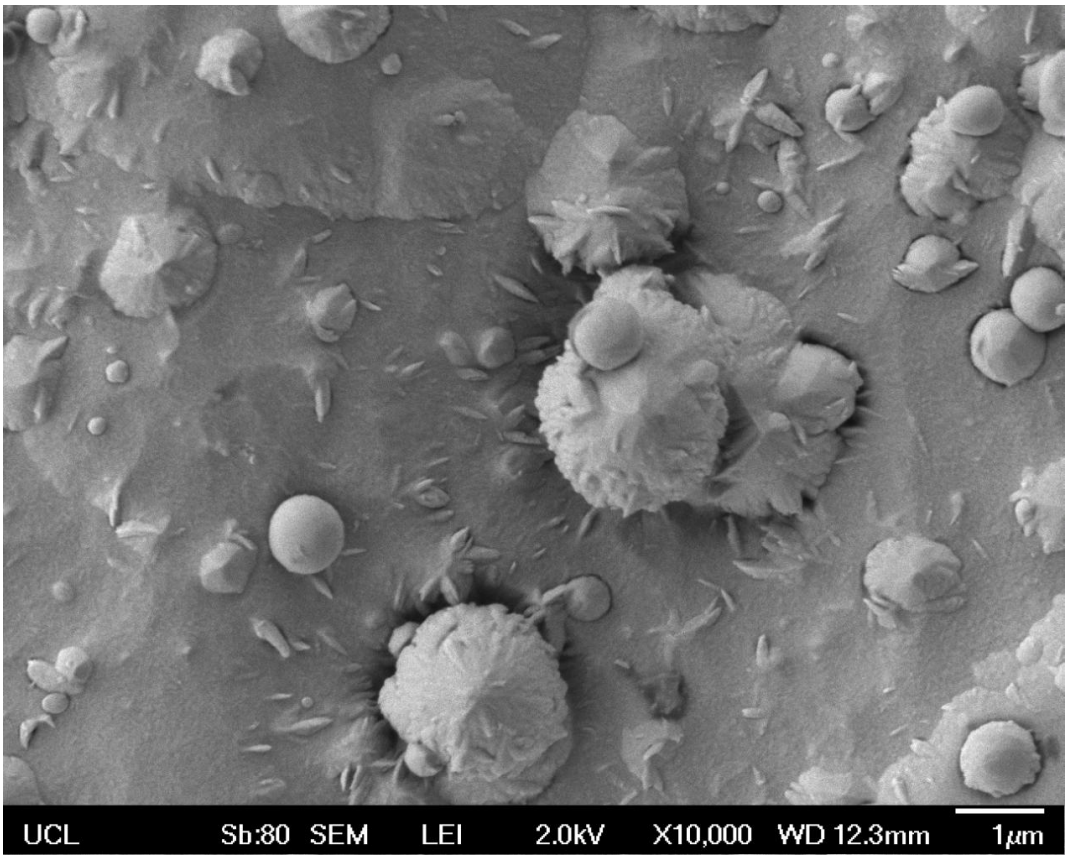

Figure 7.18 SEM image of Ti coated capsule (CAD) (x10,000)

Further magnification allows the observation (especially on nodules) of what is seemingly the columnar morphology we have described in section 7.1.4. Granular and columnar boundaries can facilitate gas permeation (Carcia et al. 2007). This is because each column can be bonded effectively to the substrate separately without being adequately bonded to each other (Prater & Moss 1983). Columnar morphology is therefore generally associated with porosity, which in our case is a big issue and can be another explanation as to why this coating does not act as an effective barrier against moisture.

Using a similar evaporation technique, a thin film of a different material is applied to new samples. Aluminium is deposited with a thickness of 3 μm (three 1 μm layers superimposed). Previous customers of the company which performed the coating have reported an increase in barrier properties when a base lacquer is applied prior to deposition. This is therefore tested by applying such a pre treatment, stoving the capsule, and then performing the Al thin film deposition. The lacquer used was MBASE 045A manufactured by Marbo Milan Italy. These packages are shown in Figure 7.19 and the

results are plotted in Figure 7.20, alongside the results corresponding to the previous experiment with the titanium thin film, for comparison purposes.

Figure 7.19 PEEK capsules with evaporation deposited aluminium thin film - with (bottom) and without (top) base lacquer applied beforehand and stoved

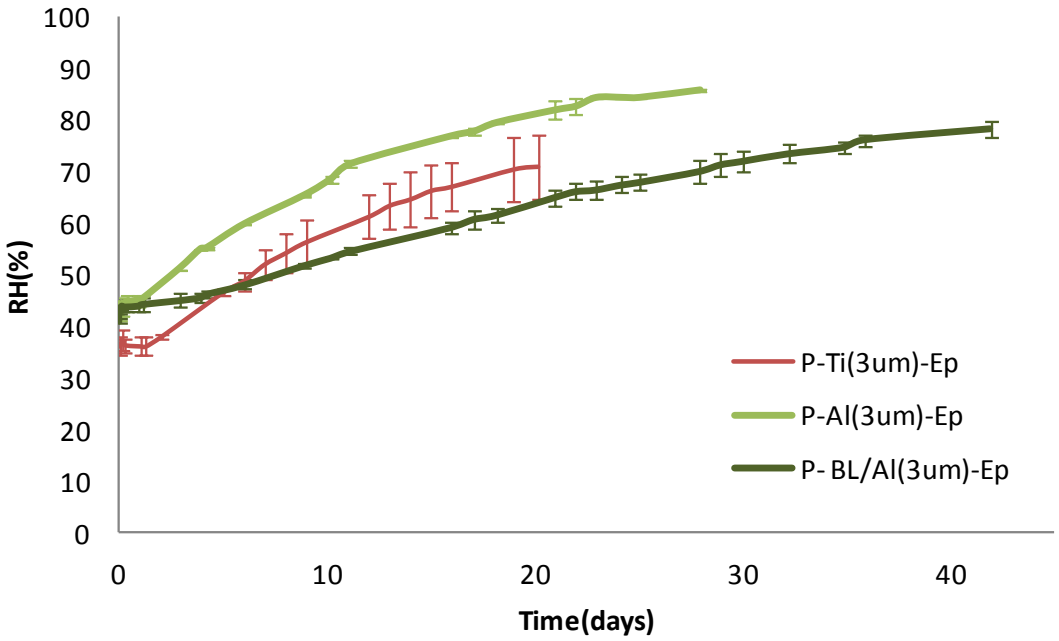

Figure 7.20 Evolution of RH in evaporation PVD coated capsules (Al -3 µm)

The time constant of the aluminium coated capsule is 18.7 days, which is very similar to the uncoated capsule (18 days), but actually less than the lifetime of the Ti coated capsule (23.5 days). This coating is therefore completely porous and ineffective as a barrier to moisture. However, the result of the package with base lacquer applied prior to deposition is extremely interesting. The lifetime in this case is 41.7 days, which represents an improvement of more than 130%. This operation allowed an increase of the time constant by a factor of 2.3. As we have seen, shadowing or step coverage can be problematic with evaporation processes, as it affects film growth and can promote columnar or granular morphology and porosity. The lacquer can to some extent limit this

by smoothing the deposition surface and providing better adhesion properties to the first layer of metal deposited, which in turns affects the whole process of film growth in a positive manner. This is clearly seen in Figure 7.21 and Figure 7.22 by comparing the surfaces of both types of samples. The surface of the lacquered capsule is clearly much smoother after deposition than the one where no lacquer was applied. The film is still porous, but to a much lesser extent. Some bigger defects also subsist. We can see a cracked patch in Figure 7.22, which is presumably due to loss of adhesion and 'lifting off' of the coating (because of the action of water). The bright reflection on the 'patch' (which is observed with further SEM magnification in Figure 7.23) is due to electrons being conducted away because of this 'lifting off'. Small dust particles can be also be seen. These were trapped when the base lacquer was applied and the metal film was deposited on top.

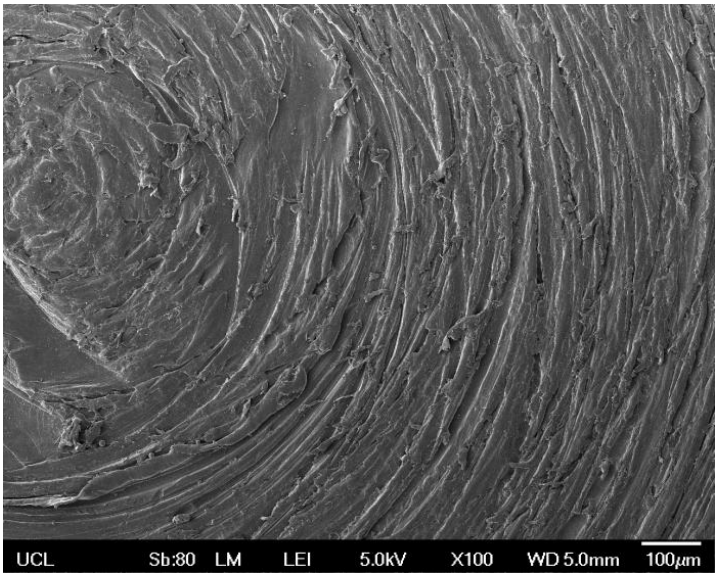

Figure 7.21 SEM image of Al coated capsule (evaporation) without base lacquer (x100)

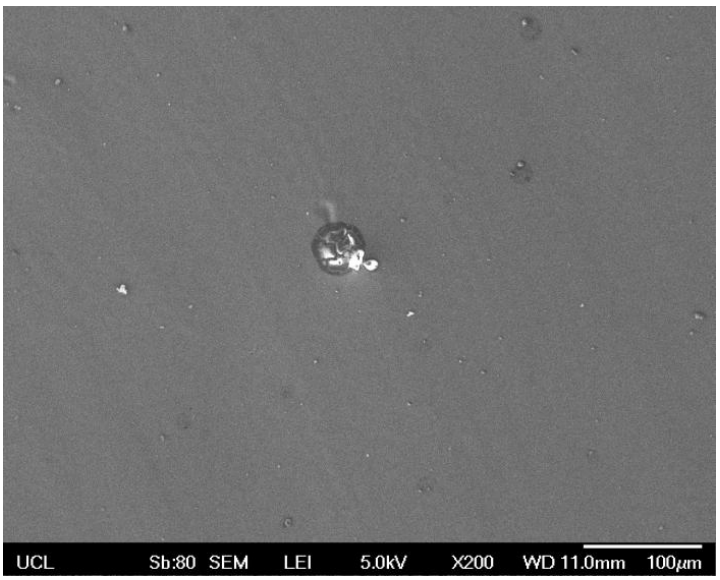

Figure 7.22 SEM image of Al coated capsule (evaporation) with base lacquer (x200)

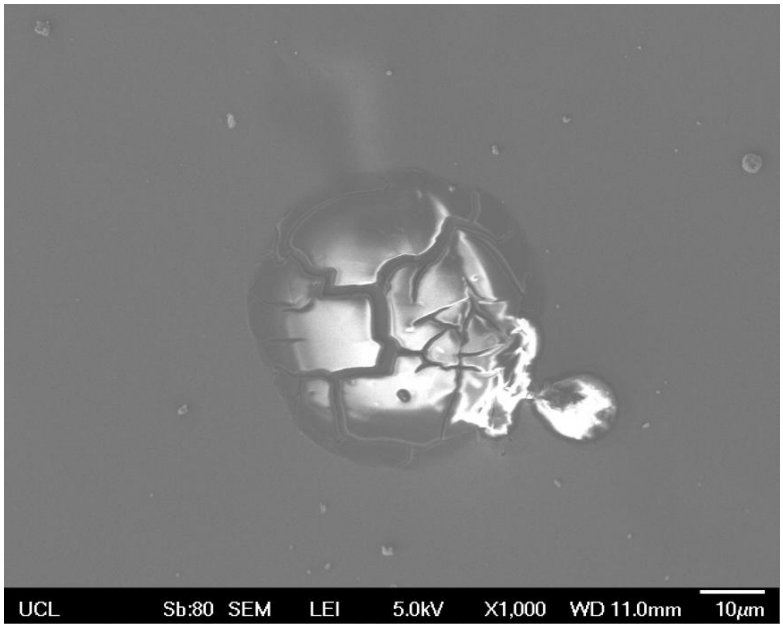

Figure 7.23 SEM image of Al coated capsule (evaporation) with base lacquer (x1,000)

7.2.3 Sputtering coating

After trying evaporation PVD techniques, we can look at sputtering and see if the thin films produced result in increased barrier properties. A PEEK package is coated with Zirconium at a thickness of 1.9 µm (2 stages) using magnetron sputtering (see 7.1.1.2 'Sputter deposition techniques'). Results are plotted in Figure 7.24.

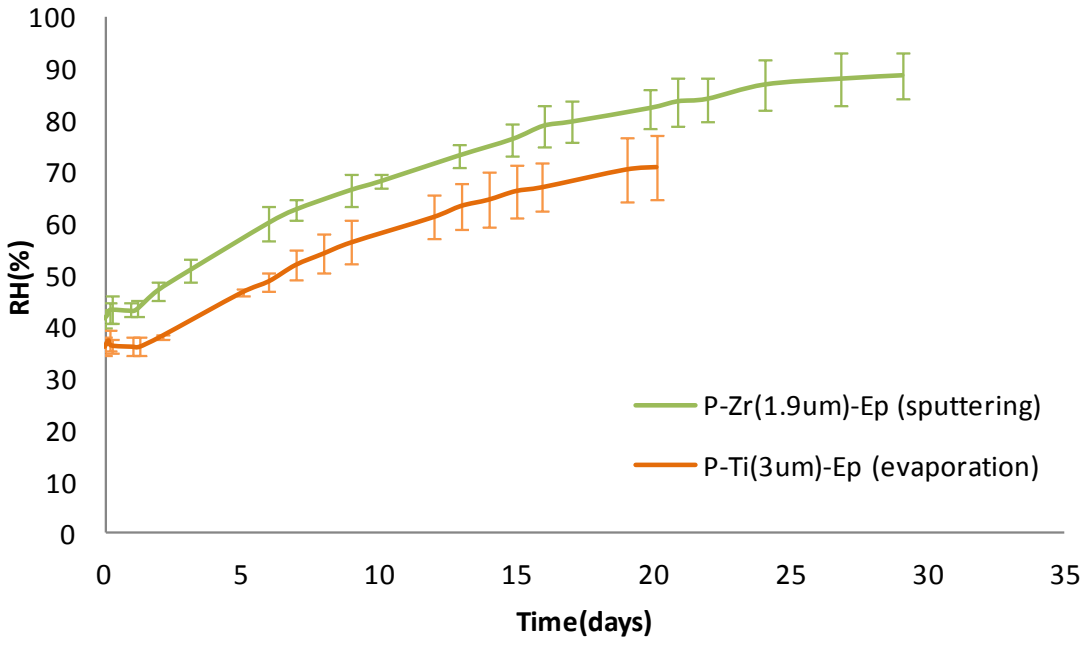

Figure 7.24 Evolution of RH in magnetron sputtering PVD coated capsules (Zr – 1.9 µm)

The lifetime obtained is 16.7 days, which is shorter than both the coated (3 μm Ti) and uncoated capsules. This method is therefore highly ineffective. Upon opening the package, we can see a lot of blistering of the film, as can be observed in Figure 7.25.

Figure 7.25 Zr coated PEEK capsule (magnetron sputtering) - blistering of the film

As was the case for the delamination experiment of the Ti coated capsule, this can be explained by high residual compressive stress in the film which is relieved when water induces a lack of adhesion at the interface. There is always a trade off between thickness of the film, which presumably we want to maximise, and residual stress, which we should be looking to minimise. There are recommendations in the literature to limit the thickness of high modulus materials such as Chromium, in order to limit residual stresses in the deposited film (Mattox 1998, p.645). In the case of PEEK and other polymers however, all metallic materials comparatively have a significantly higher modulus, and therefore the film thickness should be minimised irrespective of the metal used.

We can therefore try thinner coatings with different materials. PEEK capsules are coated with a thin film of thickness 0.5 μm only (in this case, n=1, because of resources available). The process used this time is Argon sputtering (see 7.1.2), and the film materials used are aluminium, titanium, and chromium. Those capsules are presented in Figure 7.26, and results are plotted in Figure 7.27.

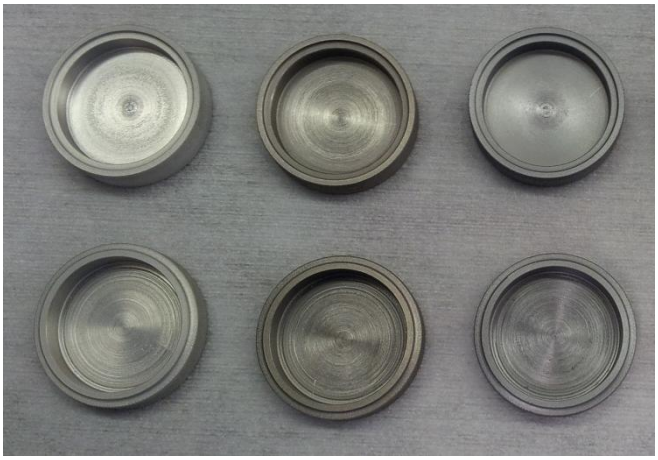

Figure 7.26 Ar sputtering of PEEK capsules with (from left to right): Al, Ti, and Cr (500nm thickness)

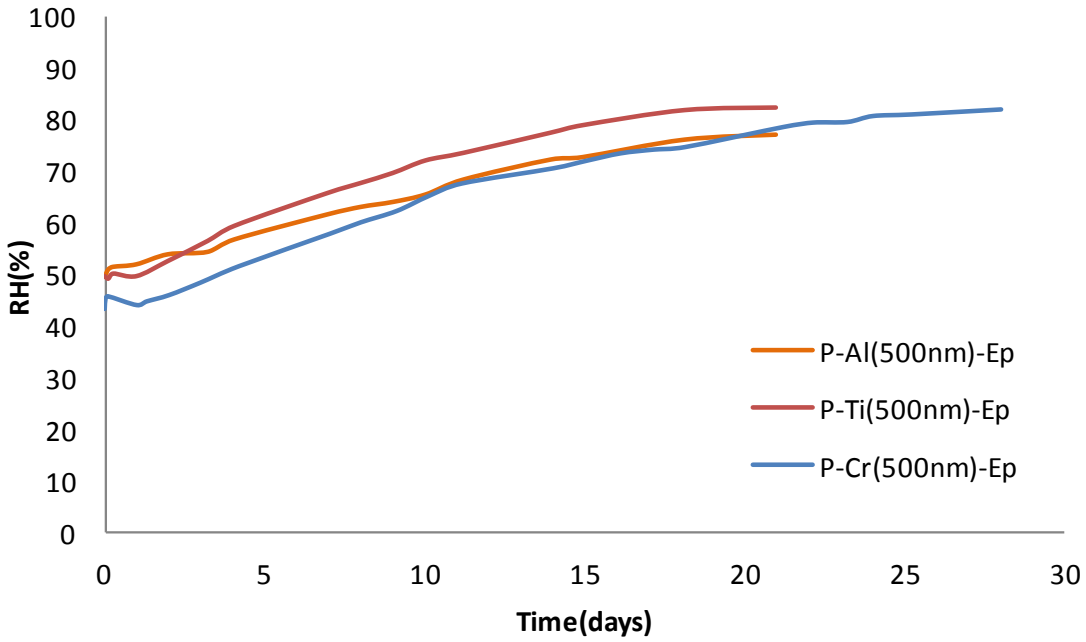

Figure 7.27 RH in Ar sputtering PVD coated PEEK capsules (Al, Ti, Cr – 0.5 µm)

Results are summarised in Table 7-3. The aluminium coating provides a 39% increase in time constant compared to the uncoated package, whereas the chromium coating sees an increase of 10% and the titanium coating has no effect. Once again, these films failed to provide a significant increase in lifetime. Unlike previously though, the film thickness has been minimised (0.5 µm) to reduce residual film stress. The main culprit here is the porosity of the film, and residual stress in the film is not as much of an aggravating factor.

Parameters	P-Ep	P-Al-Ep	P-Ti-Ep	P-Cr-Ep
Time constant (days)	18	25	17.9	19.8
Change coated/uncoated	-	+39%	-0.6%	+10%

Table 7-3 Time constants of Ar sputtering PVD coated PEEK packages (Al, Ti, Cr – 0.5 µm)

This is confirmed by Figure 7.28 which shows an SEM view of the surface of the Ti coated capsule with a x20,000 magnification. The granular/columnar morphology is clearly visible here, and the grain/columns have a width of about 0.1-0.3 µm. This is 300-1000 times the size of water molecules, which explains the porosity of such films, as the space between poorly bonded structures is sufficient for water molecules to diffuse through.

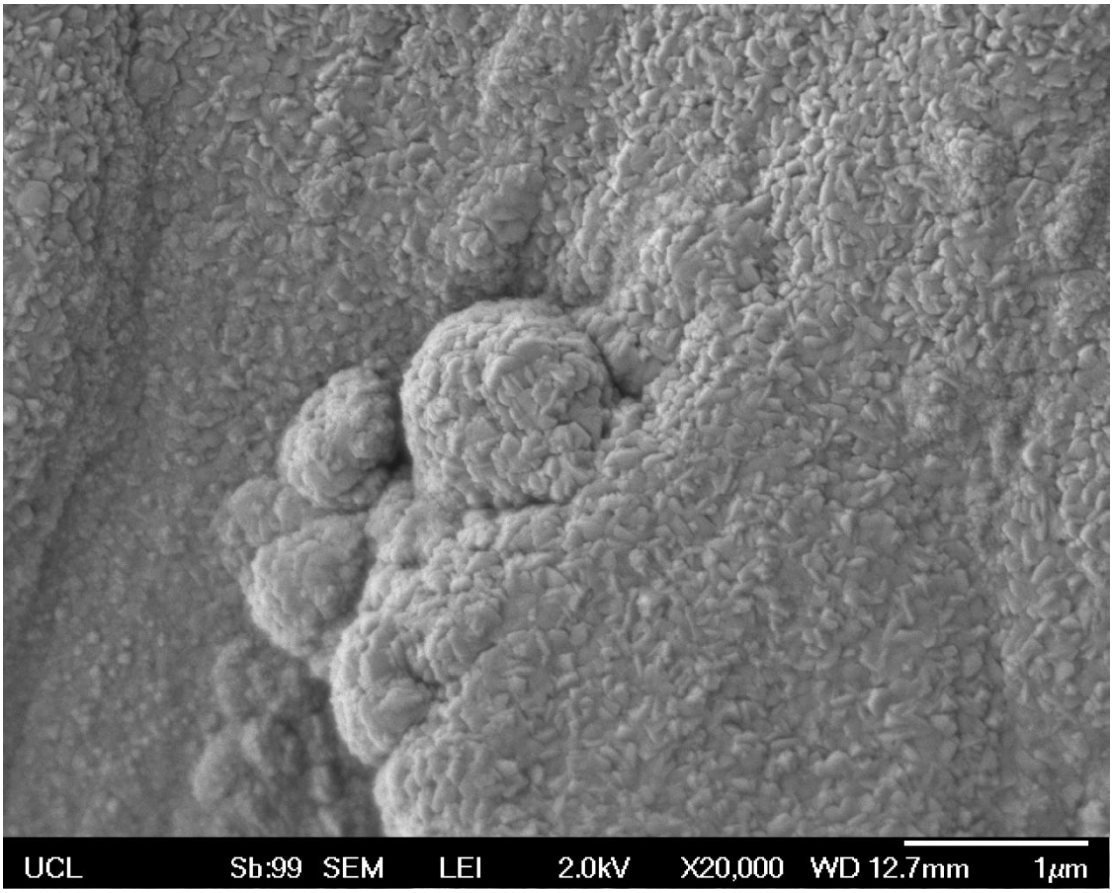

Figure 7.28 SEM image of Ti coated capsule (sputtering) (x20,000)

Finally, we can test the effect of multi-layer and compound films on the barrier properties of the film. Using Ar sputtering, 2 sets of PEEK capsules were coated with a seed layer of 0.05 μm of titanium for one, chromium for the other, followed by 0.45 μm of gold for both. The capsules are displayed in Figure 7.29. Another set of capsules is coated with a 2 μm thick film of nichrome using Ar sputtering. The results from these experiments are plotted in Figure 7.30 and summarised in Table 7-4.

Figure 7.29 Ar sputtering of PEEK capsules with (from left to right): Ti+Au and Cr+Au (500 nm thickness)

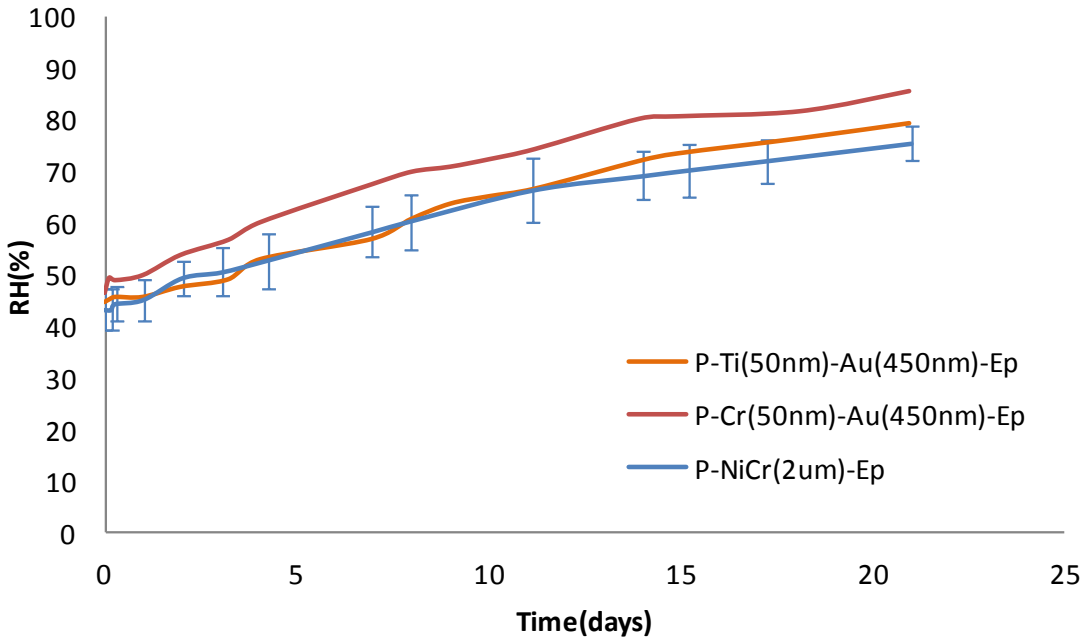

Figure 7.30 RH level in Ar sputtering PVD coated PEEK capsules (Ti+Au, Cr+Au - 0.5 µm, NiCr – 2 µm)

Parameters	P-Ep	P-Ti-Au-Ep	P-Cr-Au-Ep	P-NiCr-Ep
Time constant (days)	18	20.2	15.9	25
Change coated/uncoated	-	+12%	-12%	+39%

Table 7-4 Time constants PVD coated PEEK packages (Ti+Au, Cr+Au - 0.5 µm, NiCr – 2 µm)

The NiCr coating provides a 39% increase in time constant compared to the uncoated package, whereas the titanium-gold coating sees an increase of 12% and the chromium-gold shows a 12% decrease. None of these succeed in providing effective barrier properties against moisture, for the same reason as previously. Figure 7.31 shows that the titanium gold film also exhibits granular morphology.

In multilayer systems, poor adhesion can also occur if the first layer deposited is contaminated before the second layer deposits. The example of Ti-Au metallisation is given in the literature (Mattox 1998, p.645), where titanium can be oxidised, in which case the subsequent Au layer would not adhere well.

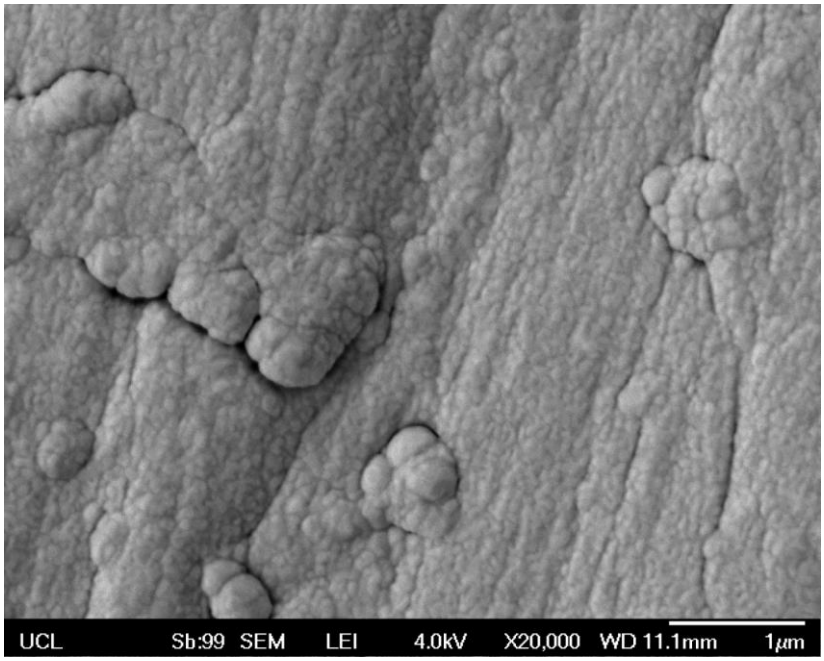

Figure 7.31 SEM image of Ti-Au coated capsule (sputtering) (x20,000)

7.3 Plasma enhanced CVD

As reported in the literature review section of this chapter (see 7.1.2), chemical vapour deposition can also be used to deposit thin films at temperatures which are compatible with PEEK.

In a first instance, capsules are coated using PVD (titanium, 1 μm), followed by plasma assisted CVD (PaCVD) of Diamond-Like Carbon (DLC) (2 μm). It is a film of amorphous carbon (a-C) which has a number of properties similar to those of bulk diamond, such as inertness, hardness or coefficient of friction, as well as the same cubic chemical structure (Monaghan et al. 1993). In order to get optimum properties, CVD at 600 – 900ºC is generally used. In our case however, PaCVD is used, close to 100ºC. Although it ensures that this is compatible with our substrate material, it can also potentially affect the properties of the deposited film.

Another set of PEEK capsules is coated with a thin film of siloxane (SiOx) (1 μm), using PaCVD. The result is a transparent coating which is presumably quite uniform and continuous, as suggested by Figure 7.32, which shows how it refracts incident light and produces a 'rainbow effect' on the surface.

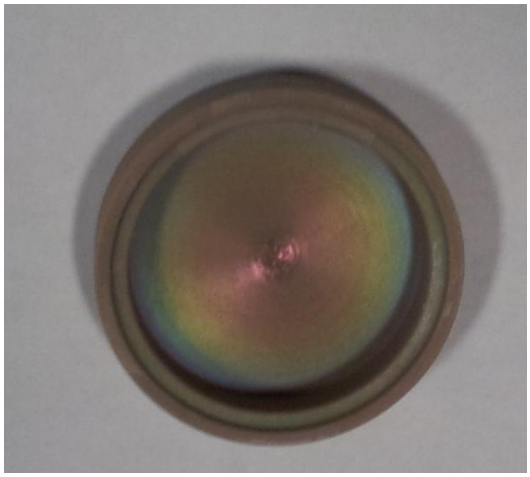

Figure 7.32 PEEK capsule coated with SiOx by PaCVD (1 µm thickness)

The two types of packages produced are tested in the usual fashion, and results are plotted in Figure 7.33. Results for both packages are extremely similar, and the time constants found are 20.8 and 20.9 days.

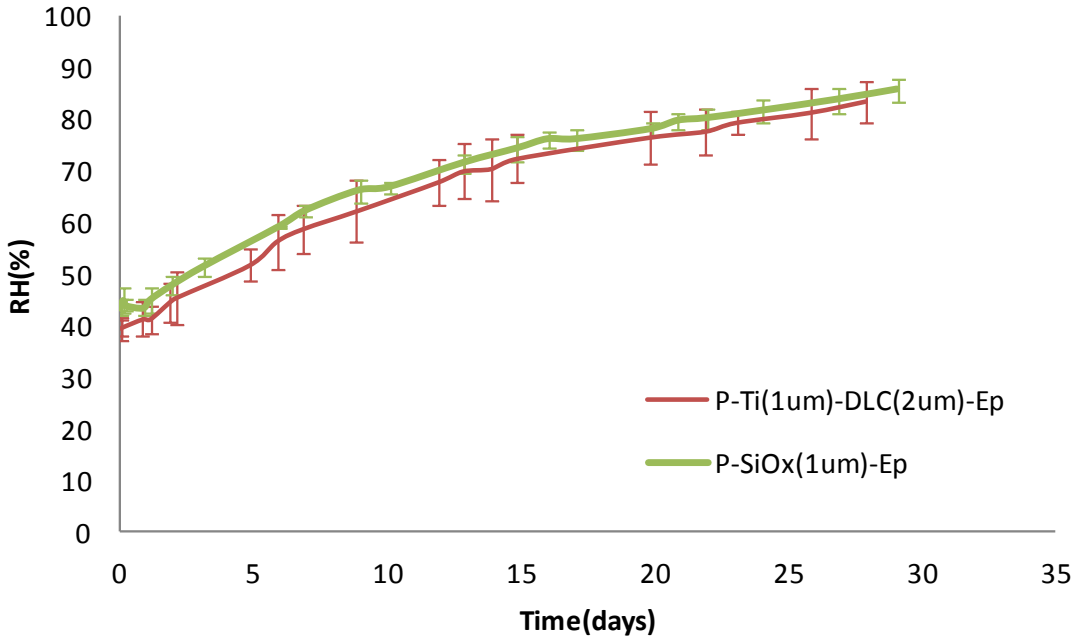

Figure 7.33 RH level in PaCVD coated PEEK capsules - Ti (1 µm)+DLC (2 µm), SiOx (1 µm)

It is interesting to notice that both DLC and SiOx are hydrophobic. However, this does not affect the diffusion of gaseous molecules of water, which are very small (less than 0.3 nm) and which flow is driven by the pressure difference between the two sides of the package walls. Figure 7.34 shows the peeling off of the DLC coating because of the action of water. The peeling off and curling of the film this time is due residual internal tensile stress (Laugier 1979). This can be attributed to the low deposition temperature, which generates a high amount of residual stress. (Monaghan et al. 1993)

Figure 7.34 DLC coating peeling off

Figure 7.35 presents SEM images of the siloxane coated surface with x100 and x20,000 magnification. The former shows that the film is smoother than what was obtained with PVD coatings (see Figure 7.21), while the latter refines this to show discontinuities in the film at a smaller scale, explaining the failure to decrease significantly the transmission rate of water through the package walls.

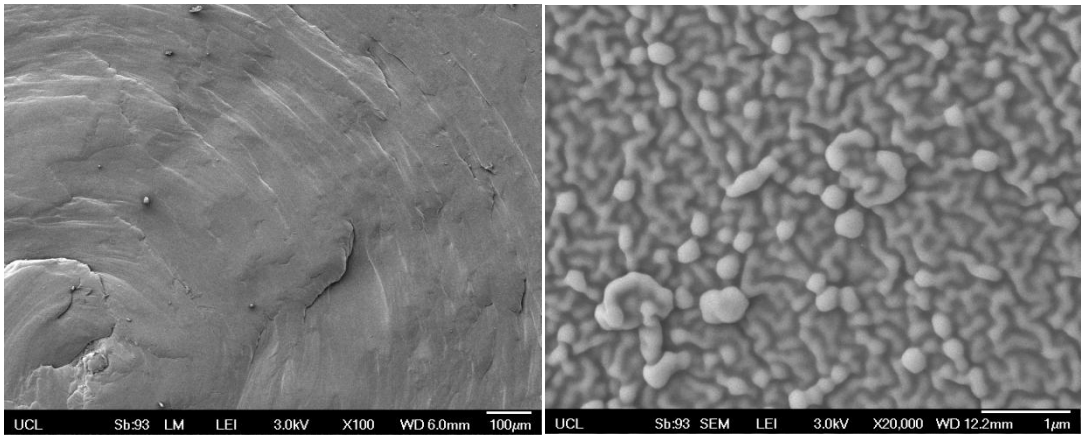

Figure 7.35 SEM image of SiOx coated capsule (PaCVD) (x100, x20,000)

PaCVD grown SiOx thin films on other polymers have also been reported in the literature to exhibit pinhole densities which are compatible with our observations (Carcia et al. 2007; da Silva Sobrinho et al. 2000). As with other vacuum thin film coatings, permeation occurs through pinholes, pores or defects.

7.4 Other coating techniques

After testing PVD and PECVD coatings, we can now look at a few other deposition methods and assess their impact on permeability.

7.4.1 Atomic Layer Deposition of alumina

Atomic Layer Deposition (ALD) is a variation of CVD, which provides very fine control over the film thickness. In ALD, two precursors are deposited alternately, and produce a self limiting reaction which results in the formation of the wanted compound. This

sequential reaction of the precursors with the substrate surface is the main difference with CVD. The substrate surface adsorbs one of the precursors until saturation, before the second precursor is introduced. Between the depositions of each species, all excess and non reacted material is purged from the system using pulses of an inert gas. With each cycle, the same amount of material is deposited, and the film thickness can be controlled very accurately. Moreover, this technique has the advantage of producing highly conformal and uniform coatings (Carcia et al. 2009). This is of particular interest when coating a machined polymer surface such as that of our PEEK capsule. ALD also offers the advantage of a low deposition temperature (Groner et al. 2004), which was the limiting factor to the use of CVD.

As we have seen in the previous section, PVD and PECVD films either have pinholes or granular/columnar morphologies which allow water vapour permeation. ALD deposition of a 25 nm thick alumina (Al_2O_3) film on a polyester film has been reported to reduce the water vapour transmission rate by a factor of up to 10^5 compared to the uncoated polymer film alone (Carcia et al. 2007). Other studies report an improvement of three orders of magnitude (George 2010). This is because ALD films are highly conformal (Ritala et al. 1999) and nearly pinhole-free (Groner et al. 2002).

In order to deposit Al_2O_3, the substrate is exposed sequentially to trimethylaluminium [$Al(CH_3)_3$] (TMA) and water in an ABAB... binary reaction sequence (Dillon et al. 1995). This binary reaction is:

$$2Al(CH_3)_3 + 3H_2O \rightarrow Al_2O_3 + 6CH_4$$

For this experiment, a 40 nm Al_2O_3 film is deposited on PEEK capsules of uniform thickness (2 mm – see Figure 7.36) using ALD, and the capsules are tested in the usual fashion. The evolution of the humidity inside the package is plotted in Figure 7.37, alongside the RH level in an uncoated PEEK capsule and in a solid titanium capsule (see 5.2.3.2 Water diffusion through the joint only – Metal capsules) for comparison. All these packages are sealed using Loctite Hysol M-31CL (epoxy). The time constants are summarised in Table 7-5.

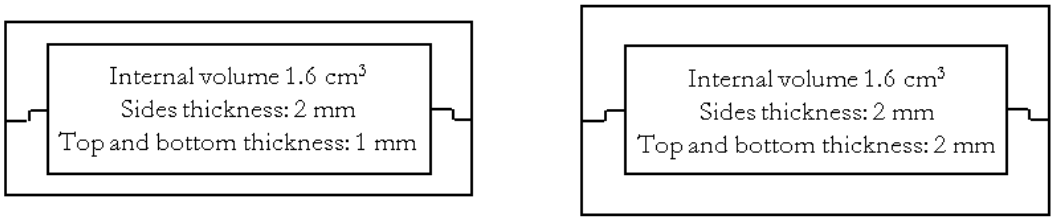

Figure 7.36 Cross section of cylindrical PEEK capsules used for PVD/PaCVD tests (Type A -left) and ALD tests (Type B - right)

Parameters	PEEK - Epoxy seal	PEEK - Al2O3 ALD coating - Epoxy seal	Titanium – Epoxy seal
Time constant (days)	42.8	101	458
Change coated/uncoated	-	+136%	+970%

Table 7-5 Time constants of uncoated and ALD PEEK packages, coated PEEK packages, and titanium packages

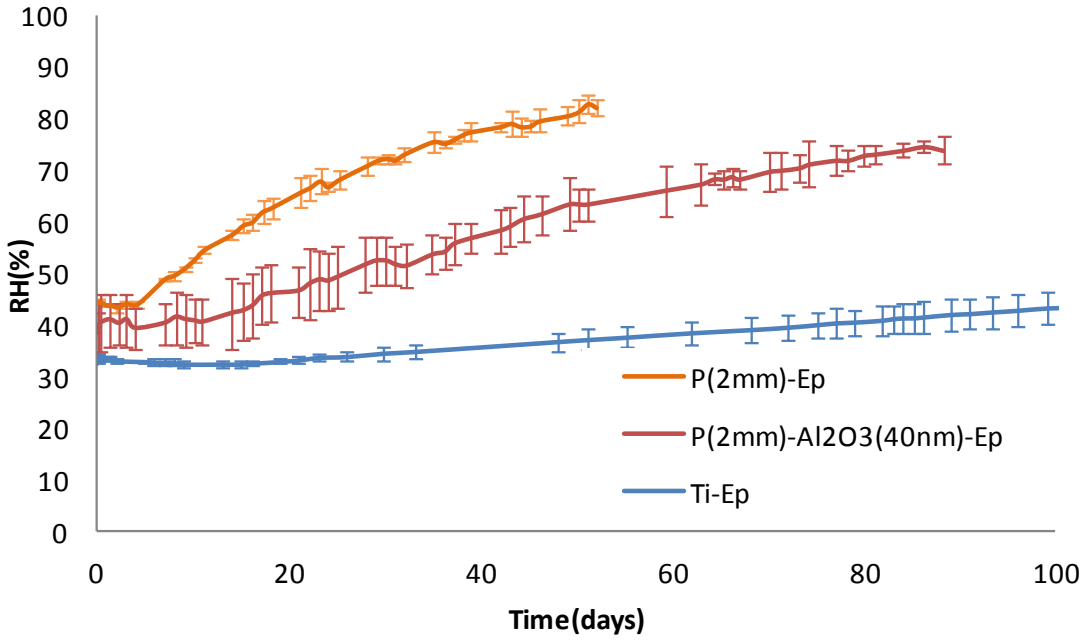

Figure 7.37 Evolution of the RH level in adhesively joined titanium and PEEK capsules (with and without ALD coating)

The uncoated PEEK capsule has a time constant of nearly 43 days, and the ALD coated package has a time constant of 101 days, which represents an improvement of 136%. The ideal case is represented by the adhesively joined titanium capsule (τ = 458 days), where water only permeates through the adhesive seal. Although the improvement of lifetime when using ALD is significant, it should be much closer to the ideal case of the Ti capsule, according to the results previously reported from the literature (George 2010; Carcia et al. 2007).

One possible explanation for this mismatch could be that the results reported refer to deposition on low roughness surfaces such as polymer membranes. Our machined PEEK capsules however have a much greater surface roughness, the scale of which is greater than the thickness of the Al_2O_3 film (40 nm). Nevertheless, it has been shown before that such ALD films are perfectly conformal even in similar conditions (Ritala et al. 1999). This explanation is therefore unlikely to be the main cause of the difference between the expected and observed effects.

The most likely explanation lies in the level of moisture the film is exposed to. While the studies which report a 10^3 - 10^5 decrease in water vapour transmission rate were done at 85% RH, other studies report that when exposed to saturated water vapour, the barrier properties are degraded significantly after 4-5 days (Dameron et al. 2008; Nahar 2000; Nahar 2002):

'Water exposure on Al_2O_3 can lead to the corrosion and reconstruction of the Al_2O_3 film. This degradation may lead to the formation of pinholes in the Al_2O_3 ALD film and result in barrier failure' (Dameron et al. 2008)

However, the same study reports that this issue can be resolved by using Al_2O_3/SiO_2 bilayers as SiO_2 does not form a hydrate with water and can therefore protect the alumina film.

7.4.2 Electrodeposition with copper

Electrodeposition, otherwise known as electroplating, consists in using an electric current to produce a (usually) metallic coating. The object to be coated is the cathode of an electrolytic cell, and is immersed into an aqueous solution containing a salt 'MA' of the metal 'M' to be deposited. The metallic cations 'M^+' of the salt are attracted to the cathode of the cell, and therefore plate the object. The anode is generally made of the metal we want to plate, and is used to replenish the solution in metal ions as these are progressively deposited on the cathode. Another method consists in using a non consumable anode, but the bath must then be periodically replenished with metal ions.

PEEK is a non conductive polymer, and therefore cannot be used directly as the cathode of the electrolytic cell. I used a technique called brush plating in order to electroplate the sample. The surface of our capsule must be made conductive beforehand. This is done using a conductive ink which is painted onto the surface in successive layers with oven baking between each layer.

According to manufacturer's specifications, a layer of lacquer is first applied to improve adhesion of the conductive ink to the substrate. The first layer of conductive ink, applied in a circular motion, is left to dry for 24 hours at room temperature and placed in a fan oven at 50°C. A second layer is then applied across the sample and placed in the oven for

the same amount of time. Instead of plunging the substrate into a bath, an absorbent swab dipped into the copper solution is placed on a carbon electrode (anode). The conductive surface to be coated is linked to the negative pole of the power supply with a crocodile clip, and the electrode with the swab on top is run through the surface to coat, and periodically dipped into the copper solution to replenish it in copper ions.

However, the copper turns out to deposit very unevenly across the surface, which may be due to uneven spreading of the conductive ink during drying and hence differences in conductivity. As a result, the layer deposited becomes quite thick by the time all the sample surface is coated. This is observed on more than 30 samples, and I did not manage to find deposition conditions (supply voltage, amount of solution used, rate of replenishing) which allowed a uniform thin film to be deposited. The best and most uniform result obtained is shown in Figure 7.38. Unfortunately, none of the capsules could be tested in water as the deposited copper layer is too thick to be used with our telemetry system and did not allow reading of the humidity level inside the package.

Figure 7.38 PEEK capsule electroplated with copper

7.4.3 Dip coating with titania

Titania can be deposited via a sol-gel dip coating method. This is a chemical procedure where a colloidal solution (sol) is a precursor, which after hydrolysis and polymerisation evolves into a network (gel). The sol is made at room temperature from titanium n-butoxide, n-butanol, isopropanol, acetonitrile and water. The overall reaction formula is

$$Ti(OBu)_4 + 2H_2O \rightarrow TiO_2 + 4BuOH$$

After deposition by dip coating, the substrate is then generally calcinated at high temperature (500°C) to remove any trace solvent and promote crystallisation (Dunnill et al. 2011; Kafizas et al. 2009). PEEK however cannot resist such a high temperature, which means that the deposited film will remain largely amorphous.

The preparation procedure is detailed in (Kafizas et al. 2009). To prepare the sol, acetylacetone (2.5246 g, 0.02526 mol) is first dissolved in butan-1-ol (32 cm^3, 0.35 mol). The purpose of this colourless solution is to moderate the reaction rate (Su et al. 2004).

Titanium n-butoxide is then added (17.50 g, 0.05 mol) and stirred for an hour using a magnetic stirrer. After this stage, distilled water (3.64 ml, 0.20mol) dissolved in isopropanol (9.05 g, 0.15 mol) is added to the solution and stirred for one hour. The prepared sol is aged over night and then ready for dip coating. The apparatus used for dip coating is shown in Figure 7.39.

The substrate is dipped in the sol and withdrawn at a steady rate of 0.2 $cm.s^{-1}$, producing a 100nm thick layer at each dip (Kafizas et al. 2009). As mentioned previously, deposited TiO_2 is generally baked afterwards at 500°C to promote crystallisation and form anatase. However this is not possible with PEEK, which has a glass transition temperature of 143°C. Nevertheless, it is still necessary to bake the samples in order to remove any trace of solvent. Samples are baked at 120°C, with the consequence that the deposited films remain amorphous. A certain degree of shrinkage of the film is expected upon baking, so adding more layers can be beneficial. 3 sets of parameters are therefore tested (n=3):

1 Single coat + baking at 120°C for one hour
2 Three successive coats, with one hour room temperature drying between each. After all layers are deposited, baking at 120°C for one hour
3 Three coats are applied, with baking at 120°C for one hour between each

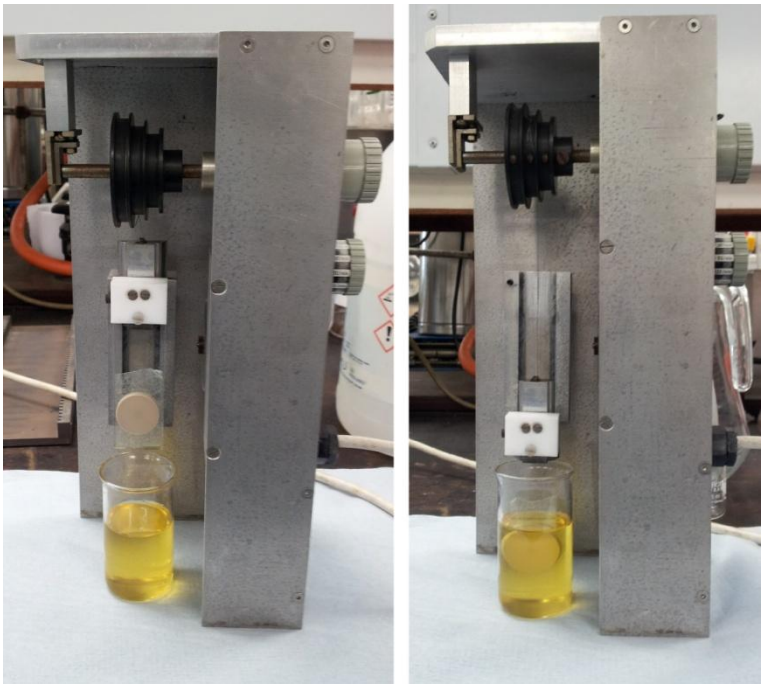

Figure 7.39 Deposition of titania thin films by sol-gel dip coating preparation

All capsules in this experiment are joined adhesively with Loctite 4061 (cyanoacrylate). The results are plotted in Figure 7.40. The corresponding time constants are identical for all tested parameters and equal to 13.5 days, which is shorter than the uncoated capsule result (15.9 days).

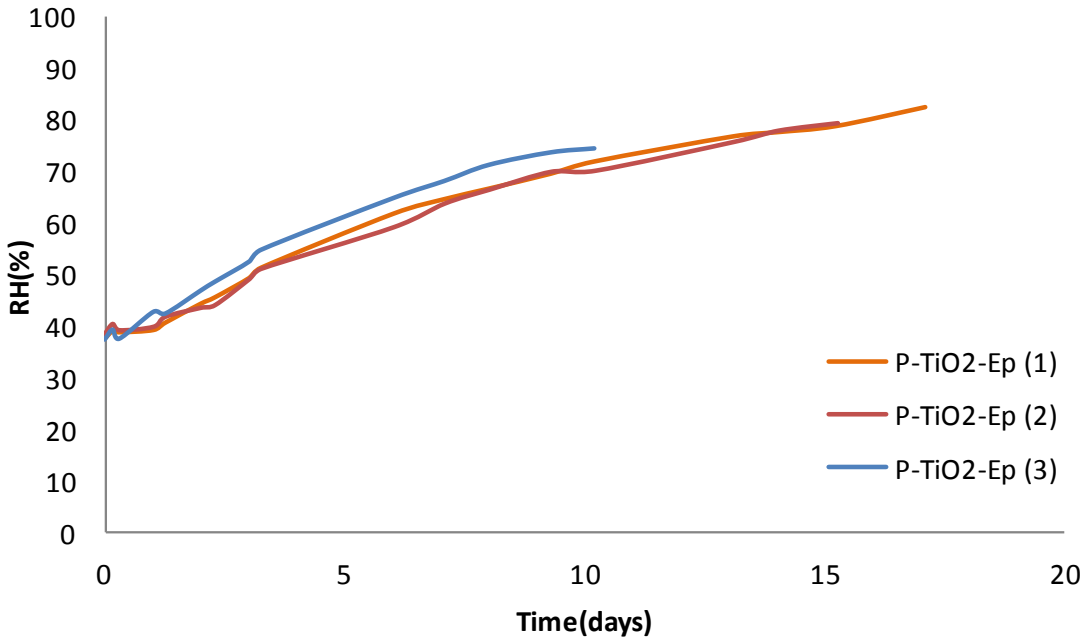

Figure 7.40 RH level in TiO_2 coated PEEK capsules

This type of coating is ineffective largely because of the shrinkage which occurs and creates large cracks in the coating, as shown in Figure 7.41. This was observed for all samples.

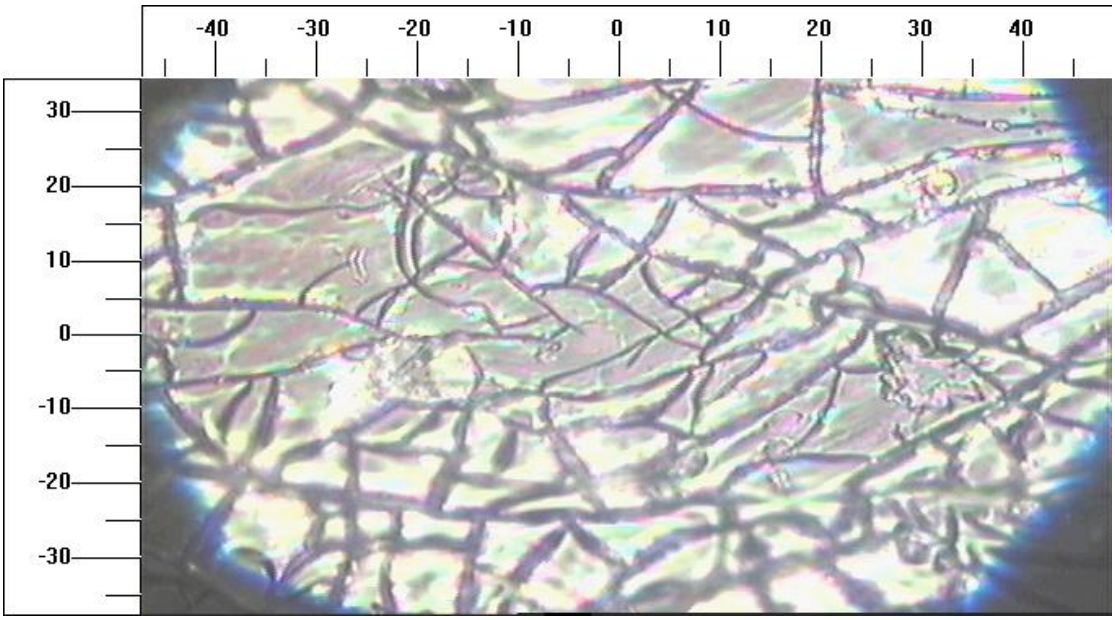

Figure 7.41 Microscope view of the titania coating for sample (3) (scale in μm)

7.4.4 Dip coating with ceramic

A ceramic coating by dip coating was produced by Invibio Ltd. The thick coatings produced (three) are tested in the usual fashion and results are presented in Figure 7.42.

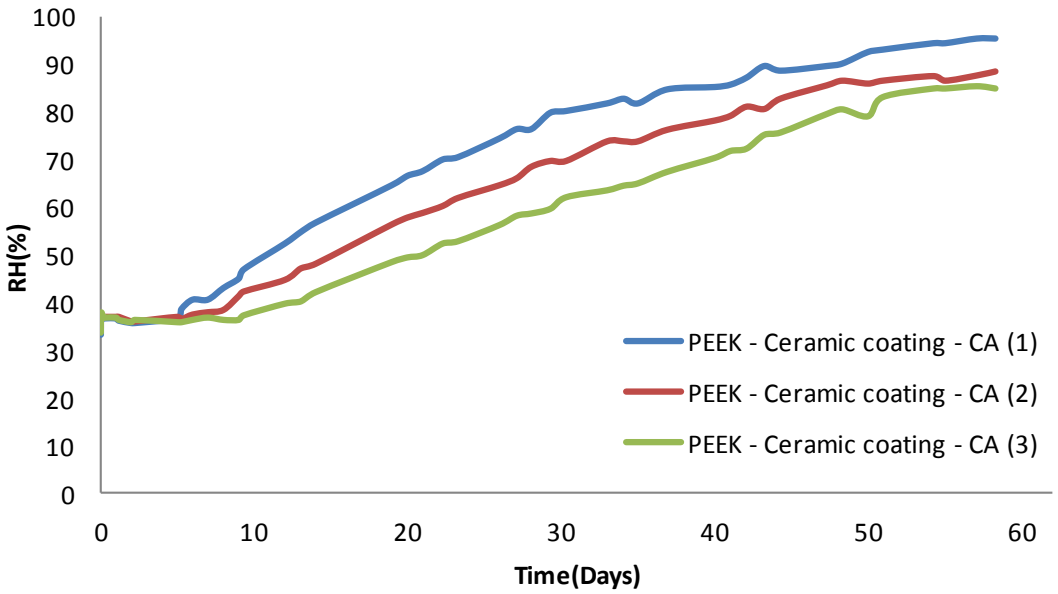

Figure 7.42 RH level in ceramic coated PEEK capsules

The results produced are different for all three samples, which is due to different thicknesses of coatings which is not uniform (between 1 and 1.5 mm). The associated time constants are 22.5, 31.5 and 38.6 days respectively. Although this may seem like an improvement, compared to the time constant obtained for the uncoated PEEK capsule, it must be kept in mind that there is an extra thickness of material involved here. Calculations show that an equivalent thickness of PEEK would produce a lifetime of about 65 days. This proves that the ceramic coating is in fact porous, and even more so than the PEEK. This is confirmed by performing a sorption test, where pieces of the ceramic coating are dried (120°C, overnight), placed in water at 37°C, and their mass gain is recorded periodically with a precision balance (Sartorius BP211D – Precision 10^{-5} g). As can be seen from Figure 7.43, which plots the evolution of this mass gain, the ceramic pieces from the coatings absorb up to 1.7% of their weight, which is more than three times the absorption capacity of PEEK. This demonstrates the porosity of this coating, and also explains the time lag in RH increase in the cavity observed in Figure 7.42.

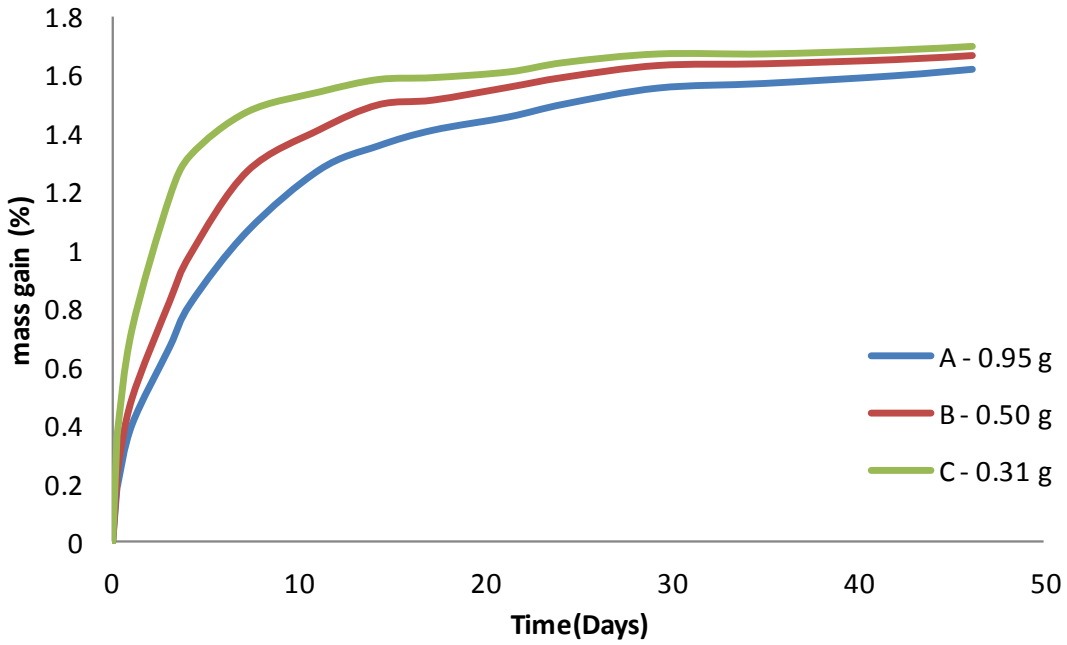

Figure 7.43 Mass gain of ceramic coating in water

7.5 Summary and conclusion

In this chapter, we have reviewed and tested a wide range of coating methods in order to assess whether the lifetime of our package can be prolonged. The results of these tests are summarized in Table 7-6 (20 experiments – n=3 – so 60 capsules were tested overall).

We have seen that the PVD and PaCVD processes produce films which fail to act as effective barrier against moisture. This has been linked to either (or both) failure of film adhesion to the substrate due to residual stress, or to the structure of the film itself.

Residual stress depends on the process used and the thickness of film deposited. We have seen that there is a clear trade-off between increasing the thickness of the film in order to improve barrier properties, and reducing it to minimise residual stress as well as eddy losses for the telemetry.

Structural problems have been attributed to columnar and granular morphologies of the film, which facilitate permeation. The growth of a film with such morphology is promoted by particles and surface roughness of the substrate which shadow the arriving flux of coating material, therefore influencing film formation.

Interestingly, we have noticed that the application of a layer of lacquer prior to PVD coating significantly mitigates this effect and increases barrier properties by 132%, although defects are still present. In all cases however, lateral diffusion between pores and pinholes can also be blamed for increased diffusion (Lewis & Weaver 2004).

Another notable exception is atomic layer deposition of Al_2O_3 films which results in an increase of the time constant of 136%, although exposure to saturated water vapour prevents a much better result.

Nevertheless, we have successfully identified two methods (ALD and PVD + lacquer) which provide a significant improvement in time constant in the context of short term implantable electronic devices.

Parameters	Coating method	Time constant (days)	Change in time constant (%)
PEEK + CA seal (loctite 4061)	-	16.3	--
PEEK + Epoxy seal (Loctite Hysol M-31CL)	-	18.0	--
PEEK + 3 µm Ti + CA seal	CAD	11.4	-29.7
PEEK + 3 µm Ti (except at joint) + CA seal	CAD	13.4	-17.6
PEEK + TiO_2 coating (100-300 nm) + CA seal	Dip coating	13.5	-17.1
PEEK+ 50 nm Cr + 450 nm Au + Epoxy seal	Ar sputtering	15.9	-11.3
PEEK+ 1.9 µm Zr + Epoxy seal	Magnetron sputtering	16.7	-7.2
PEEK+ 500 nm Ti + Epoxy seal	Ar sputtering	17.9	-0.2
PEEK + 3 µm Al + Epoxy seal	Evaporation	18.7	4.2
PEEK+ 500 nm Cr + Epoxy seal	Ar sputtering	19.8	10.2
PEEK+ 50 nm Ti + 450 nm Au + Epoxy seal	Ar sputtering	20.5	14.4
PEEK + 1 µm Ti + 2 µm DLC + Epoxy seal	PVD + PaCVD	20.8	15.6
PEEK+ 1 µm SiOx + Epoxy seal	PaCVD	20.9	16.5
PEEK + 3 µm Ti coating + Epoxy seal	CAD	23.5	31.1
PEEK + 3 µm Ti (except at joint) + CA seal	CAD	22.3	37.2
PEEK+ 2 µm NiCr + Epoxy seal	Ar sputtering	25.0	39.0
PEEK+ 500 nm Al + Epoxy seal	Ar sputtering	25.0	39.3
PEEK + base lacquer+ 3 µm Al + Epoxy seal	Evaporation	41.7	132.1
PEEK 2 mm + Epoxy seal	-	42.8	--
PEEK 2 mm + 40 nm Al_2O_3- Epoxy seal	ALD	101	135.9

Table 7-6 Coatings - summary of results

Chapter 8 Summary, discussion, and future work

In order to gather the findings of our study in a more compact and accessible way, this brief final chapter summarises the results presented in the previous chapters, discusses some general points which have not yet been addressed in previous discussions, presents the maximum achievable lifetime of PEEK packages, and puts forward some areas for future work

8.1 Summary, discussion and maximum achievable lifetime

The aims of this thesis were to identify the parameters which influence the lifetime of a PEEK package for implantable electronic devices, to establish the lifetime of such a package and to investigate ways to prolong it.

Chapter 2 provided an introduction and reviewed the properties of PEEK, the difference between encapsulation and packaging for implants, joining technologies for thermoplastic polymers which can be used to seal the packages, the mechanism of water permeation through non permeable (via defects) and permeable materials, as well as existing calculation methods to predict moisture ingress through permeable materials such as PEEK. The two methods presented were the full transient solution to Fick's laws of diffusion (Paul & DiBenedetto 1965), and Tencer's 'quasi steady state' approximation (Tencer 1994).

After the objectives of this study were stated in a more detailed manner, the PEEK package used was presented (cylindrical package of internal volume 1.6 cm^3, with a wall thickness of 1 mm on the top and bottom, and 2 mm on the side). Chapter 3 then compared those two methods and established that Tencer's model provides a good approximation of the full transient solution, by combining the two extreme cases of diffusion through a non absorbing membrane (very large cavity volume V) and into a permeable slab (negligible cavity volume). Tencer's model also offers the advantage of being much easier to use than the full transient solution, which requires to be solved numerically.

However, both solutions are limited to permeation through a single wall, or to a package with walls of uniform thickness. An original, simple calculation method was therefore developed which allows one to take into account those differences in thickness or even material (Dahan et al. 2012). This method is an improvement of Tencer's, and uses an electrical analogy to model the package as a system of capacitors and resistors, representing the ability of package elements to store water and resist its flow respectively. '*This is the exact approach used for thermal diffusion modelling but applied to moisture diffusion. [...] For thermal diffusion the technique is documented in many textbooks and articles. However, there are*

no equivalent papers on applying it to "moisture diffusion". Even for those familiar with it from thermal analysis the paper is useful since the parameters of the analogy are clearly spelled out' (Reviewer's comment when presented for publication).

As it is based on Tencer's model (the resistance and the capacitance are identified from Tencer's time constant), it shares its flaws and qualities: it is not the most accurate description of the actual physical process, but it is simple to use and provides a good approximation of the time constant, as proved experimentally. Using our method, the resistance and capacitance of the seal of an unmodified PEEK capsule was estimated to be negligible (see Figure 3.11).

Chapter 4 presented the telemetry system used throughout this thesis to measure the relative humidity inside the PEEK packages. This system is based on the method of 'passive signalling' and made of a 'transmitter' (external) and a 'receiver' (implant) which are inductively coupled. This system has proved to be reliable and robust (more than 140 packages have been tested in this fashion), and its simplicity makes it accessible to anyone wishing to pursue similar studies. To this effect, the design of both transmitter and receiver circuits were detailed, as well as components lists, circuit diagrams and microcontroller program. It was also highlighted that the thickness of any metal coating applied to act as a moisture barrier should be limited to 3-4 μm in order to limit attenuation and eddy current losses.

In Chapter 5 we assessed experimentally the lifetime of adhesively joined PEEK capsules. The chapter began with a quick review of the basic concepts of primary, secondary forces, and surface energy, which are essential to understand how adhesive bonding works. From the literature, the different theories of adhesion were also presented, and the relevant ones in our case were the adsorption theory, the mechanical theory and the weak boundary layer theory. Three types of adhesives were selected and tested to bond the package: cyanoacrylate (Loctite 4061), epoxy (Loctite Hysol M31-CL), and silicone (NuSil MED3-4013). The time constants of such packages were experimentally determined to be between 16 and 18 days, with epoxy being the least permeable type of seal as expected. In order to determine the influence of the seal only, metal capsules made of titanium and brass were adhesively joined with the same adhesives and tested, and the epoxy seal alone presented a time constant 20 times larger (458 days) than the adhesively joined PEEK capsule alone, which confirmed the estimation made of the seal having a negligible influence. This is an important result which tells us that adhesive bonding may be sufficient to join polymer parts, and that using other fusion welding method, which are more costly and potentially harmful to the electronics is not necessary. However, this remains true for non coated packages, and should an effective coating material (as a water vapour barrier) be found, then the influence of the seal would become much greater. Nevertheless, the length of the seal's

time constant (458 days) means than in this eventuality useful lifetimes could still be reached for adhesively joined packages.

Using the calculation method presented in the previous chapter, a guideline graph was then produced, which allows prediction of the time constant of a cylindrical PEEK package, depending on the walls' thickness and the cavity volume (see Figure 5.25). This can be used to establish what package dimensions are needed depending on the lifetime needs of the application. As an example, a 2 mm thick cylindrical PEEK package of internal volume 1.5 cm^3 would have a time constant of 34 days.

Although this lifetime could already be useful for some very short term experiments such as animal experiments, a longer lifetime would increase the breadth of potential applications. One of the solutions, which was investigated in Chapter 6, consists in using a desiccant to adsorb water as it enters the package cavity, therefore maintaining a lower level of relative humidity until saturation of the desiccant. This chapter first included some background on desiccants and the adsorption process. The various types of desiccants available and the corresponding adsorption isotherms were presented. Our time constant calculation model was also extended to account for the presence of the desiccant as an extra purely capacitive element. For our application, two types of desiccant were selected and tested:

- 4A molecular sieve, which has a type I isotherm behaviour, high adsorption at low relative humidity and can was found to adsorb up to 17% of its dry weight in water
- Silica gel desiccant, which has a type IV isotherm behaviour and a variable adsorption capacity depending on the surrounding relative humidity (e.g. 27% at 45% RH, 35% when exposed to saturated water vapour).

Experimentally, silica gel proved to be much more effective than 4A molecular sieve, with a time constant of the package increased by more than 120% for an equal mass of desiccant. Our updated calculation model provided an accurate estimation of the time constant in the case of silica gel (2.8%) but very inaccurate in the case of 4A molecular sieve. This result was linked to the type of isotherm behaviour exhibited by the adsorbents, with the molecular sieve's behaviour being incompatible with our electrical analogy calculation model. Nevertheless, it was proved that silica gel was the most effective type of desiccant to be used for our application and that our calculation model allowed an accurate prediction of the time constant of the PEEK package containing this type of desiccant. Similarly to Chapter 5, guideline graphs were produced, which can be used to establish what package dimensions are needed depending on the lifetime needs of the application. They provide the time constant of a cylindrical PEEK package with desiccant as a function of:

- The wall thickness and the cavity volume, when 10% of this volume is occupied by silica gel desiccant (see Figure 6.14)
- The wall thickness and the amount of silica gel desiccant, for a fixed cavity volume of 1.5 cm^3 (see Figure 6.15)

As an example, a 2 mm thick cylindrical PEEK package of internal volume 1.5 cm^3 would have a lifetime of 9.4 months when filled with 20% of desiccant, and 13.6 months when filled with 30% desiccant.

Another approach to improving the lifetime was taken in Chapter 7, which dealt with thin film coatings on PEEK. The chapter started with a review of the main PVD and CVD thin film vacuum coating techniques available and applicable to PEEK. A range of coating techniques and materials were then tested experimentally. Most of them proved ineffective in stopping the ingress of water vapour and prolonging the lifetime of the package significantly. This was attributed mostly to the growth of a columnar or granular morphology, where the columns are bonded effectively to the substrate, but are poorly bonded together, resulting in a porous structure. This growth, inherent to the PVD and PECVD processes in particular, was promoted by the surface roughness of the PEEK capsules and the presence of contaminants. Interestingly, this effect was mitigated to a great extent by the deposition of a layer of lacquer (then stoved) prior to PVD to smooth down the rough machined surface and promote good adhesion of the first deposited layer of metal, which conditions the morphology of the film. Packages PVD coated with lacquer prior to aluminium showed an improvement of more than 130% compared with the uncoated capsule and the same type of coating without lacquer. This is all the more interesting that most manufacturers did not show awareness of the ineffectiveness of their films and believed that they would significantly reduce the ingress of water vapour. One reason for this is that they are used to depositing this type of films on polymer membranes which have a low surface roughness. This is the case for example for crisp bags or helium balloons, which deflate in 1-2 weeks instead of 1-2 days for regular balloons. There is therefore a problem of perception from manufacturers, due to a lack of understanding of the processes at work. As is reported in the literature, '*it is easier to suppress the oxygen transport than the water transport, due to the additional active penetration of water through hydrogen bonds [...], capillary condensation, and swelling with high internal pressure, leading to new defects'* (Vasko et al. 2009).

Based on the positive result of the lacquer/PVD combination, it could be interesting for future improvement to look into depositing a thin layer of polymer such as PET or parylene (between 10-40 μm thick) in order to smooth the machined surface prior to PVD metallisation, and look at the effect on water vapour ingress.

In Chapter 7, we also found that there is a clear trade-off between increasing the film thickness to improve barrier properties, and reducing it to avoid internal residual stress, whether compressive or tensile, which results in blistering and curling of the film respectively, especially when exposed to water. However, there is evidence from the literature that in most cases increasing the film thickness beyond 1 μm has little influence in decreasing the transmission rate further (Vasko et al. 2009). We therefore recommend limiting the thickness of deposited thin films to 1-2 μm in order to reduce internal stress and minimise eddy current losses.

Other non-PVD or CVD techniques were also tried without success, with the exception of Atomic Layer Deposition of Al_2O_3 thin films, which, although they were only 40 nm thick, improved the time constant by more than 130%. Despite providing a reasonable improvement, this technique remained less successful than what could have been expected from the literature. This was attributed to direct exposure to saturated water vapour pressure which can degrade the film, but does not happen at lower RH levels (Nahar 2000; Nahar 2002; Dameron et al. 2008). Future work could investigate the use of Al_2O_3/SiO_2 ALD bilayers, or SiN PVD/Al_2O_3 ALD bilayers (one or more bilayers, separated by polymer interlayers), which have been reported to improve nucleation of the film and to protect it from such corrosion effects. (Dameron et al. 2008; Carcia et al. 2009).

ALD provided a lifetime improvement of 136%, which is seemingly the same as the improvement of the lacquer + PVD. It is therefore important to highlight that the sets of capsules used were not the same (see Figure 7.36); the ALD coated capsules were thicker (2 mm) and therefore although the improvement factor was the same, ALD is actually more effective as a moisture barrier than the lacquer/PVD combination.

However, the former was almost four times as expensive (coating 9 capsules cost £1350 with ALD, and only £350 with PVD. These costs would of course be greatly reduced in case of mass production, but the ratio should remain similar). However, ALD presents the advantage of causing no eddy current losses. So the use of one or the other technique would depend on the needs of the application, as well as whether any of these coatings can be improved in the suggested ways.

In this study, I have been looking for a manufacturer capable of producing an effective thin film which would act as a barrier against moisture, and I have tested many different techniques. Due to time and resources constraints, it was not possible to try them all, but a reasonable range of the most commonly used coating techniques (PVD and CVD), as well as some more recent and less used ones (ALD) were tested. Nevertheless, it should be kept in mind that many factors affect the morphology and adhesion properties of these films, and therefore it is also possible that the processes tried may indeed be appropriate, but that the right coating parameters were not used.

Using the results we have reported, we can now establish the maximum achievable lifetime by PEEK capsules with both desiccant and a thin film coating for capsules types A and B (see Figure 7.36). In this thesis we have produced enough information to allow implant designers to quickly determine the size and type of package they need depending on their application (coated? with desiccant? how much of it?), using either the guideline graphs, or simple calculations. The difficult part is actually to obtain accurate characteristics (diffusion, solubility and permeation constants) for the various materials used. Another difficulty is that the results with the coatings are valid only for the geometry tested and cannot be extended to other types of capsules.

As a guideline, Table 8-1 presents time constants for PEEK packages using both silica gel desiccant and a thin film coating. The results with coating refer to the use of lacquer/PVD for the type A capsule (1 mm thick on top and bottom, 2 mm on sides – see Fig. 11) and to ALD coating for the type B capsule (2 mm thick walls). For example, the predicted time constant of such a package with 2 mm thick walls (using 20% desiccant) is of almost two years, which would be a useful lifetime for many applications.

Amount of desiccant used	Coating	Type A capsule (see Figure 7.36) d= 1-2 mm	Type B capsule (see Figure 7.36) d= 2 mm
No desiccant	**No**	10 days	33.9 days
10%	**No**	2.8 months	5.3 months
20%	**No**	5.3 months	9.4 months
30%	**No**	7.7 months	13.6 months
No desiccant	**Yes**	23 days	2.6 months
10%	**Yes**	6.4 months	12.2 months
20%	**Yes**	12.2 months	**21.6 months**
30%	**Yes**	17.7 months	31.3 months

Table 8-1 Calculated time constant for cylindrical PEEK capsule using varying amounts of desiccant and a thin film coating

For a certain number of applications which fall within this range of achievable lifetimes PEEK can therefore be used to advantageously package implantable electronic devices, and make the most of its properties:

- Biocompatibility
- Light weight
- Thermal insulation (low heat conductivity)
- Does not corrode
- Unlike metal packages, PEEK packages do not interfere with inductive links or electrical signals in and out of the device (Amanat, James, et al. 2010)
- Unlike ceramic packages, they are not brittle

- PEEK can be injection moulded into complex designs and at high volumes, resulting in reduced manufacturing costs
- One of the strongest polymers

Potential applications depending on the lifetime are showed in Table 1-1 p.18, and some of these could clearly benefit from the advantages of PEEK packages. This is the case for example for animal experiments with neurostimulators, which may require a lifetime as small as a few days (e.g. 9 days in (Lexell, Jarvis, Downham, & Salmons, 1992)). Other prototypes may obviously require longer lifetimes, depending on the aim of the experiment. An example of such an application can be an instrumented tibial nail (e.g. Smartnail, Smith & Nephew - (Faroug et al., 2011)) made of PEEK, which requires a lifetime of 9 months. Potential applications could therefore benefit from such a cheap and versatile packaging option in the fields of orthopaedics, neuroprosthetics, veterinary and patient monitoring, especially when it comes to prototyping and clinical trials.

Another advantage of PEEK is that its mechanical properties can be tailored to the application using fibre reinforcement, which is of particular interest for instrumented orthopaedic implants, where we look to minimise stress shielding by matching the material's Young's modulus with that of bone. With metal implants, where those moduli are mismatched, the bone healing process can be affected and result in bone atrophy. Using PEEK in this case can be beneficial. Although CFR-PEEK has not been tested in this study, we can expect our conclusions to be still true, as the diffusion and sorption properties of PEEK composites are not significantly different from those of natural PEEK; Moreover, PEEK composites have been proved to exhibit excellent resistance to a saline environment (Tsai & Lin 1998; Kurtz & Devine 2007).

However, we must highlight that all the packages in this study were not submitted to any kind of external stress. In orthopaedic applications, this is obviously not the case, and this may affect the package, especially when a coating is applied. PVD coatings are actually expected to behave quite well in that respect, as they are commonly used in foil flexible films (crisp bags, helium balloons), although the effect of applied stress on their water vapour permeability has not yet been tested. This can be part of a body of future work, which would look into the effect of applied stress on the integrity and water permeability of thin film coatings. Depending on the level of stress or deformation applied to the package, this could also affect the adhesive seal. The type of adhesive used is also important. For example silicone has an adhesive strength which is less than that of cyanoacrylate, but is more flexible and durable when exposed to water. This is therefore also something which should be investigated when looking at orthopaedic applications. Presumably this could be minimised in some cases by placing the seal and coating appropriately in the implant design (e.g. in unstressed or least stressed part of the implant, or near the neutral axis in case of pure bending).

Alternatively, we could also examine other possible sealing methods. This would also become necessary if we managed to increase the efficacy of thin film coatings significantly. Our results so far show that among all the thin films we have tested, we have obtained at most an improvement of the lifetime of a factor 2.3. In this case the amount of water permeating through the thin seal vs. the walls/coating is still fairly limited.

Should a more important improvement be found in the future, (e.g. polymer/metal bilayers, Al_2O_3/SiO_2 ALD bilayers), then the influence of the seal would be more significant, and it would be worth looking into fusion welding methods to seal the package. Nevertheless, it must be kept in mind that many fusion bonding methods '*are not suitable because of excessive heat load which may be delivered to sensitive components within the capsule'* (Amanat, James, et al. 2010). This is especially true for PEEK, which has a high melting temperature (340°C). In this respect, laser welding seems to be the most promising technique, but is limited in the thickness of the parts that can be bonded (up to 1mm only). There will be therefore a trade off which would need to be offset by the performance of the coating as a sealing method.

8.2 Future work

After reviewing and discussing the main results and achievements of this thesis, we can finish by summarising the future areas of investigation mentioned, which could follow up on this work:

For all types of applications

- Polymer/PVD bilayer (subcoat of polymer such as PET or parylene between 10-40 μm)
- Polymer/ALD bilayer
- Other bilayers (e.g. Al_2O_3/SiO_2, Al_2O_3/SiN)
- If any of the above is successful, other sealing methods such as laser welding might be needed

For orthopaedic applications

- Effect of applied stress on the integrity and water permeability of thin film coatings
- Effect of applied stress on the integrity and water permeability of the adhesive seal

8.3 Conclusion

In this final chapter, the main achievements and results from this thesis have been reviewed. These provide sufficient basis for using of PEEK as a packaging material for

electronic implanted devices with a lifetime of less than 2-3 years. Areas of future work have also been presented in order to develop further the lifetime and range of applications which could be reached for such packages.

Appendix 1. Assembler code for the receiver circuit

```
;*****************************************************************
;   Files Required: P10F222.INC                                 *
;*****************************************************************
        list    p=10F222                ; list directive to define processor
        #include <p10F222.inc>          ; processor specific variable definitions
        __CONFIG H'0FEA'
; '__CONFIG' directive is used to embed configuration word within .asm file.
; The lables following the directive are located in the respective .inc file.
; See respective data sheet for additional information on configuration word.

;*****************************************************************
;***** VARIABLE DEFINITIONS
                UDATA
fd1     res  1                  ;delay loop counters
fd2     res  1
dc1     res  1
time1   res  1
time2   res  1
temp    res  1
time    res  1


;*****************************************************************
;CONFIGURATION SECTION
        ORG     0xFF            ; processor reset vector
; Internal RC calibration value is placed at location 0xFF by Microchip
; as a movlw k, where the k is a literal value.
        ORG     0x000           ; coding begins here
        movwf   OSCCAL                  ; update register with factory cal value
;Calibrate oscillator.

por                             ; test if Power on Reset has happened
        btfss   STATUS,3
        goto    por

gpwu
        btfsc   STATUS,7        ;test if change on port reset has happened
        goto    gpwu

clrf    ADRES

;1 SEC DELAY TO MAKE SURE THE SUPPLY VOLTAGE/CURRENT ARE
STABLE (PB WITH SURGE OF CURRENT OTHERWISE
;DELAY ALSO TO MAKE SURE THE HUMIDITY SENSOR HAS SENT SIGNAL
BEFORE
        movlw .244              ;delay is 244*(1023+1023+3)+2=499,458 cycles=0.5s
        movwf time2
```

```
        clrf    time1           ;inner loop:256x4-1
timedly1                        ;inner loop 1:1023 cycles
        nop
        decfsz  time1,f         ;decrement counter, skip next line if 0
        goto    timedly1
timedly2                        ;inner loop 2:1023 cycles
        nop
        decfsz  time1,f         ;decrement counter, skip next line if 0
        goto    timedly2
        decfsz  time2,f         ;decrement counter, skip next line if 0
        goto    timedly1

        movlw .244              ;delay is 244*(1023+1023+3)+2=499,458 cycles=0.5s
        movwf time2
        clrf    time1           ;inner loop:256x4-1
timedly3                        ;inner loop 1:1023 cycles
        nop
        decfsz  time1,f         ;decrement counter, skip next line if 0
        goto    timedly3
timedly4                        ;inner loop 2:1023 cycles
        nop
        decfsz  time1,f         ;decrement counter, skip next line if 0
        goto    timedly4
        decfsz  time2,f         ;decrement counter, skip next line if 0
        goto    timedly3



        movlw B'00000111'   ;Sets prescaler.sets TOCS to make GPIO available as
I/O.
        OPTION
        bcf     ADCON0,7    ;ANS1=0, GP1 is digital I/O
        bsf     ADCON0,6    ;ANS0=1, GP0 is analog I
        clrf    GPIO        ;Clear GPIO to a known state
        movlw B'00001001'   ;GP0 is input, GP1 is output
        tris    GPIO        ;
        bcf     ADCON0,2    ;CHS0=0, GP0 is ADC input channel
        bcf     ADCON0,3    ;CHS1=0, GP0 is ADC input channel
        bsf     ADCON0,0    ;ADON=1, Turn on ADC module
        goto    start
;*****************************************************************

;*****************************************************************
start

;DELAY TO MAKE SURE THE ACQUISITION HAS HAPPENED
        movlw .255
        movwf time
timestart                       ;total delay=255*4-1+2=1021uS. Normally, 8uS is enough
        nop
        decfsz  time,f          ;decrement counter, skip next line if 0
```

```
        goto    timestart

;DO A/D CONVERSION
        bsf     ADCON0,1    ;sets GO/DONE as 1. starts A/D conversion
waitadc
        btfsc   ADCON0,1    ;checks if GO/DONE bit is 0 <=> A/Dconversion
done
        goto    waitadc     ;if not, check again

        movf    ADRES,w     ;copy ADRES to temp
        movwf   temp

output
;SENDING THE OUTPUT SIGNAL WITH THE REQUIRED FREQUENCY
;SETS GP1 HIGH + FIXED DELAY
        bsf     GPIO,1              ;Sets GP1 high (for fixed delay=15uS)
        movlw   .3              ;fixed delay counter N=3
        movwf   fd1
        nop                     ;uses 1 instruction cycle
fixdly1                         ;total delay=N*4-1+4=15uS
        nop
        decfsz  fd1,f           ;decrement counter, skip next line if 0
        goto    fixdly1

;SETS GP1 LOW + FIXED + VARIABLE DELAY
        bcf     GPIO,1              ;Sets GP1 low (for variable delay=84uS)
        movlw   .20             ;fixed delay counter N=20
        movwf   fd2
fixdly2                         ;total delay=N*4-1+3=82uS
        nop
        decfsz  fd2             ;decrement counter, skip next line if 0
        goto    fixdly2


        movf    temp,w          ;copy ADRES to counter
        movwf   dc1
vardly                          ;total delay=N*4-1+4=ADRES*4+3
        nop                     ;uses 1 instruction cycle
        decfsz  dc1             ;decrement counter, skip next line if 0
        goto    vardly

        goto    output          ;repeat forever

        END                             ;directive 'end of program'
```

Appendix 2. List of components for the telemetry system

List of components for receiver (implant side) on PCB						
Denomination	**Type**	**Value**	**Manufacturer**	**Manufacturer part nb**	**Package type**	**Farnell order nb**
CRS1	Capacitor	47 pF	Kemet	C0402C470J5GAC	0402	1414592
CRS2	Trimm Capacitor	5-20 pF	AVX	CTZ2E-20C-W2-P	CTZ2	1189327
DR1	Diode, schottky	0.4V FD	NXP	1PS76SB21	SOD-323	8734038
DR2	Diode, schottky	0.4V FD	NXP	1PS76SB21	SOD-323	8734038
DR3	Zener diode	15 V	ON Semiconductor	MM3Z15VT1G	SOD-323	1431192
CR1	Tantalum Capacitor	6.8 µF	Kemet	T491A685K016AT	case A	1457431
CR2	Capacitor	2.2 µF	Kemet	C0402C225M9PAC-TU	0402	1650817
FETR1	MOSFET N-channel	3 V	ON Semiconductor	MMBF170LT1G	SOT-23	1431321
VR	Voltage regulator	3 V out	Microchip	MCP1702T-3002E/CB	SOT-23	1331489
PIC10F222	Microcontrolleur	N/A	Microchip	PIC10F222T-I/OT	SOT-23-6	1332177
SHT21	Humidity sensor	N/A	Sensirion	SHT21S	DFN	1888014
CHS	Capacitor	100 nF	Kemet	C0402C104K4RACTU	0402	1288252
CLP	Capacitor	220 nF	Kemet	C0402C224K9PAC 7867	0402	1572610
RLP	Resistor	100 kΩ	VISHAY DRALORIC	CRCW0402100KFKED	0402	1469671

List of components for transmitter						
Denomination	**Type**	**Value**	**Manufacturer**	**Manufacturer part nb**	**Package type**	**Farnell order nb**
C1,C2	Capacitor	0.47 µF	AVX	12061C474KAT2A	1206	1833899
C3,C4	Capacitor	4.7 µF	MURATA	GRM31CR71H475KA12L	1206	1735545
C5	Trimm capacitor	4-40 pF	VISHAY BC COMPONENTS	BFC280908002	2 pins	1215715
C6-C11	Capacitor	0.47 µF	KEMET	C1206C474K3RACTU	1206	1288280
C12-C16	Capacitor	0.1 µF	AVX	12061C104KAZ2A	0603	1740540
CT3	Capacitor	390 pF	MULTICOMP	MCCA000452	1206	1759331
C19	Capacitor	510 pF	VISHAY VITRAMON	VJ1206A511JXBMT	1206	1650955
L	choke coil	680 µH	PANASONIC	ELC12D681E	N/A	1749142
R1	Resistor	0 Ω	VISHAY DRALORIC	CRCW08050000Z0EA	0603	1469846
R2	Resistor	1 MΩ	MULTICOMP	MCHV06W8J0105T5E	1206	1576211
RT1	Resistor	2 kΩ	VISHAY DRALORIC	CRCW12062K00FKEA	1206	1469985
R4	Resistor	1 kΩ	PANASONIC	ERA8AEB102V	1206	1717745
DT1,DT2	Schottky diode	30 mA FWD	VISHAY SEMICONDUCTOR	BAT83S-TR	DO-35	1651141
XTAL	Crystal	13.56 MHz	ABRACON	ABM3-13.560MHZ-B2-T	5x3.2mm SMD	1611805
IC1-IC3	IC, CMOS, Inverter	N/A	TEXAS INSTRUMENTS	SN74AC14N	14 pins, DIP	1470853
DEI420	IC, Driver, MOSFET DE275	N/A	IXYS RF	DEI420	DEIC420	1347728

Appendix 3. Solid Titanium capsule and feedthrough

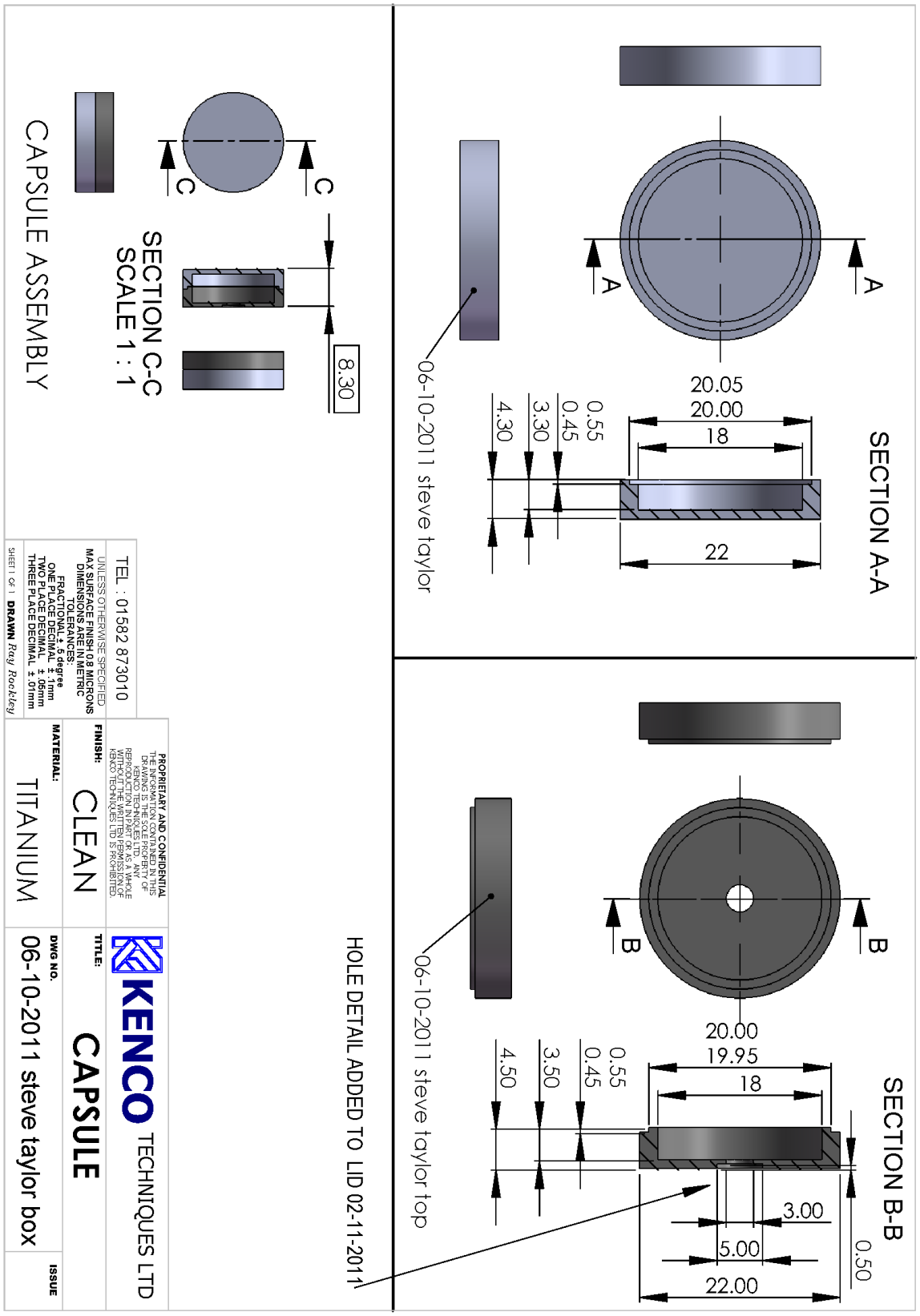

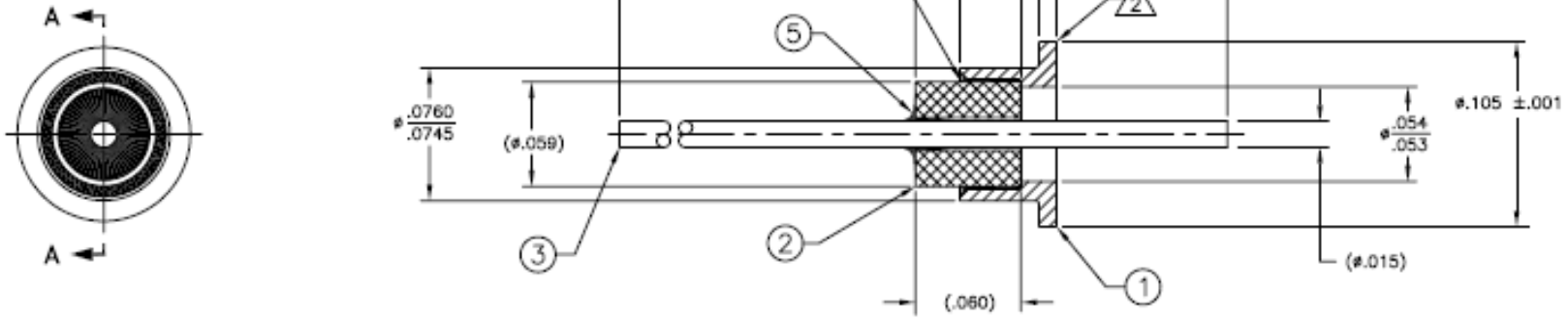
A
A
.323 ±.010
.080 ±.010
.097 ±.010
.055 ±.002
(.020)
.010 ±.001
4
2
5
ø.0760
.0745
(ø.059)
ø.105 ±.001
ø.054
.053
3
2
1
(ø.015)
(.060)

SECTION A–A

Bibliography

Adamson, A.W. & Gast, A.P., 1997. *Physical Chemistry of Surfaces*, Wiley-Blackwell.

Ageorges, C., Ye, L. & Hou, M., 2001. Advances in fusion bonding techniques for joining thermoplastic matrix composites: a review. *Composites Part A: Applied Science and Manufacturing*, 32(6), pp.839–857.

Amanat, N., Chaminade, C., et al., 2010. Transmission laser welding of amorphous and semi-crystalline poly-ether–ether–ketone for applications in the medical device industry. *Materials & Design*, 31(10), pp.4823–4830.

Amanat, N., James, N.L. & McKenzie, D.R., 2010. Welding methods for joining thermoplastic polymers for the hermetic enclosure of medical devices. *Medical engineering & physics*, 32(7), pp.690–9.

Aristov, Y.I. et al., 2006. Kinetics of water adsorption on silica Fuji Davison RD. *Microporous and Mesoporous Materials*, 96(1-3), pp.65–71.

Bauer, W., 1994. Intrinsic resputtering during film deposition investigated by Monte Carlo simulation. *Journal of Vacuum Science & Technology A: Vacuum, Surfaces, and Films*, 12(6), p.3157.

Bikerman, J.J., 1961. *The science of adhesive joints*, New York: Academic Press.

Birkholz, M., Genzel, C. & Jung, T., 2004. X-ray diffraction study on residual stress and preferred orientation in thin titanium films subjected to a high ion flux during deposition. *Journal of Applied Physics*, 96(12), p.7202.

Blundell, D.J. & Osborn, B.N., 1983. The morphology of poly(aryl-ether-ether-ketone). *Polymer*, 24(8), pp.953–958.

Bonniau, P. & Bunsell, A.R., 1981. A Comparative Study of Water Absorption Theories Applied to Glass Epoxy Composites. *Journal of Composite Materials*, 15(3), pp.272–293.

Borton, D.A. et al., 2013. An implantable wireless neural interface for recording cortical circuit dynamics in moving primates. *Journal of neural engineering*, 10(2), p.026010. Available at: http://stacks.iop.org/1741-2552/10/i=2/a=026010 [Accessed August 14, 2013].

Braden, M., 1964. The absorption of water by acrylic resins and other materials. *The Journal of Prosthetic Dentistry*, 14(2), pp.307–316.

Breck, D.W., 1974. *Zeolite Molecular Sieves: Structure, Chemistry and Use*, New York: John Wiley & Sons Inc.

Broughton, W.R. & Mera, R.D., 1997. *Review of life prediction methodology and adhesive joint design and analysis software*, Available at: http://www.adhesivestoolkit.com/Docu-Data/NPLDocuments/P A J/Other documents/PAJ-Report Lists.pdf.

Brunauer, S., 1938. Adsorption of Gases in Multimolecular Layers. *Journal of the American Chemical Society*, 60(2), pp.309 – 319.

Brunauer, S. et al., 1940. On a Theory of the van der Waals Adsorption of Gases. *J. Am. Chem. Soc.*, 62(7), pp.1723–1732.

Bunch, J.S. et al., 2008. Impermeable atomic membranes from graphene sheets. *Nano letters*, 8(8), pp.2458–62. Available at: http://dx.doi.org/10.1021/nl801457b [Accessed November 4, 2012].

Burnett, M.G., Galwey, A.K. & Lawther, C., 1996. Ideality of water vapour and its adsorption on the glass surfaces of a conventional glass vacuum apparatus at 295 K between 0 and 10 Torr. *Journal of the Chemical Society, Faraday Transactions*, 92(21), p.4301.

Callister, W.D. & Rethwisch, D.G., 2008. *Fundamentals of materials science and engineering : an integrated approach*, John Wiley & Sons.

Carcia, P.F. et al., 2007. Application of Atomic Layer Deposition for Gas Permeation Barrier Thin Films. In *ECS Transactions*. ECS, pp. 15–21. Available at: http://ecst.ecsdl.org/content/11/7/15.abstract [Accessed September 28, 2012].

Carcia, P.F. et al., 2009. Gas diffusion ultrabarriers on polymer substrates using Al[sub 2]O[sub 3] atomic layer deposition and SiN plasma-enhanced chemical vapor deposition. *Journal of Applied Physics*, 106(2), p.023533. Available at: http://link.aip.org/link/?JAPIAU/106/023533/1 [Accessed August 29, 2012].

Carslaw, H.S. & Jaeger, J.C., 1959. *Conduction of Heat in Solids*, Oxford University Press. Available at: http://adsabs.harvard.edu/abs/1959chs..book.....C.

Chin, J.W., Nguyen, T. & Aouadi, K., 1999. Sorption and diffusion of water, salt water, and concrete pore solution in composite matrices. *Journal of Applied Polymer Science*, 71(3), pp.483–492.

Crank, J., 1975. *The mathematics of diffusion*, Clarendon Press.

Crittenden, B. & Thomas, W.J., 1998. *Adsorption Technology & Design*, Butterworth-Heinemann.

Dahan, N. et al., 2013. The Application of PEEK to the Packaging of Implantable Electronic Devices: Water Permeation Calculation Method and Maximum Achievable Lifetime with Desiccant. *Journal of Microelectronics and Electronic Packaging*, 10(1), pp.15–22.

Dahan, N., Vanhoestenberghe, A. & Donaldson, N., 2012. Moisture Ingress into Packages With Walls of Varying Thickness and/or Properties: A Simple Calculation Method. *IEEE Transactions on Components, Packaging and Manufacturing Technology*, 2(11), pp.1796–1801.

Dai Jiang et al., 2011. A Stimulator ASIC Featuring Versatile Management for Vestibular Prostheses. *IEEE transactions on biomedical circuits and systems*, 5(2), pp.147–59. Available at: http://ieeexplore.ieee.org/articleDetails.jsp?arnumber=5759288 [Accessed August 14, 2013].

Dameron, A. et al., 2008. Gas Diffusion Barriers on Polymers Using Multilayers Fabricated by Al2O3 and Rapid SiO2 Atomic Layer Deposition. *Journal of Physical Chemistry C*, 112(12), pp.4573–4580. Available at: http://pubs.acs.org/doi/abs/10.1021/jp076866+ [Accessed March 19, 2013].

Davis, G.D., 2003. Durability of Adhesive Joints. In *Handbook of adhesive technology*. CRC Press, p. 273.

Davis, R.F., 1993. Diamond Films and Coatings. Available at: http://www.knovel.com/web/portal/browse/display?_EXT_KNOVEL_DISPLAY_bookid=81.

Davy, J., 1975. Model calculations for maximum allowable leak rates of hermetic packages. *Journal of Vacuum Science and Technology*, 12(1), pp.423–429.

Desiccare Inc., 2010. Bulk Desiccants. *Technical Product Information*.

Dillon, A.C. et al., 1995. Surface chemistry of Al2O3 deposition using Al(CH3)3 and H2O in a binary reaction sequence. *Surface Science*, 322(1-3), pp.230–242. Available at: http://dx.doi.org/10.1016/0039-6028(95)90033-0 [Accessed March 19, 2013].

Donaldson, N., 1992. Effect of the metallic seal of a hermetic enclosure on the induction of power to an implant. *Medical and Biological Engineering and Computing*, 30(1), pp.63–68.

Donaldson, N., 1988. Low-technology sealing method for implantable hermetic packages. *Medical and Biological Engineering and Computing*, 26(1), pp.111–116.

Donaldson, N., 1986. Passive signalling via inductive coupling. *Medical and Biological Engineering and Computing*, 24(2), pp.223–224.

Donaldson, N., 1990. *The electrical design of an implantable stimulator to restore motor control to the paralysed*. University College London.

Donaldson, N. et al., 2012. The permeability of silicone rubber to metal compounds: relevance to implanted devices. *Journal of biomedical materials research. Part A*, 100(3), pp.588–98.

Donaldson, N. & Perkins, T.A., 1983. Analysis of resonant coupled coils in the design of radio frequency transcutaneous links. *Medical and Biological Engineering and*, 21(5), pp.612–627.

Donaldson, P.E.K. & Sayer, E., 1981a. A technology for implantable hermetic packages. Part 1: Design and materials. *Medical and Biological Engineering and*, 19(4), pp.398–402.

Donaldson, P.E.K. & Sayer, E., 1981b. A technology for implantable hermetic packages. Part 2: An implementation. *Medical and Biological Engineering and*, 19(4), pp.403–5.

Drain, K.F. et al., 1985. The effect of moisture on the strength of polycarbonate-cyanoacrylate adhesive bonds. *International Journal of Adhesion and Adhesives*, 5(3), pp.133–136.

Duffin, E.G., 2006. Implantable defibrillators. *The electrical engineering handbook*, 20063932, p.58.

Dunnill, C.W. et al., 2011. Nanoparticulate silver coated-titania thin films—Photo-oxidative destruction of stearic acid under different light sources and antimicrobial effects under hospital lighting conditions. *Journal of Photochemistry and Photobiology A: Chemistry*, 220(2-3), pp.113–123. Available at: http://dx.doi.org/10.1016/j.jphotochem.2011.04.001 [Accessed August 1, 2011].

Dupré, A., 1869. Théorie Mécanique De La Chaleur. In Paris: Gauthier-Villars, p. 369.

Faroug, R. et al., 2011. Strain response of an instrumented intramedullary nail to three-point bending. *Journal of medical engineering & technology*, 35(5), pp.275–82. Available at: http://informahealthcare.com/doi/abs/10.3109/03091902.2011.582227 [Accessed July 26, 2013].

Faupel F., Willecke R. & Thran A., 1998. Diffusion of metals in polymers. *Materials Science and Engineering: R: Reports*, 22(1), p.55.

Forde, M., 2006. Implantable Cardiac Pacemakers.

George, S.M., 2010. Atomic layer deposition: an overview. *Chemical reviews*, 110(1), pp.111–31. Available at: http://www.ncbi.nlm.nih.gov/pubmed/19947596.

Gille, G. & Rau, B., 1984. Buckling instability and adhesion of carbon layers. *Thin Solid Films*, 120(2), pp.109–121.

Gledhill, R.A., Kinloch, A.J. & Shaw, S.J., 1980. A Model for Predicting Joint Durability. *The Journal of Adhesion*, 11(1), pp.3–15.

Grayson, M.A. & Wolf, C.J., 1987. The solubility and diffusion of water in poly(aryl-ether-ether-ketone) (PEEK). *Journal of Polymer Science Part B: Polymer Physics*, 25(1), pp.31–41.

Greenhouse, H., 2000. *Hermeticity of electronic packages*,

Grimm, R.A., 1995. Welding processes for plastics. *Advanced Materials and Processes*, 147(3).

Groner, M.D. et al., 2002. Electrical characterization of thin Al2O3 films grown by atomic layer deposition on silicon and various metal substrates. *Thin Solid Films*, 413(1-2), pp.186–197. Available at: http://dx.doi.org/10.1016/S0040-6090(02)00438-8 [Accessed March 22, 2013].

Groner, M.D. et al., 2004. Low-Temperature Al 2 O 3 Atomic Layer Deposition. *Chemistry of Materials*, 16(4), pp.639–645. Available at: http://dx.doi.org/10.1021/cm0304546 [Accessed April 25, 2013].

Ha, S.W., Eckert, K.L., et al., 1997. NaOH treatment of vacuum-plasma-sprayed titanium on carbon fibre-reinforced poly (etheretherketone). *Journal of Materials*, 8(12), pp.881–6.

Ha, S.W., Kirch, M., et al., 1997. Surface activation of polyetheretherketone (PEEK) and formation of calcium phosphate coatings by precipitation. *Journal of Materials*, 8(11), pp.683–690.

Ha, S.W., Gisep, A., et al., 1997. Topographical characterization and microstructural interface analysis of vacuum-plasma-sprayed titanium and hydroxyapatite coatings on carbon fibre-reinforced poly. *Journal of Materials*, 8(12), pp.891–896.

Hemmerich, K.J., 1998. General Aging Theory and Simplified Protocol for Accelerated Aging of Medical Devices. *Med Plastics Biomater*, 4, pp.16–24.

Hoffman, D.W., 1990. Intrinsic resputtering—theory and experiment. *Journal of Vacuum Science & Technology A: Vacuum, Surfaces, and Films*, 8(5), p.3707.

Hubler, G.K. & Chrisey, D.B., 1994. *Pulsed Laser Deposition of Thin Films*, New York: Wiley-Interscience.

Kafizas, A. et al., 2009. Titanium dioxide and composite metal/metal oxide titania thin films on glass: A comparative study of photocatalytic activity. *Journal of Photochemistry and Photobiology A: Chemistry*, 204(2-3), pp.183–190. Available at: http://dx.doi.org/10.1016/j.jphotochem.2009.03.017 [Accessed September 22, 2011].

Kaufman, H.R., 1986. Broad-beam ion sources: Present status and future directions. *Journal of vacuum science & technology. A. Vacuum, surfaces, and films*, 4(3), p.764.

Keller II, G.E., 1987. Adsorption. In R. W. Rousseau, ed. *Handbook of separation process technology*. Wiley-IEEE, pp. 644–669.

Kim, Y.H. & Wool, R.P., 1983. A theory of healing at a polymer-polymer interface. *Macromolecules*, 16(7), pp.1115–1120.

Kinloch, A.J., 1987. *Adhesion and Adhesives: Science and Technology*, Springer.

Kinloch, A.J., 1995. Predicting the Lifetime of Adhesive Joints in Hostile Environments, Report No 5. Available at: http://www.adhesivestoolkit.com/PDFFiles/Project 3/P3r5.pdf.

Kornilov, S.V. & Barinova, O.P., 1996. Humidity measurements in a sealed package with sorption sensors. *Sensors and Actuators B: Chemical*, 30(2), pp.89–93.

Kurtz, S.M. & Devine, J.N., 2007. PEEK biomaterials in trauma, orthopaedic, and spinal implants. *Biomaterials*, 28(32), pp.4845–69.

Langmuir, I., 1916. The constitution and fundamental properties of solids and liquids. I. solids. *J. Am. Chem. Soc.*, 38, pp.2221–95.

Laugier, M., 1979. A note on the curling of thin films and its connection with intrinsic stress. *Thin Solid Films*, 56(1-2), pp.L1–L2.

Lee, L.-H., 1987. Adhesives and sealants for severe environments. *International Journal of Adhesion and Adhesives*, 7(2), pp.81–91. Available at: http://dx.doi.org/10.1016/0143-7496(87)90093-5 [Accessed January 11, 2013].

Lewis, J.S. & Weaver, M.S., 2004. Thin-Film Permeation-Barrier Technology for Flexible Organic Light-Emitting Devices. *IEEE Journal of Selected Topics in Quantum Electronics*, 10(1),

pp.45–57. Available at: http://ieeexplore.ieee.org/xpl/articleDetails.jsp?arnumber=1288072 [Accessed September 28, 2012].

Lexell, J. et al., 1992. Quantitative morphology of stimulation-induced damage in rabbit fast-twitch skeletal muscles. *Cell & Tissue Research*, 269(2), pp.195–204. Available at: http://link.springer.com/10.1007/BF00319609 [Accessed July 26, 2013].

Lin, D. et al., 2007. Hermeticity investigation of MEMS vacuum packaging. *Electronic Packaging*, pp.542–545.

Loeb, G., 2001. BION™ system for distributed neural prosthetic interfaces. *Medical Engineering & Physics*, 23(1), pp.9–18.

Lu, T. et al., 1997. Validation of a lower limb model with in vivo femoral forces telemetered from two subjects. *Journal of biomechanics*, 31(1), pp.63–9.

Mahan, J.E., 2000. *Physical Vapor Deposition of Thin Films*, Wiley-Interscience.

Malone, L.J., 2003. *Basic Concepts of Chemistry*, Wiley.

Martin, P.J., 1996. Vacuum Arc Desposition. In R. L. Boxman, D. M. S. David M. Sanders and Philip J. MartinA2 - Raymond L. Boxman, & P. J. M. B. T.-H. of V. A. S. and Technology, eds. Park Ridge, NJ: William Andrew Publishing, pp. 367–396.

Mattox, D.M., 1998. Handbook of Physical Vapor Deposition (PVD) Processing.

McDermott, H., 1989. An advanced multiple channel cochlear implant. *IEEE transactions on bio-medical engineering*, 36(7), pp.789–97. Available at: http://www.ncbi.nlm.nih.gov/pubmed/2744794 [Accessed August 14, 2013].

Meyer, D., 2007. Miniature moisture sensors for in-package use by the microelectronics industry. *Reliability Physics Symposium, 1975. 13th Annual*, pp.48–52.

Molitor, P., Barron, V. & Young, T., 2001. Surface treatment of titanium for adhesive bonding to polymer composites: a review. *International Journal of Adhesion and Adhesives*, 21(2), pp.129–136. Available at: http://dx.doi.org/10.1016/S0143-7496(00)00044-0 [Accessed May 1, 2013].

Monaghan, D.P. et al., 1993. Deposition of wear resistant coatings based on diamond like carbon by unbalanced magnetron sputtering. *Surface and Coatings Technology*, 60(1–3), pp.525–530.

Morosanu, C.E., 1990. *Thin films by chemical vapour deposition*, Elsevier.

Nahar, R.K., 2002. Physical understanding of moisture induced degradation of nanoporous aluminum oxide thin films. *Journal of Vacuum Science & Technology B: Microelectronics and Nanometer Structures*, 20(1), p.382. Available at: http://link.aip.org/link/?JVTBD9/20/382/1 [Accessed April 26, 2013].

Nahar, R.K., 2000. Study of the performance degradation of thin film aluminum oxide sensor at high humidity. *Sensors and Actuators B: Chemical*, 63(1-2), pp.49–54. Available at: http://dx.doi.org/10.1016/S0925-4005(99)00511-0 [Accessed April 26, 2013].

Ng, K., 2001. Experimental investigation of the silica gel–water adsorption isotherm characteristics. *Applied Thermal Engineering*, 21(16), pp.1631–1642.

Nonclercq, A. et al., 2010. Sacro-lumbar Anterior Root Stimulator Implant for Exercising. In *15th Annual Conference of the International Functional Electrical Stimulation Society*. Available at: http://ifess.org/node/401 [Accessed August 14, 2013].

Novoselov, K.S. et al., 2012. A roadmap for graphene. *Nature*, 490(7419), pp.192–200. Available at: http://www.nature.com/nature/journal/v490/n7419/full/nature11458.html#/ref9 [Accessed January 11, 2013].

Oura, K. et al., 2003. *Surface Science: An Introduction*, Springer.

Paul, D.R. & DiBenedetto, A.T., 1965. Diffusion in Amorphous Polymers. *JApplPolymSci*, (10), pp.17–44.

Pawlowski, L., 2009. Suspension and solution thermal spray coatings. *Surface and Coatings Technology*, 203(19), pp.2807–2829.

Petrie, E.M., 2000. *Handbook of Adhesives and Sealants*, McGraw-Hill.

Pierson, H.O., 1999. *Handbook of Chemical Vapor Deposition (CVD): Principles, Technology and Applications: Materials Science and Process Technology Series*, Noyes Publications.

Prater, J.T. & Moss, R.W., 1983. Effect of the coating structure on the adherence of sputter-deposited oxide coatings. *Thin Solid Films*, 107(4), pp.455–462.

Ramakrishna, S., 2001. Biomedical applications of polymer-composite materials: a review. *Composites Science and Technology*, 61(9), pp.1189–1224.

Reichelt, K., 1988. Nucleation and growth of thin films. *Vacuum*, 38(12), pp.1083–1099.

Ritala, M. et al., 1999. Perfectly Conformal TiN and Al2O3 Films Deposited by Atomic Layer Deposition. *Chemical Vapor Deposition*, 5(1), pp.7–9. Available at: http://doi.wiley.com/10.1002/(SICI)1521-3862(199901)5:1<7::AID-CVDE7>3.0.CO;2-J [Accessed April 25, 2013].

Rossnagel, S.M., 1998. Interaction between gas rarefaction and metal ionization in ionized physical vapor deposition. *Journal of Vacuum Science & Technology B: Microelectronics and Nanometer Structures*, 16(6), p.3008.

Rossnagel, S.M., 2003. Thin film deposition with physical vapor deposition and related technologies. *Journal of Vacuum Science & Technology A: Vacuum, Surfaces, and Films*, 21(5), p.S74.

Ruthven, D.M., 1984. *Principles of adsorption and adsorption processes*, Wiley-Interscience.

Schneider, G., 1988. Non-metal hermetic encapsulation of a hybrid circuit. *Microelectronics Reliability*, 28(1), pp.75–92.

Schuettler, M. et al., 2011. Ensuring minimal humidity levels in hermetic implant housings. *Conference proceedings : ... Annual International Conference of the IEEE Engineering in Medicine and Biology Society. IEEE Engineering in Medicine and Biology Society. Conference*, 2011, pp.2296–9.

Sedlak, S. & Donaldson, N., 1993. A direct technique for investigating the factors which detetermine the longevity of implanted packages for electronic devices. In *Proc.Ljubljana FES Conference*.

Da Silva Sobrinho, A.S. et al., 2000. Defect-permeation correlation for ultrathin transparent barrier coatings on polymers. *Journal of Vacuum Science & Technology A: Vacuum, Surfaces, and Films*, 18(1), p.149.

Singh, J., Peck, R.A. & Loeb, G.E., 2001. Development of BION/spl trade/ technology for functional electrical stimulation: hermetic packaging. In *2001 Conference Proceedings of the 23rd Annual International Conference of the IEEE Engineering in Medicine and Biology Society*. IEEE, pp. 1313–1316.

Singh Raman, R.K. et al., 2012. Protecting copper from electrochemical degradation by graphene coating. *Carbon*, 50(11), pp.4040–4045.

Sinnadurai, N., 1996. Plastic packages survive where hermetic packages fail. *Microelectronics and Reliability*, 36(7-8), pp.1001–1018.

Smith, D., 2006. PIC in practice: A Project-based approach. , Second Edi.

Spalvins, T., 1974. Nodular growth in thick-sputtered metallic coatings. *Journal of Vacuum Science and Technology*, 11(6), p.1186.

Spear, K.E., 1976. Chapt. 3 in Treatise on Solid State Chemistry, Vol. 4 (NB Hannay, ed.).

Srivastava, N., 1998. A review of adsorbents and adsorbates in solid–vapour adsorption heat pump systems. *Applied Thermal Engineering*, 18(9-10), pp.707–714.

Stokes, V.K., 1989. Joining methods for plastics and plastic composites: An overview. *Polymer Engineering and Science*, 29(19), pp.1310–1324.

Stowell, M.J., 1974. The initial stages of thin film growth. *Journal of Crystal Growth*, 24-25(null), pp.45–52.

Su, C., Hong, B.-Y. & Tseng, C.-M., 2004. Sol–gel preparation and photocatalysis of titanium dioxide. *Catalysis Today*, 96(3), pp.119–126. Available at: http://dx.doi.org/10.1016/j.cattod.2004.06.132 [Accessed October 8, 2011].

Tatz, A. & Gottlieb, D., 2004. *Letters to a buddhist Jew*, Targum Press. Available at: http://books.google.com/books?id=UkBKx2tDxiYC&pgis=1 [Accessed May 17, 2013].

Tavakoli, M. et al., 2004. An Assessment of Adhesive Bonding of PEEK-OPTIMA for Medical Device Applications. *Proceedings of Medical Polymers*, pp.35–51.

Taylor, S., 1996. A telemetry system for measurement of forces in massive orthopaedic implants in vivo. *Engineering in Medicine and Biology Society, 1996.*, 1, pp.290–292.

Taylor, S., Perry, J. & Meswania, J., 1997. Telemetry of forces from proximal femoral replacements and relevance to fixation. *Journal of*, 30(3), pp.225–234.

Taylor, S. & Walker, P., 2001. Forces and moments telemetered from two distal femoral replacements during various activities. *Journal of biomechanics*, 34(7), pp.839–848.

Tencer, M., 1994. Moisture ingress into nonhermetic enclosures and packages. A quasi-steady state model for diffusion and attenuation of ambient humidity variations. *Electronic Components and Technology*, pp.196–209.

Traeger, R., 2002. Nonhermeticity of polymeric lid sealants. *Parts, Hybrids, and Packaging, IEEE Transactions*, PHP-13(2), pp.147–152.

Tsai, H. & Lin, S., 1998. Effects of saline environment on the properties of PEEK and epoxy composites. *Medical plastics: degradation resistance & failure analysis*, p.143.

Vanhoestenberghe, A. & Donaldson, N., 2011. The limits of hermeticity test methods for micropackages. *Artificial organs*, 35(3), pp.242–4.

Vasko, K. et al., 2009. Multilayer coatings for flexible high-barrier materials. *Central European Journal of Physics*, 7(2), pp.371–378. Available at: http://www.springerlink.com/index/10.2478/s11534-009-0056-2 [Accessed March 12, 2013].

Venables, J.A., Spiller, G.D.T. & Hanbucken, M., 1984. Nucleation and growth of thin films. *Reports on Progress in Physics*, 47(4), pp.399–459.

Venables, J.D., 1984. Adhesion and durability of metal-polymer bonds. *Journal of Materials Science*, 19(8), pp.2431–2453.

Wang, J. et al., 2012. Integrated device for combined optical neuromodulation and electrical recording for chronic in vivo applications. *Journal of neural engineering*, 9(1), p.016001. Available at: http://iopscience.iop.org/1741-2552/9/1/016001/article/ [Accessed August 8, 2013].

Warwick, M. & Green, S., 2008. Laser welding of PEEK-OPTIMA for medical devices. In *Poster P-Sat-B-305*.

Weiland, J.D., Liu, W. & Humayun, M.S., 2005. Retinal prosthesis. *Annual review of biomedical engineering*, 7, pp.361–401. Available at: http://www.ncbi.nlm.nih.gov/pubmed/16004575 [Accessed August 9, 2013].

Williams, D.S., Rapp, R.A. & Hirth, J.P., 1986. Phase Suppression in the Transient Stages of Interdiffusion in Thin Films,.

Yang, R.T., 2003. *Adsorbents: Fundamentals and Applications*, Wiley-Blackwell.

Yasuda, H., 1975. Units of gas permeability constants. *Journal of Applied Polymer Science*, 19(9), pp.2529–2536.

Young, T., 1805. An Essay on the Cohesion of Fluids. *Philosophical Transactions of the Royal Society of London*, 95, pp.65–87 CR – 1805 The Royal Society.

Zanni-Deffarges, M., 1995. Diffusion of water into an epoxy adhesive: comparison between bulk behaviour and adhesive joints. *International Journal of Adhesion and Adhesives*, 15(3), pp.137–142.

Zaporojtchenko, V. et al., 2000. Formation of metal–polymer interfaces by metal evaporation: influence of deposition parameters and defects. *Microelectronic Engineering*, 50(1-4), pp.465–471.